UNIVERSITY OF CALIFORNIA,
MERCED

Negative Regulators of Toll-Like Receptors During *Chlamydia trachomatis* Infection

DISSERTATION

Submitted in partial satisfaction of the requirements for the degree of

DOCTOR OF PHILOSOPHY

in Quantitative and Systems Biology

by

Mufadhal Mohammed Al-Kuhlani

Dissertation Committee:
Associate Professor Jennifer Manilay, Chair
Professor David M Ojcius
Professor Maria Pallavicini
Associate Professor Jinah Choi
Associate Professor Wei-Chun Chin

2013

The Dissertation of Mufadhal Mohammed Al-Kuhlani is approved, and it is acceptable in quality and form for publication on microfilm and electronically:

Dr. Wei-Chun Chin

Dr. Jinah Choi

Dr. Maria Pallavicini

Dr. David Ojcius

Dr. Jennifer Manilay, Chair

University of California, Merced
2013

DEDICATION

”وَاخْفِضْ لَهُمَا جَنَاحَ الذُّلِّ مِنَ الرَّحْمَةِ وَقُلْ رَبِّ ارْحَمْهُمَا كَمَا رَبَّيَانِي صَغِيراً“

“And lower to them (parents) the wing of humility out of tenderness. And say, ‘My Lord, bestow on them your mercy as they nourished me when I was young” Quran 17.25

This thesis is dedicated in loving memory of my parents. My father Mohammed, who realized the importance of pursuing education and instilled this in my brothers and I; and my mother Amenah, who passed away while I was abroad pursuing my dream of earning higher education. May your souls rest in peace.

This thesis is also dedicated to my brothers and sisters and my entire loving family of many nephews and nieces. Thank you for your support, guidance, encouragement and love over the years.

Finally, to my wife, Sarah, whose constant love and support pushed me forward and made it possible. Thank you for your diligent efforts that enabled me to take the necessary time to complete this work.

TABLE OF CONTENTS

LIST OF ABBREVIATIONS

BCAP	B-cell adaptor for PI3K
BM	Bone marrow
BMDM	Bone marrow derived macrophages
CAC	Colitis-associated cancer
cDNA	Complementary DNA
CLR	C-type lectin receptor
CPAF	*Chlamydia* protease-like activity factor
Ct	Threshold cycle
DAMPs	Damage-associated molecular patterns
DC	Dendritic cells
DD	Death domain
DRIL	Double RING finger-linked domain
dsRNA	Double-stranded RNA
EAE	Experimental autoimmune encephalomyelitis
EBs	Elementary bodies
ELISA	Enzyme-linked immunosorbent assay
FADD	Fas-associated death domain
GAPDH	Glyceraldehyde 3-phosphate dehydrogenase
GM-CSF	Granulocyte-macrophage colony-stimulating factor
HEK293	Human Embryonic Kidney 293
HeLa	human cervical carcinoma cell line
Hpi	Hours post infection
hTRAIL-Rs	Human TRAIL-Receptors
IFN	Interferon
IFN-I	Type –I interferon
IFU	Inclusion Forming Unit
IKK	IκB kinase
IL-	Interleukin -8, -6, -18, -1alpha and beta
IL-1Rs	Interleukin-1 receptors
IRAK	IL-1 receptor-associated kinase
IRF-7	Interferon regulatory factor 7
IκB	Inhibitor of NF-κB
KO	Knockout
LBP	LPS-binding protein
LGV	Lymphogranuloma venereum
LPS	Lipopolysaccharide
LRR	Leucine-rich-repeat
MAL	MyD88-adaptor like
MD2	Myeloid differentiation factor 2
MEFs	Mouse embryonic fibroblasts

MOI	Multiplicity of infection
MOMP	Major outer membrane protein
MoPn	Mouse pneumoniti (*Chlamydia muridarum*),
mRNA	Messenger RNA
mTRAILR	Murine-TRAIL-R
MyD88	Myeloid differentiation primary-response protein 88
NF-κB	Nuclear factor-kabba B
NK	Natural Killer cells
NLRs	NOD-like receptors
NOD	Nucleotide-binding oligomerization domain
PAMPs	Pathogen-associated molecular patterns
PI	propidium iodide
PI3K	Phosphoinositide 3-kinase
PID	Pelvic inflammatory disease
PKR	Protein kinase RNA-activated
PMN	Polymorphonuclear
PRR	Pathogen Recognition Receptors
qPCR	Quantitative polymerase chain reaction
RBs	Reticulate bodies
RIG-I	Retinoic acid inducible gene-I
RLRs	RIG-I-like receptors
RT	Reverse transcription
SD	Standard deviation
SEAP	Embryonic Alkaline Phosphatase
shRNA	Short hairpin RNA
SIGIRR	Single Ig IL-1 receptor-related
siRNA	Small interfering RNA
SOCS	Suppressor of cytokine signaling
sST2	Soluble ST2
STD	sexually-transmitted diseases
TAG	TRAM adaptor with GOLD domain
TANK	TRAF family member-associated NF-κB activator
Th1	T helper-1 cells
THP1	human acute monocytic leukemia cell line
TIR	Toll/IL-1R domain
TIR8	Toll interleukin-1 receptor 8
TIRAP	TIR-containing adaptor proteins
TLRs	Toll-like receptors
TNF	Tumor necrosis factor
TNFAIP3	Tumor necrosis factor-alpha-induced protein 3
TNFRSF	TNF receptor superfamily
Tollip	Toll-interacting protein

TRAF6	TNF-receptor-associated factor 6
TRAIL	Tumor necrosis factor-related apoptosis-inducing ligand
TRAIL-R	TRAIL Receptor
TRAP	Translocated actin-recruiting phosphoprotein
Triad3A	Two RING fingers and DRIL protein 3A
TRIF	TIR-related adaptor protein inducing interferon
WT	Wild Type
ZIN	Zinc-finger protein inhibiting

LIST OF FIGURES

ACKNOWLEDGMENTS

I would like to express my sincere appreciation to my advisor and mentor; Dr. David Ojcius, for his invaluable guidance. I am grateful for his insights, word of encouragement, motivation and generous support throughout my thesis project.

I would like to thank the chair of my thesis committee, Dr. Jennifer Manilay, for her guidance throughout the years. Her support has always inspired me to work hard and complete my graduate education. I would also like to thank members of my thesis committee Dr. Maria Pallavicini, Dr. Jinah Choi and Dr. Wei-Chun Chin for their support and advice throughout my research.

I thank the John Wiley and Sons for permission to include Appendix D of my dissertation, which was originally published in Cellular Microbiology Journal. I like to thank the University of California-Merced and the NIH grant R56 AI078419 for providing the financial support.

Finally, I would like to take this opportunity to thank lab mates and colleagues at the University of California-Merced and everyone who helped me perfecting my research and writing of this thesis.

Curriculum Vitae

Mufadhal M Al-Kuhlani

TELEPHONE: 209-505-0029 EMAIL: almufadhal@gmail.com

Education:

2006- Present- University of California- Merced

- Ph.D. candidate, Quantitative and Systems Biology program, emphasis in Immunology.

2000—2004- University of Kansas

- B.S. in Clinical Laboratory Sciences, **emphasis in Molecular Biotechnology**.

Research And Professional Experience:

***Graduate Student Researcher*: University of California- Merced.** Program of Quantitative and Systems Biology. *Principal Investigator: David Ojcius, PhD*

- Studying the innate immune system and the negative regulation mechanisms that control pro-inflammatory response to *Chlamydia trachomatis* infection.

Research Specialist: **Ellis Fischel Cancer Center, University of Missouri**, September 2004- June 2006

- Conducted an independent-development of CpG island DNA microarray to discover the potential epigenetic biomarkers of genes methylation behavior in Multiple Myeloma,
- Performed genome wide analysis of DNA methylation of histone H3 Lysine 9 to identify novel epigenetic targets in breast cancer

Undergraduate internship: **Stowers Institute for Medical Research**. Kansas City**. Flow Cytometry Core Facility. January-February 2004**.

- Designed a project to isolate and harvest muscle stem cells, also known as satellite cells, from skeletal muscle tissues of adult mice.

Teaching Experience:

Teaching Associate: **University of California- Merced.** 2009-2013

Classes taught: The Cell, Bio 110 (4 semesters) Molecular Immunology (Bio 150 and Bio 151L). **Duties include:** organizing and leading discussion, leading wet and computer lab, holding office hours, preparing review sessions, preparing and grading homework, quizzes and lab assignments, grading midterms and final exams and guest lecturing.

Teaching Assistant: **University of California- Merced.** 2006-2009.

Classes taught: Contemporary Biology, Bio 1 (2 semester); Molecular Machinery of Life, Bio 2 (2 semester); The cell, Bio 110 (2 semesters); General Microbiology, Bio120 & Bio120L (1 semester). **Duties include:** organizing and leading discussion, leading wet and computer Lab, holding office hours, grading homework, quizzes and lab assignments, writing and grading midterm and final questions.

Publication:

Anyou Wang, **Mufadhal Al-Kuhlani,** S. Clayborne Johnston, David Ojcius, Joyce Chou, and Deborah Dean. "*Transcription factor complex AP-1 mediates inflammation initiated by Chlamydia pneumoniae infection*". *Cell Microbiol*, doi:10.1111/cmi.12071 (2012).

J. Ciriza, D. Hall, A. Lu, J. Robert De Sena**, *M. Al-Kuhlani,*** and Marcos E. García-Ojeda "*Single-Cell Analysis of Murine Long-Term Hematopoietic Stem Cells Reveals Distinct Patterns of Gene Expression during Fetal Migration"* PLoS One. 2012; 7(1): e30542

H. Shi, J. Guo, D. J. Duff, F. Rahmatpanah, R. Chitima-Matsiga, ***M. Al-Kuhlani***, K. H. Taylor, O. Sjahputera, M. Andreski, J. E. Wooldridge and C. W. Caldwell **"***Discovery of novel epigenetic markers in non-Hodgkin's lymphoma"* Carcinogenesis 2007 28: 60-70

Manuscripts Submitted or in Preparation:

Jesús Ciriza, **Mufadhal Al-Kulani**, Dominique Hall, Alison Lu, Joseph Robert Desena, Marcos E. García-Ojeda. *Multiplex single cell RT-qPCR analysis of fetal and adult murine long-term hematopoietic stem cells*. Stem Cell Review and Reports journal. *In review.*

Mufadhal M Al-Kuhlani, Luis De La Maza, Deborah Dean, David M Ojcius. *Human TRAIL-R1 is a negative regulator of pro-inflammatory response induced by Chlamydia Trachomatis*. PLOS Pathogen journal. *In review.*

Hsin-Chih Lai, **Mufadhal Al-Kuhlani**, and David M. Ojcius**.** *Inflammasome activation and IL-1b secretion.* Chapter in the Encyclopedia of Human Biology. *In review.*

Mufadhal M Al-Kuhlani, Ye Zhu, Graham Lambert, Karina Bermudez, David M Ojcius. *SIGIRR associates with MyD88 to down-regulates proinflammatory response to Chlamydia Trachomatis*. Submission plan June 2013.

Research Abstracts and Oral Presentation:

Mufadhal Al-Kuhlani, James Rothchild, Sukumar Pal, Luis M. de la Maza, Sander Ouburg, Servaas A. Morré, Deborah Dean, David M. Ojcius. *"Human TRAIL-R1 is a negative regulator of pro-inflammatory response induced by Chlamydia trachomatis"***.** Poster at the 6th Biennial Meeting of the Chlamydia Basic Research Society, March 2013. San Antonio, Texas .

Al-Kuhlani. M.M, Ojcius. D.M. "*Turning off TLR-dependent inflammation during C trachomatis infection*". Oral presentation for UC Merced/ Irvine/ Los Angeles Chlamydia Group Seminar Series. June, 2011

Al-Kuhlani. M.M, Ciriza. J, Ramos. JH, Carroll. T, Peiris. H, Garcia-Ojeda, M.E. "*Molecular Interaction Between GATA-3 and Notch-1 That Regulate T Cell Commitment"* Symposium Talk, The 10th Annual UC Systemwide Bioengineering Symposium June, 2009. Merced, California.

Al-Kuhlani. M, Carroll. T, and Garcia-Ojeda. ME. "*Single Cell q-PCR Analysis of The Molecular Regulation of T Cell Commitment".* Poster at the Experimental Biology Conference for the American Association of Immunologists (AAI) 661.1A, April 2008. San Diego, California.

Durtschi. D, **Al-Kuhlani. M**, Duff. D, Taylor. K, Caldwell. C, and Shi. H. *"Integrated epigenomic scanning in multiple myeloma cell lines reveals regulatory pathways of epigenetic alterations"* Poster at the AACR Meeting 97: 3236A, 2006, April 2006. Washington, DC.

Honors and Awards:

- Graduate Students Fellowships, University of California-Merced. 2010 and 2011
- John Traylor Conner Award University of Kansas, 2003
- Betha Martha Award, University of Kansas, 2003
- Qatar Award, Ministry of Higher Education and Scientific Research (Yemen) 1999-2004

ABSTRACT OF THE DISSERTATION

Negative Regulators of Toll-Like Receptors During *Chlamydia trachomatis* Infection

By
Mufadhal Mohammed Al-Kuhlani

Doctor of Philosophy in Quantitative and Systems Biology

University of California, Merced 2013

Professor Jennifer Manilay, Chair

Chlamydia trachomatis is the most common bacterial sexually-transmitted disease (STD) around the world. The response of the immune system to eliminate *C. trachomatis* infection through inflammation is a very efficient process. However, persistent infection or uncontrolled inflammation causes a complication in the upper genital tract, which can ultimately lead to infertility and chronic pelvic pain. Therefore, inflammation has to be tightly regulated to avoid an uncontrolled immune response. The genetic factors that regulate inflammation during *Chlamydia* infection have not been clearly characterized. SIGIRR, Triad3A and TRAIL-R are proteins that have been shown to manipulate inflammation in response to various pathogens and diseases. However, little is known about their role during *C. trachomatis* infection.

Our results indicate that in the absence of SIGIRR, epithelial cells induce higher levels of proinflammatory cytokines in response to chlamydia infection. In addition, overexpression analysis reveals that SIGIRR associates with MyD88 and localizes around the inclusion of the *Chlamydia* and the nucleus of the

infected cell. Additionally, our data indicates that the absence of Triad3A in HEK cells that express individual TLRs does not affect the levels of IL-8 in TLR2, TLR3 or TLR4, when activated by *C. trachomatis*. However, the absence of Triad3A in cells that express both TLR2 and TLR4 induces lower level of IL-8 compared to wild type cells as a result of the inhibitory effect that TLR4 exerts on TLR2.

Ex-vivo analysis shows that *Chlamydia* infection of bone marrow derived macrophages (BMDM) and primary lung fibroblasts from TRAIL-R deficient mice, induces higher levels of MIP2 mRNA expression and IL-1β secretion compared to cells from the wild type mice. In addition, *in vitro* study of human TRAILR1 shows that reduction of TRAIL-R1 expression on HeLa cells correlates with an increase of IL-8 expression and secretion in *Chlamydia*-infected cells.

Taken together, our data shows that SIGIRR, Triad3A and for the first time human TRAIL-R1, function as regulators of the immune response to *C. trachomatis* infection. This finding provides an insight into the immune-pathogenesis of *C. trachomatis* that can be used to develop novel intervention and diagnostic strategies to treat and identify individuals at high risk.

CHAPTER 1

INTRODUCTION

1.1 *CHLAMYDIA TRACHOMATIS* AND CHLAMYDIAL DISEASES

1.1.1. *Chlamydial* Strains and virulence:

Chlamydia is an obligate intracellular bacterial pathogen with a unique biphasic developmental life cycle that is capable of infecting various types of tissues in humans and animals. Initially, the family of *Chlamydiae* had been strictly classified as a mammalian pathogen with four different species [3]. In the late 1990s, a controversial classification of *Chlamydia* to pathogenic and environmental groups with 9 different species was introduced based on their 16S rRNA sequences [3,4]. The pathogenic group contains four major species; *C. trachomatis, Chlamydia pneumoniae, Chlamydia psittaci* and *Chlamydia pecorum*, and each one causes unique health risks for humans [5-7]. Despite the differences of the genomic size and their hosts, all *Chlamydia* species share many common mechanisms in infection, growth cycle, metabolism and manipulation of host cells to survive and obtain nutrients [3,8,9].

C. trachomatis is one of the leading cause of bacterial sexually-transmitted diseases (STD), and a major cause of preventable blindness around the world [10]. The number of the reported cases in the United States in 2011, according to the Centers for Disease Control (CDC), is more than 1.4 million cases, which corresponds to an increase of about 8% in comparison with the rate of 2008 [11].

The World Health Organization reports that *Chlamydia* is the cause of blindness to about 6 million with overall infection of more than 140 millions around most part of the world [12]. *C. trachomatis* in both men and women causes asymptomatic infection, which further complicates the spread of the bacteria as the infected individuals serve as a carriers[13]. Infected women suffer from major and long-term complications that can cause irreversible damages. Acute salpingitis, pelvic inflammatory disease (PID), tubal factor infertility, ectopic pregnancy and chronic pelvic pain are some examples of the consequences that women face as a result of *Chlamydia* infection [14,15].

Based on the major outer membrane protein (MOMP), *C. trachomatis* is categorized into 19 different strains [16]. Depending on the site and intensity of infection, the 19 strains are commonly divided into three disease groups; ocular (strains A, B, Ba, and C), urogenital (strains D, Da, E, F, G, H, I, Ia, J, Ja and K), and the invasive urogenital (strains L1, L2, L2a and L3), known as lymphogranuloma venereum (LGV) [16]. Compared to other strains, the fast growing LGVs are associated with more severe forms of the infection and are the cause of major outbreaks in humans [17-19]. Despite their effects, the major virulence factors that explain LGVs' invasiveness and severity are yet to be discovered [20]. *Chlamydia muridarum,* widely known as mouse pneumonitis (MoPn), was initially identified as a causative agent of pneumonitis in mice, but was later identified as a strain of *Chlamydia* that is capable of infecting the lung and the urogenital tract of the mouse [21]. Both *Chlamydia muridarum* and the

human strain of LGVs are closely related and usually used on mice to study the host-pathogen interaction [22,23].

Chlamydia pneumonia, is a widely spread bacteria among humans that causes acute upper and lower respiratory tract infections [24,25]. Reports have estimated that *Chlamydia pneumoniae* is responsible for about 10% of the community acquired-pneumonia and that almost everyone has been infected with the bacteria at least once [26]. Like *C. trachomatis, C. pneumoniae* has been linked to many chronic infections such as asthma and cardiovascular diseases [27,28]. Even though that *Chlamydia pneumoniae* found on humans was originally an animal pathogen, and still can be detected in various animals, the transmission mechanism has been reported to be only through human-to-human interaction [25].

Chlamydia psittaci and *Chlamydia pecorum* both are pathogenic strains that generally cause infection for birds and some mammals with wide range of symptoms [29]. However, human contact with infected birds can cause severe pneumonia as a result of a rare transmission of *Chlamydia psittaci* [26].

1.1.2. *Chlamydial* developmental cycle:

As it was mentioned earlier, different species of *Chlamydiae* share a unique biphasic developmental life cycle. In their life cycle, *Chlamydiae* species alternate between the small, infectious and metabolically inactive extracellular elementary bodies (EBs); and the large, noninfectious and metabolically active reticulate bodies (RBs) [30]. The 300 nm spore-like EBs initially attach to the host

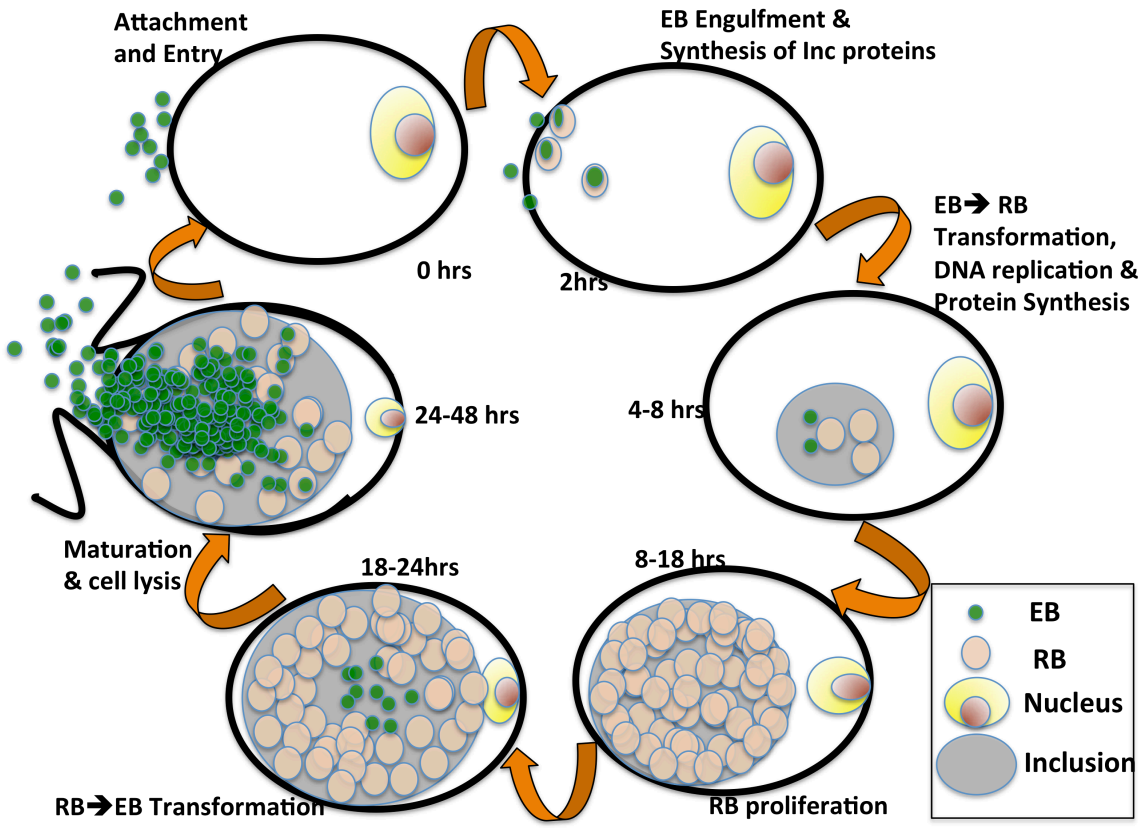

Figure 1.1: Life cycle of *Chlamydia Trachomatis*. Infection starts by the entry of the elementary bodies (EBs) followed by the formation of the inclusion in the first 2 hrs of infection. EBs transform into reticulate bodies (RB), which actively proliferate for the next 12 hrs. RBs convert back to EBs and burst outside of the host cell between 24-48 hrs of infection [31].

cells via undefined mechanism. Once they irreversibly attach to the host cells, EBs release translocated actin-recruiting phosphoprotein (TARP) via type III secretion. TARP is a *Chlamydia* effector protein that manipulates the actin filaments of the host to allow the internalization of the EBs into the cytosol via endocytosis [32].

As illustrated in Figure1.1, *Chlamydiae* species replicate within a membrane bound vacuole, called inclusion, where they can multiply without lysosomal fusion[33]. Therefore, immediately after entering the host cells, transcription mechanisms of EBs begin to synthesize proteins that are required for the inclusion formation, such as IncD-G, along with other proteins that are necessary for the transformation of EBs to RBs [34,35]. The formation of the inclusion and the synthesis of proteins needed for the EB-RB transformation is dominant during the first 8 hours of infection. Over time, the inclusion that contains the dividing RBs keep expanding until they dominate the cytoplasm of the host cells.

For the next 10 hours, the cellular machinery is dedicated for the rapid growth and expansion of the RBs via binary fusion [35]. *Chlamydia* starts activating the genes needed for the transformation of RB to EB, where the DNA becomes condensed around 12 hours post infection (hpi) [35]. During the late phase of the cycle, the EBs can be detected at 18 hpi. Twenty-four hpi, DNA replication and RB proliferation continue but at a slower rate, while the number of EBs increases. Depending on the *Chlamydia* strain, the multiplication of the RBs

and their transformation to EBs continue for additional 24-48 hours until the cells burst and release EBs [36].

1.2. *CHLAMYDIA* – HOST CELL INTERACTIONS

1.2.1 Activation of the immune system

Innate immunity is an ancient form of host defense that is shared by many species, including the vertebrates, invertebrates and plants [37]. It is the major contributor to inflammation and is considered the first line of defense against invading microbial and viral pathogens [38,39]. Contribution of the innate immune system is not limited to the professional immune cells, such as dendritic cells (DC), macrophages or polymorphonuclear (PMN) leukocytes, but also extends to non-immune cells such as epithelial, endothelial and fibroblast cells[38,39].

Even though they are not considered as immune cells, epithelial cells have been shown to initiate inflammation by producing several cytokines such as tumor necrosis factor-α (TNF-α), Granulocyte macrophage-colony stimulating factor (GM-CSF), interleukin (IL)-1, IL-6 and IL-8 [40,41]. IL-8 functions as a chemokine that attracts and activates various immune cells to the site of infection. The signal that triggers the production of IL-8 in response to *Chlamydia* infection is linked to an internal signal within the host cell rather than the soluble factors produced by other infected cells [42]. Unlike other pathogens, where the IL-8 synthesis begins shortly after infection, the level of IL-8 in response to *Chlamydia* infection begins 15 hpi. Secretion of IL-8 attracts neutrophils, macrophages, dendritic cells (DCs), T-cells and NK cells to the infected site[43,44].

In addition to the IL-8, various immune cells induce the secretion of proinflammatory cytokine IL-1β that is known to contribute to the oviduct pathology of infected mice in response to *Chlamydia* infection [44-46]. Clearance of *Chlamydia* infection from IL-1β deficient mice was greatly delayed compared to WT mice, indicating its role in response to the infection[45]. Reports have shown that PMNs' capability to eradicate *Chlamydia* is strain specific, where some strains can multiply inside these PMNs instead of being killed [47,48]. Macrophages are also one of the immune cells that are effective in fighting *Chlamydia* infection via phagocytosis and the production of IFNγ [49,50]. In addition to their phagosomal activity against *Chlamydia*, activated macrophages, as well as DCs, recruit and activate NK, B and T cells to the infected site [49].

Epithelial cells are the main target for *Chlamydial* infection, and therefore are considered the first responder cells that initiate and sustain the release of proinflammatory cytokines against *Chlamydia* [40]. The epithelial cells lining various tissues of the reproductive tract of humans are known to express many of the pattern-recognition receptors (PRRs), including members of the Toll-like receptors (TLRs) such as TLR1, TLR2, TLR3, and TLR4[51]. Recognition of conserved pathogenic structures, known as pathogen-associated molecular patterns (PAMPs) such as peptidoglycan (PG); lipopolysaccharides (LPS); or double stranded RNA (dsRNA), by the appropriate TLR stimulates the production of various pro-inflammatory mediators. Besides LPS, which is believed to activate TLR4, *Chlamydia* species express a lipoprotein known as macrophage infectivity potentiator (MIP) that has been shown to activate TLR2 [52]. In addition,

Chlamydia encodes enzymes for PG synthesis and known to be sensitive to penicillin treatment, but all the attempts to detect any level of PG have not been successful [53,54]. However, it is not clearly defined wither TLR2 or TLR4 is responsible for the recognition of *Chlamydia's* PAMPs that leads to the induction of the immune response.

1.2.2 Toll-Like receptors (TLRs)

Before recognizing Toll's role in innate immunity in mid-1990's, it was first identified as a critical component of Drosophila's embryogenesis [55,56]. Toll-Like receptors (TLRs), the mammalian homolog of Drosophila Toll, are members of the large interleukin-1 receptors (IL-1Rs) superfamily. There are about 10 TLRs receptors that have been characterized in human and 12 in mice with broad range of PAMPs that can be detected by these receptors [2]. TLRs are integral glycoproteins that can be present on the surface of the cells or within the intracellular endosomes or lysosomes of the cells [38]. They are characterized by leucine-rich-repeat (LRR) motifs of variable lengths in the extracellular domains as well as a highly conserved cytoplasmic Toll/IL-1R (TIR) domain[57].

TLR2 is a well-studied member of TLR family. It has the ability to detect variety of microbial components more than any other TLRs. Microbial components like lipoproteins from gram-negative or mycoplasma's origin, peptidoglycan and lipoteichoic acid from gram-positive bacteria, fungal zymosan and even some lipopolysaccharide (LPS) that are structurally different from those recognized by TLR4, are all examples of the microbial ligand that can activate TLR2 [57-59]. The fact that TLR2 is capable of forming homodimers or

heterodimers with either TLR1 or TLR6 as well as its ability to work together with other receptors, such as Dectin-1, offers an explanation to TLR2's ability to recognize such a broad selection of ligands [60,61].

TLR3 is predominantly expressed in dendritic cells and has been widely known to detect viral double-stranded (ds) RNA within the endolysosomes [62]. However, few reports have recently indicated that TLR3 is also capable of recognizing bacterial components [63]. One unique structure of TLR3 that separates it from all the other known TLRs is the absence of the conserved proline residue in its cytoplasmic domain [64]. Activation of TLR3 results in the induction of type –I interferon (IFN-I) along with other pro-inflammatory cytokines [63].

TLR4 is the first member of mammalian TLRs family to be linked to the induction of pro-inflammatory response [65]. The ability of TLR4 to induce an immune response to LPS has been thoroughly investigated. Three accessory proteins are required for the TLR4 signaling to take place in response to LPS [66]. First, gram-negative LPS must be extracted by LPS-binding protein (LBP) and then transferred to CD14, which will then bring it to the TLR4-myeloid differentiation factor 2 (MD2) complex [66,67]. Activation of TLR4 leads to its translocation, and later its degradation via Triad3A, into the endosome without effecting the activation of the downstream nuclear factor-kabba B (NF-κB) [68,69,70]. Activation of these TLRs, which are expressed in immune cells such as macrophages, dendritic cells and neutrophils as well as the mucosal epithelial cells, are known to drive the immune response[56,71].

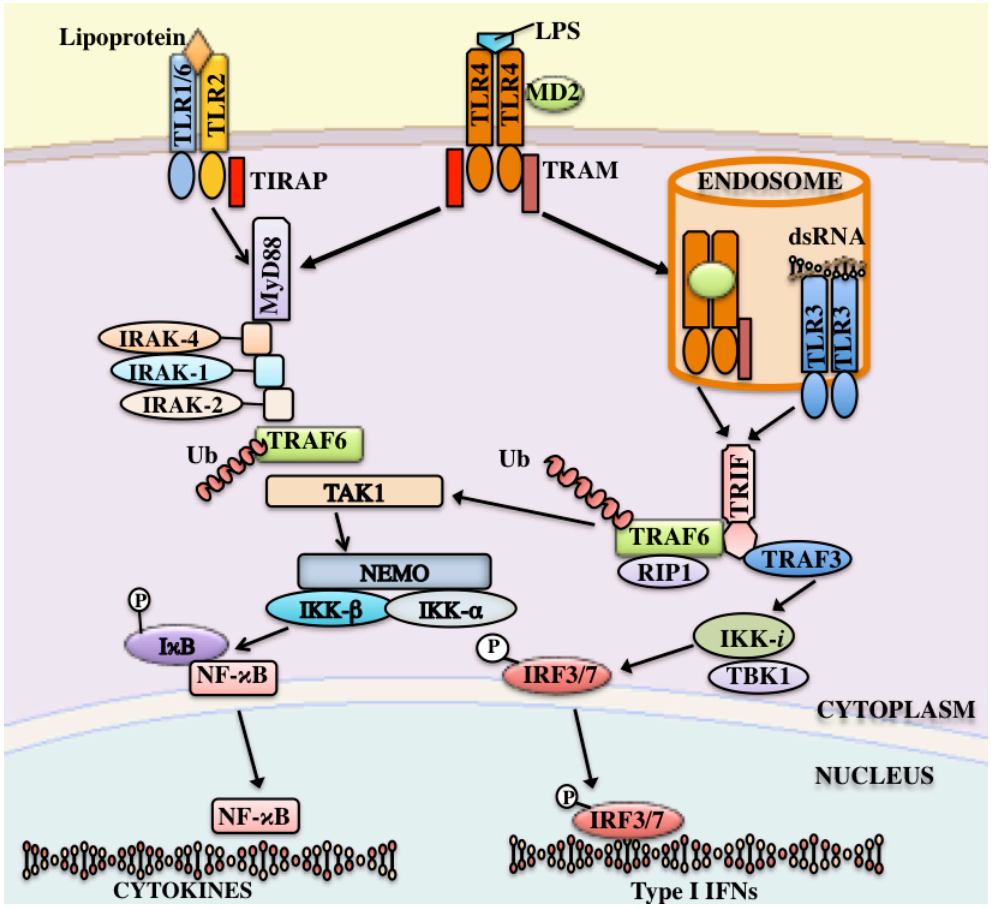

Figure 1.2: Summary of the signaling pathways for TLR2, 3 and 4. Engagement of the appropriate ligand with TLR2 or TLR4 recruits TIRAP and MyD88 to the cytosolic domain of the TLRs. More adaptors like IRAKs and TRAF6 also recruited to form complex that dissociates from the MyD88-TIRAP complex and ultimately phosphorylates NEMO complex and activates IKK. Subsequently IκB is phosphorylated and degraded via ubiquitination which allows the activated NF-κB to translocates into the nucleus and induce the expression of proinflammatory cytokines. TRIF-dependent pathway for TLR4 requires the translocation of the receptor into the endosome. TLR3 and TLR4 TRIF-dependent pathways interacts with either TRAF6 or TRAF3 that leads to the activation of NF-κB, or the phosphorylation of IRF3 that results in the induction of proinflammatory cytokine genes and type I IFNs [2].

1.2.3. Activation of TLR signaling pathways

As illustrated in Figure 1.2, the engagement of the host TLRs with the appropriate ligands causes conformational change to the receptor that allows them to recruit various adaptors to their TIR domains [2]. Activated TLRs, with exception to TLR3, use myeloid differentiation primary-response protein 88 (MyD88) as a universal adaptor [42]. Signaling through TLR2 and TLR4 also recruits TIR-containing adaptor proteins (TIRAP), also known as MyD88-adaptor like (MAL) [72]. MyD88 further recruits and activates the IL-1 receptor-associated kinase 4 (IRAK4) through its Death Domain (DD) to this complex [73,74]. This complex leads to the recruitment and phosphorylation of another adaptors, like IRAK1/2, which will further attract the (TNF)-receptor-associated factor 6 (TRAF6) to this complex [73,75,76]. Activated TRAF6 initiates its own lys-63 polyubiquitination and then dissociates the IRAKs-TRAF6 complex from MyD88 [77]. This complex then engages with various proteins that ultimately leads to the phosphorylation of inhibitor of NF-κB (IκB) kinase (IKK), which subsequently phosphorylates IκB [78]. IκB then undergoes degradation via ubiquitination and releases the activated nuclear factor-κB (NF-κB). Finally, activated NF-κB translocates into the nucleus and ultimately up-regulates the expression of proinflammatory components, such as IL-8, IL-6, IL-18, IL-1α and GM-CSF, which recruit and activate various immune cells [41,42,79,80]. In addition to their activated NF-κB, TLR7, 8 and 9 activate an alternative pathway that involves the phosphorylation of TRAF3 in addition to TRAF6 [81,82]. This pathway

phosphorylates the Interferon regulatory factor 7 (IRF7) and translocates it into the nucleus, which then induces the expression of IFN-I molecules [82].

The signaling pathway of both TLR3 and TLR4 is a MyD88 independent pathway that utilizes TIR-related adaptor protein inducing interferon (TRIF). Unlike TLR4 that is also capable of recruiting MyD88, TLR3 signaling is restricted to TRIF [2]. Activated TLR3 binds directly to TRIF through its TIR domain, while TLR4 requires TRIF-related adaptor molecule (TRAM) to bring TRIF to its TIR domain [83]. TRIF binding to the TIR domain of both TLR3 and TLR4 recruits and activates either TRAF3 or TRAF6 [84]. Activated TRAF3 further activates other kinases that will ultimately lead to the phosphorylation of IRFs and consequently the induction of IFN-I. On the other hand, activated TRAF6 engages with kinases, other than the IRAKs, that in return activates NF-κB [84].

1.2.4. Clearance and persistence of *Chlamydia* infection

Clearance of infection through inflammation is a very efficient process. However, the mechanisms for clearing infection by the immune system varies among individuals where the pathogen can also cause a chronic inflammation, or develop to become persistent [85,86]. Persistent infection of *Chlamydia* is a reversible process that is caused by inappropriate exposure to antibiotics, nutrient deprivation, re-infection, or the ability of the bacteria to escape macrophages' phagosomal activity [87,88]. Even though *C. trachomatis* infection can be easily treated with a dose of antibiotics if diagnosed early, the asymptomatic nature of the infection often leads to severe complications ranging

from blindness to pelvic inflammatory disease and infertility [44]. These complications and the damage caused by *Chlamydia* are mainly linked to the chronic inflammation triggered by persistent infection. Since TLR signaling pathways play major role to initiate inflammation, the immune response must be down-regulated following the resolution of the infection to avoid the development of chronic inflammation.

1.3. NEGATIVE REGULATORS OF TLR PATHWAYS

Chronic inflammation and tissue damage are associated with diseases like rheumatoid arthritis, asthma, and inflammatory bowel disease organisms [89]. Therefore, inflammation has to be tightly regulated to avoid uncontrolled immune response. The mechanism that negatively regulates inflammation is accomplished at multiple levels throughout the TLR signaling pathways. Liew *et al*. reviewed these levels and mainly categorized them, based on their location in the cell, to extracellular decoy receptors, intracellular inhibitors and membrane-bound regulators [1]. Here, we review the literature for previous effectors and the most recently discovered ones and classify them based on the regulatory mechanism they exert on the TLR signaling pathways (Figure 1.3).

1.3.1 Alternative Splicing:

Alternative splicing is the processing of mRNA from a sequence of a single gene that produces different isoforms of the protein with different functions. The different variants produced by this mechanism have shown to negatively regulate

the TLR signaling. Different isoforms of TLRs have been naturally detected in their soluble form [90,91]. The existence of soluble form of membrane receptors, which work as decoys, as well as some of their accessory proteins, ensures that signaling pathway can be blocked at the early stages so that an overreaction of the host immune system does not occur. Soluble TLR2 isoforms are found in breast milk and plasma [92]. These soluble isoforms were capable of dampening inflammation, marked by reduced NF-κB activity, without compromising the host efficiency to clear bacterial infection[93]. In macrophage cell lines, the expression of soluble isoforms of TLR4 is increased as a result of LPS stimulation. This soluble TLR4 is capable of inhibiting NF-κB activity as well as TNF production [90]. In addition to the soluble TLR4, the TLR4 accessory protein, MD2, also exists as an isoform that reduces the activity of NF-κB by competing with the full length MD2 for the binding to TLR4 [94].

Adaptors like MyD88, IRAK1, IRAK2 and TRIF are the main targets for negative regulations. An isoform of MyD88, known as MyD88s, that is missing the interdomain and is detected in few tissues, does not activate NF-κB [95]. MyD88s forms a heterodimer with MyD88 and IRAK1, but not to IRAK4. Therefore, IRAK1 does not get phosphorylated and accordingly NF-κB activity is blocked, indicating MyD88s role as a negative regulator of TLRs. Signaling through TRIF adaptor is also regulated by a splice variant of TRAM called TAG (TRAM adaptor with GOLD domain), where overexpression of the protein affects signaling downstream of IRF3, but not NF-κB [96]. Similarly, IRAK1 and IRAK2 exist in different isoforms, known as IRAK1C and IRAK2c, that are incapable of

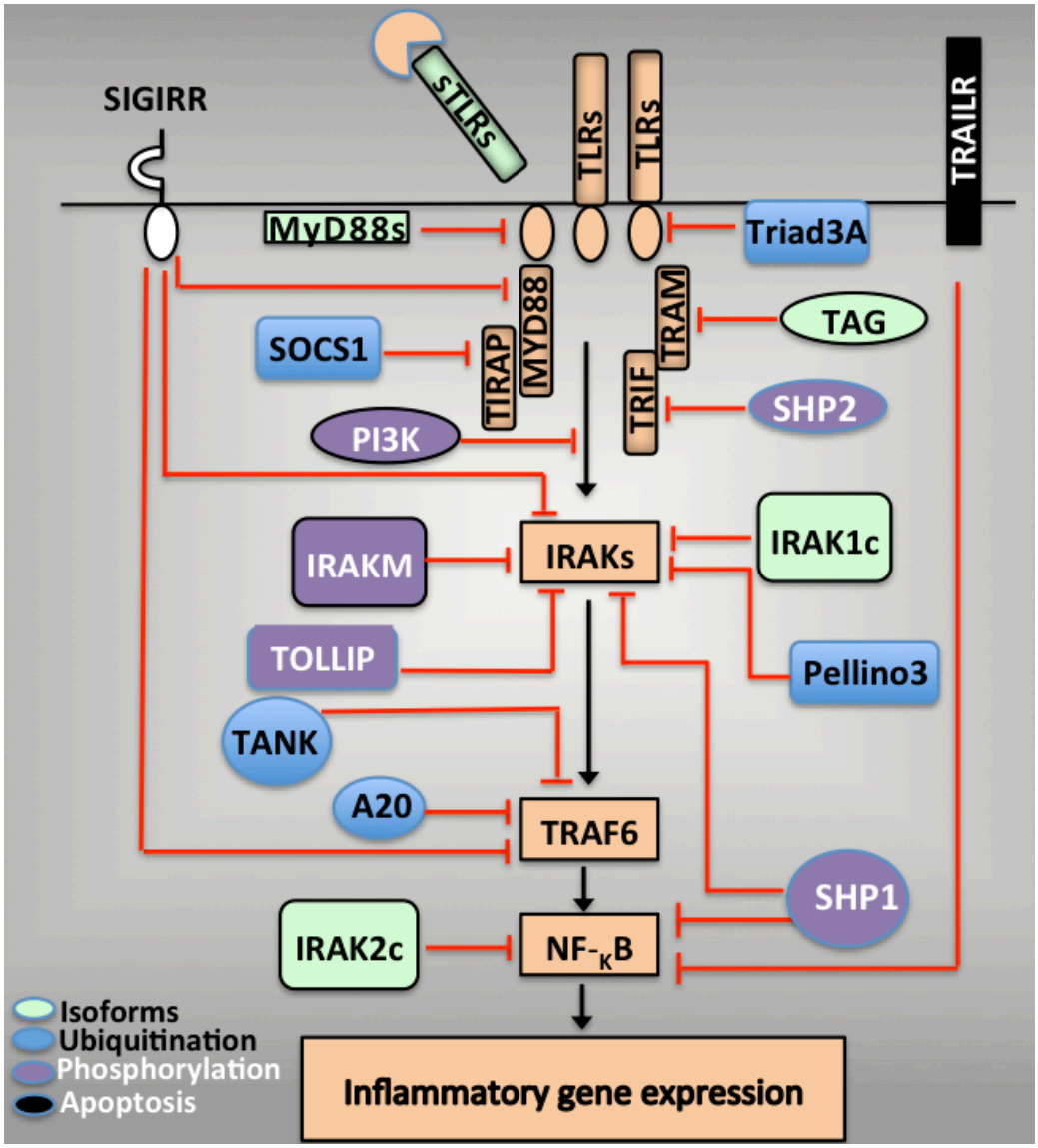

Figure 1.3: Summary of the various proteins that have shown to regulate the immune response to various stimuli and their targets. Regulation by different protein isofroms (green), ubiquitination (blue), phosphorylation (purple) or apoptosis (black) blocks TLR activation process by targeting various proteins (orange) at different stages of the signaling pathways [1].

being activated by IRAK4 even though they strongly bind to the MyD88-IRAK4 complex and interact with NF-κB complex indicating their role as negative regulators of TLR signaling [97,98].

1.3.2. Regulation via Ubiquitination

Ubiquitination is a reversible process that affects protein conformation and regulates the localization and activity of targeted proteins [99] . Ubiquitin protein uses its lysine residues to bind covalently to the Lys residues of its targets and to other ubiquitins to form polyubiquitin chains. Lys-63-linked-ubiquitination leads to the activation of the targeted proteins, while Lys-48- linked Ubiquitin leads to its degradation [99]. Components of the TLR signaling like TRAF6, IRAK1 and IkB go through ubiquitination as part of their signaling pathways. Therefore, regulation of TLR signaling of these proteins and others, via ubiquitination, has been thoroughly investigated.

As discussed earlier, TRAF6 is involved in the signaling pathways of all TLRs signaling where ubiquitination is an important aspect of its activities [77]. Studies of the mechanisms that regulate TRAF6 revealed that proteins like A20, the TRAF family member-associated NF-κB activator (TANK), manipulate the activation of TRAF6 by adding or removing Lys63-linked ubiquitin to the protein [100,101,102]. Stimulation of various TLRs in the absence of A20 or TANK resulted in higher levels of pro-inflammatory cytokines and that elevated levels were associated with higher Lys-63 polyubiquitination of TRAF6 [103,101].

Suppressor of cytokine signaling-1 (SOCS) and Triad3A proteins regulate TLR signaling pathways via Lys-48-linked polyubiquitination that lead to the

degradation of the targeted proteins [69,104-106]. While SOCS-1 targets the p65 subunit of NF-κB, Triad3A promotes the degradation of TLR themselves [69,107,108]. On the other hand, Pellino3 is a protein that competes with Lys-48-linked polyubiquitination to promote Lys63-linked polyubiquitination on the single ubiquitination site found on IRAK1 [109]. Therefore, deficiency in Pellino3 promotes the degradation of IRAK1 and subsequently the reduction of TLR signlaing [110].

1.3.3. Regulation via Phosphorylation:

Phosphorylation and de-phosphorylation is a mechanism that regulates the activities of many proteins by the tight coordination between kinases and phosphatases [111]. Phosphorylation process that involves TLR signaling pathways usually targets tyrosone residues and causes conformational changes that allow these proteins to become activated and recruit others. Therefore, activity of these proteins requires a mechanism that controls the duration and the intensity of their phosphorylation.

Phosphorylation of phosphoinositide 3-kinase (PI3K) causes an accumulation of phospholipids in cell membranes which function as a second messenger that control many cellular functions on the cell [112]. There are conflicting reports on the role of PI3K as positive or negative regulator of TLR signaling κB [113,114,115-118]. However, this discrepancy is explained by the fact that PI3K exist in different classes that play multiple roles at different signaling pathways on different cells with the help of different proteins [112,119].

Activation of IRAK1 and IRAK4 proteins take place through

phosphorylation. IRAK-M, Single Immunoglobulin IL-1 related receptor (SIGIRR), Toll-interacting protein (Tollip), and Src homology 2 domain-containing protein tyrosine phosphatase-1 (SHP-1) are all proteins involved in manipulating the activation of the IRAK proteins [120-122,123,124]. Even though that only IRAK-M is known to block the phosphorylation of IRAK1 and IRAK4, both SIGIRR and IRAK-M act in the same way by preventing the recruitment and dissociation of signaling component MyD88-IRAKs-TRAF6 complex [123,124]. On the other hand, stimulation of TLR pathways in the presence of either TOLLIP or SHP-1 diminishes the autophosphorylation of IRAK1 [125,120,121]. Unlike SHP-1, SHP-2 has been shown to negatively regulate the production of IFN-I by exerting an inhibitory effect on TRIF-dependent pathway by suppressing the phosphorylation of TBK1 protein [126].

1.3.4. Regulation via Apoptosis

Apoptosis, is a programmed cell death that controls the development, maintains homeostasis and functions as a defense mechanism by the immune system to remove infected or damaged cells [127]. Activation of death receptors or the release of mitochondrial proteins are the two signaling pathways that have been identified to initiate apoptosis [127]. NF-κB activity mediates survival of host cells by inducing anti-apoptotic proteins and therefore preventing apoptosis. On the other hand, pathogens like Yersinia induces apoptosis in the host cells as a way to manipulate the immune response so the pathogen can multiply and spread[128]. Other pathogens, like C*hlamydia*, can both inhibit and induce

apoptosis in the host cells depending on the strain and the stage of the bacteria's life cycle [129]. A microarray analysis revealed that the induction of apoptosis, following PMN phagocytosis, significantly down regulates the expression of more than 42 genes that are critical for the inflammatory response [130].

Fas-associated death domain (FADD) is a proapoptotic protein that gets recruited to the death receptor via its death domain (DD) that is associated with caspase-dependent proapoptotic signaling pathways [131]. Reports have shown FADD's involvement in manipulating NF-κB activity, where its over-expression reduces the activity of IL-1β- and LPS-induced NF-κB [132]. This inhibitory effect takes place through the interaction with MyD88 and IRAKs through their DDs [133,134].

Besides FADD, which is caspase-8 dependent, stimulation of TLR2 or TLR4 upregulate Nur77, which in return induces caspase-independent apoptosis pathways [135]. In addition, TLR2 and TLR4 signaling pathways have been also shown to activate protein kinase RNA-activated (PKR) that facilitates the release of damaged-associated molecular patterns (DAMPs) that induce apoptosis [136-139]. In addition to PKR, stimulation of TLR3 upregulates the tumor necrosis factor-related apoptosis-inducing ligand (TRAIL) and its receptors, TRAIL-R 1 and 2, which in return initiates the proapoptotic pathway [140]. Manipulation of Apoptosis via TLR5 and TLR9 has been also reported, but the mechanisms are not clearly defined [141,142].

1.3.5. Negative regulation of inflammation during *Chlamydia* infection

Chlamydia species are dependent on the host cell for survival and development. Therefore, the bacteria have developed many strategies that manipulate the host cells to the bacteria's advantage. For instance, *C. trachomatis* manipulates the host's microtubules and move the inclusion near the Golgi and acquire nutrients such nucleic acid, amino acids and phospholipids from the host cell [143,144,145]. In addition, *C. trachomatis* escapes macrophages' phagosomal activity, down regulates MHC molecules, inhibits apoptosis, and modifies the cytoskeleton of the host [81,82,83,129,87,88,146]. Few of the virulence factors of *C. trachomatis* have been associated with manipulation of phosphorylation, ubiquitination, and apoptosis. It is well established that many of *Chlamydia* species encode two deubiquitinating proteins, known as *Chla*Dub1 and *Chla*Dub2, that inhibit the ubiquitination and the degradation of IκB [147,148]. Additionally, *Chlamydia* encodes an apoptotic mediator, known as *Chlamydia* protein associating with death receptors (CADD), that interacts with Fas through its death domain-like region [129,149]. Even though phosphorylation is not directly involved in the regulation of the immune response against *Chlamydia*, entry of EBs is associated with increased tyrosine phosphorylation involving Tarp [150]. Collectively these factors support the survival and development of *C. trachomatis* while minimizing the effect of inflammation during infection.

Utilization of phosphorylation, ubiquitination, and apoptosis by the virulence factors of *Chlamydia* during infection raised the question of whether host cells exploits similar mechanisms to negatively regulate the activities of the

immune response against *Chlamydia*. Although TLRs play a major role in the initiation of inflammation, little is known about the down-regulation mechanism of inflammation during successful resolution of *C. trachomatis* infection. Preliminary investigation of the genes expressed in cervical epithelial cells narrowed the potential regulators for this study into three genes; the single-immunoglobulin interleukin-1 receptor-related (SGIRR), two RING fingers and DRIL (Triad3A) and TNF-related apoptosis-inducing ligand receptor (TRAIL-R).

1.4. SIGNIFICANCE:

The tight regulation of the innate immune signaling is an essential mechanism that ensures that abnormal immune responses that lead to severe or even fatal consequences do not occur. Inflammation is a process that is very efficient in eliminating invading pathogens. The ability of *Chlamydia* to cause a chronic inflammation or develop to become a persistent infection is subjective to the individual's ability to clear the infection. The biological and genetic factors that lead to an aberrant inflammation in the host cells have not been clearly characterized.

This work is aimed to address an important aspect that contributes to the severity of infection and the chronic inflammatory stage that causes irreversible tissue damage caused by *Chlamydia* to the female genital tract. The effects of SIGIRR, Triad3A and TRAIL-R activities on *C. trachomatis* diseases have never been investigated. Thus, elucidating the molecular mechanisms that regulate the proinflammatory response by these proteins may help us to better understand

the biological basis that causes complications during *C. trachomatis* infection. Here I investigated the role of SIGIRR, TRAIL-R and Triad3A in regulating inflammation and determined how they influence the innate immune response in the *Chlamydia*–infected cells.

Revealing the factors that are involved in down-regulating the immune response of *Chlamydia*-challenged cells will help us understand how chronic inflammation is established. Ultimately, this study may eventually lead to the development of novel diagnostic, therapeutic and intervention techniques that minimize complication of the *Chlamydial* diseases as well as an anti-*Chlamydia* vaccine that can control the spread of *Chlamydia.*

CHAPTER 2: MATERIALS AND METHODS

2.1. CELL CULTURE AND *CHLAMYDIA* INFECTION

2.1.1. Growth of Cell lines and bacteria:

The human cervical carcinoma cell line, HeLa 229, was obtained from American Type Culture Collection (ATCC). HeLa cells were cultured in a humidified incubator at 37 °C with 5% CO2 in DMEM/F12 medium (Invitrogen) supplemented with 10% heat-inactivated fetal bovine serum (FBS) (Invitrogen), 50 U/ml Penicillin, 50 ug/ml Streptomycin (Invitrogen) and 10 ug/ml gentamycin. The LGV/L2 strain of C. trachomatis were obtained from Roger Rank, University of Arkansas and grown and harvested in HeLa as described before [151,152]. Briefly, $1x10^7$ HeLa cells were plated on 150 mm plate until they reached about 60% confluence in antibiotic free media. The monolayer of the HeLa cells was infected with frozen stock of LGV-L2 EBs at a multiplicity of infection (MOI) of 2 EBs/host cell and incubated at 37◦C. Forty-four hpi, cells were collected using sterile cell scraper and stored at -80°C. Collected cells went through a freeze-thaw cycle and vortexed for about 1 minute. Cell suspension were centrifuged for 15 min at 500*xg* at 4°C. Supernatant was centrifuged again for 30 min at 30,000 *xg* at 4°C. Supernatant was discarded and the pellet was resuspended in 2 ml Sucrose/phosphate/glutamate buffer (SPG), aliquoted into appropriate volume and stored at -80°C until ready for use. The number of bacterial inclusion-forming units (IFU) of C. trachomatis was determined by infecting HeLa cell monolayer cultures as described previously [152,153].

2.1.2. Culturing and treatments of HEK-Blue-hTLR and Null cells:

HEK-Blue SEAP reporter cell lines Null1; Null2; hTLR2; hTLR3 or hTLR4 (Invivogen, San Deigo, CA) were grown in T75 flasks with DMEM high glucose media (Invitrogen) supplemented with 10% FCS(Invitrogen), 50 U/ml Penicillin, 50 ug/ml Streptomycin(Invitrogen) and selected with the appropriate antibiotic according to the manufacturer's instructions. Twelve hours prior to stimulation, 1x10^5/well (24 well plate) of HEK- Blue cells were plated. At ~50% confluency, cells were left untreated or stimulated with the following stimuli (unless otherwise noted): *C. trachomatis (LGV)* at MOI of 1; 2.0 ug/ ml of Poly I:C (pI:C); 5ug/ml Pam3SCK4, 0.5ug/ml ultra pure *E.coli* lipopolysaccharide (LPS) as indicated (Invivogen, San Deigo, CA). Supernatants were collected at the indicated times for the NF-κB activity assay. Whole cells were collected for RNA isolation or western blot.

2.1.3. Animals:

Lungs and femurs from six-eight weeks old wild type (WT) C57Bl/6 mice were kind gifts from Roy Hoglund (vivarium facility at the University of California, Merced), and the TRAIL-R knockout (KO) mice were provided by our collaborator Dr. Luis De La Maza, UC-Irvine as a kind gift from Dr. Winoto (University of California-Berkeley) [154] .

2.1.4. Isolation of bone marrow (BM) and differentiation of bone marrow derived macrophages (BMDM):

Briefly, femurs from two WT and KO mice were cleaned from tissues and briefly sterilized in 70% ethanol and then washed in PBS. Using RPMI media

(Invitrogen) with 1%FBS, bones were flushed with 25-gauge needle. The cells were then centrifuged at 1200 rpm for 5 min at 4°C. Red blood cells (RBC) were lysed by treating pellets with ACK (Invitrogen) on ice for 5 min. Then the cells were centrifuged again. $1x10^7$ bone marrow cells were resuspended in 10 ml BMDM media (RPMI-1640 supplemented with 15% FBS, 20ng/ml m-CSF (Sigma M9170), 100 U/ml penicillin and 100 µg/ml streptomycin) into100 mm tissue culture dish and incubated at 37°C and 5% CO2. 5 mls of fresh BMDM media were added on the third day and left to grow for another 4 days. Finally, the BMDM cells were harvested using trypsin and the cell populations were either re-plated in 12 well plate for the infection assays or analyzed by flow cytometery.

2.1.5. Isolation of primary lung fibroblasts:

Lungs were minced into very small pieces using scalpels and then were digested with 20 ml DMEM-F-12 media (invtirogen) supplemented with 1mg/ml of collagenase (Sigma-C1639) for two consecutive cycles of 30 minutes with gentle stirring. Suspension was passed through 70 uM nylon strainer (BD Falcon) to remove debris and washed twice in DMEM-F12 media supplemented with 15%FBS to remove traces of collagenase by spinning samples at 1200 rpm for 5 min at 4°C. Cells were resuspended in 10 ml DMEM-F12 +15%FBS and 1x antibiotic/antimycotic mix (invitrogen) into 100 mm culture dish and incubated at 37°C and 5% CO2. Using TrypLE-Express solution (Life Technologies), fibroblasts were maintained for two weeks by splitting cells and changing media when necessary to remove non-adherent cells. Fourteen days

post isolation, the primary lung fibroblasts were seeded into 12 well plates for infection assays.

2.1.6. Ex-vivo and in vitro cell culture and infection:

16-24 h prior to infection, $1x10^6$ of murine BMDM, $1x10^6$ murine lung fibroblast/ well of 12 well plate or $5x10^4$ cells/well of HeLa cells were plated on 24 well plate in antibiotic free culture media. The cells were grown to about 60% confluency, then were infected with either *C. trachomatis* **(**LGV/L2) or C. *muridarum* (MoPn) *as indicated at* MOI of 1.0 and incubated at 37 °C with 5% CO2. Twenty-four hpi, supernatants were then collected for ELISA analysis and the infected cells were lysed in RLT buffer for RNA isolation.

2.2. MOLECULAR BIOLOGY METHODS

2.2.1. Generation of transient siRNA knockdowns of HeLa Cells:

Transient reduction of SIGIRR and Triad3A was accomplished by transfecting the cells with gene-specific siRNA. Lipofectamine 2000 reagent was used to transfect HeLa cells following the manufacturer's instructions. Briefly, HeLa cells were plated 24 hrs prior to transfection so the cells would be 70% confluent at the time of transfection. Lipofectamine 2000 mixture was prepared in the appropriate amount of serum-free medium Opti-MEM. Cells were transfected with siRNA non-target control (Cell Signaling), SIGIRR-specific siRNA(NM_021805 oligo #1269132 for Seq A, and 1269134 for Seq B) or Triad3A-specific siRNA sequences (NM_021805 oligo #1305372 for Seq A, and 1305366 for SeqB, Sigma-Aldrich) and then were incubated at 37 °C with 5%

CO2 for 24 h. Cells then were detached by TrypLE-Express (Invitrogen), and plated to obtain 80% confluency after 18 h to be evaluated for the knockdown efficiency via qPCR or be treated with stimuli as indicated.

2.2.2. Generation of cells stably expressing shRNA:

$3x10^4$/well of HeLa cells were seeded in 96-well plates and then transduced, in the presence of 8ug/ml Polybrene for 48 hrs, with shRNA-SIGIRR (catalog number NM_021805), shRNA-TRAIL-R1 (catalog number NM_003844) or shRNA-Triad3A (catalog number NM_207111) specific lentiviral particles purchased from Sigma-Aldrich (catalog number NM_003842) at multiplicity of infection (MOI) of 1. Non-target shRNA control cells were also generated using an irrelevant sequence (Sigma, SHC002 V). Cells successfully transduced with lentiviral particles were selected by the addition of media containing 2.5 ug/ml puromycin (Sigma-Aldrich). Knockdown efficiency of each gene was verified by q-PCR analysis.

2.2.3. Transfection of Flag-Tagged-SIGIRR Plasmid:

$5x10^5$/well of HEK-Blue hTLR2 cells or $5x10^5$/well of HeLa cells were seeded on 6-wells (or 60 mm) plate and incubated at 37 °C with 5% CO2 until they reached 60% confluency. HEK-TLR2 cells were then transfected with SIGIRR-FLAG plasmids, at different concentration as indicated (0.1, 0.5, 1.0, 2.0 or 4.0 µg), using Lipofectamine 2000 reagent (Invitrogen) following the manufacturer's instructions. HeLa cells were transfected with 4ug of MyD88 HA and with either SIGIRR-FLAG plasmids or empty vector pCDNA3.1+ plasmids. Transfection media was changed 6 hours post transfection and the cells were

replated as needed and left to grow for total time of 48hrs. Cells then were infected with LGV/L2 at MOI of 1. Twenty-four hpi, supernatant were collected for ELISA assays and the cells were used for either qPCR or co-immunoprecipitation assays. The overexpression constructs for SIGIRR-FLAG was a kind gift from Dr.Li Xiaoxia at Cleveland Clinic Foundation, Ohio.

2.2.4. RNA isolation, reverse transcription and PCR (RT-PCR):

Total RNA was isolated from cells using the Qiagen RNeasy kit (Qiagen) following the manufacturer's instructions. The synthesis of the complementary DNA (cDNA) template was conducted according to the manufacturer's instruction (TaqMan, Roch). PCR was then performed using the primers listed in Table 1. The PCR was conducted using Qiagen Fast Cycling PCR Kit. PCR condition included an activation step of 95 °C for 5 min; followed by 35 cycles of 96 °C for 5 sec, 60 °C for 5 sec and 68 °C for 5 sec; followed by one cycle of 72 °C for 1 min. The PCR products were then separated by 2% agarose gel electrophoresis and visualized using ethidium bromide.

2.2.5. Quantitative real-time PCR (qPCR):

Total RNA and cDNA were generated as explained above. The q-PCR analysis was conducted in triplicates in a 20 ul final volume using Mx3000P (Stratagene, La Jolla, CA) with Brilliant III Ultra Fast STBR Green qPCR master mix (Stratagene). Negative controls include a no-RT control and no cDNA template control (H_2O alone). Real-time PCR included initial denaturation at 95

Table 2.1: List of Primers

	Gene	Forward (5'à3')	Reverse (5'à3')	Product Size	Accession #
Human	**SIGIRR**	TCAGTGGCTCTGAACTGCAC	GTACCAGAGCAGCACGTTGA	352	NM_021805.2
	TRAIL-R1	GGAGCCTGTAACCGGTGCACAG	CCTCTGGGGCACCCTCTGCT	214	NM_003844
	TRAIL-R2	AAGACCCTTGTGCTCGTTGT	CAGGTGGACACAATCCCTCT	145	NM_147187
	TRAIL-R3	CCTTGAAGCTGTGCCTCTGT	GGATCCCCAAGACCCTAAAG	141	NM_003841
	TRAIL-R4	GAGTCCTTTTCCGGCGGCGT	AAGGTGCTGATGTCAGCGGAGTCA	271	NM_003840
	TRIAD3A	CCTCAGAGATCACGACCCAAT	TGCCCCAGAATCAAACAATGG	159	NM_207111.3
	IL-8	AATCTGGCAACCCTAGTCTGCTA	AGAAACCAAGGCACAGTGGAA	64	NM_000584.3
	IL-6	CTGCAGCCACTGGTTCTGT	CCAGAGCTGTGCAGATGAGT	143	NM_000600.3
	GM-CSF	GTCTCACTCCTGGACTGGCT	ACTACAAGCAGCACTGCCCT	140	NM_000758.2
	IL-1A	ATTCAGCTCTCTGGGCTGTGATC	CATCACACAGGACTCCAGGTCATT		NM_002170.3
	IFN-B	CCAACAAGTGTCTCCTCCAAA	CCTCAGGGATGTCAAAGTTCA	185	NM_002176.2
	GAPDH	TTAAAAGCAGCCCTGGTGAC	CTCTGCTCCTCCTGTTCGAC	144	NM_002046.3
Mouse	**TRAIL-R**	CAGGCTGTCTTTGTTCCA	TCTTGCCAGGTTCCGTG	624	NM_020275.4
	MIP-2	GAGCTTGAGTGTGACGCCCCCAGG	GTTAGCCTTGCCTTTGTTCAGTATC	141	NM_009140.2
	IL-1B	CAACCAACAAGTGATATTCTCCATG	GATCCACACTCTCCAGCTGCA	152	NM_008361.3
	GAPDH	GAAGGTCGGTGTGAACGGATTTGGC	GATGGGCTTCCCGTTGATGACAAGC	211	NM_008084.2
Chlamydia	**C.Trach-16S R**	GGCGTATTTGGGCATCCGAGTAACG	TCAAATCCAGCGGGTATTAACCGCCT	315	

°C for 3 min, followed by 40 cycles of 95 °C for 5 s, 60 °C for 20 sec, and one cycle of 95 °C for 1 min, 55 °C for 30 s, 95 °C for 30 s. The average of the collected data was normalized to the activity of a house-keeping gene, GAPDH. For mouse BMDM and Lung fibroblast, the relative expression (ΔΔCt) was calculated using un-infected cells (WT or KO) as a baseline. For human samples, infected wild type HeLa cells were used as a baseline for the ΔΔCt calculation.

2.3. PROTEIN ANALYSIS

2.3.1. HEK-Blue NF-κB activity assay:

Collected supernatant from each sample was mixed at a ratio of 9:1 with QUANTI-Blue solution (Invivogen, San Deigo, CA) in a flat-bottom 96-well plate. The samples were incubated at 37°C for 2 hrs and then the secretion levels of Secreted Embryonic Alkaline Phosphatase (SEAP) were measured using a spectrophotometer at 630 nm.

2.3.2. Immunocytochemical Staining and Fluorescence Microscopy:

HeLa cells that were transfected with SIGIRR-FLAG construct, as described above, were plated on coverslips and then infected with LGV/L2 strain of C. trachomatis at an MOI of 1. Twenty-four hpi, cells were fixed with freezing cold methanol for 10 minutes then washed with 1xPBS after each step. The cells were then permeabilized with 0.1% of Tritonx100 in PBS for 15 minutes then blocked in 1% BSA for 30 minutes. Cells were then stained with primary antibodies of Mouse-anti-FLAG monoclonal antibody M2 at a ratio of 1:500

(Sigma) (or stained with Cy3 conjugated anti-FLAG monoclonal antibody M2) and goat anti-MyD88 (SantaCruz-8196) at a ratio of 1:50 for 1 h. The appropriate conjugated secondary antibodies were then used to stain the cells at a ratio of 1:100 for 30 minutes. The cells were then stained with Hoechst (and FITC-conjugated anti-*Chlamydia*l antibody, as indicated, (Argene, Massapequa, NY)) for 10 minutes. Finally, the cells were mounted on a glass slide, sealed with nail polish, and viewed with a Leica wide-field fluorescence microscope and the images were processed on ImageJ software (Version 1.440).

2.3.3. Co-immunoprecipitation:

Immunoprecipitation analysis of HeLa cells overexpressing MyD88-HA and with either SIGIRR-FLAG or empty vector proteins was conducted using FLAG Immunoprecipitation Kit (Sigma) following manufacturer's instructions. Briefly, supernatant from 60mm dish, LGV/L2 infected (or uninfected) HeLa cells that overexpressed SIGIRR-FLAG protein were removed and the cells were washed 3 times in 1x PBS. Performing all steps at 2–8°C, the cells from each plate were then lysed in 300ul lysis buffer (SIGMA), with 1x protease inhibitor cocktail, for 20 minutes on a shaker, and then the lysates were collected by centrifuging for 10 minutes at 12,000x g.

The cell lysates and positive control were then added to the thoroughly resuspended, washed and pre-cleared ANTI-FLAG M2 resin (lysate:resin ratio is 20:1) and were left overnight on a roller shaker. Samples were then collected via several rounds of centrifugation (8000x g) and washes in 1x wash buffer. To elute the samples, packed resins were boiled for 3 minutes in a 2x sample buffer

that did not contain any reducing agents. Samples then were centrifuged again, and the supernatants were then boiled again for 5 minutes in a 5x sample buffer that contained 2-mercaptoethanol. Samples were loaded on SDS-PAGE gel and immunoblotted using rabbit anti-SIGIRR (abcam), Mouse-anti-MyD88 (Millipore) or mouse anti-FLAG M2 (Sigma) antibodies.

2.3.4. Western Blot:

Samples were treated as described above in 12 well-plate and collected 24 hpi. Monolayers were washed twice with ice-cold phosphate-buffered saline and lysed in 150 ul ice-cold lysis buffer (1% Nonidet P-40, 50 mM Tris-HCL, pH 8.0, 150 mMNaCl, 10% glycerol, 1 mM EDTA, 1 mM DTT, 2 mM PMSF, 1 mM sodium orthovanadate and 1× protease inhibitor cocktail from Roche) for 30 minutes in 4 °C, and then protein lysates were collected at 10,000*x g* and stored at −20 °C. Concentrations of proteins were measured using a Bradford protein assay (Bio-Rad). Equal amounts of proteins were used (30ug) and boiled in 5× SDS loading buffer (250 mM Tris-HCl, pH 6.8, 500 mM DTT, 10% sodium dodecylsulfate, 0.5% bromophenol blue, 50% Glycerol and 12% 2-Mercaptoethanol).

Samples were ran through 12% SDS-PAGE gel and proteins were transferred to PVDF membranes (Millipore). The membranes were blocked with 5% BSA (sigma) in Tris-buffered saline containing 0.05% Tween 20. Membrane was incubated with 1:1000 P-AKT primary antibodies (Cell Signaling), 1:100 rabbit anti-SIGIRR (abcam), 1:200 mouse anti-MyD88 (Millipore); 1:1000 mouse anti-FLAG M2 (sigma); 1;1000 or mouse-anti-HA (Invivogen) overnight and in the

appropriate secondary HRP-conjugated antibodies (1:1000). The protein of interest was visualized by adding ECL Plus Western blotting detection reagents (Millipore) following manufacturer's instructions. Images of the bands and their intensity were detected and measured using a Gel Doc system (Bio-Rad).

2.3.5. Flow Cytometery:

Seven days post-isolation, collected BMDM cells were washed in 1xPBS and centrifuged at 1,200 rpm for 5 minutes at 4°C. FcBlock was added to the cells and incubated for 10 minutes on 4°C fridge before adding BMDM specific markers, anti-mouse CD11b-PE *and* F4/80-APC *(*eBiosciences*)* at a ratio of 1:100. Thirty minutes later, BMDM cells were washed with 1x PBS and centrifuged *at* 1200 rpm for 5 min at 4°C*.* Samples were then resuspended in 300 µl of 0.1 µg/ml propidium iodide (PI). Samples were analyzed using a BD LSRII flow cytometer and the data analysis was performed using FlowJo software (version 7.6.1, TreeStar*).*

2.3.6. Mouse IL-1β ELISA:

Mouse IL-1β ELISA Kit (eBioscience Cat# 88-7013-76) was used according to the manufacturer's instructions. Initially, 96 well plate was coated with capture antibody and incubated overnight at 4°C. Plates were blocked with 1x assay diluent for 1 hour at room temperature. Then, 100 µl of the 2 fold-serial diluted standards and samples were loaded in duplicate and incubated overnight at 4°C. Detection antibody was added to the plate and incubated for 1 hour at room temperature. The plate was incubated in100 µl of diluted Avidin-HRP for 30 minutes at room temperature. Then, the substrate solution was added and the

plate was incubated for 15 minutes at room temperature before adding the Stop Solution 2 N H2SO4). The absorbance was measured immediately at 450 nm and corrected by subtracting the values from the 570 nm reading. The plate was washed five times with wash buffer (0.05% Tween20 in PBS, pH 7.2) after each step and 7 times before adding the substrate. A standard curve was established by a 2-fold serial dilution of recombinant mouse IL-1β as a reference for quantification (1000 pg/mL- 8 pg/ml).

2.3.7. Human IL-8 ELISA:

Human CXCL8/IL-8 cytokine ELISA kit (R&D Systems, DY208) was used according to manufacturer's instruction. Briefly, capture antibody in PBS was coated on a 96Wells microplates for 16 hrs at room temperature. Plate was blocked (1% BSA, in PBS with 0.05% NaN3) for 1 hr at room temperature, and then samples were loaded in duplicates and incubated for 2 hrs at room temperature. Plate was incubated with the detection antibody diluted in reagent diluent (0.1% BSA,5 0.05% Tween 20 in Tris-buffered Saline (20 mM Trizma base, 150 mM NaCl), pH 7.2) for 2 hrs at room temperature. Streptavidin-HRP was added and the plate was incubated for 20 min in the dark at room temperature. The substrate solution (R&D Systems Catalog # DY999) was then added for 20 min and stopped with Stop Solution (2 N H2SO4). The absorbance at 450 nm was measured with correction at 540 nm using ELISA plate reader. The plate was washed three times with wash buffer (0.05% Tween_ 20 in PBS, pH 7.2) after each step. A standard curve was established by a 2-fold serial dilution of recombinant human IL-8 as a reference for quantification (2000 pg/mL-

8 pg/ml).

2.4. STATISTICAL ANALYSIS

The statistical significance was evaluated using GraphPad Instat software (GraphPad Software Inc, La Jolla, CA) by unpaired Student's **t**-test. A value of $p < 0.05$ was considered significant. Data presented in each figure as the cumulative result of at least 3 times, unless stated otherwise.

CHAPTER 3

The Role Of Single Ig IL-1 Receptor (IL-R)-Related Receptor (SIGIRR) During *C. trachomatis* Infection

3.1 INTRODUCTION:

Single Ig IL-1 receptor (IL-R)-related molecule (SIGIRR), also known as toll interleukin-1 receptor (IL-1R) 8 (TIR8), is a member of the Toll/IL-1 receptor (TIR) superfamily that includes TLRs and ILRs subfamilies. Unlike the ILRs members that contain three Ig domains, SIGIRR has a single domain in the extracellular region, with no known ligand, and a TIR domain in the cytoplasmic side of the cell. It is highly expressed in the tissues of the digestive tract, dendritic cells, various organs, epithelial cells lines and various immune cells, but not in the bone marrow derived macrophages [124,155-157]. Disregulation of the expression level of SIGIRR has been associated with some diseases and abnormalities in the development of some cells[156,158,159].

Current knowledge of the role of SIGIRR has been mostly obtained from studies of SIGIRR deficient mice. Overall, these studies have shown that SIGIRR deficiency mediates kidney graft rejection, enhances the development of colitis-associated cancer (CAC) and intestinal inflammation, increases susceptibility to lupus and bacterial/fungal infections[155,156,160-163]. The immune responses in these SIGIRR deficient mice were associated with induced expression of

proinflammatory agents, elevated infiltration of PMNs and observed damage to the tissues. On the other hand, reports on the effect of stimulation of the immune system on the expression levels of SIGIRR mRNA have been conflicting. For example, stimulation of the immune system with LPS or a pathogen reduces the mRNA and protein levels of SIGIRR in mice[164]. However, another group has reported an opposite observation on monocytes during sepsis or sterile inflammation, where the expression of SIGIRR is greatly increased [165].

SIGIRR does not associate with NF-κB directly, but it triggers an inhibitory effect through its interaction with other adaptors via TIR domain [164]. Stimulated lymphocytes and liver cell lines that are overexpressing SIGIRR have higher levels of NF-κB activity compared to unstimulated cells[155]. Two reports by Huang *et al.* and Rodriguez *et al.* show that resistance against *P. aeruginosa* infection of lung and cornea is mediated by SIGIRR[164,166]. The neutralization of SIGIRR protein with anti-SIGIRR antibody resulted in increased damage to the host cells, higher titer of the bacteria and increased levels of proinflammatory cytokines in response to *P. aeruginosa* infection. Moreover, it was clearly demonstrated that the inhibitory effect of SIGIRR is dose-dependent since the stimulation of IL-1R1 and TLR4, but not TLR3, reduces NF-κB activity as the expression level of SIGIRR increases[164]. Even though this report indicates that SIGIRR exerts its inhibitory effect through MyD88-dependent pathways, other reports have shown that SIGIRR's inhibition of TLR3 signaling might be cell-type specific[155,157,164].

In addition to TLR3 and 4, SIGIRR negatively regulates the signaling pathways of TLR2, 5, 7, and 9 in various tissues[155,167-169]. The inhibitory

mechanism that SIGIRR exerts on TLR signaling reveals that TIR domain, but not the extracellular Ig domain, is necessary to interfere with the recruitment of other adaptors to the TLRs[167]. Beside its self-dimerization, SIGIRR also interacts strongly with IL-1R as well as other signaling molecules such as MyD88, IRAK and TRAF6[124,167,168]. Studies of immature dendritic cells, which express high level of SIGIRR, indicate that association of MyD88 with SIGIRR through the TIR domain is constitutive and necessary to remain immature [170]. Disruption of this connection or the decrease of SIGIRR's expression, leads to the maturation of the dendritic cells and enhances the immune response[160,170]. In addition to MyD88, Qin and colleagues reported that SIGIRR interferes with the recruitments of IRAK1 and 4 as well as TRAF6, to stimulated IL-1R[171].

SIGIRR's variable effects appear to be dependent on its expression levels observed in various tissues and cell type. The ability of SIGIRR to interact with various components of the TLR signaling pathways in a way that influences the immune response of various epithelial cells during bacterial infection indicates its importance as a negative regulator. The aim of our study was to investigate the role of SIGIRR's activity on the complications caused by *C. trachomatis* infection and whether SIGIRR's interaction with components of the TLR signaling pathways may explain the mechanism by which it negatively regulates inflammation.

3.2. RESULTS

3.2.1. SIGIRR expression during infection:

It is necessary to evaluate first the presence of SIGIRR in various cell lines that are commonly used for immunological studies since the mRNA level is subject to variation depending on the expression profile of a given cell. Here, we first examined via PCR the presence of SIGIRR in the human cervical carcinoma cell line (HeLa), Human Embryonic Kidney 293 (HEK293), the human acute monocytic leukemia cell line (THP1) and the modified HEK293 cells that are expressing human TLR2, TLR3 or TLR4. As shown in Figure 3.1A, high levels of SIGIRR were detected in HeLa and THP-1, but slightly reduced level in HEK293. In contrast, all modified HEK-Blue cells with hTLR2, 3 and 4 did not express any detectable levels of SIGIRR mRNA.

HeLa cells are the most physiologically relevant cell line in which investigate *Chlamydia* infection since they are isolated from human genital tract. In order to determine the effect of *C. trachomatis* on the expression of SIGIRR, the level of SIGIRR mRNA in *C. trachomatis* infected HeLa cells was measured over five different time points (0, 3, 6, 12 and 24 hours). Real-time PCR analysis of the expression level shows that SIGIRR is induced as early as 3 hpi (Figure 3.1B). However, the expression level of SIGIRR was declining for the next nine hours before it start increasing back to reach its base level at 24 hpi. Variation between replicates were extreme and affected the statistical significance calculation, however, the expression patterns of SIGIRR were similar across all

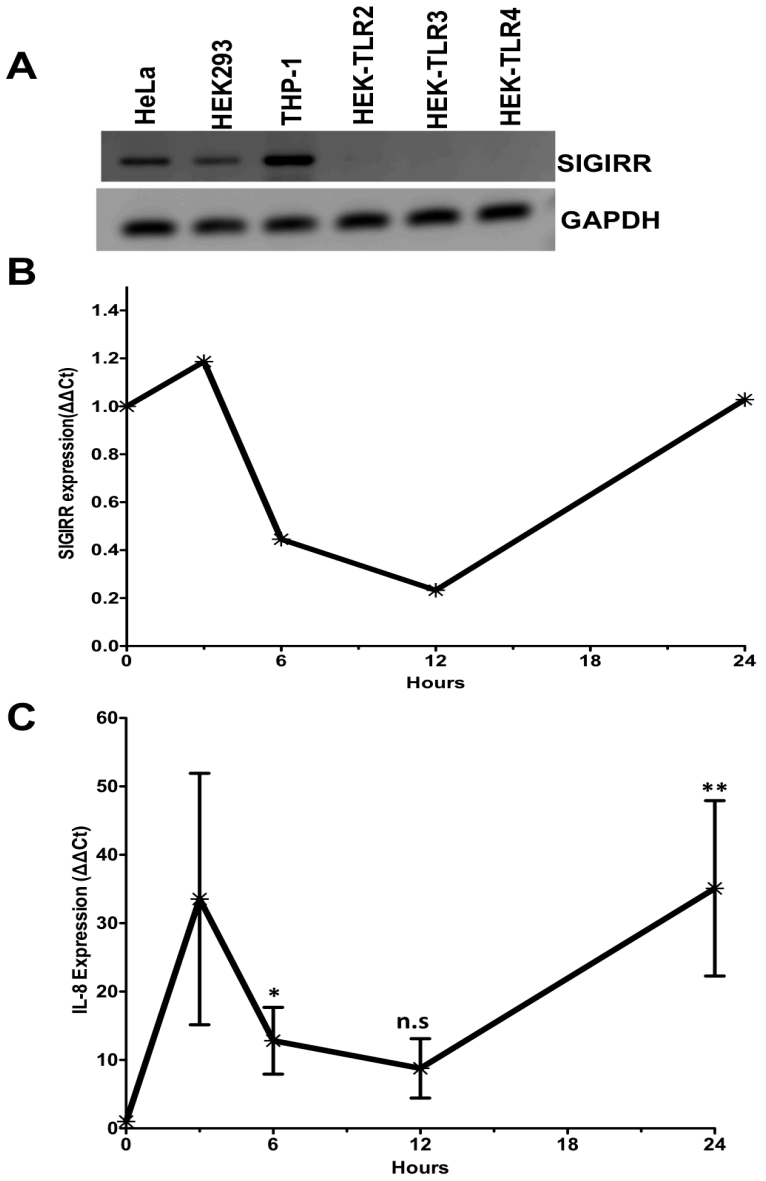

Figure 3.1: Expression of SIGIRR and IL-8 fluctuates overtime in response to C. trachomatis infection. **(A)** PCR analysis of SIGIRR in various human cell lines. Cervical epithelial HeLa cells,HEK293 and THP-1 cells express SIGIRR, while HEK-Blue-TLR2, 3 and 4 do not. **(B&C)** HeLa cells were infected with C. trachomatis serovar L2 (MOI of 1) at the indicated time. The mRNA levels of SIGIRR and IL-8 were measure via qPCR. Ct values are normalized to GAPDH and relative expression (ΔΔCt) is calculated compared to non-infected cells (0HR) **(B)** A representative data of the expression level of SIGIRR. *Chlamydia* infection the expression of SIGIRR 3hpi. Expression level fluctuates over time until it reaches its highest level at 36hpi. **(C)** Three hours post LGV/L2 infection of HeLa cells significantly induces the expression level of IL-8. The expression declines for the next 9 hours and increases again by 24hrs before reaching its highest levels at 36hpi. Data for IL-8 expression collected from 4 independent experiments. Error bars on **B** were not added due to the great variations between the replicates. Error bars represent ±SD, and the statistical significant analysis was conducted by comparing each data point to its preceding time point using Student's t test. n.s (not significant), *$p < 0.05$, **$p < 0.01$.

the replicates. In the meantime, the expression of the proinflammatory IL-8 was significantly induced in response to infection 3 hpi (Figure 3.1C). Levels of IL-8 were significantly reduced at 6 and 12 hpi compared to the 3 hours time point. Twenty-four hpi, the expression of IL-8 was as high as the level observed at early point at 3 hpi. Measuring the significant changes of IL-8 expression between each time point, as shown in Figure 3.1C, the statistical significant analysis for the expression of IL-8 was calculated by comparing each data point to its preceding time point. With the exception of the measurement at 12 hpi, the expression level of IL-8 significantly changed at each time point.

3.2.2. Reduced level of SIGIRR induces higher mRNA of IL-8.

To investigate the role of SIGIRR in *Chlamydia* infected cells, HeLa cells were transfected with SIGIRR specific siRNA. Real-time PCR analysis of the efficiency of the transfection indicated that there was no significant difference of the expression levels of SIGIRR in HeLa cells treated with Lipofectamine only (Lipo Cont) or siRNA non-target control (siRNA CONT) compared to the wild type (WT) cells (Figure 3.2A). However, both SIGIRR-siRNA specific sequences (sequence A or B) reduced the mRNA level by 40 and 80%, respectively, relative to the untransfected WT cells (Figure 3.2A).

Next, the effect of SIGIRR on *Chlamydia*-infected cells was tested. Real-time PCR analysis of HeLa cells infected with *C. trachomatis* revealed thae expression level of IL-8 was higher in cells that have reduced levels of SIGIRR

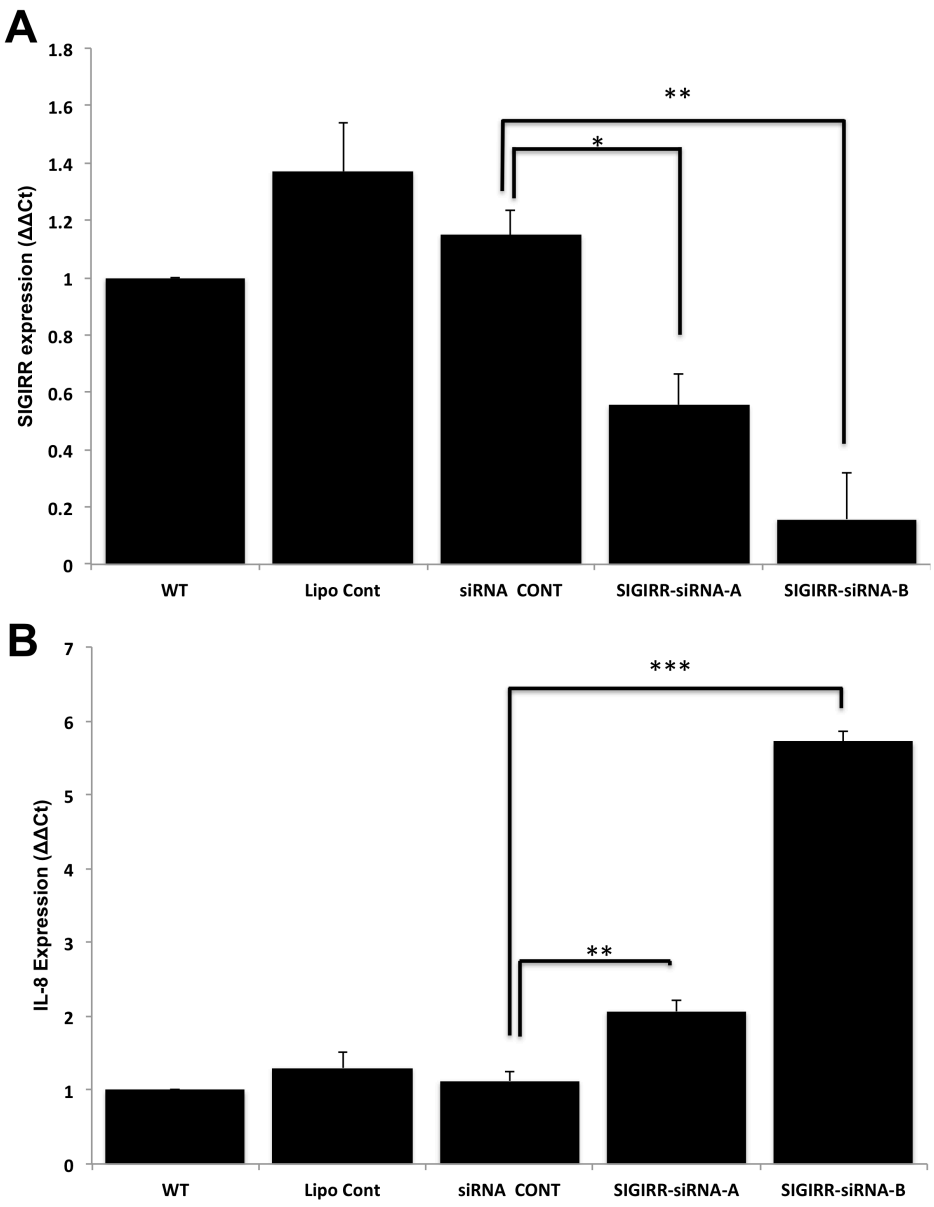

Figure 3.2: Transient silencing of SIGIRR in HeLa cells induces higher levels of IL-8. (A) Using Lipofectamine 2000 transfection reagent, HeLa cells were transfected with siRNA non-target control (siRNA CONT); SIGIRR-siRNA (sequence A or B); Lipofectamine treated (Lipo Cont) or untreated wild type (WT). Relative expression level of SIGIRR compared to WT was reduced by 40 to 80% in SIGIRR-siRNA A and B respectively. (B) 24 hpi, IL-8 expression in C. trachomatis serovar L2 infected HeLa cells, at MOI of 1, shows higher levels of the proinflammatory cytokines in the cells that are expressing lower level of SIGIRR compared to WT infected cells. The increase of IL-8 expression inversely correlates with the expression levels of SIGIRR as shown in part A. Data are collected from 4 independent experiments. Error bars represent ±SD, and Student's t test was conducted. n.s (not significant), (*$p < 0.05$, **$p < 0.01$, , ***$p < 0.001$.

compared to the WT infected HeLa cells (Figure 3.2B). Both siRNA sequences used (SIGIRR-siRNA-A and B) had 2-6 fold increase of IL-8, respectively, which inversely associated with the reduced levels of SIGIRR that have been observed in Figure 3.2A. No significant differences were detected in the two control groups. This data suggests that SIGIRR is involved in reducing the immune response against *C. trachomatis* infection.

3.2.3. SIGIRR distribution and localization in infected cells

Distribution of SIGIRR around the cell under normal circumstances or during *Chlamydia* infection was tested through immunofluorescent staining. Transiently transfected HeLa cells with 2.0ug of SIGIRR-FLAG construct were either left untreated or infected with *C. trachomatis*. SIGIRR localization was not limited to the cell membrane, but we show here that it was also distributed around the cytoplasm of non-infected cells, with slightly higher concentration toward the outer sides of the cells (Figure3.3A, top panel). On the other hand, SIGIRR localization in *Chlamydia* infected HeLa cells was concentrated around the nucleus of the HeLa cells and the inclusion of the bacteria (Figure 3.3A middle).

Next, we questioned whether SIGIRR co-localizes with different components of the TLR signaling pathways during *Chlamydia* infection. MyD88 adaptor protein is the likely candidate to interact with SIGIRR through the TIR domain[124]. HeLa cells transfected with SIGIRR-FLAG construct were stained with Cy3-conjugated anti-FLAG antibody (red) and anti-MyD88 antibody (green).

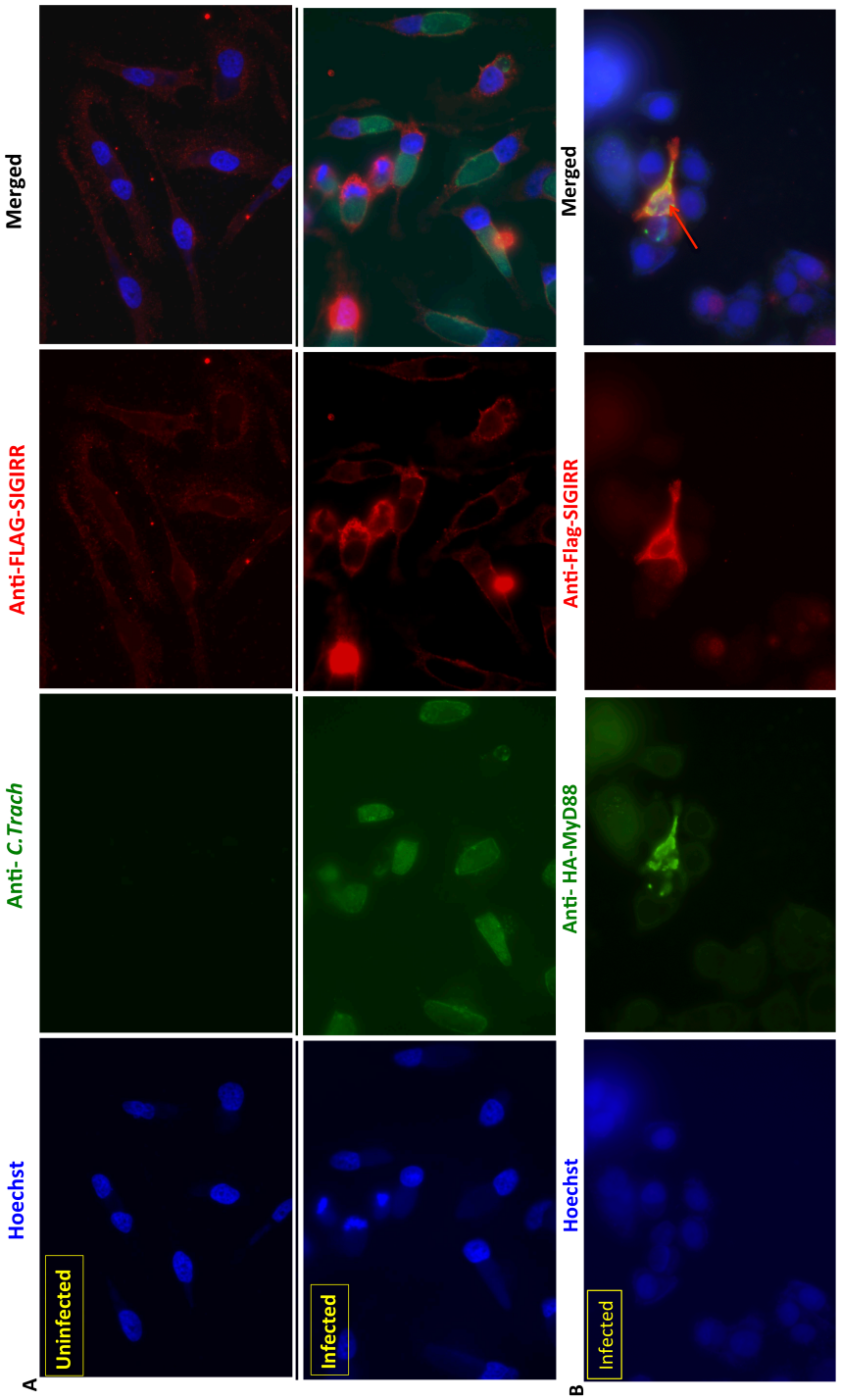

Figure 3.3: SIGIRR and MyD88 localization in *C. trachomatis* infected cells. HeLa cells were transiently transfected with SIGIRR-FLAG construct alone (A) or with MyD88-HA construct (B). Forty-eight hrs post transfection, cells were grown on coverslips and left untreated or infected with C. trachomatis serovar L2, MOI of 1 for 24 hrs. Fixed cells stained with Hoechst stain (blue), Cy3-conjugated anti-FLAG antibody (red), and anti-*Chlamydia* or anti-HA antibody (green) and visualized on a fluorescence microscope. **A)** SIGIRR localizes on the surface and around the cytoplasm of uninfected cells (top panel). In *Chlamydia* infected cells, SIGIRR localizes around the bacterial inclusion and the nucleus of the host cells (middle panel). **B)** SIGIRR and MyD88 co-localizes around *Chlamydia* inclusion (red arrow)2.

Both SIGIRR and MyD88 were distributed around the nucleus of the uninfected HeLa cells *Chlamydia* infection of the HeLa cells redistributed both SIGIRR and MyD88 to co-localize around the inclusion of the bacteria (Figure 3.3A bottom).

3.2.4. SIGIRR association with MyD88

Since localization of SIGIRR with MyD88 has been shown here and elsewhere, we further investigated whether SIGIRR can physically associate with MyD88 during *Chlamydia*-infection [124]. HeLa cells transfected with 4.0 ug of MyD88-HA along with 4.0 ug of SIGIRR-FLAG, or 4.0 ug of pCDNA3.1+ empty vector were either left uninfected or infected with *C. trachomatis*. Immunoblotting of the immunoprecipitated cell lysate showed that immunoprecipitation of SIGIRR-FLAG has been successful and specific since transfection with empty vector did not have a signal for SIGIRR (Figure 3.4 top panel-left). However, co-immunoprecipitation results also showed that MyD88 was associated with SIGIRR regardless of *Chlamydia* infection (Figure 3.4 top panel-right). Interestingly, infected samples show increased intensity of the MyD88 band compared to non-infected samples indicating *Chlamydia* infection increases the association between MyD88 and SIGIRR. Cell lysate from all the samples successfully express MyD88-HA (Figure 3.4 bottom panel).

3.2.5. SIGIRR overexpression reduces the mRNA level of IL-8

Since our data from Figure 3.2B showed that SIGIRR deficiency induces the expression of IL-8, we next examined the impact of SIGIRR overexpression

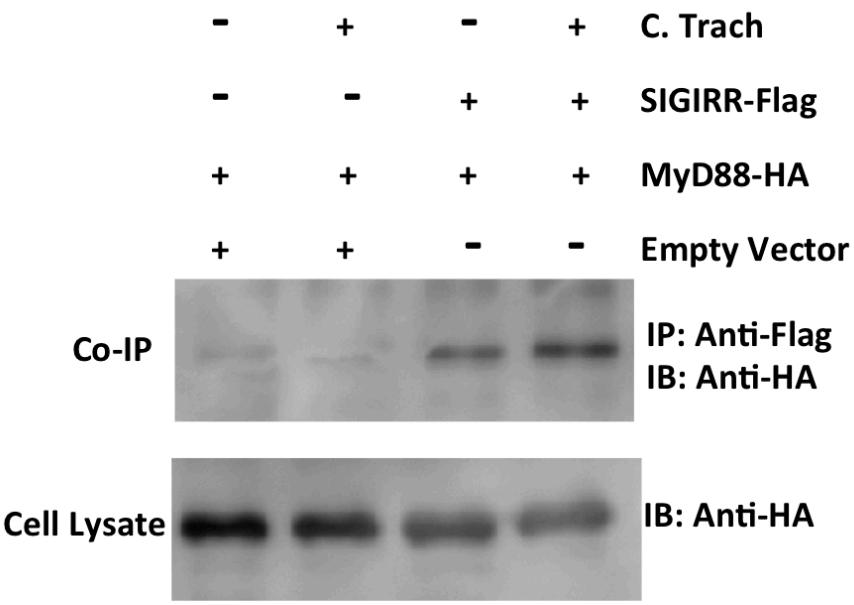

Figure 3.4: SIGIRR associates with MyD88. HeLa cells on 60mm tissue-culture dish were transfected with 4.0 ug of MyD88-HA and with either SIGIRR-FLAG construct or mock-transfected with 4.0 ug of pCDNA3.1+ empty vector as described before. Forty-eight 48 hours post transfection, cells were either left uninfected or infected with LGV/L2 as indicated. Seventy-two hours post transfection, cells were lysed in lysis buffer and immunoprecipitated using FLAG Immunoprecipitation Kit (IP) . Samples were loaded into SDS-PAGE gel and immunoblotted (IB) using anti-FLAG M2 or anti-HA. Bothe L2 infected or uninfected HeLa cells shows an association of MYD88 with SIGIRR.

on *Chlamydia* infected cells. Unlike HEK- 293 cells, HEK-Blue-hTLR2 cells are ideal for the overexpression experiment since they constantly express TLR2, have no endogenous SIGIRR, and provides rapid measurement of NF-κB activities (Figure 3.1A). HEK-Blue-hTLR2 cells transiently transfected, or mock-transfected, with 0.1 ug and 1.0 ug of SIGIRR-FLAG construct or pCDNA3.1+ empty vector. Real-time PCR showed that the level of SIGIRR mRNA in the transfected cells was proportional to the amount of plasmid DNA introduced to the cells, while cells transfected with the empty vector had undetectable level of SIGIRR as expected (Figure 3.5A). Infecting the cells with *C. trachomatis* induced IL-8 expression in both SIGIRR-FLAG and empty vectors transfected cells (Figure 3.5B). However, HEK-Blue-hTLR2 cells that expressed lower level of SIGIRR, 0.1 ug, showed slightly reduced, but statistically significant, levels of IL-8 compared to the cells that were not expressing SIGIRR (Figure 3.5B, left).

On the other hand, cells transfected with higher level of the SIGIRR-FLAG construct have also showed reduced, but statistically insignificant, level of IL-8 mRNA. To evaluate whether the reduction of IL-8 in SIGIRR expressing cells would also impact the secretion of the cytokine, we tested the level of IL-8 in the supernatant of *Chlamydia* infected HEK-Blue-hTLR2 via ELISA. As shown in Figure 3.5C, both SIGIRR-FLAG and empty vector transfected cells secreted high levels of the cytokine with no significant difference being observed between the two groups of variable concentrations of the plasmids (concentrations of IL-8 from all groups reached the higher end of the kit's maximum level).

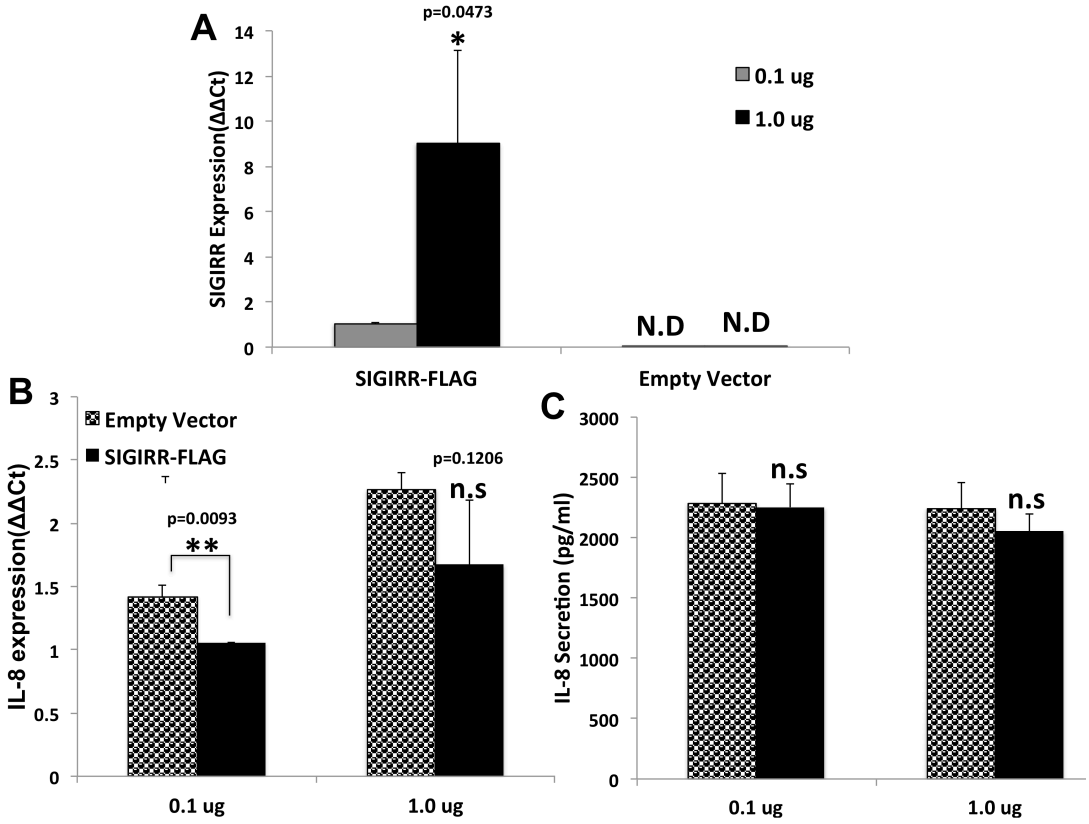

Figure 3.5: Overexpression of SIGIRR slightly reduces the expression level, but not the secretions, of IL-8. HEK-Blue-hTLR2 cells transiently transfected, or mock-transfected, with 0.1 ug and 1.0 ug of SIGIRR-FLAG construct or pCDNA3.1+ empty vector using Lipofectamine reagents. (A) The expression of SIGIRR in HEK-Blue hTLR2 cells was detected only in SIGIRR-FLAG trnasfected cells. The expression levels of SIGIRR mRNA was proportional to the level of the plasmid DNA introduced to the cells. (B) Both mock-cells and SIGIRR-FLAG infected with C. trachomatis serovar L2 strain at m.o.i of 1 for 24 hrs. The mRNA expression level of IL-8 was reduced in cell transfected with SIGIRR-FLAG construct compared to the empty vector. This reduction was statically significant only at the lower concentration of SIGIRR (0.1 ug). (C) ELISA analysis of supernatant of chlamydia infected HEK-Blue-hTLR2 cells had similar levels of IL-8 secretion for both groups that are transfected with SIGIRR-FLAG vector or the empty vector. Data are collected from at least 3 independent experiments. Error bars represent ±SD, and Student's t test was conducted. N.D (not detected), n.s (not significant), *$p < 0.05$, **$p < 0.01$.

3.3. DISCUSSION:

3.3.1. Function of SIGIRR during *Chlamydia* infection

As a member of the Toll/IL-1 receptor superfamily that plays a major role in activating the innate immune system, an orphan receptor like SIGIRR is expected to function as a regulator of these pathways. Indeed, studies have shown that manipulation of SIGIRR affected the activities of various signals that are associated with induced immune response [156,158,159]. Therefore, we hypothesized that SIGIRR may negatively regulate the TLR signaling pathways during *C. trachomatis* infection.

SIGIRR expression in various human and murine tissues has been reported [124,164]. Our data shows that the humans cell lines HeLa, HEK293 and THP1 all express SIGIRR. Unexpectedly, SIGIRR mRNA was completely absent in the modified HEK cells that express hTLRs. Since the stimulation of the immune system affects SIGIRR expression in different ways depending on the stimulus and the type of cells, we first measured the levels of SIGIRR during *Chlamydia* infection at various time points [164,165]. The decreased level of SIGIRR at 6 and 12 hpi before returning to its base level 24 hpi indicates its involvement during the early stages of *Chlamydia* infection, which correlates with similar findings for other pathogens by other reports [164,172]. Production of proinflammatory cytokines is a crucial mechanism by which infected cells modulate inflammation. Since it is considered as one of the early markers of bacterial infection, including *Chlamydia*, our study focused on the expression and

the secretion levels of IL-8 cytokine during *Chlamydia* infection [42,173]. We observed that *Chlamydia* infection of HeLa cells induces IL-8 expression as early as 3 hpi before declining at 6 and 12 hpi (Figure 3.1C). Since it has been shown that the induction of IL-8 as a result of NF-κB activation by *Chlamydia trachomatis* infection does not take place until 15 hpi, we believe that the early induction of IL-8, followed by a reduction, was not directly related to NF-κB activities [42]. Instead, we believe this early increase of IL-8 is caused by the entry of the EBs of *Chlamydia trachomatis* to the cells, a phenomena that has been reported for other stimuli [42,174,175]. Therefore, the correlation between SIGIRR and IL-8 expression seen in Figure 3.1B and C in the early stages of the infection is not related to SIGIRR's effect on TLR signaling. However, since the expression of SIGIRR returns to its base level by the time RBs start transforming into EBs, we predict that SIGIRR up-regulation takes place as a results of EBs' presence.

The goal of this study was to determine if SIGIRR functions as a down-regulator of the innate immune system in response to *Chlamydia* infection. siRNA knockdown of SIGIRR indicated that SIGIRR is a down-regulator during *Chlamydia* infection as the IL-8 expression is elevated in the absence of SIGIRR. This increase of IL-8 level when SIGIRR level is being reduced seems to contradict the observed correlation between SIGIRR and IL-8 24 hpi, as seen in Figure 3.1 B and C. However, it is clear that the level of SIGIRR in Figure 3.1B, 24 hpi, was similar to the expression level observed in the non-infected cells, while IL-8 expression for the same time point was 30 fold higher than non-infected cells. Hence, we predict that the increase of SIGIRR at later stages of

the infection is part of its temporal and spatial dynamics to reduce the immune response against *Chlamydia.* Therefore, when the level of SIGIRR is reduced as seen in Figure 3.2, the expression of IL-8 is greatly increased compared to the infected control groups. The literature limits SIGIRR distribution to the cell membrane, however, SIGIRR on the non-infected cells appears to be localized around the cytoplasm as well. Immunocytochemistry showed that during infection, SIGIRR localizes around the nucleus of the infected cells as well as around the *Chlamydia* inclusion. Unlike other pathogens that have been used to investigate SIGIRR's role in regulating the immune response, this is the only report that shows localization of SIGIRR protein around the pathogen inside the cell [164,172].

A report by O'Connell *et al.* showed that TLR2 and MyD88 co-localize around *C. trachomatis* inclusion of the infected cells [176]. Since SIGIRR has been shown to interact with MyD88 and based on our observation that SIGIRR localizes around the inclusion, we sought to investigate whether both SIGIRR and MyD88 co-localize around the inclusion of *C. trachomatis.* Our results show that SIGIRR indeed co-localizes with MyD88 around the inclusion of infected HeLa cells. Co-immunoprecipitation studies confirmed a specific association between SIGIRR and MyD88 in both infected and non-infected HeLa cells.

SIGIRR's role as a negative regulator was confirmed by an overexpression of the protein and observing its effect on the production of proinflammatory cytokines. Since the knockdown analysis of SIGIRR induced higher level of IL-8 expression during infection, we expected that SIGIRR

overexpression will result in a lower level of IL-8. Certainly, the level of IL-8 expression in *C. trachomatis*-infected HEK-blue-hTLR2 cells that are overexpressed lower levels of SIGIRR (0.1 ug) were significantly lower than the level observed in mock-transfected cells. However, due to the toxicity of the transfection with higher levels of plasmids (1.0 ug) on HEK-blue-hTLR2, there was no significant difference on the expression level of IL-8 compared to mock-transfected cells (Figure 3.5B). However, the secretion levels of IL-8 in response to *Chlamydia* infection did not show any significant difference between the cells overexpressing SIGIRR, both 0.1 and 1.0 ug, and the ones that maintain normal level of the endogenous protein of mock-transfected cells (Figure 3.5C). Once again, the toxicity effect of the transfection process on these cells greatly increased the secretion of IL-8 regardless of the treatment and we cannot predict the effect of SIGIRR's overexpression on the secretion of IL-8.

Our in *vitro* findings correlate with the preliminary *in vivo* results collected by our collaborator at UC Irvine. In these experiments, mice that were intra-nasally challenged with MoPn strain showed that SIGIRR KO mice lost less body weight, and at a slower rate, than the WT C57BL/6 mice 10 dpi. Additionally, the number of MoPn inclusion forming units (IFU) recovered from the lungs of SIGIRR KO mice was greatly less than those recovered from the WT mice. Preliminary analysis of human SNPs provided the promising results that indicate significant correlation in the SIGIRR gene (G allele) with reduced risk of both infection and tubal pathology in women.

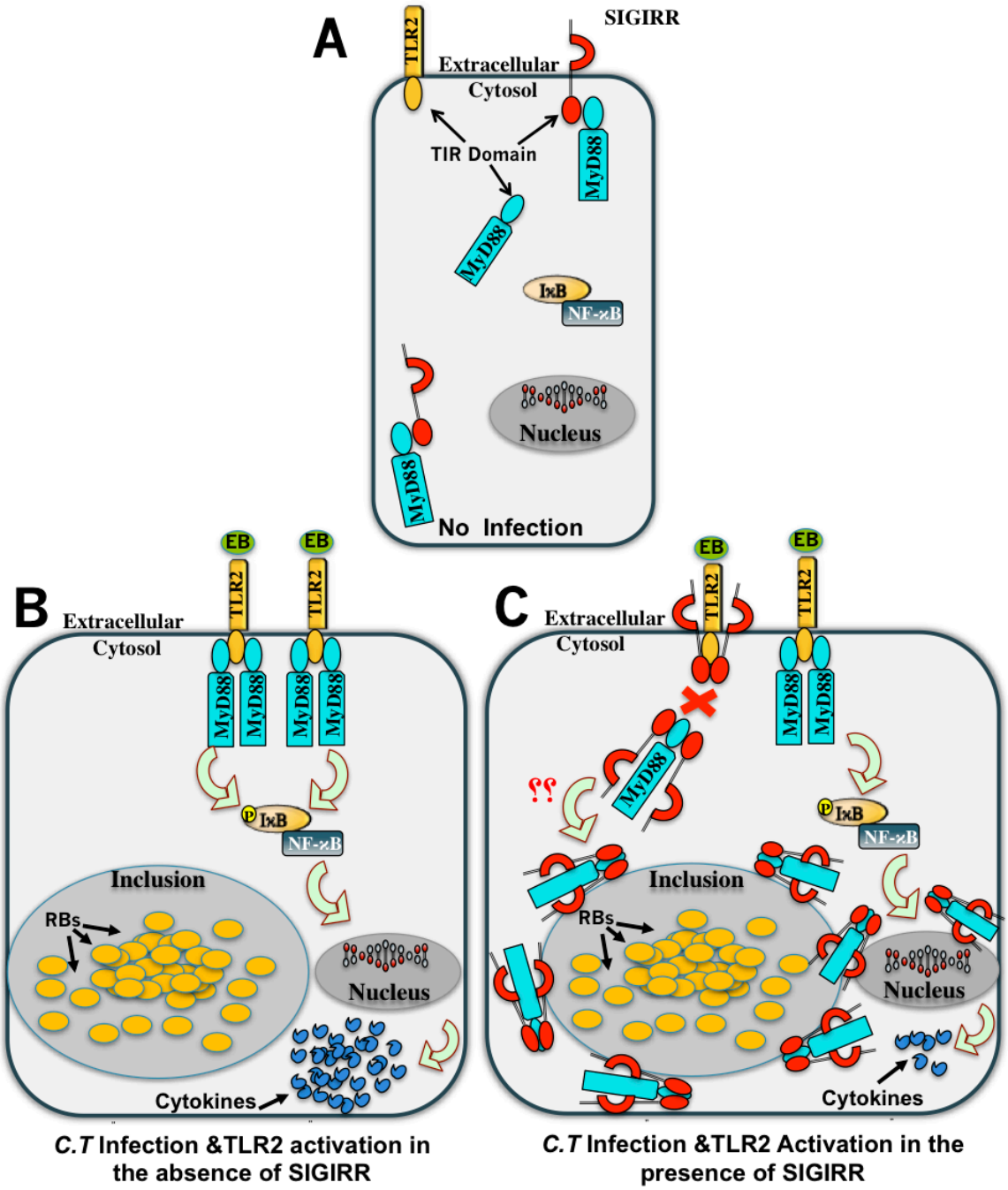

Figure 3.6: SIGIRR down-regulation model: A) SIGIRR localizes in the membrane and the cytosol and associates with MyD88 in un-infected cells. **B)** *C. trachomatis* (*C.T*) infected cells induces higher levels of pro-inflammatory cytokines in the absence of SIGIRR. **C)** Presence of SIGIRR blocks TLR2 activation by binding to the TIR domain of MyD88. Both MyD88 and SIGIRR localizes around the nucleus and *C.T* inclusion of the infected cells.

In summary, our in *vitro, in vivo* and SNPs data suggest that SIGIRR is a negative regulator of the immune response induced by *C. trachomatis* infection. The changes of IL-8 levels, body weight and IFU in the absence of SIGIRR as well as the reduced risk of infection all support the notion that SIGIRR influences the immune response. These data also shows that SIGIRR localizes with pathogens inside the cells and that MyD88's physically association with SIGIRR during *Chlamydia* infection partially explains the mechanism that SIGIRR utilizes to exert its inhibitory effect on the immune system.

CHAPTER 4

Triad3A Role During *Chlamydia trachomatis* Infection

4.1. INTRODUCTION:

The Two RING fingers and DRIL protein, Triad3A:

The two RING fingers and DRIL proteins, TRIADs, were first identified by Van Der Reijden and colleagues as conserved cysteine-rich zinc-binding domain that is flanked by two RING finger structures known as double RING finger-linked (DRIL) domain[177]. Triad3, also known as zinc-finger protein inhibiting NF-κB (ZIN), has been identified as an E3 ubiquitin –protein ligase that promotes Lys-48 linked ubiquitination[69,178]. The use of the yeast two-hybrid system by the Chuang group indicated that Triad3 interacts with the cytoplasmic domain of TLR3, 4, 5, and 9 but not with TLR2. Further analysis revealed that there are 5 splice variants of Triad3, named Triad3A-E, with Triad3A being the most abundant isoform and the largest in size. In addition to being moderately expressed in many tissues like the brain and the heart, Triad3A is highly expressed in the lungs, spleen and pancreas as well as many cell lines such as THP-1, HeLa and HEK293[69]. The role of Triad3A on reducing the activities of NF-κB by promoting ubiquitination and degradation of various proteins in different pathways has been reported repeatedly[69,178-181].

Even though the Chuang group demonstrated that Triad3A has the ability to interact with the TIR domain of TLR3, 4, 5 and 9, the authors reported that the

effect of Triad3A on the activities of TLR4 and 9 was more apparent than that observed for TLR3 and 5[69]. The group showed that transfection of Triad3A into HEK293 cells that expresses human TLRs induces complete degradation of both TLR4 and 9, and minimal degradation of TLR3 and 5 without affecting the expression levels of any of these receptors[69]. However, co-transfection of Triad3A and TLR3 into 293T cells blocks the activities of IL-1B completely, but partially affects NF-κB activities upon stimulation of the cells [181]. This inhibitory effect of Triad3A on IFN-β and NF-κB activities was mediated through RIG-1/MAVS signaling pathway instead of TLR3 by directly targeting TRAF3 for degradation. The increase of the endogenous Triad3A protein in response to viral infection of human bronchial epithelial A549 cell line was accompanied by an increase in the degradation of TRAF3 protein[181]. On the other hand, stimulation of TLR4 and TLR9 signaling pathways in various cell types that overexpress Triad3A resulted in a reduction of the NF-κB activity compared to control cells[69]. Similarly, the silencing of Triad3A via siRNA stabilizes the protein level of TLR9 in un-stimulated cells and induces higher level of NF-κB activation in response to TLR4 and 9 stimulation [69].

Using the same discovery tool of yeast two-hybrid system, other groups showed that Triad3A also interacts with receptor-interacting protein (RIP) and promotes its degradation[178]. The authors further showed that Triad3A is capable of inhibiting RIP, IKK, TNF and IL-1 induced-NF-κB activity. Since the activity of Triad3A seems to be mediated through the TIR domain, another study that focused on the interaction between RIP and Triad3A investigated the possible

involvements of other TLRs' adaptors. The group reported that Triad3A mediates protein degradation of TIRAP and TRIF without affecting the level of mRNA expression[180]. On the other hand, they also showed that the protein levels of other adaptors in the TLRs signaling pathways, such as MyD88, IRAK1, IRAK4, IRAK-M, TRAF2 and TRAF6, are not affected by Triad3A activities [180].

Triad3A ubiquitination and degradation capabilities of various TLRs, along with other adaptors downstream these pathways, makes it a potential regulator of the immune response during *C. trachomatis* infection. This study aimed to investigate the ability of Triad3A to regulate inflammation in *Chlamydia*- infected cells.

4.2. RESULTS:

4.2.1. Triad3A expression during infection

Expression of Triad3A in various cell lines was tested via PCR as described above. All the tested cell lines, HeLa, HEK293, THP1, HEK-blue-hTLR2, 3, and 4 expressed Triad3A at a very high levels as shown in Figure 4.1A. Determining the level of Triad3A during the course of *Chlamydia* infection is necessary to evaluate the effect of *Chlamydia* and Triad3A on each other. Real-time PCR analysis of WT HeLa cells infected with *C. trachomatis* at 0, 3, 6, 12, 24 and 36 hours shows that expression of Triad3A remained low throughout the 36 hrs compared to the uninfected cells (Figure 4.1B). However, statistical analysis revealed that Triad3A expression level at 6 hpi was significantly lower than its preceding time point of 3hpi (Figure 4.1B). The

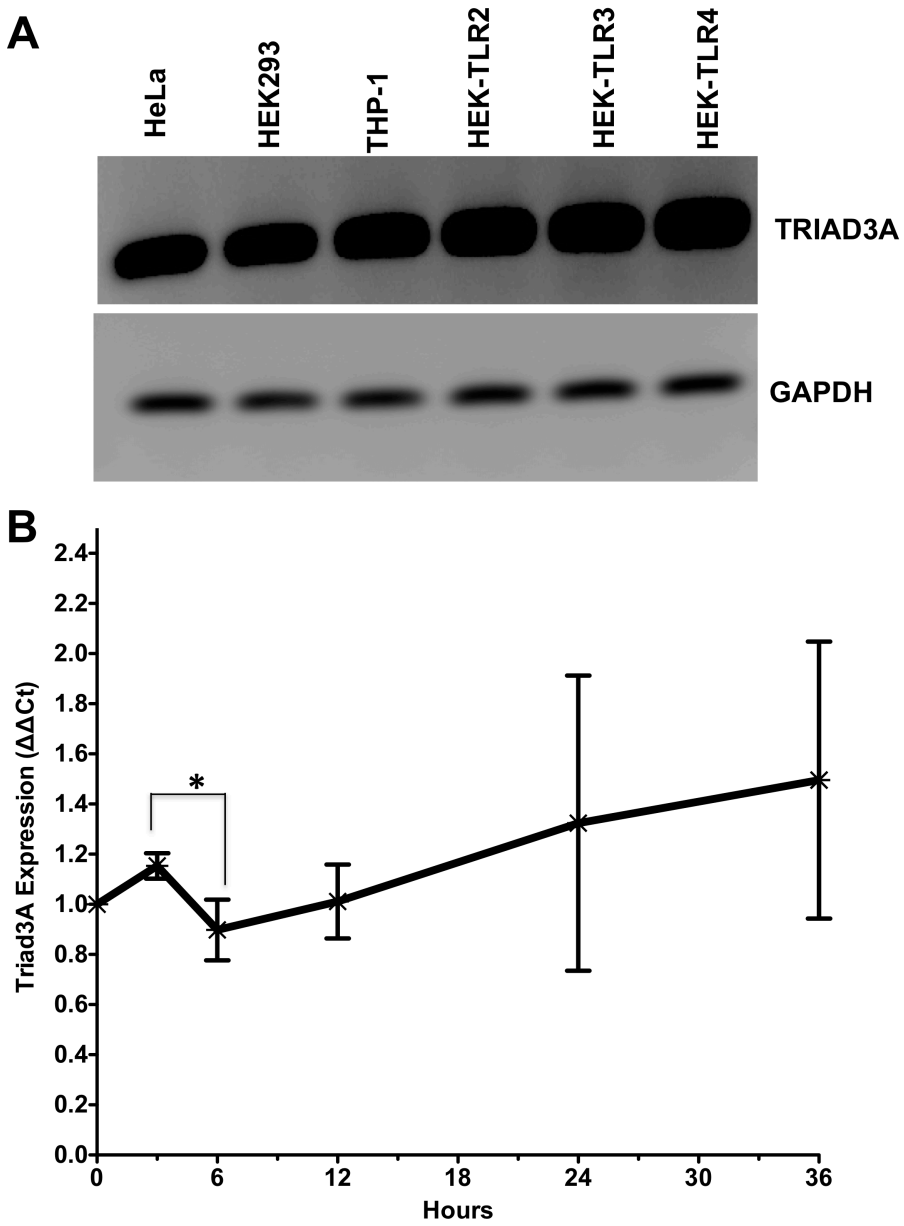

Figure 4.1: Cell lines highly express Triad3A, and Triad3A expression remain stable overtime. (A) PCR analysis of Triad3A in various human cell lines. HeLa, HEK293, THP-1, HEK-Blue-TLR2, 3 and 4 cell lines highly express Triad3A. (B) wild type HeLa cells were infected with C. trachomatis serovar L2 (moi of 1) at the indicated time. The mRNA levels of Triad3A was measure via qPCR. Ct values are normalized to GAPDH and relative expression (ΔΔCt) is calculated compared to non-infected cells (0HR). (B) Triad3A expression level remain stable throughout the 5 time points, with the exception of a slight decrease 6 hpi. The slight increase in the expression at 24 hrs is statistically not significant. Data were collected from 4 independent experiments. . Error bars represent ±SD, and the statistical significant analysis was conducted by comparing each data point to its preceding time point using Student's t test. n.s (not significant), *$p < 0.05$.

increased level of Triad3A at 24 and 36 hpi were not statistically different than the 0 or 12 hpi.

4.2.2. C. trachomatis Activates TLR2 and TLR3 pathways

Triad3A targets TLR3 and TLR4, but not TLR2, for degradation as it has been previously reported [69]. Therefore, we sought to determine which signaling pathway of these three receptors that *C. trachomatis* activates. To do so, we utilized HEK-Blue cell lines that stably express hTLR2, 3 or 4 to allow for the evaluation of the role of each of these receptors independently from the other receptors. These cells also express NF-κB-inducible secreted embryonic alkaline phosphatase (SEAP) reporter gene that is used to measure NF-κB activity. As shown in Figure 4.2A, NF-κB activity in HEK-Blue-hTLR2 was increasing in response to stimulation with *C. trachomatis* and TLR2 agonist (Pam3CSK4) over a period of 24 hours. Even though HEK-Blue-hTLR2 stimulated with TLR4 agonist (Pure-LPS) did show a minimal increase of NF-κB activity at later time point, this increase was most likely due to impurity of LPS. On the other hand, *C. trachomatis*-stimulated HEK-Blue-hTLR4 cells did not induce any detectable levels of NF-κB (Figure 4.2B). Therefore, *C. trachomatis* activates NF-κB through TLR2, but not TLR4 signaling pathway.

Since TLR2 is not affected by Triad3A activities, activation of TLR3 by *C. trachomatis* PAMPs was investigated. The TLR3 signaling pathway is known to induce IFN-β expression in response to viral stimulation[62]. Stimulation of HEK-Blue hTLR3 cells by

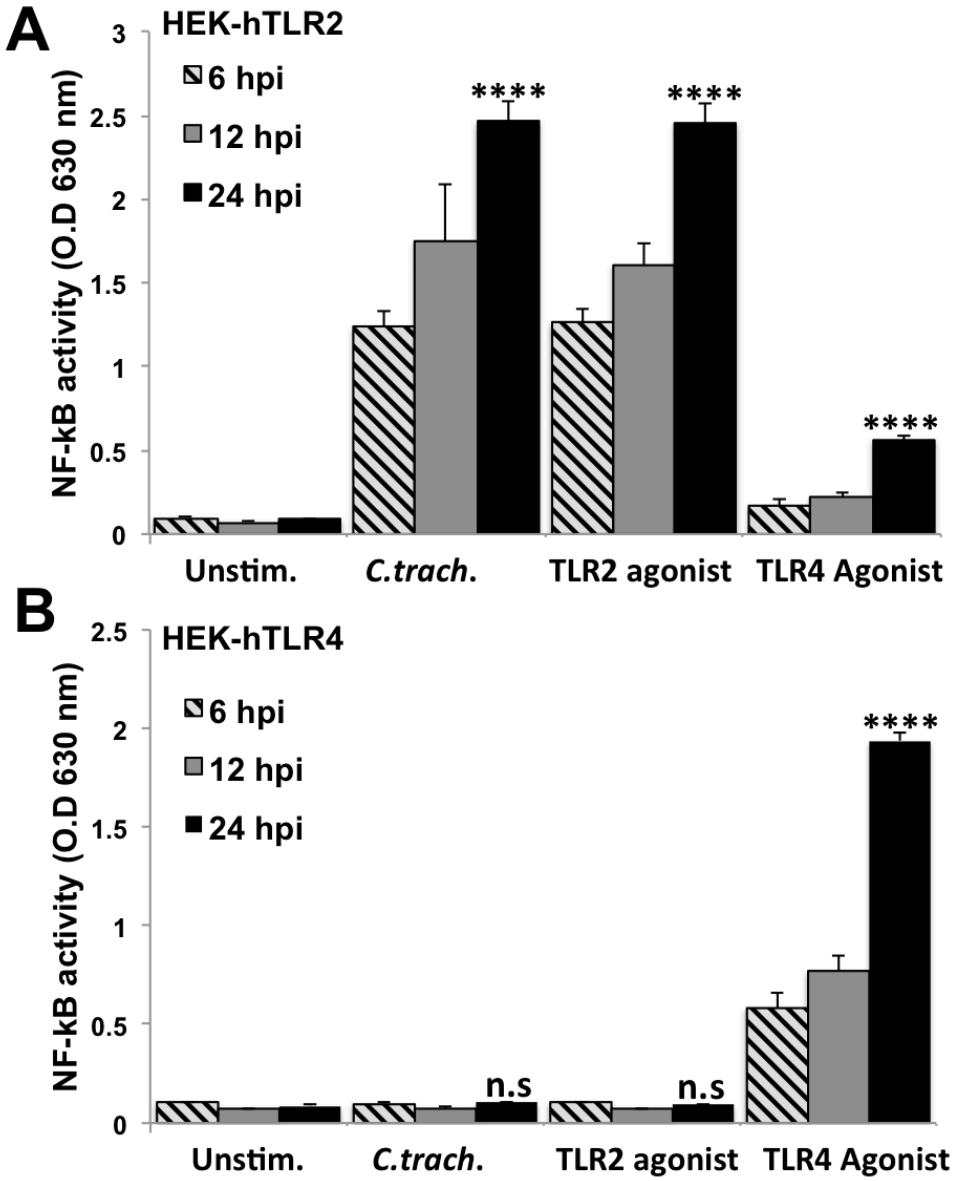

Figure 4.2: ***C. trachomatis induces cell signaling through*** **TLR2, but not TLR4**. HEK-Blue cells expressing human TLR2 or 4 were stimulated with C. trachomatis serovar L2 (moi of 1), TLR2 agonist (Pam3CSK4, 5ug/ml) or TLR4 agonist (ultra Pure *E.Coli* lipopolysaccharide (LPS), 500 ng/ml), or left unstimulated as indicated. NF-κB activities were measured at 6, 12 and 24 hpi using the supernatant of the cultured cells. **(A)** C. Trachomatis, Pam3CSK4, and to a lesser degree, pure LPS induced NF-κB activities as measured by the level of secreted SEAP. (**B)** NF-κB activities on HEK-hLR4 cells increased with time in response to LPS only. C. Trachomatis and Pam3CSK4 failed to induce any significant level of NF-κB compared to the unstimulated HEK-hTLR4 cells. Error bars represent SD values, and the statistical significant analysis was conducted by comparing the readings from the treated samples to the untreated controls using Student's t test (n.s (not significant), and ****$p < 0.0001$).

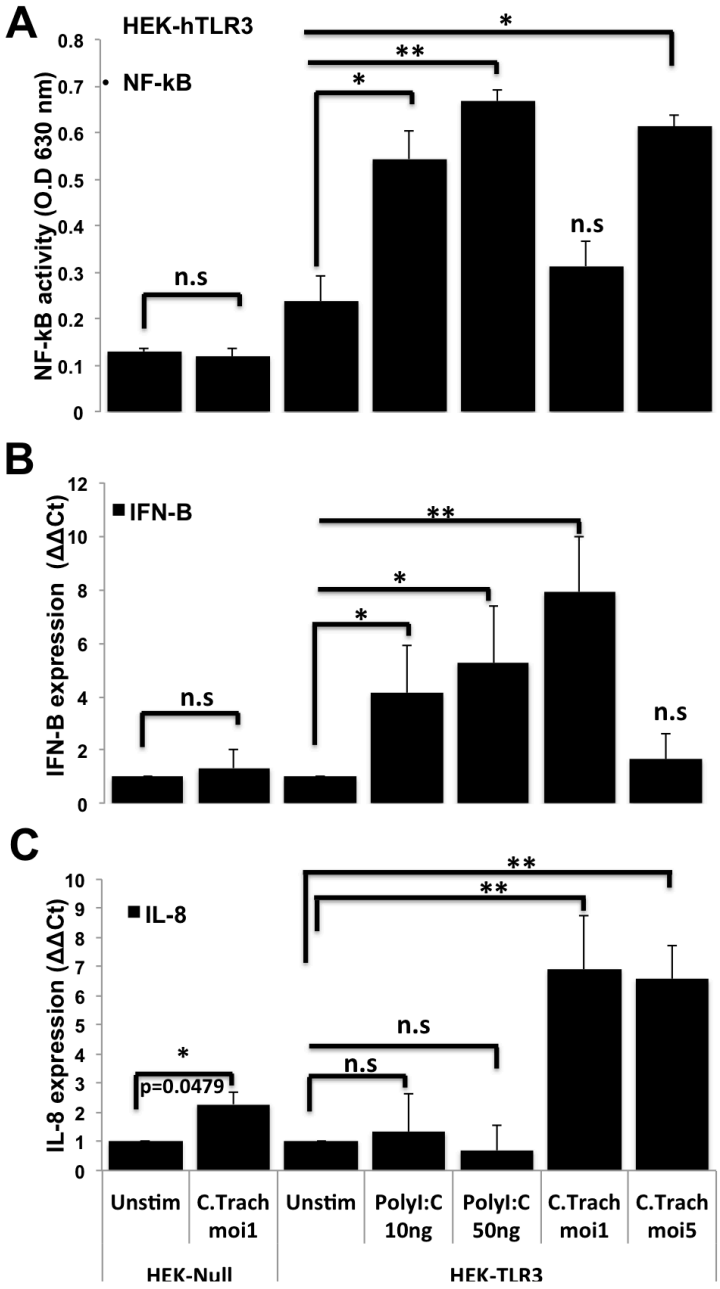

Figure 4.3: TLR3 is activated by *C. trachomatis.* HEK-Blue cells expressing human TLR3, as well as HEK-Null 1 cells were stimulated with C. trachomatis serovar L2 (MOI of 1 or 5) or TLR3 agonist (Poly(I:C), 10ng or 50 ng/ml) or left unstimulated as indicated. Activities of NF-κB were measured at 24 hpi as described in Figure 4.2 and the cell lysate were used for real-time PCR. (A) C. Trachomatis infection of HEK-hTLR3 induced NF-κB activities compared to non-infected HEK-hTLR3cells. Higher MOI of the bacteria (MOI of 5) induced higher levels of NF-κB activities. (B&C) Real-time PCR analysis of IFN-β and IL-8 in HEK-hTLR3. Both PolyI:C and C. Trachomatis treated HEK-hTLR3, at lower MOI only, induced higher mRNA levels of IFN-β;D. *C. trachomatis*,but not PolyI:C, treated cells induced significant levels of IL-8 mRNA. Data are collected from at least 3 independent experiments. Ct values are normalized to GAPDH and relative expression (ΔΔCt) is calculated compared to non-infected cells. Error bars represent SD values, and the statistical significant analysis was conducted by comparing the readings from the treated samples to the untreated controls using Student's t test (n.s (not significant), *$p < 0.05$, and **$p < 0.01$.

C. trachomatis and TLR3 agonist (Poly I:C) induced the activity levels of NF-κB (Figure 4.3A). NF-κB activity in HEK-Blue hTLR3 cells stimulated with lower MOI of *C. trachomatis* was slightly lower than those cells stimulated with higher MOI of the bacteria. On the other hand, lower doses of *C. trachomatis* induced higher levels of IFN-β mRNA, that is 8-folds higher than non-infected HEK-hTLR3 cells, but, paradoxically, higher doses of the bacteria failed to induce any significant level of the IFN-β (Figure 4.3B). However, both low and high MOI of *C. trachomatis* induced significantly higher, but similar, levels of IL-8 mRNA compared to the uninfected cells (Figure 4.3C). Stimulation of HEK-Blue hTLR3 by Poly I:C failed to induce any significant level of IL-8. As a result of the low level of endogenous TLR3 that HEK293 cells normally express, HEK-Blue Null1 cells expressed slightly higher levels of IL-8 mRNA compared to uninfected cells (Figure 4.3C)[182,183]. However, the level of IL-8 remained more than 4 fold lower than HEK-blue-hTLR3 cells. Based on this finding, the role of Triad3A during *C. trachomatis* infection can be now investigated using HEK-Blue-hTLR3 cells since Triad3a interacts with TLR3.

4.2.3. Triad3A silencing has no significant impact on HEK-Blue TLR2 cells

Since HEK-Blue cells are resistant to puromycin, the use of Triad3A-shRNA specific lentiviral particles to generate stable cell line is not feasible. To investigate the role of Triad3A on the signaling pathways of individual TLRs, we used siRNA to reduce the expression level of Triad3A in HEK-Blue TLR2. Real

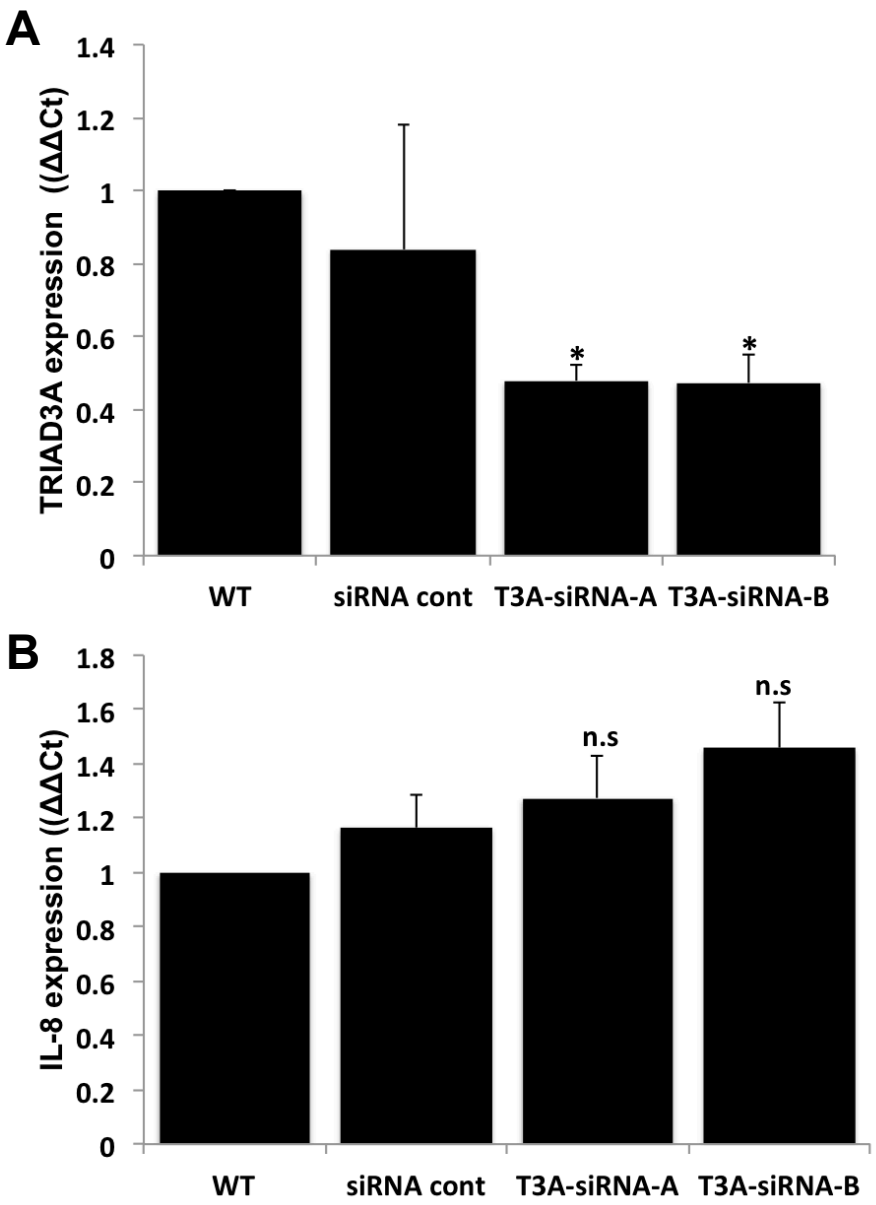

Figure 4.4: Levels of IL-8 unchanged as Triad3A decreases in HEK-hTLR2. Efficiency of Triad3A silencing via siRNA on HEK-hTLR2 as described in figure 10above, were evaluated by real-time PCR. (A) Expression level of Triad3A mRNA was reduced by 50% in these cells compared to the wild type cells. No significant difference of the NF-κB activities were observed as a result of the Triad3A silencing for all of the three cell lines in response to any of the stimulators. Error bars represent SD values, and the statistical significant analysis was conducted by comparing the readings of each time point to the untransfected WT cells. **(B)** Twenty-four hpi with C. trachomatis serovar L2, MOI of 1, the cDNA templates were generated from the isolated mRNA of the HEK-hTLR2 cell lysate. Changes in IL-8 expression between untransfected cells and Triad3A silenced cells were not significant. Data are collected from 4 independent experiments. Error bars represent ±SD, and Student's t test was conducted. n.s (not significant), (*$p < 0.05$, **$p < 0.01$, , ***$p < 0.001$.

time PCR analysis for the knock-down efficiency showed that both siRNA sequences (siRNA-A and B) significantly reduced the expression level of Triad3A by 50% in HEK-Blue-hTLR2 (Figure 4.4A). Stimulation of the siRNA transfected cells with *C. trachomatis,* or TLR2 agonist, pam3CSK, showed no significant difference in Triad3A knocked-down cells relative to cells transfected with siRNA control sequences (Figure 4.4B). The findings from Figure 4.4B show, as expected, that Triad3A does not affect TLR2 signaling pathways. Further analysis of the effect of Triad3A deficiency on stimulated HEK-Blue-hTLR3 and TLR4 cells is planned.

4.2.4. Reduced levels of Triad3A negatively effect IL-8 mRNA

HeLa cells that are stably expressing Triad3A-shRNA vectors and maintaining puromycin resistance were generated to evaluate Triad3A's effects on IL-8 expression during *Chlamydia* infection. Knock–down efficiency of Triad3A was evaluated using real-time PCR. HeLa cells expressing Triad3A-shRNA-A and B displayed significantly reduced levels of Triad3A mRNA expression by about 40% compared to the WT cells (Figure 4.5A). No significant difference was observed for the expression of Triad3A between WT and the shRNA non-target control (sh CONT). Surprisingly, the expression levels of IL-8 in response to infection by *C. trachomatis,* as shown in Figure 4.5B, was greatly reduced by 70-80% in cells that expressed either sequence of Triad3A shRNA. This reduction was statistically significant when compared to the level of IL-8 in the *C. trachomatis* infected non-target shRNA control. Taken together, it is likely that

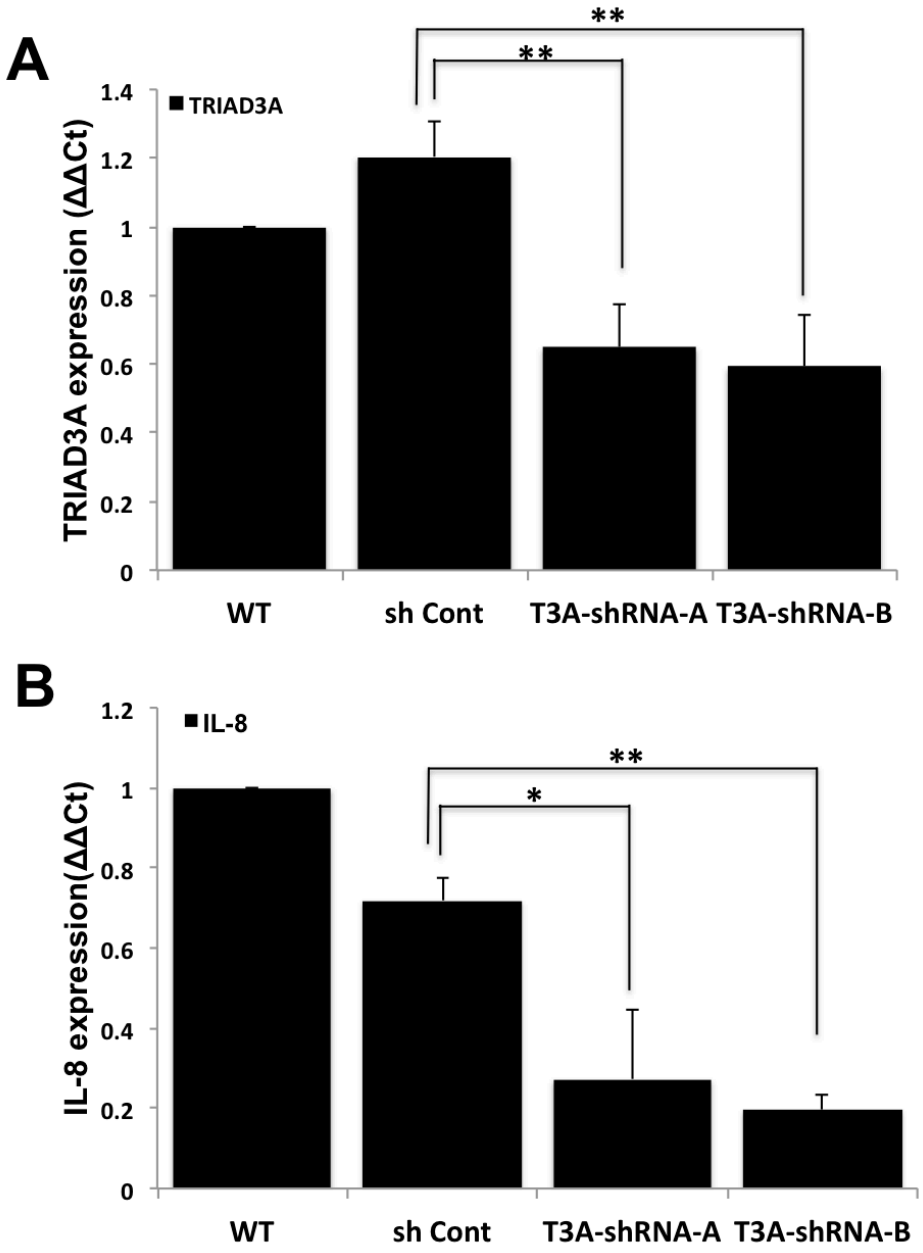

Figure 4.5: Triad3A contributes to the production of IL-8 in *Chlamydia* infected HeLa cells. HeLa cells were transduced for 48 h with lentiviruses expressing either non-target shRNA control (sh Cont) or Triad3A Sequence A and B (T3A-shRNA-A or B). (A) real-time PCR analysis of the efficiency of Triad3A silencing. Relative expression level of Triad3A compared to wild type (WT) was reduced by about 40% for both sequences. (B) HeLa WT, sh Cont, T3A-shRNA-A and B cells were infected with C. trachomatis serovar L2 at MOI of 1. 24 hpi, real-time PCR analysis of IL-8 expression was lower in the Triad3A knocked-down cells compared to WT infected cells. Data are collected from at least 3 independent experiments. Error bars represent ±SD, and the statistical significant analysis was conducted by comparing the expression level of IL-8 on the Triad3A knocked-down cells to the non-target shRNA control using Student's t test (n.s (not significant), *$p < 0.05$, and **$p < 0.01$).

Triad3A exerts its effect on *Chlamydia* infected cells through indirect mechanism that manipulates TLR2 signaling pathways.

4.3. DISCUSSION:

Triad3A indirectly regulate TLR2 activity during infection

Triad3A is the most abundant variant isoform of the known TRIADs and is known to reduce NF-κB activities by promoting the degradation of various TLRs [69,178-181]. In addition to the increased levels of Triad3A protein in response to viral stimulation, it has been suggested that degradation of Triad3A's targets is dependent on the activation of the target itself [69,181]. Therefore, we first investigated if the activation of the innate immune system by *C. trachomatis* caused any changes to the level of Triad3A mRNA. Our results clearly indicated that *Chlamydia* infection of HeLa cells did not have a significant effect on the expression level of Triad3A compared to the non-infected cells. However, 6 hpi, Triad3A level was significantly reduced to its lowest level compared to the earlier point of 3 hours. The reduction of Triad3A at the 6 hpi coincides with the early activation of NF-κB as reported before.

Chuang and colleagues showed that Triad3A interacts with the TIR domain and promotes the degradation of TLR3, 4, 5 and 9, but not TLR2 [69]. At the onset of our work, it was not fully illustrated whether TLR2, TLR4 or both, are the receptors that detect microbial components of *C. trachomatis* that lead to the induction of the immune system. Therefore, we first characterized the role that TLR2 and TLR4 play during *Chlamydia* infection utilizing HEK-Blue cells that are

expressing individual TLRs. Our results clearly show, for the first time, that the recognition of *C. trachomatis* by the immune system that leads to the activation of NF-κB, is mediated through the TLR2, but not TLR4 signaling pathway.

Since Triad3A targets TLR4, but not TLR2, for degradation, our focus shifted toward the possible role of TLR3 in inducing a proinflammatory cytokines in response to *C. trachomatis* infection. TLR3 is a receptor that has been historically associated with the induction of IFN-β in response to viral dsRNA stimulation[62]. Recently, few studies focused on the ability of some bacterial species, including *Chlamydia muridarum*, to induce the production of TLR3-dependent IFN-β [63,184,185]. However, there is no indication that dsRNA associates with Chlamydia species[186]. Using HEKBlue-hTLR3 cells, our results show that *C. trachomatis* activates NF-κB. To our knowledge, this is the first report ever to show that *C. trachomatis* activates TLR3 signaling pathway in a way that leads to the production of proinflammatory cytokines, such as IL-8 and IFN-β, in a NF-κB dependent manner. Interestingly, stimulation of these cells with synthetic dsRNA and PolyI:C, induced the production of IFN-β but not the IL-8, emphasizing the existence of separate mechanisms for the production of these cytokines in response to different stimuli. Even though such observation has not been described in bacterial infection, Ye *et al.* showed that the level of TLR3-induced IFN-β decreases in response to HBV polymerase in a dose-dependent manner [187]. Therefore, the reduction of IFN-β expression observed at higher MOI can be explained by the inhibitory effect that higher dose of *C. trachomatis* that cause the decrease observed in figure 4.3B. The slight increase of IL-8

expression in HEK-Blue-Null1 cells came as result of the endogenous, but low, level of TLR3 that HEK cells are expressing [182]. The higher precision and increased sensitivity of qPCR over the NF-κB activity assay could explain the discrepancy observed between the expression of IL-8 and NF-κB activation in the HEK-Blue-Null1 cells that were infected with *Chlamydia.* It is also possible that there are factors other than NF-κB that regulate the expression of IL-8.

Based on the present evidence of the role of TLR2, TLR3 and TLR4 during *Chlamydia* infection, and the role of Triad3A on regulating these receptors, we hypothesized that silencing of Triad3A in cells expressing TLR2 alone will not cause a change in the inflammatory response against *C. trachomatis.* Indeed, HEK-Blue-hTLR2 cells that expressed lower levels of Triad3A showed no significant difference in their ability to activate NF-κB or to induce proinflammatory cytokines in response to *C. trachomatis* and TLR2 agonist (PAM3CSK) stimulation compared to the control groups, WT and siRNA control.

On the other hand, Triad3A silencing in a physiologically relevant cell line for *C. trachomatis* infection, such as HeLa cells that express all three receptors; TLR2, 3 and 4, would cause an increase in the proinflammatory cytokines in response to *C. trachomatis* infection [188]. This increase is expected to be the result of TLR3 stabilization in the absence of Triad3A. Surprisingly, *C. trachomatis* infections of HeLa cells that have reduced level of Triad3A induced lower levels of IL-8 compared to the WT and sh-control groups. However, our lab had previously showed that TLR4 deficient macrophages and fibroblasts

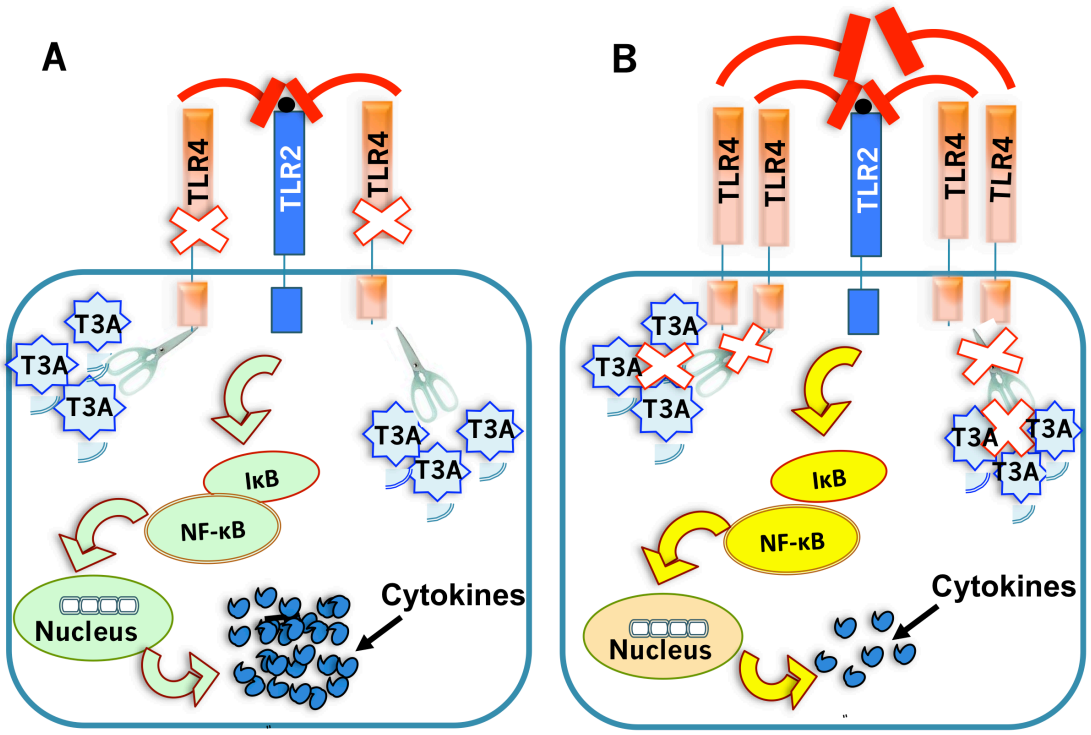

Figure 4.6: Regulation model of inflammation via Triad3A. A) The presence of Triad3A protein induces the ubiquitination and degradation of TLR4 leading to the reduction of the inhibitory effect that TLR4 exerts over TLR2 activity (heterotolerance) leading to increased production of pro-inflammatory cytokines. **B)** Absence of Triad3A prevents TLR4 degradation and increases its stability. Increased TLR4 stability further enhances its inhibitory effect over TLR2, which ultimately leads to the production of reduced levels of pro-inflammatory cytokines.

induced higher proinflammatory cytokines, such as MIP-2 and IL-6, in response to *Chlamydia miriudarum* infection [189]. This observation of an increased proinflammatory response was attributed to the possible increase of TLR2 activities due to the absence of the heterotolerance effect of TLR4 that it exerts over TLR2 [189,190]. TLR-induced heterotolerance known to cause a decrease in the activity of NF-κB to a given stimulus that is different from stimuli of another TLR [191]. Since Triad3A targets TLR4 for ubiquitination and degradation, therefore, the absence of Triad3A in HeLa cells further stabilizes the level of TLR4 and prevents its degradation. Hence, it is very likely that the increased stability of TLR4 lead to greater inhibitory effect on TLR2 activities that caused the observed reduction of the proinflammatory cytokines (Figure 4.6). Attempts to detect the protein levels of TLR2, TLR3 and TLR4 in Triad3A KD HeLa cells have failed despite the use of antibodies from different vendors.

Our results here show for the first time that *C. trachomatis* induce the activities of TLR2 and TLR3 but not TLR4 signaling pathways. We report that *C. trachomatis* activates TLR3 signaling pathway that leads to the induction of IFN-β, and IL-8. More interestingly, interactions between different TLRs are manipulated by the involvement of other factors such as Triad3A, where the absence of Triad3A results in the increase of TLR4 that in return leads to reduced activity of TLR2. Further investigation of this phenomenon will advance our knowledge of the exact mechanisms that TLR4 uses to overshadow TLR2 activity.

CHAPTER 5

TRAIL-R's Role As A Negative Regulator Of TLR Signaling Pathway

5.1. INTRODUCTION:

The trans-membrane receptor of TNF-related apoptosis-inducing ligand receptor (TRAIL-R), is a member of the tumor necrosis factor receptor superfamily (TNFRSF) that lacks a TIR domain[192]. There are four different TRAIL-Rs that have been identified in humans (hTRAIL-R1-4) and one full-length receptor in mice (mTRAIL-R) [193,194]. The cytoplasmic region of both TRAIL-R1 and 2, also known as Death Receptor (DR) 4 and 5 (alternative name is TNFRSF10A and B), contain functional death domains that can induce apoptosis[195]. Both TRAIL-R1 and TRAIL-R2 are capable of selectively killing transformed cells but not normal cells, while TRAIL-R3 and TRAIL-R4 (alternative name is TNFRSF10C and D) serve as decoys [196,197]. The interaction between TRAIL-R and its ligand (TRAIL) has been shown to play a role in the prognosis of various autoimmune diseases and have undergone clinical trials as promising proapoptotic anti-cancer therapy for solid malignancies or non-Hodgkin lymphomas [195,198-201]. In addition to its well-established role in inducing apoptosis through FADD-caspase-8, TRAIL-R is one of several trans-membrane proteins that have been reported to manipulate inflammation of the host cells in response to various pathogens and diseases [154,202-204]. These reports implicate TRAIL-R as a negative regulator in TLR signaling.

The blockage of TRAIL-R signaling pathway, by neutralizing the ligand for TRAIL-R, induced higher inflammatory response for mice that have gone through MOG-induced experimental autoimmune encephalomyelitis (EAE)[205]. In addition, the activation of autoreactive T cells in these mice was also increased when TRAIL signaling was blocked indicating that TRAIL-R inhibits autoimmune inflammation. Another report has showed that TRAIL-R deficient lymphomas express higher levels of basophils, NK and T-cells, indicating higher infiltration of various immune cells[201]. Sublethal irradiation of TRAIL-R deficient mice induced higher levels of NF-κB activity associated with inflammation and fibrosis in the lung that was more frequent and severe than TRAIL-R+/– mice [201].

TRAIL-R deficient mice develop normal populations of immune cells with some contradiction on the effect of such deficiency on the development of T cells [154,206,207]. However, challenging TRAIL-R deficient mice with different pathogens and stimuli for TLR2, 3 and 4 receptors, but not TLR9, showed an enhanced the ability of the innate immune system to clear out the infection and increased production of different pro-inflammatory-cytokines such as IFN-β [154]. While the activation level of the MAPK pathway was similar in WT and TRAIL-R deficient macrophages, the regulatory mechanisms of TRAIL-R on TLR signaling seem to be through the stabilization of IκBα subunit [154]. Interestingly, the degradation level of IκBα subunit of WT and TRAIL-R deficient macrophages was similar in the early stages of LPS-stimulation. Consistent with the increased level of TRAIL 4 hours post LPS stimulation, the level of replenished IκBα subunit on the TRAIL-R deficient cells was much lower than the level observed in WT [154]. This clearly

indicates that TRAIL-R is involved in the TLR signaling by preventing the translocation of NF-κB to the nucleus. In contradiction to the previous reports, Tang *et al.* showed that overexpression of TRAIL-R1 and 2 in HEK293 induces the production of proinflammatory cytokines in NF-κB-dependent manner [208]. The report showed that NF-κB activation is dependent on the cytoplasmic domain of the receptors and that TRAIL-R2 is more potent than TRAIL-R-1 in inducing cytokines release. Despite this contradiction, the report further confirmed the involvement of IκB on TRAIL-R signaling.

Despite its role in apoptosis and regulation of NF-κB activity, the involvement of TRAIL-R during *C. trachomatis* infection has never been addressed. Here we proposed to elucidate the biological factors that cause the abnormal immune response during *C. trachomatis* infection and the role that TRAIL-R plays in regulating TLR signaling pathway in *Chlamydia*–infected cells.

5.2. RESULTS:

5.2.1. TRAIL-R KO fibroblasts express higher levels of cytokines

With few exceptions, studies on the role of TRAIL-R in regulating inflammation have been mainly focused in mice. Therefore, we first evaluated the role of murine TRAIL-R during *Chlamydia* infection using primary cells from TRAIL-R knock-out (KO) mice. *Chlamydia muridarum* (MoPn) is the ideal strain for infecting lung fibroblast since it is known to cause pneumonitis in mice, in addition to the LGV strain of *Chlamydia trachomatis* (L2) that is known to induce

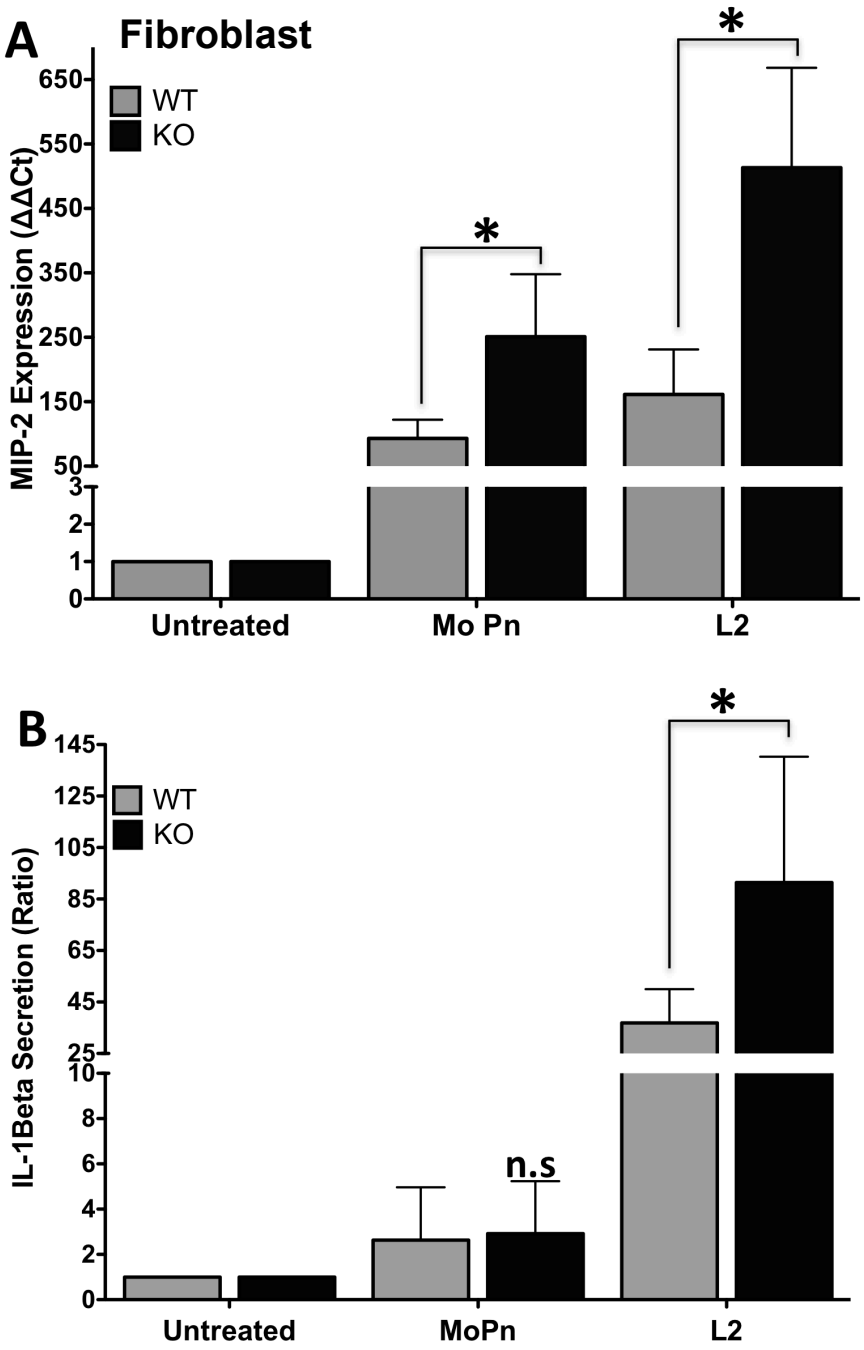

Figure 5.1: TRAIL-R deficiency increases MIP-2 and IL-1β levels in primary lung fibroblasts. WT and KO cells were infected with MoPn or L2 strains at MOI of 1 for 24 hrs. A) mRNA levels of MIP-2 are measure via qPCR. Ct values are normalized to GAPDH and relative expression (ΔΔCt) is calculated compared to non-infected cells. Significant difference of MIP-2 expression in both MoPn and L2 infected KO cells. B) ELISA measurement for IL-1β. The ratio of increased IL-1β level with respect to uninfected cells. Only L2 infected fibroblast secreted adequate IL-1β, where KO cells have significantly higher level of IL-1β compared to WT. Error bars represent standard deviations from 3 separate experiments. * indicates $p < 0.05$; ** indicates $p < 0.01$; compared to infected WT cells.

a stronger response in the infected cells [21,22,23]. Since *Chlamydia muridarum* is closely related to the LGVs of human, it has been widely used to study the pathogenesis of *Chlamydial* diseases in the reproductive and respiratory tracts of mouse model [22,23]. As shown in Figure 5.1A, real-time PCR analysis of MIP-2 (a mouse homologue of human IL-8) indicated that the mRNA level was greatly induced in response to *Chlamydia* infection from both L2 and MoPn compared to the non-infected lung fibroblasts. However, L2 induction of MIP-2 expression in cells from both WT and KO mice was one fold higher than the response induced by the MoPn strain. On the other hand, the expression level of MIP-2 in the lung fibroblasts from TRAIL-R KO mice was significantly higher than the WT cells regardless of the bacterial strain used (Figure 5.1A). The level of IL-1β beta secreted by these fibroblasts was measured using ELISA. The levels of IL-1β secreted from lung fibroblast were normalized to the levels measured for the uninfected cells. Despite the increase in the mRNA level of the pro-inflammatory cytokine, MIP-2, the ratio of IL-1β secreted from both WT and KO lung fibroblasts in response to MoPn infection was low and insignificant compared to the level of uninfected cells (Figure 5.1B). In contrast to MoPn-infected cells, fibroblasts infected with *C. trachomatis* serovar L2 induced the secretion of IL-1β to more than 50 fold compared to the uninfected cells (Figure 5.1B). In addition, the lung fibroblasts that are TRAIL-R deficient secreted higher levels of IL-1β compared to the infected WT cells (Figure 5.1B).

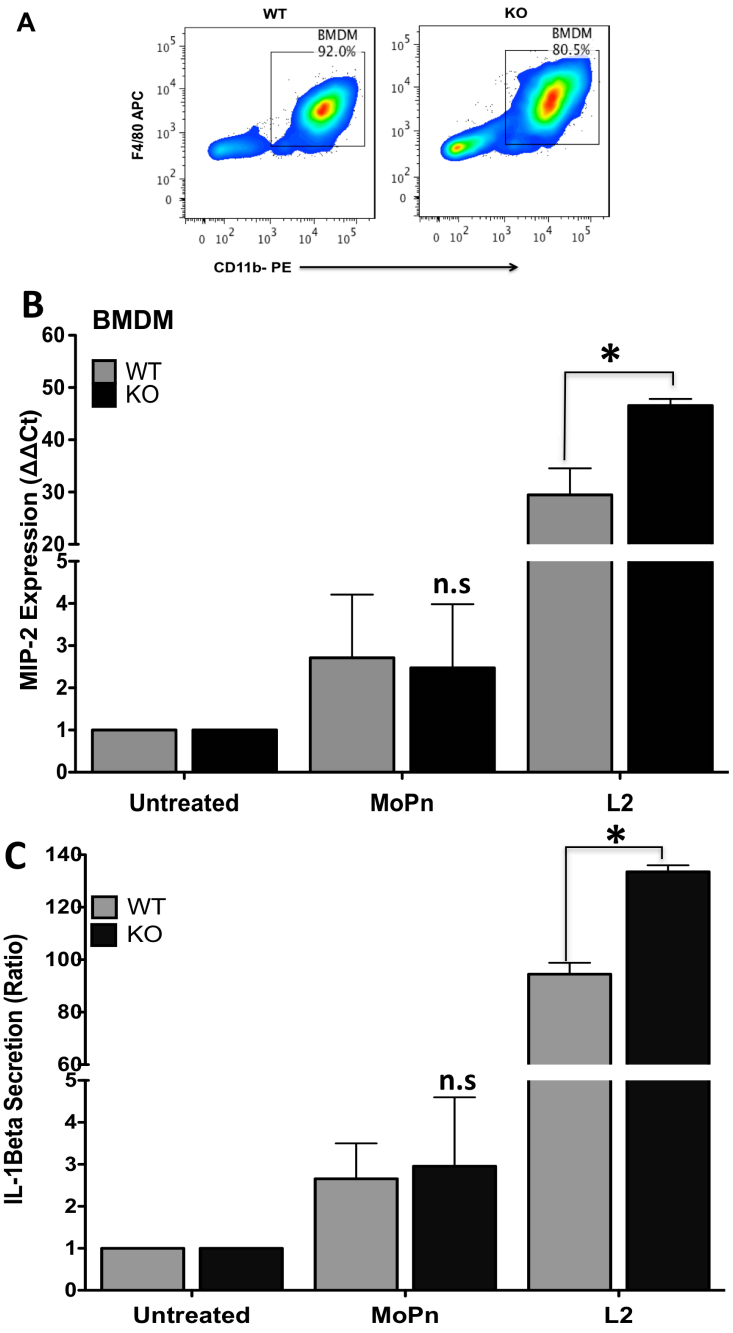

Figure 5.2: TRAIL-R deficient BMDMs have higher MIP-2 and IL-1β levels in L2, but not MoPn infected cells. (A) Representative flow cytometry dot plot of differentiated BMDM cells. Bone marrow cells were isolated and cultured in the presence of M-CSF. Seven days post-isolation, cultured bone marrow cells were stained with BMDM specific receptor using anti-mouse *CD11b-PE* and *F4/80-APC.* (B&C) BMDM infected with MoPn and with C. trachomatis serovar L2. qPCR analysis of MIP-2 (B); and ELISA level of IL-1β secretion (C). Both L2 and MoPn infected BMDMs induced MIP-2 expression, but only L2 infected KO cells have significantly higher level than the WT cells as seen in B. Similarly, MoPn and L2 infected cells induce the secretion of IL-1β where the levels of IL-1β of the KO BMDMs are higher than the WT (C). Error bars represent standard deviations from 3 independent experiments, and Student's t test was conducted where n.s (not significant) and *$p < 0.05$, compared to infected WT cells.

5.2.3. TRAIL-R KO BMDMs induces higher levels of cytokines

Since macrophages are effective immune cells that engulf *Chlamydia* and induce an immune response against it, differentiated bone marrow derived macrophages (BMDMs) from WT and KO mice were infected with both MoPn and *C. trachomatis* L2 strains [49,50]. Initially, cultured cells were tested for the presence of differentiated BMDMs using BMDM specific markers CD11b and F4/80. As shown in Figure 5.2A, seven days post isolation, more than 80% of cultured BM cells have been differentiated into BMDMs that expressed both markers of CD11b and F4/80. BMDM cells infected with both MoPn and L2 strains induced higher levels of MIP-2 mRNA compared to non-infected cells (Figure 5.2B). However, only *C. trachomatis* infected BMDM induced higher expression of MIP-2 in TRAIL-R deficient cells compared to infected WT (Figure 5.2B). Additionally, MIP-2 mRNA expression level was 10-fold lower than the levels observed in the lung fibroblasts (Figure 5.1A and 5.2B).

IL-1β secretion in BMDM, as measured by ELISA, showed that MoPn-level in the BMDM was 10-folds lower than the levels observed in the lung fibroblasts (Figure 5.1B and 5.2C). Infected BMDMs secreted low levels of the cytokine compared to the uninfected cells (Figure 5.2C). However, no significant difference of the level of IL-1β was observed between WT and TRAIL-R deficient cells (Figure 5.2C). *C. trachomatis L2* infected cells, on the other hand, induced higher secretion levels of IL-1β than MoPn- infected cells. The ratio of secreted IL-1β in TRAIL-R KO BMDM, compared to uninfected cells, was about 50% higher than infected cells from WT mice (Figure 5.2C).

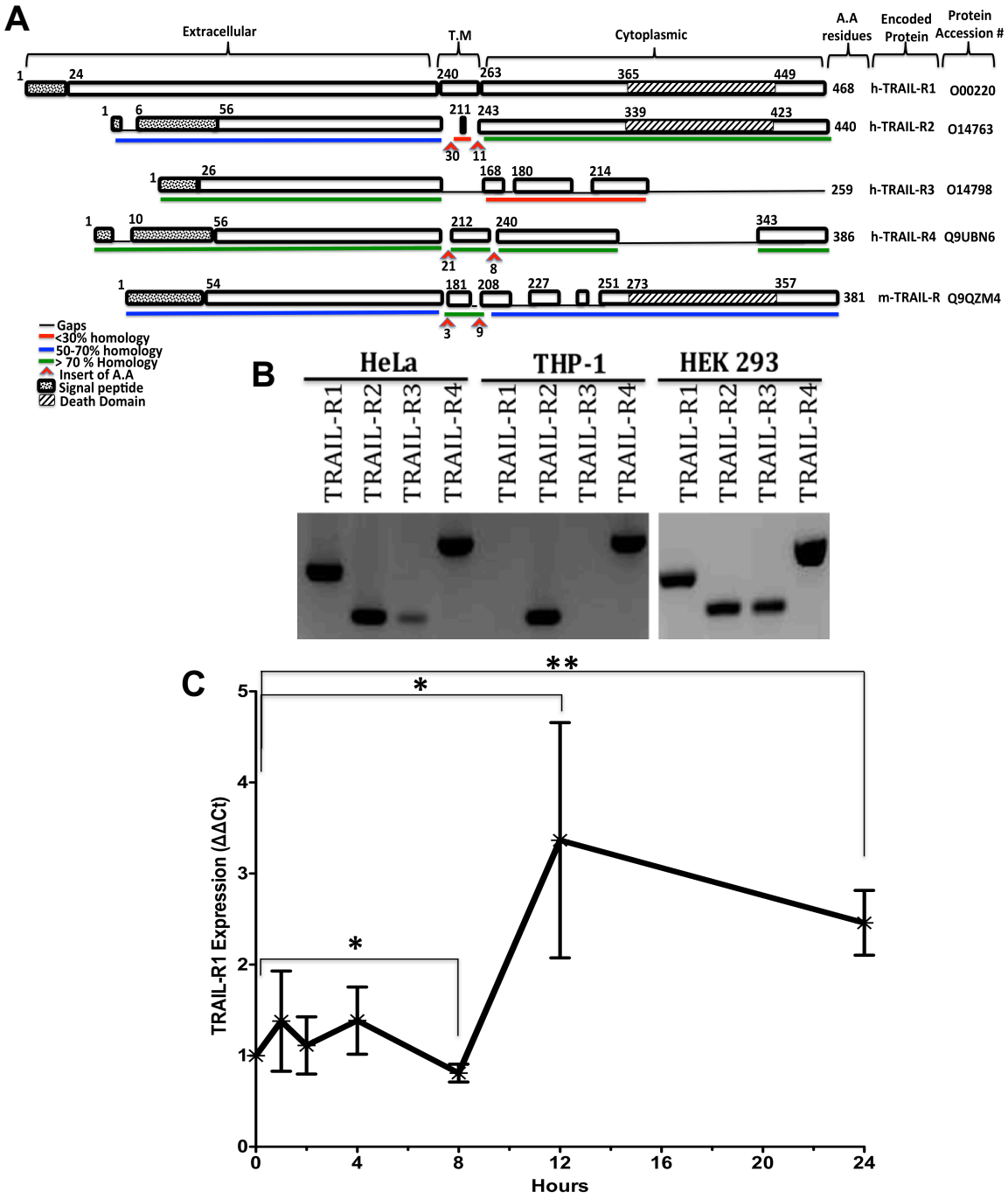

Figure 5.3: Amino acid alignment, expression of TRAIL-R1-4 and the effect of *C. trachomatis* infection on TRAIL-R1 expression. **A)** Amino acid (A.A) sequence alignment of TRAIL-R-2,3,4 and mTRAIL-R compared toTRAIL-R1. **B)** 2% agarose gel electrophoresis showing RT-PCR amplification of TRAIL-R1 (214 bp), 2 (145 bp), 3 (141 bp) and 4 (271 bp) mRNAs from HeLa, THP-1 and HE293 cell lines. **C)** Wild type HeLa cells were infected with *C. trachomatis* serovar L2 (MOI of 1). Cells were collected at the indicated time and the mRNA levels of TRAIL-R1 was measure via qPCR. Ct values are normalized to GAPDH and relative expression (ΔΔCt) is calculated compared to non-infected cells (0HR). Expression of TRAIL-R1 was constant during the early stages of the infection before slightly decreases at 8 hpi and then increases at 12 and 24 hpi. Data were collected from 3 independent experiments. Error bars represent ±SD, and the statistical significant analysis was done by comparing data points to the uninfected sample (0HR) using Student's t test. n.s (not significant), *p < 0.05, **p < 0.01.

5.2.4. Expression of human TRAIL-R1 during infection

The homology between the mTRAIL-R and hTRAIL-R1 and 2 has been reported previously[192]. We ran multiple alignments at the protein level for all TRAIL-Rs using UniProt knowledgebase by comparing the amino acid sequences of murine and hTRAIL-R2-3-4 to TRAIL-R1[209]. Our data showed that the extracellular domain of all receptors carried about 50% similarities to TRAIL-R1. While the overall homology of the cytosolic domain varied between the different receptor, the homology of the death domain was very high and ranged between 70-80% (Figure 5.3A). The presence of the four different TRAIL-Rs (TRAIL-R1-4) in the human cell lines; HeLa, THP-1 and HEK-293, was tested via PCR. Both HeLa and HEK293 cells highly expressed all four subtypes of TRAIL-Rs, with the exception to TRAIL-R3 that was slightly expressed in HeLa cells, and the THP-1 cell line which expresses TRAIL-R2 and 4 only (Figure 5.3B).

Since TRAIL-R1 is involved in the apoptosis pathway, a process that is inhibited in the early stages of *Chlamydia* infection, the expression level of TRAIL-R1 in *Chlamydia*- infected HeLa cells was monitored over a 24-hour period [129]. Real-time PCR analysis of TRAIL-R1 expression at 1, 2, 4, 8, 12 and 24 hours showed that changes of the expression levels of TRAIL-R1 remained insignificant for the first 4 hours of the infection compared to the uninfected WT cells at 0 hr (Figure 5.3C). However, statistical analysis indicated that TRAIL-R1 significantly decreased in the period between 4-8 hpi before it greatly increased at the period of 12 and 24 hpi compared to the uninfected samples.

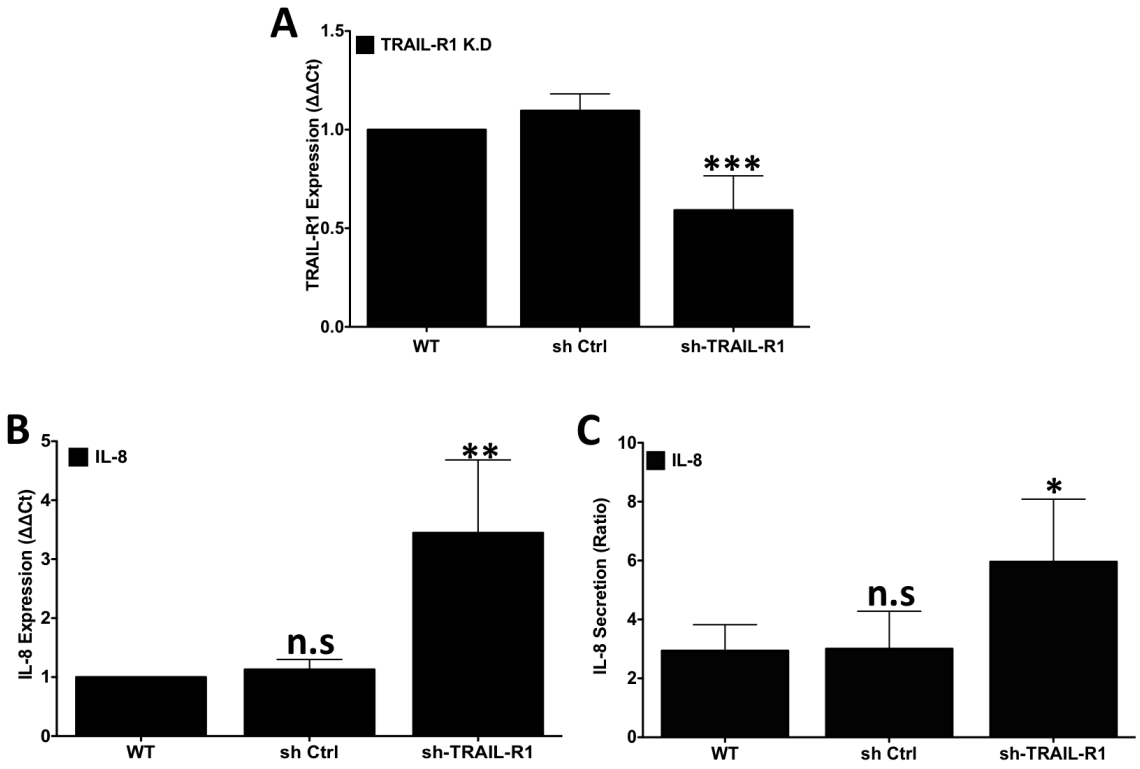

Figure 5.4: Increased IL-8 expression and secretion in TRAIL-R1 Knockdown HeLa cells. (A) HeLa cells transduced with TRAIL-R1 specific shRNA (sh-TRAIL-R1) have a reduced level of TRAIL-R1 mRNA by about 50% when quantified by real-time PCR and compared with wild-type (WT) and non-target control (sh Ctrl). (B&C) HeLa cells were infected with C. trachomatis serovar L2 at MOI of 1. (B)RNA was harvested 24 hpi for quantification of IL-8 expression using qPCR. Data is normalized to GAPDH and infected wild type HeLa used to calculate the relative expression (ΔΔCt). (C) ELISA measurement of IL-8 secretion. The ratio of increased IL-8 secretion, with respect to uninfected cells, in response to *C. trachomatis* serovar L2 infection at MOI of 1, 24 hpi. TRAIL-R1 KD cells express higher level of IL-8 mRNA (B); and secreted more IL-8 (C) to the supernatant compared to both WT and shRNA control. Error bars represent SD from least 3 separate experiments and Student's t test was conducted . "n.s" indicate not significant; * indicates $p < 0.05$; . ** indicates $p < 0.01$; and *** indicates $p < 0.001$ compared to infected WT cells.

5.2.5. Silencing of hTRAIL-R1 increases proinflammatory cytokines

Transduction of HeLa cells with shRNA non-target control (sh CONT) and TRAIL-R1-shRNA specific vectors to establish stable knockdown of the target gene was performed as described before. Real-time PCR confirmed that HeLa cells transduced with TRAIL-R-1 specific shRNA vector have 40% reduction in the mRNA level of the gene compared to WT cells (Figure 5.4A). Both WT HeLa and non-target shRNA control maintained similar level of the TRAIL-R1 mRNA.

To determine whether TRAIL-R1 reduction influences the response of HeLa cells to *Chlamydial* infection, WT, non-target shRNA control and TRAIL-R1 knocked-down cells were infected with *C. trachomatis* serovar L2. Real-time PCR analysis of IL-8 expression in the infected cells indicated that WT and non-target shRNA control expressed similar levels of the cytokines in response to *Chlamydia* infection (Figure 5.4B). However, *C. trachomatis* infection of HeLa TRAIL-R1 KD cells induced level of TRAIL-R1 induced higher expression of IL-8 mRNA that was 4 fold higher than the level measured for both WT and non-target-shRNA control (Figure 5.4B). Similarly, ELISA analysis of TRAIL-R1 knocked-down HeLa cells showed that the ratio of IL-8 secretion during *Chlamydia* infection of these cells, compared to the uninfected ones, was significantly greater than infected WT and non-target control cells (Figure 5.4C). Collectively, this data shows that both mTRAIL-R and hTRAIL-R1 down-regulate the proinflammatory response of cells that are infected with *C. trachomatis*.

5.3. DISCUSSION

Function of mouse and human TRAIL-R during *Chlamydia* infection

Several studies have focused on the role of TRAIL-R to induce apoptosis, with few emerging studies that shift their focus on the role of TRAIL-Rs in regulating the innate immune response against bacterial and viral pathogens. In this study, to elucidate the potential role of TRAIL-R in regulating *Chlamydia* infection, we first examined the effect of TRAIL-R absence in the response of murine primary lung fibroblast to C. *muridarum* (MoPn) *and C*. *trachomatis* **(**LGV/L2) infection. Our results show that the absence of TRAIL-R KO in lung fibroblasts increased the expression level of MIP-2 mRNA in response to both MoPn and *C. trachomatis* infection compared to the uninfected cells.

The secretion of the proinflammatory cytokines of IL-1β in response to infection shows some differences between the two-*Chlamydia* strains. Here, MoPn-infected lung fibroblast failed to secrete adequate levels of IL-1β with no significant difference between the WT and TRAIL-R KO fibroblasts despite the increased level of MIP-2. Activation TLR signaling up-regulates the expression of pro-inflammatory cytokines, such as MIP-2 and inactive IL-1β, known as pro-IL-1β. However, the secretion of the active form requires the presence of a second signal that activates the inflammasome complex, which in return leads to the cleavage of pro-IL-1β and the secretion of mature IL-1β [151,210]. Therefore, the different trends seen between MIP-2 expression and IL-1β secretion in MoPn infected fibroblasts can be explained simply by the absence of the second signal due to the weak response to MoPN infection. On the other hand, the more

invasive strain of *C. trachomatis*, the L2, induced a high secretion level of IL-1β. Similar to increased MIP-2 expression, TRAIL-R KO fibroblasts that were infected with L2 secreted higher levels of IL-1β than that seen from the WT. The extreme difference in the fibroblasts' response to the two strains is caused by the ability of L2 strain to induce a stronger immune response than other strains.

Macrophages are one of the main components of the innate immune response to many pathogens including *Chlamydia*. However, some *Chlamydia* species are unique in their ability to infect macrophages and survive in them [211,212]. In addition, macrophages infected with *C. trachomatis* have been shown to induce apoptosis of T cells by up-regulating Fas, a caspase-8-dependent apoptosis pathway that is also used by TRAIL-R, contributing to the persistent of the infection [213]. We show here that isolated bone marrow cells that have been differentiated into BMDMs respond to stimulation by both strains of *Chlamydia*. However, MIP-2 expression and IL-1β secretion in MoPn-infected BMDMs were extremely low with no significant difference between cells isolated from WT and TRAIL-R deficient mice. In contrast, *C. trachomatis* L2-infected BMDMs induced much higher levels of both MIP-2 and IL-1β, where TRAIL-R deficient cells clearly had a higher amount of both cytokines than the WT cells. Even though *Chlamydia* infection induced a proinflammatory response in BMDM cells, the expression level of MIP-2 appeared to be 10-fold lower than the levels observed in the lung fibroblasts. Such reduction in BMDMs is most likely linked to the ability of macrophages to suppress the growth of *C. trachomatis* [214]. The results

from lung fibroblasts and BMDMs collectively confirm the role of mTRAIL-R as a negative regulator of the immune system.

Since the hTRAIL-R1 and 2 proteins are closely homologous to the mTRAIL-R, we predicted that TRAIL-R1 functions as a down-regulator of the immune response during *C. trachomatis* infection [192]. The pattern of low mRNA level of TRAIL-R1 at the early point of the infection and the increase at later stage can be related to the observed effect of *C. trachomatis* on the apoptosis process of the infected cells[129]. It is not clearly understood what mechanism or factors that *Chlamydia* uses to inhibit apoptosis during the early stages of the infection and this result indicates a possible role that TRAIL-R1 plays during this process [129,203].

The protein structures of both TRAIL-R1 and TRAIL-R2 greatly resemble each other. However, there are few distinct differences in which the N-linked glycosylation sites are present in TRAIL-R1 but not in TRAIL-R2, as wells as the absence of the sequences adjacent to the trans-membrane in TRAIL-R1 that TRAIL-R2 has [215]. Therefore, only TRAIL-R1-shRNA specific lentiviral particles were used to knockdown HeLa cells. The increased expression of IL-8 seen in TRAIL-R1 KD cells in response to *Chlamydia* infection further illustrates that TRIAL-R1 negatively regulates the immune response against *C. trachomatis*. The secretion of IL-8 has been associated with *C. trachomatis* infection of HeLa cells and used as an indication of the inflammatory response of the immune system[41,42,216]. Our results here show that TRAIL-R1 KD cells secreted higher

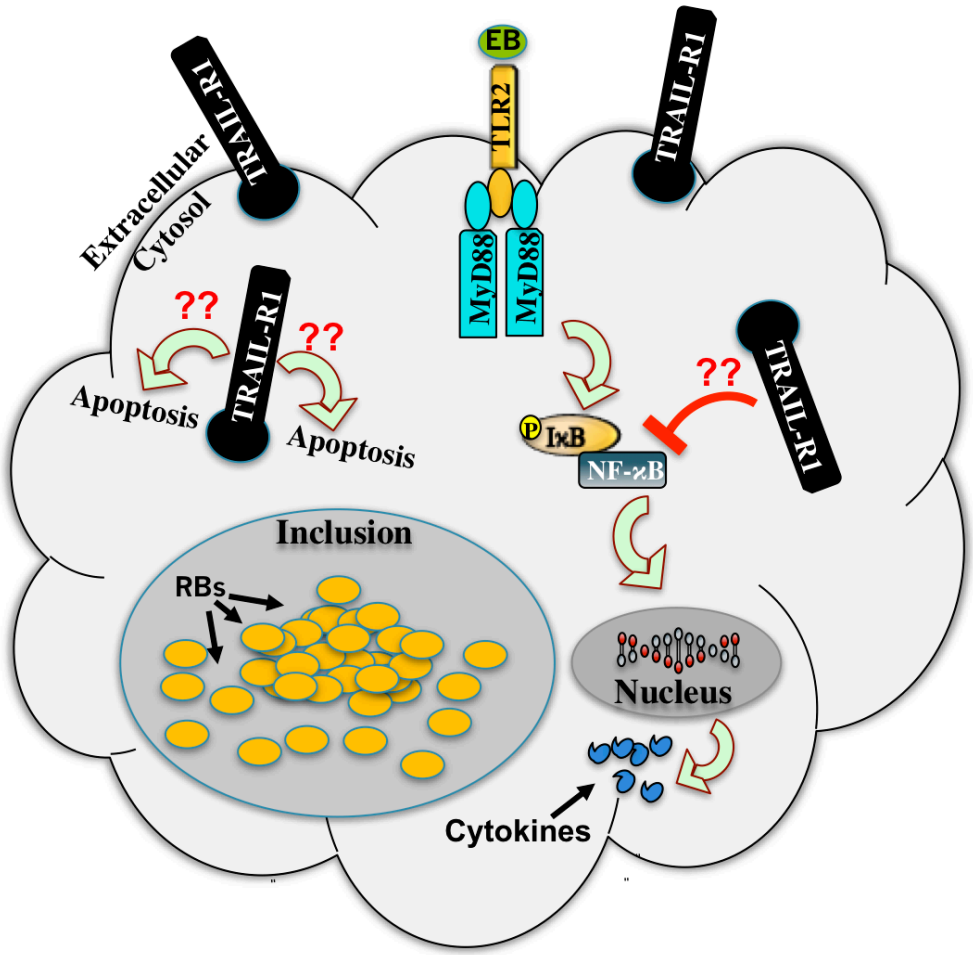

Figure 5.5: TRAIL-R1 model for regulating TLR activity. The presence of TRAIL-R1 during *C. trachomatis* infection leads to the reduction of pro-inflammatory cytokines via unknown mechanism. Cell death via TRAILR-R1 apoptotic pathway is likely to be involved.

levels of IL-8 compared to infected WT cells indicating its role in regulating inflammatory response.

In conclusion, the ex-vivo results presented here demonstrate that TRAIL-R is involved in the mechanisms that regulate some pro-inflammatory cytokines of primary lung fibroblast in response to infection of either *C. trachomatis* or *C. muridarum.* However, infection with *C. trachomatis*, but not *C. muridarum*, is capable of inducing such response in the BMDM cells. The different responses to *C. muridarum* infection observed between lung fibroblasts and BMDMs; and between *C. trachomatis* vs. *C. muridarum* infected BMDM raise the question of whether TRAIL-R negative regulation is tissue/strains specific.

This is the first report to show that hTRAIL-R1 functions as a negative regulator for inflammation in response to *C. trachomatis* in vitro. The mRNA expression and protein secretion of IL-8 is greatly increased in TRAIL-R1 KD cells. The exact mechanism, or the mediators that TRAIL-R1 interacts with, that leads to the reduction of pro-inflammatory response in humans is yet to be investigated. It is likely that the absence of TRAIL-R prevents apoptosis from occurring in the inflamed tissue, and therefore causes higher levels of proinflammatory response (Figure 5.5). Understanding these components and their cross-reaction with TRAIL-R1 could ultimately lead to the development of a therapeutic approach to minimize the side effects of inflammation when infection occurs.

Conclusion and Future Directions:

We have shown that absence of SIGIRR increases the level of IL-8 in *Chlamydia* infected cells. Our data also discloses the association of MyD88 with SIGIRR during *Chlamydia* infection that potentially links SIGIRR's inhibitory effect of the immune system. Our data also illustrates for the first time that TLR2 and TLR3, but not TLR4 signaling pathways are activated by *C. trachomatis*. Despite the fact that Triad3A does not affect TLR2, we predict that its interaction with TLR4 indirectly manipulates the activities of TLR2 during *C. trachomatis* infection. This phenomenon of TLR4 interaction with TLR2 in the absence of Triad3A that leads to a reduced activity of TLR2 is an interesting observation that is worth investigating. The study of genetic polymorphisms of both SIGIRR and Triad3A may also elucidate the variations in the immune responses during *Chlamydial* infection that may contribute to the persistence of *Chlamydia* and the complications that the bacteria cause.

Murine TRAIL-R functions as a negative regulator of pro-inflammatory response to both *C. trachomatis* and *C*. *muridarum.* The observed discrepancy of pro-inflammatory response between lung fibroblasts and BMDMs during *C*. *muridarum* infection*;* as well as the difference observed in BMDMs that were infected with either *C*. *trachomatis* or *C*. *muridarum* emphasizes the specificity of tissue/strains interaction. Our data illustrates, for the first time, that human TRAIL-R1, that normally involved in apoptosis, functions here as a negative regulator for inflammation during *C. trachomatis* infection. Since TRAIL-R1

known trigger apoptosis via FADD and caspase-8, and that *C. trachomatis* manipulate cell death during the infection, evaluating the effect of TRAILR-R1 absence or over expression on the activation of the apoptotic pathway during *Chlamydia* infection may explain the mechanism of action of TRAIL-R1 as a negative regulator.

Although we have shown that TRAIL-R1 is a negative regulator during *Chlamydia* infection, similar functions of TRAIL-R2, which is homologous to TRAIL-R1, remains unknown. Therefore, further analysis of the role of TRAIL-R2 could be carried out to determine if the absence of TRAIL-R2 alone, or in combination with TRAIL-R1, increases the pro-inflammatory cytokines in response to *Chlamydia* infection and establishes its role as negative regulator. In addition, TRAIL-R3 and 4, which both lack the death receptors in their cytosolic domain, are known as decoy receptors that could possibly neutralize TRAIL-R1 and 2 function. Experiments that overexpress either TRAIL-R3, 4, or both could reveal any possible role that these receptors may have in manipulating the innate immune response. Overall, the studies conducted here for SIGIRR, Triad3A and TRAIL-R were all done *in vitro*. Hence, conducting *in vivo* studies for these three genes, using *C*. *trachomatis* or *C*. *muridarum* strains, further confirms our finding about the role of these genes during infection.

Finally, in addition to the genes encoding intracellular negative regulators of TLR mediated inflammation, other genes, such as NLRx1 and NLRC5 are worth exploring since they have been reported to regulate inflammation [217,218]. A better understanding the different components and the cellular mechanisms that

regulate inflammation will be valuable in revealing host-pathogen interactions that can be utilized during the development of new therapeutic approaches and effective vaccine.

BIBLIOGRAPHY

1 Liew, F. Y., Xu, D., Brint, E. K. & O'Neill, L. A. Negative regulation of toll-like receptor-mediated immune responses. *Nat Rev Immunol* **5**, 446-458, doi:10.1038/nri1630 (2005).

2 Takeuchi, O. & Akira, S. Pattern recognition receptors and inflammation. *Cell* **140**, 805-820, doi:10.1016/j.cell.2010.01.022 (2010).

3 Clarke, I. N. Evolution of Chlamydia trachomatis. *Ann N Y Acad Sci* **1230**, E11-18, doi:10.1111/j.1749-6632.2011.06194.x (2011).

4 Everett, K. D., Bush, R. M. & Andersen, A. A. Emended description of the order Chlamydiales, proposal of Parachlamydiaceae fam. nov. and Simkaniaceae fam. nov., each containing one monotypic genus, revised taxonomy of the family Chlamydiaceae, including a new genus and five new species, and standards for the identification of organisms. *Int J Syst Bacteriol* **49 Pt 2**, 415-440 (1999).

5 Morrison, R. P., Lyng, K. & Caldwell, H. D. Chlamydial disease pathogenesis. Ocular hypersensitivity elicited by a genus-specific 57-kD protein. *The Journal of experimental medicine* **169**, 663-675 (1989).

6 Campbell, L. A. & Kuo, C. C. Chlamydia pneumoniae and atherosclerosis. *Semin Respir Infect* **18**, 48-54, doi:10.1053/srin.2003.50006 (2003).

7 DeGraves, F. J., Gao, D., Hehnen, H. R., Schlapp, T. & Kaltenboeck, B. Quantitative detection of Chlamydia psittaci and C. pecorum by high-sensitivity real-time PCR reveals high prevalence of vaginal infection in cattle. *Journal of clinical microbiology* **41**, 1726-1729 (2003).

8 Zhong, G., Fan, P., Ji, H., Dong, F. & Huang, Y. Identification of a chlamydial protease-like activity factor responsible for the degradation of host transcription factors. *The Journal of experimental medicine* **193**, 935-942 (2001).

9 Hueck, C. J. Type III protein secretion systems in bacterial pathogens of animals and plants. *Microbiol Mol Biol Rev* **62**, 379-433 (1998).

10 Miller, W. C. *et al.* Prevalence of chlamydial and gonococcal infections among young adults in the United States. *JAMA : the journal of the American Medical Association* **291**, 2229-2236, doi:10.1001/jama.291.18.2229 (2004).

11 Prevention. (ed CDC) (CDC, 2010).

12 World.Health.Organization. in http://www.who.int/vaccine_research/diseases/soa_std/en/index.html (2012).

13 Hamdad-Daoudi, F., Petit, J. & Eb, F. Assessment of Chlamydia trachomatis infection in asymptomatic male partners of infertile couples. *J Med Microbiol* **53**, 985-990 (2004).

14 Batteiger, B. E., Fraiz, J., Newhall, W. J., Katz, B. P. & Jones, R. B. Association of recurrent chlamydial infection with gonorrhea. *The Journal of infectious diseases* **159**, 661-669 (1989).

15 Somboonna, N. *et al.* Hypervirulent Chlamydia trachomatis clinical strain is a recombinant between lymphogranuloma venereum (L(2)) and D lineages. *MBio* **2**, e00045-00011, doi:10.1128/mBio.00045-11 (2011).

16 Gomes, J. P. *et al.* Evolution of Chlamydia trachomatis diversity occurs by widespread interstrain recombination involving hotspots. *Genome Res* **17**, 50-60, doi:10.1101/gr.5674706 (2007).

17 Fraiz, J. & Jones, R. B. Chlamydial infections. *Annu Rev Med* **39**, 357-370, doi:10.1146/annurev.me.39.020188.002041 (1988).

18 Spaargaren, J. *et al.* Slow epidemic of lymphogranuloma venereum L2b strain. *Emerg Infect Dis* **11**, 1787-1788, doi:10.3201/eid1111.050821 (2005).

19 Schachter, J. & Moncada, J. Lymphogranuloma venereum: how to turn an endemic disease into an outbreak of a new disease? Start looking. *Sexually transmitted diseases* **32**, 331-332 (2005).

20 Herring, A. & Richens, J. Lymphogranuloma venereum. *Sex Transm Infect* **82 Suppl 4**, iv23-25, doi:10.1136/sti.2006.023143 (2006).

21 Ramsey, K. H. *et al.* Strain and virulence diversity in the mouse pathogen Chlamydia muridarum. *Infection and immunity* **77**, 3284-3293, doi:10.1128/IAI.00147-09 (2009).

22 Byrne, G. I. Chlamydia trachomatis strains and virulence: rethinking links to infection prevalence and disease severity. *The Journal of infectious diseases* **201 Suppl 2**, S126-133, doi:10.1086/652398 (2010).

23 Pal, S., Peterson, E. M. & de la Maza, L. M. Vaccination with the Chlamydia trachomatis major outer membrane protein can elicit an immune response as protective as that resulting from inoculation with live bacteria. *Infection and immunity* **73**, 8153-8160, doi:10.1128/IAI.73.12.8153-8160.2005 (2005).

24 Grayston, J. T. *et al.* A new respiratory tract pathogen: Chlamydia pneumoniae strain TWAR. *The Journal of infectious diseases* **161**, 618-625 (1990).

25 Myers, G. S. *et al.* Evidence that human Chlamydia pneumoniae was zoonotically acquired. *J Bacteriol* **191**, 7225-7233, doi:10.1128/JB.00746-09 (2009).

26 Campbell, L. A. & Kuo, C. C. Chlamydia pneumoniae--an infectious risk factor for atherosclerosis? *Nature reviews. Microbiology* **2**, 23-32, doi:10.1038/nrmicro796 (2004).

27 Sutherland, E. R. & Martin, R. J. Asthma and atypical bacterial infection. *Chest* **132**, 1962-1966, doi:10.1378/chest.06-2415 (2007).

28 Leinonen, M. & Saikku, P. Evidence for infectious agents in cardiovascular disease and atherosclerosis. *Lancet Infect Dis* **2**, 11-17 (2002).

29 Sheehy, N., Markey, B., Gleeson, M. & Quinn, P. J. Differentiation of Chlamydia psittaci and C. pecorum strains by species-specific PCR. *Journal of clinical microbiology* **34**, 3175-3179 (1996).

30 Birkelund, S. The molecular biology and diagnostics of Chlamydia trachomatis. *Dan Med Bull* **39**, 304-320 (1992).

31 Hammerschlag, M. R. The intracellular life of chlamydiae. *Semin Pediatr Infect Dis* **13**, 239-248, doi:10.1053/spid.2002.127201 (2002).

32 Clifton, D. R. *et al.* A chlamydial type III translocated protein is tyrosine-phosphorylated at the site of entry and associated with recruitment of actin. *Proceedings of the National Academy of Sciences of the United States of America* **101**, 10166-10171, doi:10.1073/pnas.0402829101 (2004).

33 Scidmore, M. A., Fischer, E. R. & Hackstadt, T. Restricted fusion of Chlamydia trachomatis vesicles with endocytic compartments during the initial stages of infection. *Infection and immunity* **71**, 973-984 (2003).

34 Scidmore, M. A. & Hackstadt, T. Mammalian 14-3-3beta associates with the Chlamydia trachomatis inclusion membrane via its interaction with IncG. *Molecular microbiology* **39**, 1638-1650 (2001).

35 Shaw, E. I. *et al.* Three temporal classes of gene expression during the Chlamydia trachomatis developmental cycle. *Molecular microbiology* **37**, 913-925 (2000).

36 Nicholson, T. L., Olinger, L., Chong, K., Schoolnik, G. & Stephens, R. S. Global stage-specific gene regulation during the developmental cycle of Chlamydia trachomatis. *J Bacteriol* **185**, 3179-3189 (2003).

37 Janeway, C. A., Jr. & Medzhitov, R. Innate immune recognition. *Annu Rev Immunol* **20**, 197-216, doi:10.1146/annurev.immunol.20.083001.084359 (2002).

38 Akira, S., Uematsu, S. & Takeuchi, O. Pathogen recognition and innate immunity. *Cell* **124**, 783-801, doi:10.1016/j.cell.2006.02.015 (2006).

39 Karin, M., Lawrence, T. & Nizet, V. Innate immunity gone awry: linking microbial infections to chronic inflammation and cancer. *Cell* **124**, 823-835, doi:10.1016/j.cell.2006.02.016 (2006).

40 Dessus-Babus, S., Darville, T. L., Cuozzo, F. P., Ferguson, K. & Wyrick, P. B. Differences in innate immune responses (in vitro) to HeLa cells infected with nondisseminating serovar E and disseminating serovar L2 of Chlamydia trachomatis. *Infection and immunity* **70**, 3234-3248 (2002).

41 Rasmussen, S. J. *et al.* Secretion of proinflammatory cytokines by epithelial cells in response to Chlamydia infection suggests a central role for epithelial cells in chlamydial pathogenesis. *J Clin Invest* **99**, 77-87, doi:10.1172/JCI119136 (1997).

42 Buchholz, K. R. & Stephens, R. S. Activation of the host cell proinflammatory interleukin-8 response by Chlamydia trachomatis. *Cell Microbiol* **8**, 1768-1779, doi:10.1111/j.1462-5822.2006.00747.x (2006).

43 Darville, T. & Hiltke, T. J. Pathogenesis of genital tract disease due to Chlamydia trachomatis. *The Journal of infectious diseases* **201 Suppl 2**, S114-125 (2010).

44 Roan, N. R. & Starnbach, M. N. Immune-mediated control of Chlamydia infection. *Cellular microbiology* **10**, 9-19, doi:10.1111/j.1462-5822.2007.01069.x (2008).

45 Prantner, D. *et al.* Critical role for interleukin-1beta (IL-1beta) during Chlamydia muridarum genital infection and bacterial replication-independent secretion of IL-1beta in mouse macrophages. *Infection and immunity* **77**, 5334-5346, doi:10.1128/IAI.00883-09 (2009).

46 Gervassi, A. *et al.* Differential regulation of inflammatory cytokine secretion by human dendritic cells upon Chlamydia trachomatis infection. *Infection and immunity* **72**, 7231-7239, doi:10.1128/IAI.72.12.7231-7239.2004 (2004).

47 van Zandbergen, G. *et al.* Chlamydia pneumoniae multiply in neutrophil granulocytes and delay their spontaneous apoptosis. *Journal of immunology* **172**, 1768-1776 (2004).

48 Buendia, A. J. *et al.* B-cell-deficient mice show an exacerbated inflammatory response in a model of Chlamydophila abortus infection. *Infection and immunity* **70**, 6911-6918 (2002).

49 Beckett, E. L. *et al.* TLR2, but Not TLR4, Is Required for Effective Host Defence against Chlamydia Respiratory Tract Infection in Early Life. *PLoS One* **7**, e39460, doi:10.1371/journal.pone.0039460 (2012).

50 Rothfuchs, A. G., Kreuger, M. R., Wigzell, H. & Rottenberg, M. E. Macrophages, CD4+ or CD8+ cells are each sufficient for protection against Chlamydia pneumoniae infection through their ability to secrete IFN-gamma. *Journal of immunology* **172**, 2407-2415 (2004).

51 Pioli, P. A. *et al.* Differential expression of Toll-like receptors 2 and 4 in tissues of the human female reproductive tract. *Infection and immunity* **72**, 5799-5806, doi:10.1128/IAI.72.10.5799-5806.2004 (2004).

52 Bas, S. *et al.* The proinflammatory cytokine response to Chlamydia trachomatis elementary bodies in human macrophages is partly mediated by a lipoprotein, the macrophage infectivity potentiator, through TLR2/TLR1/TLR6 and CD14. *Journal of immunology* **180**, 1158-1168 (2008).

53 Ghuysen, J. M. & Goffin, C. Lack of cell wall peptidoglycan versus penicillin sensitivity: new insights into the chlamydial anomaly. *Antimicrobial agents and chemotherapy* **43**, 2339-2344 (1999).

54 Skilton, R. J. *et al.* Penicillin induced persistence in Chlamydia trachomatis: high quality time lapse video analysis of the developmental cycle. *PLoS One* **4**, e7723, doi:10.1371/journal.pone.0007723 (2009).

55 Hashimoto, C., Hudson, K. L. & Anderson, K. V. The Toll gene of Drosophila, required for dorsal-ventral embryonic polarity, appears to encode a transmembrane protein. *Cell* **52**, 269-279 (1988).

56 Lemaitre, B., Nicolas, E., Michaut, L., Reichhart, J. M. & Hoffmann, J. A. The dorsoventral regulatory gene cassette spatzle/Toll/cactus controls the potent antifungal response in Drosophila adults. *Cell* **86**, 973-983 (1996).

57 Takeda, K., Kaisho, T. & Akira, S. Toll-like receptors. *Annu Rev Immunol* **21**, 335-376, doi:10.1146/annurev.immunol.21.120601.141126 (2003).

58 Lien, E. *et al.* Toll-like receptor 2 functions as a pattern recognition receptor for diverse bacterial products. *The Journal of biological chemistry* **274**, 33419-33425 (1999).

59 Lehner, M. D., Morath, S., Michelsen, K. S., Schumann, R. R. & Hartung, T. Induction of cross-tolerance by lipopolysaccharide and highly purified lipoteichoic acid via different Toll-like receptors independent of paracrine mediators. *Journal of immunology* **166**, 5161-5167 (2001).

60 Ozinsky, A. *et al.* The repertoire for pattern recognition of pathogens by the innate immune system is defined by cooperation between toll-like receptors. *Proceedings of the National Academy of Sciences of the United States of America* **97**, 13766-13771, doi:10.1073/pnas.250476497 (2000).

61 Gantner, B. N., Simmons, R. M., Canavera, S. J., Akira, S. & Underhill, D. M. Collaborative induction of inflammatory responses by dectin-1 and Toll-like receptor 2. *The Journal of experimental medicine* **197**, 1107-1117, doi:10.1084/jem.20021787 (2003).

62 Muzio, M. *et al.* Differential expression and regulation of toll-like receptors (TLR) in human leukocytes: selective expression of TLR3 in dendritic cells. *Journal of immunology* **164**, 5998-6004 (2000).

63 Monroe, K. M., McWhirter, S. M. & Vance, R. E. Induction of type I interferons by bacteria. *Cellular microbiology* **12**, 881-890, doi:10.1111/j.1462-5822.2010.01478.x (2010).

64 Applequist, S. E., Wallin, R. P. & Ljunggren, H. G. Variable expression of Toll-like receptor in murine innate and adaptive immune cell lines. *International immunology* **14**, 1065-1074 (2002).

65 Medzhitov, R., Preston-Hurlburt, P. & Janeway, C. A., Jr. A human homologue of the Drosophila Toll protein signals activation of adaptive immunity. *Nature* **388**, 394-397, doi:10.1038/41131 (1997).

66 Lavelle, E. C., Murphy, C., O'Neill, L. A. & Creagh, E. M. The role of TLRs, NLRs, and RLRs in mucosal innate immunity and homeostasis. *Mucosal Immunol* **3**, 17-28, doi:10.1038/mi.2009.124 (2010).

67 da Silva Correia, J., Soldau, K., Christen, U., Tobias, P. S. & Ulevitch, R. J. Lipopolysaccharide is in close proximity to each of the proteins in its membrane receptor complex. transfer from CD14 to TLR4 and MD-2. *The Journal of biological chemistry* **276**, 21129-21135, doi:10.1074/jbc.M009164200 (2001).

68 Tanimura, N., Saitoh, S., Matsumoto, F., Akashi-Takamura, S. & Miyake, K. Roles for LPS-dependent interaction and relocation of TLR4 and TRAM in TRIF-signaling. *Biochemical and biophysical research communications* **368**, 94-99, doi:10.1016/j.bbrc.2008.01.061 (2008).

69 Chuang, T. H. & Ulevitch, R. J. Triad3A, an E3 ubiquitin-protein ligase regulating Toll-like receptors. *Nature immunology* **5**, 495-502, doi:10.1038/ni1066 (2004).

70 Kagan, J. C. *et al.* TRAM couples endocytosis of Toll-like receptor 4 to the induction of interferon-beta. *Nature immunology* **9**, 361-368, doi:10.1038/ni1569 (2008).

71 Poltorak, A. *et al.* Defective LPS signaling in C3H/HeJ and C57BL/10ScCr mice: mutations in Tlr4 gene. *Science* **282**, 2085-2088 (1998).

72 O'Neill, L. A., Fitzgerald, K. A. & Bowie, A. G. The Toll-IL-1 receptor adaptor family grows to five members. *Trends Immunol* **24**, 286-290 (2003).

73 Medzhitov, R. *et al.* MyD88 is an adaptor protein in the hToll/IL-1 receptor family signaling pathways. *Mol Cell* **2**, 253-258 (1998).

74 Brikos, C., Wait, R., Begum, S., O'Neill, L. A. & Saklatvala, J. Mass spectrometric analysis of the endogenous type I interleukin-1 (IL-1) receptor signaling complex formed after IL-1 binding identifies IL-1RAcP, MyD88, and IRAK-4 as the stable components. *Mol Cell Proteomics* **6**, 1551-1559, doi:10.1074/mcp.M600455-MCP200 (2007).

75 Cao, Z., Xiong, J., Takeuchi, M., Kurama, T. & Goeddel, D. V. TRAF6 is a signal transducer for interleukin-1. *Nature* **383**, 443-446, doi:10.1038/383443a0 (1996).

76 Cao, Z., Henzel, W. J. & Gao, X. IRAK: a kinase associated with the interleukin-1 receptor. *Science* **271**, 1128-1131 (1996).

77 Walsh, M. C., Kim, G. K., Maurizio, P. L., Molnar, E. E. & Choi, Y. TRAF6 autoubiquitination-independent activation of the NFkappaB and MAPK pathways in response to IL-1 and RANKL. *PLoS One* **3**, e4064, doi:10.1371/journal.pone.0004064 (2008).

78 Ghosh, S., May, M. J. & Kopp, E. B. NF-kappa B and Rel proteins: evolutionarily conserved mediators of immune responses. *Annu Rev Immunol* **16**, 225-260, doi:10.1146/annurev.immunol.16.1.225 (1998).

79 Dessus-Babus, S., Knight, S. T. & Wyrick, P. B. Chlamydial infection of polarized HeLa cells induces PMN chemotaxis but the cytokine profile varies between disseminating and non-disseminating strains. *Cell Microbiol* **2**, 317-327 (2000).

80 Lu, H., Shen, C. & Brunham, R. C. Chlamydia trachomatis infection of epithelial cells induces the activation of caspase-1 and release of mature IL-18. *Journal of immunology* **165**, 1463-1469 (2000).

81 Negishi, H. *et al.* Evidence for licensing of IFN-gamma-induced IFN regulatory factor 1 transcription factor by MyD88 in Toll-like receptor-

dependent gene induction program. *Proceedings of the National Academy of Sciences of the United States of America* **103**, 15136-15141, doi:10.1073/pnas.0607181103 (2006).

82 Oganesyan, G. *et al.* Critical role of TRAF3 in the Toll-like receptor-dependent and -independent antiviral response. *Nature* **439**, 208-211, doi:10.1038/nature04374 (2006).

83 Fitzgerald, K. A. *et al.* LPS-TLR4 signaling to IRF-3/7 and NF-kappaB involves the toll adapters TRAM and TRIF. *The Journal of experimental medicine* **198**, 1043-1055, doi:10.1084/jem.20031023 (2003).

84 Hacker, H. *et al.* Specificity in Toll-like receptor signalling through distinct effector functions of TRAF3 and TRAF6. *Nature* **439**, 204-207, doi:10.1038/nature04369 (2006).

85 Campbell, L. A. *et al.* Detection of Chlamydia trachomatis deoxyribonucleic acid in women with tubal infertility. *Fertility and sterility* **59**, 45-50 (1993).

86 Kiviat, N. B. *et al.* Localization of Chlamydia trachomatis infection by direct immunofluorescence and culture in pelvic inflammatory disease. *American journal of obstetrics and gynecology* **154**, 865-873 (1986).

87 Fan, P., Dong, F., Huang, Y. & Zhong, G. Chlamydia pneumoniae secretion of a protease-like activity factor for degrading host cell transcription factors required for [correction of factors is required for] major histocompatibility complex antigen expression. *Infection and immunity* **70**, 345-349 (2002).

88 Hogan, R. J., Mathews, S. A., Mukhopadhyay, S., Summersgill, J. T. & Timms, P. Chlamydial persistence: beyond the biphasic paradigm. *Infection and immunity* **72**, 1843-1855 (2004).

89 Serhan, C. N. *et al.* Resolution of inflammation: state of the art, definitions and terms. *FASEB journal : official publication of the Federation of American Societies for Experimental Biology* **21**, 325-332, doi:10.1096/fj.06-7227rev (2007).

90 Iwami, K. I. *et al.* Cutting edge: naturally occurring soluble form of mouse Toll-like receptor 4 inhibits lipopolysaccharide signaling. *Journal of immunology* **165**, 6682-6686 (2000).

91 Iwaki, D. *et al.* The extracellular toll-like receptor 2 domain directly binds peptidoglycan derived from Staphylococcus aureus. *The Journal of biological chemistry* **277**, 24315-24320, doi:10.1074/jbc.M107057200 (2002).

92 LeBouder, E. *et al.* Soluble forms of Toll-like receptor (TLR)2 capable of modulating TLR2 signaling are present in human plasma and breast milk. *Journal of immunology* **171**, 6680-6689 (2003).

93 Raby, A. C. *et al.* Soluble TLR2 reduces inflammation without compromising bacterial clearance by disrupting TLR2 triggering. *Journal of immunology* **183**, 506-517, doi:10.4049/jimmunol.0802909 (2009).

94 Gray, P. *et al.* Identification of a novel human MD-2 splice variant that negatively regulates Lipopolysaccharide-induced TLR4 signaling. *Journal of immunology* **184**, 6359-6366, doi:10.4049/jimmunol.0903543 (2010).

95 Janssens, S., Burns, K., Vercammen, E., Tschopp, J. & Beyaert, R. MyD88S, a splice variant of MyD88, differentially modulates NF-kappaB- and AP-1-dependent gene expression. *FEBS letters* **548**, 103-107 (2003).

96 Palsson-McDermott, E. M. *et al.* TAG, a splice variant of the adaptor TRAM, negatively regulates the adaptor MyD88-independent TLR4 pathway. *Nature immunology* **10**, 579-586, doi:10.1038/ni.1727 (2009).

97 Rao, N., Nguyen, S., Ngo, K. & Fung-Leung, W. P. A novel splice variant of interleukin-1 receptor (IL-1R)-associated kinase 1 plays a negative regulatory role in Toll/IL-1R-induced inflammatory signaling. *Mol Cell Biol* **25**, 6521-6532, doi:10.1128/MCB.25.15.6521-6532.2005 (2005).

98 Hardy, M. P. & O'Neill, L. A. The murine IRAK2 gene encodes four alternatively spliced isoforms, two of which are inhibitory. *The Journal of biological chemistry* **279**, 27699-27708, doi:10.1074/jbc.M403068200 (2004).

99 Haglund, K. & Dikic, I. Ubiquitylation and cell signaling. *Embo J* **24**, 3353-3359, doi:10.1038/sj.emboj.7600808 (2005).

100 Shembade, N., Ma, A. & Harhaj, E. W. Inhibition of NF-kappaB signaling by A20 through disruption of ubiquitin enzyme complexes. *Science* **327**, 1135-1139, doi:10.1126/science.1182364 (2010).

101 Wertz, I. E. *et al.* De-ubiquitination and ubiquitin ligase domains of A20 downregulate NF-kappaB signalling. *Nature* **430**, 694-699, doi:10.1038/nature02794 (2004).

102 Boone, D. L. *et al.* The ubiquitin-modifying enzyme A20 is required for termination of Toll-like receptor responses. *Nature immunology* **5**, 1052-1060, doi:10.1038/ni1110 (2004).

103 Kawagoe, T. *et al.* TANK is a negative regulator of Toll-like receptor signaling and is critical for the prevention of autoimmune nephritis. *Nature immunology* **10**, 965-972, doi:10.1038/ni.1771 (2009).

104 Nakagawa, R. *et al.* SOCS-1 participates in negative regulation of LPS responses. *Immunity* **17**, 677-687 (2002).

105 Kinjyo, I. *et al.* SOCS1/JAB is a negative regulator of LPS-induced macrophage activation. *Immunity* **17**, 583-591 (2002).

106 Yasukawa, H. *et al.* IL-6 induces an anti-inflammatory response in the absence of SOCS3 in macrophages. *Nature immunology* **4**, 551-556, doi:10.1038/ni938 (2003).

107 Ryo, A. *et al.* Regulation of NF-kappaB signaling by Pin1-dependent prolyl isomerization and ubiquitin-mediated proteolysis of p65/RelA. *Mol Cell* **12**, 1413-1426 (2003).

108 Mansell, A. *et al.* Suppressor of cytokine signaling 1 negatively regulates Toll-like receptor signaling by mediating Mal degradation. *Nature immunology* **7**, 148-155, doi:10.1038/ni1299 (2006).

109 Xiao, H. *et al.* Pellino 3b negatively regulates interleukin-1-induced TAK1-dependent NF kappaB activation. *The Journal of biological chemistry* **283**, 14654-14664, doi:10.1074/jbc.M706931200 (2008).

110 Muroi, M. & Tanamoto, K. IRAK-1-mediated negative regulation of Toll-like receptor signaling through proteasome-dependent downregulation of TRAF6. *Biochimica et biophysica acta* **1823**, 255-263, doi:10.1016/j.bbamcr.2011.10.003 (2012).

111 Cohen, P. The regulation of protein function by multisite phosphorylation--a 25 year update. *Trends in biochemical sciences* **25**, 596-601 (2000).

112 Kuo, C. C., Lin, W. T., Liang, C. M. & Liang, S. M. Class I and III phosphatidylinositol 3'-kinase play distinct roles in TLR signaling pathway. *Journal of immunology* **176**, 5943-5949 (2006).

113 Rhee, S. H., Kim, H., Moyer, M. P. & Pothoulakis, C. Role of MyD88 in phosphatidylinositol 3-kinase activation by flagellin/toll-like receptor 5 engagement in colonic epithelial cells. *The Journal of biological chemistry* **281**, 18560-18568, doi:10.1074/jbc.M513861200 (2006).

114 Yum, H. K. *et al.* Involvement of phosphoinositide 3-kinases in neutrophil activation and the development of acute lung injury. *Journal of immunology* **167**, 6601-6608 (2001).

115 Diaz-Guerra, M. J., Castrillo, A., Martin-Sanz, P. & Bosca, L. Negative regulation by phosphatidylinositol 3-kinase of inducible nitric oxide synthase expression in macrophages. *Journal of immunology* **162**, 6184-6190 (1999).

116 Guha, M. & Mackman, N. The phosphatidylinositol 3-kinase-Akt pathway limits lipopolysaccharide activation of signaling pathways and expression of inflammatory mediators in human monocytic cells. *The Journal of biological chemistry* **277**, 32124-32132, doi:10.1074/jbc.M203298200 (2002).

117 Aksoy, E. *et al.* Inhibition of phosphoinositide 3-kinase enhances TRIF-dependent NF-kappa B activation and IFN-beta synthesis downstream of Toll-like receptor 3 and 4. *European journal of immunology* **35**, 2200-2209, doi:10.1002/eji.200425801 (2005).

118 Fukao, T. *et al.* PI3K-mediated negative feedback regulation of IL-12 production in DCs. *Nature immunology* **3**, 875-881, doi:10.1038/ni825 (2002).

119 Hazeki, K., Nigorikawa, K. & Hazeki, O. Role of phosphoinositide 3-kinase in innate immunity. *Biol Pharm Bull* **30**, 1617-1623 (2007).

120 Burns, K. *et al.* Tollip, a new component of the IL-1RI pathway, links IRAK to the IL-1 receptor. *Nat Cell Biol* **2**, 346-351, doi:10.1038/35014038 (2000).

121 Zhang, G. & Ghosh, S. Negative regulation of toll-like receptor-mediated signaling by Tollip. *The Journal of biological chemistry* **277**, 7059-7065, doi:10.1074/jbc.M109537200 (2002).
122 Huang, R. *et al.* Identification, characterization and the interaction of Tollip and IRAK-1 in grass carp (Ctenopharyngodon idellus). *Fish Shellfish Immunol* **33**, 459-467, doi:10.1016/j.fsi.2012.05.025 (2012).
123 Kobayashi, K. *et al.* IRAK-M is a negative regulator of Toll-like receptor signaling. *Cell* **110**, 191-202 (2002).
124 Wald, D. *et al.* SIGIRR, a negative regulator of Toll-like receptor-interleukin 1 receptor signaling. *Nature immunology* **4**, 920-927, doi:10.1038/ni968 (2003).
125 An, H. *et al.* Phosphatase SHP-1 promotes TLR- and RIG-I-activated production of type I interferon by inhibiting the kinase IRAK1. *Nature immunology* **9**, 542-550, doi:10.1038/ni.1604 (2008).
126 An, H. *et al.* SHP-2 phosphatase negatively regulates the TRIF adaptor protein-dependent type I interferon and proinflammatory cytokine production. *Immunity* **25**, 919-928, doi:10.1016/j.immuni.2006.10.014 (2006).
127 Elmore, S. Apoptosis: a review of programmed cell death. *Toxicol Pathol* **35**, 495-516, doi:10.1080/01926230701320337 (2007).
128 Ruckdeschel, K. *et al.* Yersinia outer protein P of Yersinia enterocolitica simultaneously blocks the nuclear factor-kappa B pathway and exploits lipopolysaccharide signaling to trigger apoptosis in macrophages. *Journal of immunology* **166**, 1823-1831 (2001).
129 Ying, S., Pettengill, M., Ojcius, D. M. & Hacker, G. Host-Cell Survival and Death During Chlamydia Infection. *Current immunology reviews* **3**, 31-40, doi:10.2174/157339507779802179 (2007).
130 Kobayashi, S. D., Voyich, J. M., Braughton, K. R. & DeLeo, F. R. Down-regulation of proinflammatory capacity during apoptosis in human polymorphonuclear leukocytes. *Journal of immunology* **170**, 3357-3368 (2003).
131 Nagata, S. Fas ligand-induced apoptosis. *Annu Rev Genet* **33**, 29-55, doi:10.1146/annurev.genet.33.1.29 (1999).
132 Bannerman, D. D., Tupper, J. C., Kelly, J. D., Winn, R. K. & Harlan, J. M. The Fas-associated death domain protein suppresses activation of NF-kappa B by LPS and IL-1 beta. *J Clin Invest* **109**, 419-425, doi:10.1172/JCI14774 (2002).
133 Zhande, R. *et al.* FADD negatively regulates lipopolysaccharide signaling by impairing interleukin-1 receptor-associated kinase 1-MyD88 interaction. *Mol Cell Biol* **27**, 7394-7404, doi:10.1128/MCB.00600-07 (2007).
134 Aliprantis, A. O., Yang, R. B., Weiss, D. S., Godowski, P. & Zychlinsky, A. The apoptotic signaling pathway activated by Toll-like receptor-2. *Embo J* **19**, 3325-3336, doi:10.1093/emboj/19.13.3325 (2000).

135 Kim, S. O., Ono, K., Tobias, P. S. & Han, J. Orphan nuclear receptor Nur77 is involved in caspase-independent macrophage cell death. *The Journal of experimental medicine* **197**, 1441-1452, doi:10.1084/jem.20021842 (2003).

136 Cabanski, M. *et al.* PKR regulates TLR2/TLR4-dependent signaling in murine alveolar macrophages. *Am J Respir Cell Mol Biol* **38**, 26-31, doi:10.1165/rcmb.2007-0010OC (2008).

137 Zamanian-Daryoush, M., Mogensen, T. H., DiDonato, J. A. & Williams, B. R. NF-kappaB activation by double-stranded-RNA-activated protein kinase (PKR) is mediated through NF-kappaB-inducing kinase and IkappaB kinase. *Mol Cell Biol* **20**, 1278-1290 (2000).

138 Lu, B. *et al.* Novel role of PKR in inflammasome activation and HMGB1 release. *Nature*, doi:10.1038/nature11290 (2012).

139 Hsu, L. C. *et al.* The protein kinase PKR is required for macrophage apoptosis after activation of Toll-like receptor 4. *Nature* **428**, 341-345, doi:10.1038/nature02405 (2004).

140 Sun, R. *et al.* Toll-like receptor 3 (TLR3) induces apoptosis via death receptors and mitochondria by up-regulating the transactivating p63 isoform alpha (TAP63alpha). *The Journal of biological chemistry* **286**, 15918-15928, doi:10.1074/jbc.M110.178798 (2011).

141 Zeng, H. *et al.* Flagellin/TLR5 responses in epithelia reveal intertwined activation of inflammatory and apoptotic pathways. *American journal of physiology. Gastrointestinal and liver physiology* **290**, G96-G108, doi:10.1152/ajpgi.00273.2005 (2006).

142 Lim, E. J. *et al.* Toll-like receptor 9-mediated inhibition of apoptosis occurs through suppression of FoxO3a activity and induction of FLIP expression. *Exp Mol Med* **42**, 712-720 (2010).

143 Omsland, A., Sager, J., Nair, V., Sturdevant, D. E. & Hackstadt, T. Developmental stage-specific metabolic and transcriptional activity of Chlamydia trachomatis in an axenic medium. *Proceedings of the National Academy of Sciences of the United States of America* **109**, 19781-19785, doi:10.1073/pnas.1212831109 (2012).

144 Carabeo, R. A., Mead, D. J. & Hackstadt, T. Golgi-dependent transport of cholesterol to the Chlamydia trachomatis inclusion. *Proceedings of the National Academy of Sciences of the United States of America* **100**, 6771-6776, doi:10.1073/pnas.1131289100 (2003).

145 Pokrovskaya, I. D. *et al.* Chlamydia trachomatis hijacks intra-Golgi COG complex-dependent vesicle trafficking pathway. *Cellular microbiology* **14**, 656-668, doi:10.1111/j.1462-5822.2012.01747.x (2012).

146 Fields, K. A. & Hackstadt, T. The chlamydial inclusion: escape from the endocytic pathway. *Annu Rev Cell Dev Biol* **18**, 221-245, doi:10.1146/annurev.cellbio.18.012502.105845 (2002).

147 Le Negrate, G. *et al.* ChlaDub1 of Chlamydia trachomatis suppresses NF-kappaB activation and inhibits IkappaBalpha ubiquitination and degradation. *Cellular microbiology* **10**, 1879-1892, doi:10.1111/j.1462-5822.2008.01178.x (2008).

148 Misaghi, S. *et al.* Chlamydia trachomatis-derived deubiquitinating enzymes in mammalian cells during infection. *Molecular microbiology* **61**, 142-150, doi:10.1111/j.1365-2958.2006.05199.x (2006).

149 Stenner-Liewen, F. *et al.* CADD, a Chlamydia protein that interacts with death receptors. *The Journal of biological chemistry* **277**, 9633-9636, doi:10.1074/jbc.C100693200 (2002).

150 Mehlitz, A., Banhart, S., Hess, S., Selbach, M. & Meyer, T. F. Complex kinase requirements for Chlamydia trachomatis Tarp phosphorylation. *FEMS Microbiol Lett* **289**, 233-240, doi:10.1111/j.1574-6968.2008.01390.x (2008).

151 Abdul-Sater, A. A., Said-Sadier, N., Padilla, E. V. & Ojcius, D. M. Chlamydial infection of monocytes stimulates IL-1beta secretion through activation of the NLRP3 inflammasome. *Microbes and infection / Institut Pasteur* **12**, 652-661, doi:10.1016/j.micinf.2010.04.008 (2010).

152 Scidmore, M. A. Cultivation and Laboratory Maintenance of Chlamydia trachomatis. *Curr Protoc Microbiol* **Chapter 11**, Unit 11A 11, doi:10.1002/9780471729259.mc11a01s00 (2005).

153 Perfettini, J. L. *et al.* Role of proapoptotic BAX in propagation of Chlamydia muridarum (the mouse pneumonitis strain of Chlamydia trachomatis) and the host inflammatory response. *J Biol Chem* **278**, 9496-9502, doi:10.1074/jbc.M211275200
M211275200 [pii] (2003).

154 Diehl, G. E. *et al.* TRAIL-R as a negative regulator of innate immune cell responses. *Immunity* **21**, 877-889, doi:10.1016/j.immuni.2004.11.008 (2004).

155 Garlanda, C. *et al.* Intestinal inflammation in mice deficient in Tir8, an inhibitory member of the IL-1 receptor family. *Proceedings of the National Academy of Sciences of the United States of America* **101**, 3522-3526, doi:10.1073/pnas.0308680101 (2004).

156 Xiao, H. *et al.* The Toll-interleukin-1 receptor member SIGIRR regulates colonic epithelial homeostasis, inflammation, and tumorigenesis. *Immunity* **26**, 461-475, doi:10.1016/j.immuni.2007.02.012 (2007).

157 Lech, M. *et al.* Different roles of TiR8/Sigirr on toll-like receptor signaling in intrarenal antigen-presenting cells and tubular epithelial cells. *Kidney Int* **72**, 182-192, doi:10.1038/sj.ki.5002293 (2007).

158 Batliwalla, F. M. *et al.* Microarray analyses of peripheral blood cells identifies unique gene expression signature in psoriatic arthritis. *Mol Med* **11**, 21-29, doi:10.2119/2006-00003.Gulko (2005).

159 Bulek, K. *et al.* The essential role of single Ig IL-1 receptor-related molecule/Toll IL-1R8 in regulation of Th2 immune response. *Journal of immunology* **182**, 2601-2609, doi:10.4049/jimmunol.0802729 (2009).

160 Lech, M. *et al.* Tir8/Sigirr prevents murine lupus by suppressing the immunostimulatory effects of lupus autoantigens. *The Journal of experimental medicine* **205**, 1879-1888, doi:10.1084/jem.20072646 (2008).

161 Noris, M. *et al.* The Toll-IL-1R member Tir8/SIGIRR negatively regulates adaptive immunity against kidney grafts. *Journal of immunology* **183**, 4249-4260, doi:10.4049/jimmunol.0803549 (2009).

162 Bozza, S. *et al.* Lack of Toll IL-1R8 exacerbates Th17 cell responses in fungal infection. *Journal of immunology* **180**, 4022-4031 (2008).

163 Garlanda, C. *et al.* Damping excessive inflammation and tissue damage in Mycobacterium tuberculosis infection by Toll IL-1 receptor 8/single Ig IL-1-related receptor, a negative regulator of IL-1/TLR signaling. *Journal of immunology* **179**, 3119-3125 (2007).

164 Huang, X., Hazlett, L. D., Du, W. & Barrett, R. P. SIGIRR promotes resistance against Pseudomonas aeruginosa keratitis by down-regulating type-1 immunity and IL-1R1 and TLR4 signaling. *Journal of immunology* **177**, 548-556 (2006).

165 Adib-Conquy, M. *et al.* Up-regulation of MyD88s and SIGIRR, molecules inhibiting Toll-like receptor signaling, in monocytes from septic patients. *Crit Care Med* **34**, 2377-2385, doi:10.1097/01.CCM.0000233875.93866.88 (2006).

166 Veliz Rodriguez, T. *et al.* Role of Toll interleukin-1 receptor (IL-1R) 8, a negative regulator of IL-1R/Toll-like receptor signaling, in resistance to acute Pseudomonas aeruginosa lung infection. *Infection and immunity* **80**, 100-109, doi:10.1128/IAI.05695-11 (2012).

167 Qin, J., Qian, Y., Yao, J., Grace, C. & Li, X. SIGIRR inhibits interleukin-1 receptor- and toll-like receptor 4-mediated signaling through different mechanisms. *The Journal of biological chemistry* **280**, 25233-25241, doi:10.1074/jbc.M501363200 (2005).

168 Zhang, C., Wu, X., Zhao, Y., Deng, Z. & Qian, G. SIGIRR inhibits toll-like receptor 4, 5, 9-mediated immune responses in human airway epithelial cells. *Molecular biology reports* **38**, 601-609, doi:10.1007/s11033-010-0146-7 (2011).

169 Gong, J. *et al.* Inhibition of Toll-like receptors TLR4 and 7 signaling pathways by SIGIRR: a computational approach. *J Struct Biol* **169**, 323-330, doi:10.1016/j.jsb.2009.12.007 (2010).

170 Drexler, S. K. *et al.* Evidence for a DC-specific inhibitory mechanism that depends on MyD88 and SIGIRR. *Scand J Immunol* **71**, 393-402, doi:10.1111/j.1365-3083.2010.02392.x (2010).

171 Qin, J., Qian, Y., Yao, J., Grace, C. & Li, X. SIGIRR inhibits interleukin-1 receptor- and toll-like receptor 4-mediated signaling through different mechanisms. *J Biol Chem* **280**, 25233-25241, doi:10.1074/jbc.M501363200 (2005).

172 Feng, T. *The Role of SIGIRR in LPS-Induced Acute Inflammatory Response in Human Type II Alveolar Epithelial Cells (A549)* PhD thesis, Fourth Military Medical University, (2010).

173 Urbonas, V., Eidukaite, A. & Tamuliene, I. The diagnostic value of interleukin-6 and interleukin-8 for early prediction of bacteremia and sepsis in children with febrile neutropenia and cancer. *J Pediatr Hematol Oncol* **34**, 122-127, doi:10.1097/MPH.0b013e3182446a60 (2012).

174 Fiedler, M. A., Wernke-Dollries, K. & Stark, J. M. Respiratory syncytial virus increases IL-8 gene expression and protein release in A549 cells. *The American journal of physiology* **269**, L865-872 (1995).

175 Kwon, O. J. *et al.* Tumor necrosis factor-induced interleukin-8 expression in cultured human airway epithelial cells. *The American journal of physiology* **267**, L398-405 (1994).

176 O'Connell, C. M., Ionova, I. A., Quayle, A. J., Visintin, A. & Ingalls, R. R. Localization of TLR2 and MyD88 to Chlamydia trachomatis inclusions. Evidence for signaling by intracellular TLR2 during infection with an obligate intracellular pathogen. *The Journal of biological chemistry* **281**, 1652-1659, doi:10.1074/jbc.M510182200 (2006).

177 van der Reijden, B. A., Erpelinck-Verschueren, C. A., Lowenberg, B. & Jansen, J. H. TRIADs: a new class of proteins with a novel cysteine-rich signature. *Protein Sci* **8**, 1557-1561, doi:10.1110/ps.8.7.1557 (1999).

178 Chen, D., Li, X., Zhai, Z. & Shu, H. B. A novel zinc finger protein interacts with receptor-interacting protein (RIP) and inhibits tumor necrosis factor (TNF)- and IL1-induced NF-kappa B activation. *The Journal of biological chemistry* **277**, 15985-15991, doi:10.1074/jbc.M108675200 (2002).

179 Miah, S. M. *et al.* Ubiquitylation of an internalized killer cell Ig-like receptor by Triad3A disrupts sustained NF-kappaB signaling. *Journal of immunology* **186**, 2959-2969, doi:10.4049/jimmunol.1000112 (2011).

180 Fearns, C., Pan, Q., Mathison, J. C. & Chuang, T. H. Triad3A regulates ubiquitination and proteasomal degradation of RIP1 following disruption of Hsp90 binding. *The Journal of biological chemistry* **281**, 34592-34600, doi:10.1074/jbc.M604019200 (2006).

181 Nakhaei, P. *et al.* The E3 ubiquitin ligase Triad3A negatively regulates the RIG-I/MAVS signaling pathway by targeting TRAF3 for degradation. *PLoS pathogens* **5**, e1000650, doi:10.1371/journal.ppat.1000650 (2009).

182 Hasan, U. A., Trinchieri, G. & Vlach, J. Toll-like receptor signaling stimulates cell cycle entry and progression in fibroblasts. *The Journal of biological chemistry* **280**, 20620-20627, doi:10.1074/jbc.M500877200 (2005).

183 Invivogen. in *293/Control cells* (2011).
184 Aubry, C. *et al.* Both TLR2 and TRIF contribute to interferon-beta production during Listeria infection. *PLoS One* **7**, e33299, doi:10.1371/journal.pone.0033299 (2012).
185 Derbigny, W. A., Johnson, R. M., Toomey, K. S., Ofner, S. & Jayarapu, K. The Chlamydia muridarum-induced IFN-beta response is TLR3-dependent in murine oviduct epithelial cells. *Journal of immunology* **185**, 6689-6697, doi:10.4049/jimmunol.1001548 (2010).
186 Wang, A. *et al.* Transcription factor complex AP-1 mediates inflammation initiated by Chlamydia pneumoniae infection. *Cell Microbiol*, doi:10.1111/cmi.12071 (2012).
187 Yu, S. *et al.* Hepatitis B virus polymerase inhibits RIG-I- and Toll-like receptor 3-mediated beta interferon induction in human hepatocytes through interference with interferon regulatory factor 3 activation and dampening of the interaction between TBK1/IKKepsilon and DDX3. *J Gen Virol* **91**, 2080-2090, doi:10.1099/vir.0.020552-0 (2010).
188 Nishimura, M. & Naito, S. Tissue-specific mRNA expression profiles of human toll-like receptors and related genes. *Biol Pharm Bull* **28**, 886-892 (2005).
189 Darville, T. *et al.* Toll-like receptor-2, but not Toll-like receptor-4, is essential for development of oviduct pathology in chlamydial genital tract infection. *Journal of immunology* **171**, 6187-6197 (2003).
190 Dobrovolskaia, M. A. *et al.* Induction of in vitro reprogramming by Toll-like receptor (TLR)2 and TLR4 agonists in murine macrophages: effects of TLR "homotolerance" versus "heterotolerance" on NF-kappa B signaling pathway components. *Journal of immunology* **170**, 508-519 (2003).
191 Dolganiuc, A. *et al.* Viral and host factors induce macrophage activation and loss of toll-like receptor tolerance in chronic HCV infection. *Gastroenterology* **133**, 1627-1636, doi:10.1053/j.gastro.2007.08.003 (2007).
192 Wu, G. S., Burns, T. F., Zhan, Y., Alnemri, E. S. & El-Deiry, W. S. Molecular cloning and functional analysis of the mouse homologue of the KILLER/DR5 tumor necrosis factor-related apoptosis-inducing ligand (TRAIL) death receptor. *Cancer research* **59**, 2770-2775 (1999).
193 Pitti, R. M. *et al.* Induction of apoptosis by Apo-2 ligand, a new member of the tumor necrosis factor cytokine family. *J Biol Chem* **271**, 12687-12690 (1996).
194 Wiley, S. R. *et al.* Identification and characterization of a new member of the TNF family that induces apoptosis. *Immunity* **3**, 673-682 (1995).
195 Lopez-Gomez, C. *et al.* TRAIL/TRAIL receptor system and susceptibility to multiple sclerosis. *PLoS One* **6**, e21766, doi:10.1371/journal.pone.0021766 (2011).

196 Ashkenazi, A., Holland, P. & Eckhardt, S. G. Ligand-based targeting of apoptosis in cancer: the potential of recombinant human apoptosis ligand 2/Tumor necrosis factor-related apoptosis-inducing ligand (rhApo2L/TRAIL). *Journal of clinical oncology : official journal of the American Society of Clinical Oncology* **26**, 3621-3630, doi:10.1200/JCO.2007.15.7198 (2008).

197 Wang, S. The promise of cancer therapeutics targeting the TNF-related apoptosis-inducing ligand and TRAIL receptor pathway. *Oncogene* **27**, 6207-6215, doi:10.1038/onc.2008.298 (2008).

198 Grosse-Wilde, A. *et al.* TRAIL-R deficiency in mice enhances lymph node metastasis without affecting primary tumor development. *J Clin Invest* **118**, 100-110, doi:10.1172/JCI33061 (2008).

199 Yoldas, B. *et al.* Clinical significance of TRAIL and TRAIL receptors in patients with head and neck cancer. *Head Neck* **33**, 1278-1284, doi:10.1002/hed.21598 (2011).

200 Nguyen, V. *et al.* TRAIL, DR4 and DR5 are upregulated in kidneys from patients with lupus nephritis and exert proliferative and proinflammatory effects. *Clin Immunol* **132**, 32-42, doi:10.1016/j.clim.2009.02.011 (2009).

201 Finnberg, N., Klein-Szanto, A. J. & El-Deiry, W. S. TRAIL-R deficiency in mice promotes susceptibility to chronic inflammation and tumorigenesis. *J Clin Invest* **118**, 111-123, doi:10.1172/JCI29900 (2008).

202 Bodmer, J. L. *et al.* TRAIL receptor-2 signals apoptosis through FADD and caspase-8. *Nat Cell Biol* **2**, 241-243, doi:10.1038/35008667 (2000).

203 Kuang, A. A., Diehl, G. E., Zhang, J. & Winoto, A. FADD is required for DR4- and DR5-mediated apoptosis: lack of trail-induced apoptosis in FADD-deficient mouse embryonic fibroblasts. *J Biol Chem* **275**, 25065-25068, doi:10.1074/jbc.C000284200 (2000).

204 Sprick, M. R. *et al.* FADD/MORT1 and caspase-8 are recruited to TRAIL receptors 1 and 2 and are essential for apoptosis mediated by TRAIL receptor 2. *Immunity* **12**, 599-609 (2000).

205 Hilliard, B. *et al.* Roles of TNF-related apoptosis-inducing ligand in experimental autoimmune encephalomyelitis. *Journal of immunology* **166**, 1314-1319 (2001).

206 Cretney, E. *et al.* Normal thymocyte negative selection in TRAIL-deficient mice. *J Exp Med* **198**, 491-496, doi:10.1084/jem.20030634 (2003).

207 Lamhamedi-Cherradi, S. E., Zheng, S. J., Maguschak, K. A., Peschon, J. & Chen, Y. H. Defective thymocyte apoptosis and accelerated autoimmune diseases in TRAIL-/- mice. *Nature immunology* **4**, 255-260, doi:10.1038/ni894 (2003).

208 Tang, W. *et al.* TRAIL receptor mediates inflammatory cytokine release in an NF-kappaB-dependent manner. *Cell Res* **19**, 758-767, doi:10.1038/cr.2009.57 (2009).

209 Reorganizing the protein space at the Universal Protein Resource (UniProt). *Nucleic Acids Res* **40**, D71-75, doi:10.1093/nar/gkr981 (2012).
210 Abdul-Sater, A. A., Koo, E., Hacker, G. & Ojcius, D. M. Inflammasome-dependent caspase-1 activation in cervical epithelial cells stimulates growth of the intracellular pathogen Chlamydia trachomatis. *The Journal of biological chemistry* **284**, 26789-26796, doi:10.1074/jbc.M109.026823 (2009).
211 Azenabor, A. A. & Chaudhry, A. U. Chlamydia pneumoniae survival in macrophages is regulated by free Ca2+ dependent reactive nitrogen and oxygen species. *J Infect* **46**, 120-128 (2003).
212 Wyrick, P. B. & Brownridge, E. A. Growth of Chlamydia psittaci in macrophages. *Infection and immunity* **19**, 1054-1060 (1978).
213 Jendro, M. C. *et al.* Infection of human monocyte-derived macrophages with Chlamydia trachomatis induces apoptosis of T cells: a potential mechanism for persistent infection. *Infection and immunity* **68**, 6704-6711 (2000).
214 Sun, H. S. *et al.* Chlamydia trachomatis vacuole maturation in infected macrophages. *J Leukoc Biol* **92**, 815-827, doi:10.1189/jlb.0711336 (2012).
215 Walczak, H. *et al.* TRAIL-R2: a novel apoptosis-mediating receptor for TRAIL. *Embo J* **16**, 5386-5397, doi:10.1093/emboj/16.17.5386 (1997).
216 Eckmann, L., Kagnoff, M. F. & Fierer, J. Epithelial cells secrete the chemokine interleukin-8 in response to bacterial entry. *Infection and immunity* **61**, 4569-4574 (1993).
217 Cui, J. *et al.* NLRC5 negatively regulates the NF-kappaB and type I interferon signaling pathways. *Cell* **141**, 483-496, doi:10.1016/j.cell.2010.03.040 (2010).
218 Xia, X. *et al.* NLRX1 negatively regulates TLR-induced NF-kappaB signaling by targeting TRAF6 and IKK. *Immunity* **34**, 843-853, doi:10.1016/j.immuni.2011.02.022 (2011).

APPENDICES

Appendix A: *Analysis of Signals That Regulate The Fate of Early T cell Precursors.*

This is an overview of the project that I worked on in Dr. Garcia-Ojeda's lab. The project investigated the signals that regulate the fate of early T cell precursors. The design of the project and the execution of the different experiments described here were fully developed under the supervision of Dr. Garcia-Ojeda.

Appendix B: *Multiplex single cell RT-qPCR analysis of fetal and adult murine long-term hematopoietic stem cells.*

A draft for a paper that is under review at *Stem Cell Reviews and Reports* journal that outlines the protocol for single cell q-PCR. The development of a novel multiplex single cell RT-qPCR technique was part of my project to characterize the signals that regulate the development of T cell (presented in Appendix A). The development and the optimization of the technique were conducted along with Dr. Jesus Ciriza. Data presented on Figure 7 and 8 are specifically corresponding to the population of cells that I was studying. The manuscript was prepared by Dr. Ciriza and reviewed by me.

Appendix C: *Single-Cell Analysis of Murine Long-Term Hematopoietic Stem Cells Reveals Distinct Patterns of Gene Expression during Fetal Migration.*

This is a published article on *PlosOne* journal for the work conducted by Dr. Ciriza. My contribution for this project was limited to the development of the single cell q-PCR assay (presented in Appendix B). This includes the optimization of the sorting technique and the q-PCR analysis as seen on Figure 1A.

Appendix D: *Transcription factor complex AP-1 mediates inflammation initiated by Chlamydia pneumoniae infection.*

This is a published article on the journal of *Cellular Microbiology* for our collaborative work with the lab of Dr. Deborah Dean from Children's Hospital Oakland Research Institute and UC-Berkeley. My contribution to the paper includes the characterization of NF-κB activity and IL-8 expression on cells expressing TLR3 in response to *Chlamydia pneumoniae* infection (Figure 7). Preparation of different sections of the manuscript was partially completed by me.

APPENDICES

Appendix A: *Analysis of Signals That Regulate The Fate of Early T cell Precursors.*

This is an overview of the project that I worked on in Dr. Garcia-Ojeda's lab. The project investigated the signals that regulate the fate of early T cell precursors. The design of the project and the execution of the different experiments described here were fully developed under the supervision of Dr. Garcia-Ojeda.

Appendix B: *Multiplex single cell RT-qPCR analysis of fetal and adult murine long-term hematopoietic stem cells.*

A draft for a paper that is under review at *Stem Cell Reviews and Reports* journal that outlines the protocol for single cell q-PCR. The development of a novel multiplex single cell RT-qPCR technique was part of my project to characterize the signals that regulate the development of T cell (presented in Appendix A). The development and the optimization of the technique were conducted along with Dr. Jesus Ciriza. Data presented on Figure 7 and 8 are specifically corresponding to the population of cells that I was studying. The manuscript was prepared by Dr. Ciriza and reviewed by me.

Appendix C: *Single-Cell Analysis of Murine Long-Term Hematopoietic Stem Cells Reveals Distinct Patterns of Gene Expression during Fetal Migration.*

This is a published article on *PlosOne* journal for the work conducted by Dr. Ciriza. My contribution for this project was limited to the development of the single cell q-PCR assay (presented in Appendix B). This includes the optimization of the sorting technique and the q-PCR analysis as seen on Figure 1A.

Appendix D: *Transcription factor complex AP-1 mediates inflammation initiated by Chlamydia pneumoniae infection.*

This is a published article on the journal of *Cellular Microbiology* for our collaborative work with the lab of Dr. Deborah Dean from Children's Hospital Oakland Research Institute and UC-Berkeley. My contribution to the paper includes the characterization of NF-κB activity and IL-8 expression on cells expressing TLR3 in response to *Chlamydia pneumoniae* infection (Figure 7). Preparation of different sections of the manuscript was partially completed by me.

APPENDIX A

Analysis of Signals That Regulate The Fate of Early T cell Precursors

Mufadhal Mohammed Al-Kuhlani

UC Merced 2009

Advisor:

Marcos E. García-Ojeda, PhD

A-Specific Aims:

During lymphopoiesis, the transition from Hematopoietic Stem Cell (HSC) to Common Lymphoid Progenitor (CLP) with potential to give rise to dendritic, NK, B and T cells depends on the signals they receive from their microenvironment. The transmembrane receptor Notch-1 and the zinc-finger transcription factor GATA-3 are two of the signals that regulate the commitment of CLP towards the T cell lineage. Notch-1 instructs thymic lymphocyte progenitors to differentiate into T cells while inhibiting B cell development. Disruptions of Notch-1 signaling lead to an early arrest of T cell development. GATA-3 expression in mature T_H2 T cells is regulated by Notch signals. However, the role of GATA-3 in early T cell development is poorly characterized. In vitro studies show that GATA-3 deficient (GATA-$3^{-/-}$) progenitors initiate a T cell developmental program characteristic of early T cell progenitors but become arrested at the $CD44^+CD25^+$ double negative 2 (DN2) stage. These GATA-$3^{-/-}$ DN2 cells display an aberrant capacity to generate B cells in the presence of Notch-1 signals suggesting that the final fate decision toward the T lineage is dependent on GATA-3 transcriptional activity. Gene expression profile analysis of GATA-$3^{-/-}$ DN2 cells showed elevated expression of Deltex-1, a Notch-1 regulator known to induce B cell development while inhibiting T cell differentiation. *We hypothesize that GATA-3 transcriptional activity controls the expression of Deltex-1, and possibly other regulators of Notch-1 such as Mint, Nrarp and Numb.* To determine how GATA-3 transcriptional activity influences the expression of Deltex-1, Mint, Nrarp and Numb, we will:

1) ***Evaluate the expression level of Notch-1 regulators in wild type and GATA-3 knockdown thymocytes.*** We hypothesize that GATA-3 regulates the expression of Notch-1 regulators. We will measure the expression level of GATA-3, Deltex-1, Mint, Nrarp and Numb in DN1-DN4 cells from wild type thymus as well as cocultured cells using a quantitative PCR technique in the following sets:

a) We will determine the expression levels of Deltex-1, Mint, Nrarp, Numb and Gata-3 in DN1-DN4 cells isolated from wild type thymus and from DN1-DN4 cells generated in vitro from co-cultures of OP9DL1 stroma with wild type fetal liver hematopoietic stem cells (FL-HSC). This will allow us to determine the steady state expression of these genes and will serve as a base to establish how their expression is affected by modulating the levels of GATA-3.

b) GATA-$3^{-/-}$ DN2 cells generated from wild type FL-HSC retrovirally transduced with GATA-3-GFP shRNA will be cultured on OP9Dl1 stroma for 2 weeks. The generated GATA-$3^{-/-}$ DN2 cells will be sorted on the basis of GFP expression. Molecular analysis by qPCR of GATA-3 and Notch-1 regulators will be compared to their steady state expression.

2) ***Investigate by qPCR Array the genes involved in the Notch signaling pathway that are modulated by GATA-3.*** We hypothesize that the knockdown of GATA-3 affects the expression of various Notch-1 targets and regulators. We will perform a genetic profile utilizing a Notch-1 qPCR array to examine how genes involved in Notch signaling are affected by GATA-3 deficiency. Genes whose expression are affected by GATA-3 deficiency will be evaluated for

potential GATA-3 binding sites on their promoter regions and validated by Chromatin Immunoprecipitation (ChIP) assays.

3) **Determine the threshold level of GATA-3 protein required to rescue T cell commitment in GATA-3$^{-/-}$ DN2 cells.** We hypothesize that commitment to the T cell lineage is dependent on the amount of functional GATA-3 protein. GATA-3$^{-/-}$ FL-HSC will be transduced with a destabilized FKBP:GATA-3 fusion protein whose stability depends on the concentration of FKBP's ligand Shield-1. The GATA-3 protein level will be evaluated by western blot, and the effect on gene expression for Deltex-1, Mint and Numb will be evaluated via qPCR. Commitment to the T cell lineage will be examined by culturing GATA-3$^{-/-}$ DN2 cells at various concentrations of Shield-1 in OP9 and OP9DL1 stroma at limiting dilution.

Understanding the mechanisms of interaction between GATA-3 and Notch-1, as well as other genes involved in T cell commitment, will allow us to elucidate how early lymphocyte precursors commit to the T cell fate. This will facilitate the development of new stem cell-based therapeutic approaches to treat diseases related to impaired T cell development, such as immunodeficiencies, or the reconstitution of immune function following stem cell transplantation for the treatment of cancer.

B-BACKGROUND AND SIGNIFICANCE:

I-Overview of Early T-Cell Development:

Hematopoietic stem cells (HSC) differentiate into all mature blood cells [1]. During lymphopoiesis, HSC transition through a Common Lymphoid Progenitor (CLP) that gives rise to dendritic, NK, B and T cells [2]. The final fate of CLPs depends on the signals and growth factors they receive from their microenvironment. In the thymus, early T cell precursors commit to the T cell lineage, losing the capacity to differentiate into other cell types [3]. The most immature T cell population, known as double negative (DN), is defined by the absence of CD4 and CD8 markers. This group is subdivided further into four different subgroups (DN1-4) based on the expression of CD44 and CD25 [4]. The most immature population is $CD44^{+}CD25^{-}$, and is called DN1 or 'early T cell progenitors' (ETP) [5]. This population was further characterized into five subpopulation (DN1a-DN1e) based on the expression of c-Kit and CD24 markers [6].

The DN1a and DN1b populations, which resemble the bone marrow derived stem cells as they express c-Kit and Sca-1 but not CD127 or CD3∑, serve as DN2 precursors since they have the potential to generate Natural Killer cells (NK cells) and T cells but not B cells [6]. DN2 cells have been characterized by the presence of both CD25 and CD44 [4]. However, there have been some recent challenges to the current characterization of the DN2 cells that distinguish them from the DN3 cells. DN2 cells down regulation of CD44 and c-Kit along

with the increased expression of intracellular CD3∑ all indicate their transition into the DN3 stage [7]. However, Ceredig and colleagues showed that DN2 cells, defined as $CD25^{+}CD44^{++}CD117^{++}$, have an overlapping sub-population that is both intracellular $CD3\sum^{+}$ and $CD3\sum^{-}$. This led them to conclude that CD44 expression alone cannot be used to characterize the transition of DN2 into DN3 [8]. The loss of both CD44 and CD25 from the DN3 population marks the transition to the DN4 stage, which subsequently becomes $CD4^{+}CD8^{+}$ double positive (DP) before further differentiating into single positive $CD4^{+}$ helper T cells or $CD8^{+}$ cytotoxic T cells [4].

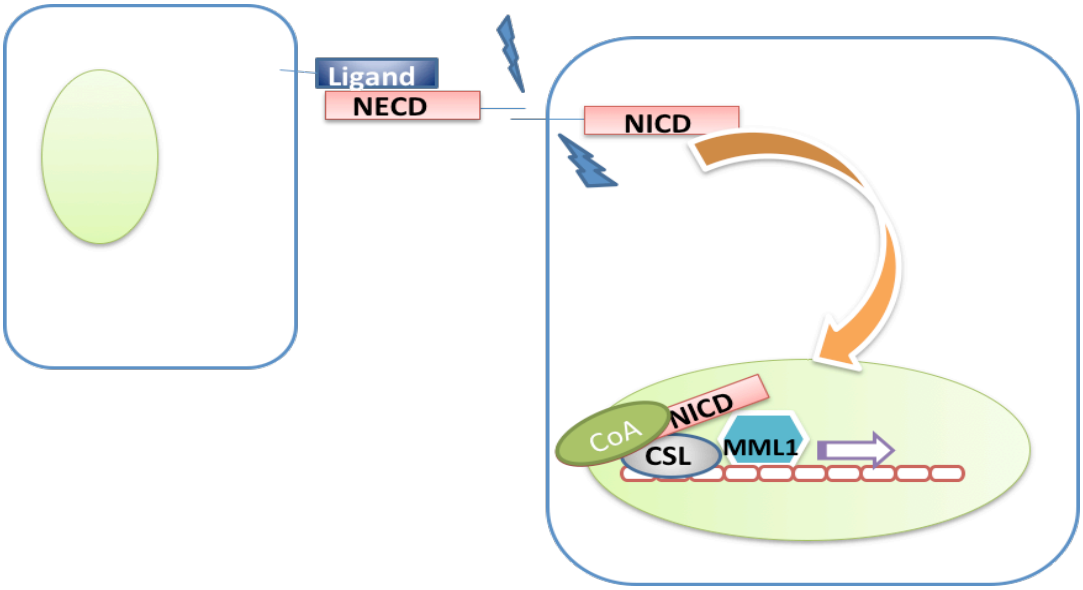

Figure1: Notch-1 signaling pathway. Engagement of the Notch's extracellular domain (NECD) with its ligand leads to two proteolytic cleavages (bolts), which release Notch's intracellular domain (NICD) and allow its translocation into the nucleus to activate the targeted genes.

everal genes, including Notch-1 and the transcription factor GATA-3, are involved at the different stages of T cell development [9]. Notch proteins are large, single pass type I transmembrane receptors conserved across many diffe
rent species [10]. They are involved in the regulation of various developmental activities during embryonic and post-natal development such as proliferation, apoptosis and cell fate decisions [11]. Mammals possess four Notch receptors (Notch1-4) and five ligands (Delta-like-1, -3, -4 and Jagged-1 and -2). Notch ligands are characterized by three motifs that are structurally related, an N-terminal Delta/Serrate/LAG-2 (DSL) motif, a Delta and OSM-11-like protein (DOS) domain, and Epidermal Growth Factor (EGF)-like repeats [12]. The binding of ligands containing the DSL and DOS domains to the Notch's extracellular domain (NECD) induces the canonical activation of Notch signaling pathway. However, several proteins lacking both the DSL and DOS domains, such as F3/Contactin1, MAGP1 and MAGP2, have been shown to act as Notch ligands that initiate an alternative, noncanonical signaling pathway [12].

As it is illustrated in Figure 1, the engagement of Notch receptors by its ligand induces two proteolytic cleavages in Notch, resulting in the release of Notch's intercellular domain (NICD) from the plasma membrane [13]. NICD translocates to the nucleus, where it binds to the transcription factor CSL (CBF-1 suppressor of Hairless-Lag1) and recruits the transcriptional co-activator Mastermind-like (MAML) [14], forming a transcriptional activator. This complex activates the expression of Notch-1 target genes including HES-1 [15], Deltex-1 [16-18], and GATA-3 [15]. During lymphocyte development, Notch-1 instructs

lymphocyte progenitors in the thymus to differentiate into T cells while blocking B cell development [19, 20]. Notch-1 involvement on T cell development spans different maturation stages, starting with TCRβ gene rearrangement, β-selection, as well as providing the signals required for specification of T helper cells [21, 22]. Gain of function and conditional knockout studies revealed that Notch-1 is necessary and sufficient for the induction of T cell development and the suppression of B cell fate [23]. Any disruption of Notch-1 signaling in hematopoietic progenitors arrests T cell development at an early stage [13, 24].

GATA transcription factors are a family of zinc-finger transcriptional regulatory proteins involved in the development and differentiation of many different types of cells [25, 26]. Only GATA-1, GATA-2 and GATA-3 are expressed in hematopoietic cells [25]. GATA-3 is predominantly expressed in lymphocytes, particularly T cells, but the expression of GATA-3 is tightly regulated during T cell development through Notch-1 signaling [15, 25], especially in the differentiation of T_H2 cells [27]. Although GATA-3 can be detected in fetal and adult HSC and increases as cell development advances toward the lymphoid lineage [28, 29], its exact role during early T cell development is poorly characterized. Fetal thymocytes over-expressing GATA-3 fail to develop beyond the DN1-DN2 stage under constant expression of Notch-1 [30]. Instead, these DN1-DN2 cells differentiate into mast cells when cocultured on OP9 stroma cells in the absence of cytokines that support such development [30]. A study by Georgescu and colleagues revealed that GATA-3 overexpression induces the expression of an early target of Notch-1, *Hes-1* [31].

However, GATA-3 overexpression down-regulates the expression of other T cell specific genes, such as *Rag1, Ptcra, Tcf7* and *Lef1,* that are needed during the transition from DN1 to DN3 stages [31].

The importance of GATA-3 in early T cell development is evidenced by the early DN stage developmental arrest observed in C57BL/6 complementation chimeras created with GATA-3 deficient embryonic stem cells [32, 33]. GATA-3 deficient embryos die by day 11.5 of gestation from developmental defects of the sympathetic nervous system and heart [34]. However, these embryos could be pharmacologically rescued to day 14.5 of gestation by treatment with α- and β-adrenergic receptor agonists [35], facilitating the study of lymphopoiesis from GATA-$3^{-/-}$ hematopoietic stem cells. The rescued embryos generate functional fetal liver HSC but lack a thymus, further complicating the study of T lymphopoiesis. To overcome these obstacles and study the role of GATA-3 in early T cell development, we used the system developed by Schmitt and colleagues where the bone marrow stroma OP9 was engineered to express the Notch-1 ligand Delta-like-1 [36]. In these experiments, GATA-$3^{-/-}$ HSC were co-cultured on OP9Delta-like-1 (OP9DL1) cells in the presence of IL-7 and Flt-3L for 2 weeks. Under these conditions, T cell development was arrested at the early $CD44^{+}CD25^{+}$ DN2 stage. These DN2 cells express a phenotypic and molecular profile characteristic of DN2 cells found in the thymus, including expression of pre-Tα, Rag-1 and Rag-2. Furthermore, these DN2 cells aberrantly generated B cells in the presence of Notch-1 signals, which are inhibitory of B cell development [37]. Hence, the balance between T and B cell commitment is

perturbed in GATA-3 deficient T cell progenitors. These results illustrate that the commitment to the T cell lineage observed after Notch-1 signaling is dependent on GATA-3 transcriptional activity, elucidating a novel functional dependence between the Notch-1 and GATA-3 signaling pathways in early T cell development [37]. The gene expression profile of GATA-$3^{-/-}$ DN2 cells revealed an increased level of Deltex-1, a regulator of Notch-1 signals [37]. Deltex-1 overexpression in HSC results in an induction of B cell development and an inhibition of T cell differentiation [38]. *Therefore, we hypothesize that GATA-3 plays a critical role in controlling the expression of Deltex-1 and other Notch-1 regulators.*

II- Regulators of Notch-1 activity:

Extracellular, cytoplasmic, and nuclear proteins regulate Notch-1 signaling. Fringe proteins are an example of extracellular regulators of Notch-1. There are three Fringe N-acetylglucosamine (GlcNAc)-transferase enzymes, known as Lunatic, Manic, and Radical Fringes, all capable of modulating NECD's affinity towards various ligands. They do so by possessing a fucose-specific β1,3 N-acetylglucosaminyl transferase activity that catalyses the elongation of O-linked fucose on the EGF repeats of Notch NECD [39].This post-translational modification of NECD skews its binding specificity to the Delta ligands, but not to the Jagged ligands.

The cytoplasmic regulators of Notch-1, such as Deltex-1, are involved in the inhibition of NICD translocation into the nucleus by binding to the ankyrin repeats of the NICD [40]. Deltex-1, Deltex-2 and Deltex-4 comprise a gene family

of mammalian orthologues of Drosophila Deltex [17]. Even though Deltex was shown to be a positive modulator of Notch in Drosophila, the overexpression of Deltex-1 on mouse HSC skews lymphoid development toward the B-cell lineage at the expense of T cell development [38]. Deletion of Deltex-1 did not impaired lymphoid development, probably as a result of functional compensation by other Deltex orthologues [41]. However, Lehar and Bevan postulated that although Deltex-1 acts as a negative regulator of Notch signals in T cell development, neither Deltex1 nor Deltex2 are important for regulating Notch signals during thymocyte development [17]. Interestingly, Notch-1 activity controls the expression of Deltex-1, but this process is not completely understood.

Numb and its homolog Numblike, form a group of membrane associated cytoplasmic adaptor proteins that act upstream of Notch [42, 43]. In Drosophila, Numb negatively regulates Notch through direct protein-protein interactions of its phosphotyrosine-binding (PTB) domain with either the RAM23 motif of CBF-1 or the C-terminal end of Notch [44]. However, the role of Numb in T lymphocyte development remains controversial. The overexpression of p66, the predominant isoform of Numb in the thymus, resulted in a reduction of Notch signaling on immature thymocytes but did not alter either the $\gamma\delta$ vs. $\alpha\beta$ or the CD4 vs. CD8 T cell fates, probably by the presence of Numblike [45]. On the other hand, simultaneous deletion of Numb and Numblike did not affect the ability of stem cells to undergo intrathymic T cell development [42]. Together, these data suggest that Numb acts as a Notch-1 antagonist in immature thymocytes, but

does not alter T cell development. However, the regulation of Numb expression in developing lymphocytes is not completely understood.

Notch regulated ankyrin repeat protein (Nrarp, formerly known as XNAP or 5D9) is a Notch/Wnt regulator protein involved in somitogenesis [46], angiogenesis [47] and T cell development [48]. It contains two ankyrin repeats that interact with CSL and NICD [49, 50]. Overexpression of Nrarp causes a decrease in Notch signaling, resulting in phenotypic alterations similar to those seen by Notch loss of function [49]. The increase of Nrarp expression on HSC impedes T cell development to proceed beyond the DN1 to DN2 stage transition [48].

Msx2-interacting nuclear target protein (Mint) is another regulator of Notch-1 that competes with NICD for binding to CSL [51]. Mint contains three RNA recognition motifs (RAM) in its N-terminus and a SPEN paralog and ortholog C-terminal (SPOC) domain at its C-terminus [52]. These characteristics lead to its classification as a SPEN family protein. The SPOC domain mediates homodimerization of Mint, an interaction that is important for its repression activity of Notch [52-54]. Mint deficiency causes an increase on fetal thymic ETP and DN4 cells. Surprisingly, it induced also the expression of Nrarp, which in turn impaired the transition from DN1 to DN2 stages [55].

Preliminary data shows that GATA-3 deficient progenitors cultured under constant Notch-1 signals undergo aberrant B cell development [37]. This could be the result of the inhibition of Notch-1 signals by Notch adaptor proteins upregulated during culture. For example, we observe that GATA-3 deficient T

cell progenitors cultured under constant Notch-1 signals express high levels of Deltex-1. *Therefore, we hypothesize that the elevated levels of Deltex-1 could inhibit Notch-1 signaling, resulting on B cell development in an environment that usually fosters T cell differentiation.* This observation led us to investigate how GATA-3 transcriptional activity influences the expression of Notch-1 regulators. Collectively, the mechanisms that control the expression of Notch-1 regulators are not clearly understood. Of the regulators mentioned above, the role of Deltex-1, Mint, Nrarp and Numb will be investigated further in this study.

III- Significance:

The regenerative power of stem cells harbors great potential to cure diseases and repair damaged tissues. Understanding the signals that direct the commitment of stem cells towards desired lineages will further improve the ability of the biomedical research community to exploit this potential through regenerative medicine. Therefore, elucidating the mechanisms governing the interaction between GATA-3 and Notch-1, as well as other genes involved in T lymphocyte cell fate decisions, will help us comprehend how these decisions are made. Such understanding will enable the development of new stem cell-based therapeutic approaches to treat cancer and diseases related to impaired T cell development.

C- PROJECT DESIGN:

Aim 1*: Evaluate the expression level of Notch-1 regulators in wild type AND GATA-3 knockdown thymocytes and DN2 cells.* We hypothesize that the expression of Notch-1 regulators is controlled by GATA-3 activity. Studies have shown that the expression of Deltex-1, a regulator of Notch-1, increases in GATA-3 deficient DN2 cells [37]. Therefore, it is possible that the expression of other Notch-1 regulators is affected also by GATA-3 deficiency. We will measure the expression level of GATA-3, Deltex-1, Mint, Nrarp and Numb genes on the different subpopulation of DN1-DN4 cells using a quantitative PCR technique. Such approach requires careful examination of the primers to be used in this process.

Aim 1a: Measuring the steady state expression of GATA-3, Deltex, Mint, and Numb in wild type DN1-4 populations from the thymus and cocultured FL-HSC:

i) Primer design and efficiency analysis:

Forward and reverse primers for GATA-3, Deltex-1, Mint, Nrarp, Numb, and HPRT were carefully designed to minimize primer dimer formation. The comparison of the qPCR amplification efficiency of all primers will be evaluated using R software (R Foundation for Statistical Computing). Statistical analysis will determine if there is a significant difference in the amplification of the gene

products between all 6 primers sets. A p-value of < 0.05 will be considered significant.

ii) Cell Culturing and Sorting:

Fetal liver (FL) cells will be harvested from wild type C57BL/6 d14 embryos and depleted of mature, lineage positive (Lin^+) cells expressing CD3, CD4, CD8, CD11b, CD19, GR1, NK1.1, and Ter119 by MACS. The Lin^- fraction will be stained with c-Kit and Sca-1 and the $Lin^-Sca\text{-}1^+c\text{-}Kit^+$ (LSK) population containing FL-HSC [56] will be sorted. Sorted LSK will be co-cultured on OP9DI1 stroma for 2 weeks in the presence of 5 ng/ml rmIL-7 and rmFlt3L [36]. After culture, the Lin^+ fraction will be depleted by MACS, followed by staining of the Lin^- population with c-Kit, CD44, and CD25. Cells from the four DN populations ($CD44^+CD25^-$ for DN1, $CD44^+CD25^+$ for DN2, $CD44^-CD25^+$ for DN3, and $CD44^-CD25^-$ for DN4) will be sorted for qPCR molecular analysis for the expression of GATA-3, Deltex-1, Mint, Nrarp, Numb and HPRT. The isolation of wild type DN1-4 thymocytes will be conducted by enriching for the DN population by removing the CD4 and CD8 positive cells by MACS. DN subpopulations (DN1-4) will be sorted based on the expression level of CD44, CD25 as explained above. The threshold cycle (Ct) values obtained from Applied Biosystems Step One Plus Real time PCR System software are used to calculate the average (Ct) values of the triplicate qPCR samples for each gene in each sorted population. The ΔCt value is calculated using the following equation:

$$\Delta Ct = (\text{Avg. Targeted gene } Ct - \text{Avg. HPRT } Ct)$$

The standard deviation for each cell and the mean for each population are determined also and the ΔCt values obtained are used as a reference for future experiments [57]. We will determine the fold change in gene expression by calculating the $2^{-\Delta\Delta Ct}$ values using the follow equation:

$\Delta\Delta C$T = (Avg. Targeted gene *C*t - Avg. HPRT *C*t) shRNA - (Avg. Targeted gene *C*t - Avg. HPRT *C*t) Steady state

<u>Aim 1b: Knockdown GATA-3 on FL-HSC by shRNA followed by quantification of the expression level of the GATA-3, Deltex-1, Mint, Nrarp, Numb and HPRT in the emerging DN2 cells.</u>

Fetal liver hematopoietic stem cells (FL-HSC) will be retrovirally transduced with a GATA-3-shRNA-GFP retrovirus [58]. Following transduction, the HSC will be cultured on OP9DI1 stroma as described before. After 2 weeks of culture, the emerging DN2 cells will be sorted based on their GFP expression. The mRNA and protein levels of GATA-3 in the transduced DN2 cells will be analyzed via qPCR and western blot to verify the level of the knockdown of GATA-3. The average of the Ct values of the triplicate qPCR samples for each gene will be normalized to the housekeeping gene HPRT. The Ct value will then be compared to the untreated control, the steady state gene expression obtained previously on Aim1a, and presented by calculating the $2^{-\Delta\Delta Ct}$ as fold change in gene expression [57].

***Expected Results*:**

The involvement of the selected genes (Deltex-1, Mint, Nrarp and Numb) in the regulation of Notch-1 through GATA-3 is expected to show upregulation of their expression level in comparison to the steady state expression obtained from the wild type control. Since the sorting of the cells will be based on the expression level of the GFP, we would expect that the higher the GFP expression of the sorted cells, the higher the expression level of the targeted genes.

Alternative Approach: GATA-3 conditional deletion mutant.

GATA-$3^{+/nlsLacZ}$ [33] or GATA-$3^{flx/flx}$ mice [59] can be used to obtain GATA-$3^{-/-}$ FL-HSC. These stem cells will be cultured on OP9Dl1 stroma for 2 weeks to generate GATA-$3^{-/-}$ DN2 cells. Gene expression and developmental potential studies will be performed as described in Aim 2b.

Aim2: ***Investigate by qPCR Array the genes involved in the Notch signaling pathway that are modulated by GATA-3.*** We hypothesize that the deletion of GATA-3 affects the expression of various targets of Notch-1. Our preliminary data shows that Deltex-1 expression is upregulated in the absence of GATA-3. *ChIP assay will be used to confirm the binding of GATA-3 protein to the promoter regions of these genes.* To test this hypothesis, we will propose the following:

Aim 2a: ***Explore the various genes that are involved in the Notch signaling pathway using qPCR Array.***

Since Notch signaling regulates the activity of several developmental genes, we will explore how GATA-3 silencing can affect the expression levels of these genes. SA Biosciences has developed an array capable of monitoring the expression level of 84 genes involved in Notch signaling. The genes in this array include Sonic Hedgehog and Wnt genes, known to cross talk with the Notch signaling pathway. Wild type HSC cells and HSC that are transduced with GATA-3-shRNA-GFP retrovirus will be cocultured on OP9Dl1 stroma cells for 14 days to isolate DN2 cells. The RNA from sorted wild type and GATA-$3^{-/-}$ DN2 will be isolated, reverse transcribed to generate cDNA, then assayed by qPCR Array following manufacturer's instructions. Gene expression analysis will be conducted as described previously using the following equation:

$\Delta\Delta C$T = (Avg. Targeted gene *C*t - Avg. HKG *C*t) GATA-3-shRNA - (Avg. Targeted gene *C*t - Avg. HKG *C*t) Wild type

Aim2b: ***Determine whether GATA-3 binds to the promoter regions of the targeted genes selected on Aim 1 and the ones revealed from the*** **qPCR array** ***analysis.***

We hypothesize that GATA-3 binds to the promoter region of the genes obtained from the qPCR Array analysis as well as the ones tested on Aim1 (Deltex-1, Mint, Nrarp and Numb). To test this hypothesis, we will utilize transcription factor binding algorithms to find putative GATA-3 DNA binding

motifs {(W)GATA(R)} on the promoter and 5' untranslated regions of these genes [60]. The 1000 base sequence of the promoter as well as the 5' untranslated regulatory region of these genes will be obtained from UCSC Genome Bioinformatics Site. The Transcription Element Search software (TESS) [61, 62] and TF Search [63] will be used to search for GATA-3 binding sites as described by Schung et al [64]. PCR primers will be design to obtain PCR products spanning the putative GATA-3 binding sites.

To confirm the binding of GATA-3 into the selected promoter regions of the target genes, we will use Chromatin Immunoprecipitation (ChIP) assays as described by Nelson et al [65]. Briefly, isolated DN2 cells will be cross-linked with formaldehyde, then lysed and sonicated to shear the chromatin into 300-800 bp DNA fragments. These fragments will be incubated with anti-GATA-3 monoclonal antibodies, followed by immunoprecipitation with Protein A beads. Following the precipitation step, the cross-linking will be reversed and the sample digested with proteinase K to eliminate residual proteins. Recovered DNA fragments will be analyzed via PCR to detect GATA-3 binding sites previously identified on the promoter and 5' untranslated regions of the targeted genes.

Expected Results:

Quantitative PCR array analysis will expand the list of Notch-1 genes affected by GATA-3 silencing. We will use the TESS mathematical algorithm to find putative GATA-3 binding sites into the promoter region of these genes. ChIP-PCR assays will confirm that GATA-3 binds the promoter regions of these

genes. Based on our preliminary data using TESS, we expect the ChIP assay to detect at least one binding site of GATA-3 on the regulatory regions of these genes including Deltex-1, Mint, Nrarp and Numb. Confirming a true GATA-3 binding site will allow us to test whether such binding affect the expression level of these genes

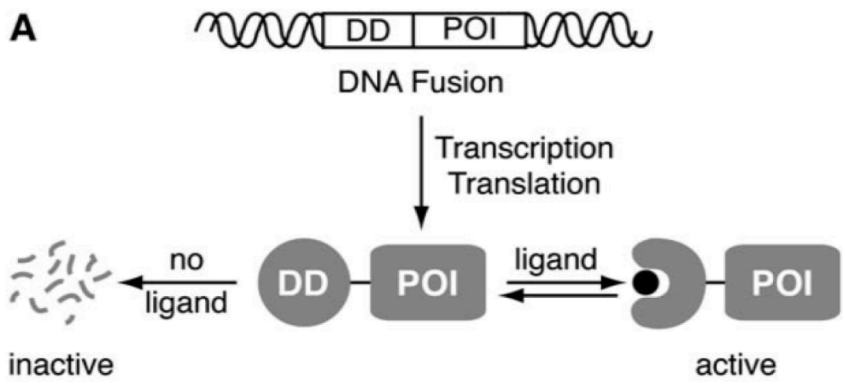

Figure 2. General method for the regulation of protein expression using Shield-1 and the destabilization domain of FKBP (66).

Alternative Approach:

The Electrophoretic Mobility Shift Assay (EMSA) is an alternative method to detect DNA:protein interactions. Using the DNA sequence of the targeted genes, we will design different DNA probes that contain the potential GATA-3 binding sequence. In order to be visualized, these DNA fragments will be radiolabeled on their 5´ end with [^{32}P]ATP and T4 polynucleotide kinase. Since we propose a DNA:protein interaction, our protein samples will be extracted from the nucleus, and not the cytoplasm, of DN2 cells. The non-specific poly (dA•dT) DNA competitor will be added to minimize the nonspecific binding of proteins to

the target sequences. DNA:protein complexes will migrate slower in the non-denaturing agarose gel, generating a higher (shifted) band than the DNA fragments alone. Since the presence of a shifted band does not identify the bounded protein, we will treat the DNA:protein complexes with GATA-3 specific antibody. If the radio-labeled DNA:protein complex contains GATA-3, the added antibody will bind to GATA-3, causing the complex to slow its mobility further and migrate at a slower rate than the DNA fragment alone and the DNA:GATA-3 complex (creating a supershift band).

Aim 3: Determine the threshold level of GATA-3 protein required to rescue T cell commitment in GATA-3$^{-/-}$ DN2 cells. We hypothesize that commitment to the T cell lineage is dependent on the amount of functional GATA-3 protein. *In vitro* studies have shown that GATA-3 deficient DN2 cells develop into B cell in the presence of Notch-1 signals, while the overexpression of GATA-3 in wild type DN2 cells induces the development of mast cells [30, 37]. GATA-3$^{-/-}$ FL-HSC will be transduced with a destabilized FKBP:GATA-3 fusion protein whose stability and function depends on the concentration of FKBP's ligand Shield-1. The protein level of GATA-3 required to affect Notch-1 regulators will be evaluated by western blot, and the gene expression analysis for Deltex-1, Mint and Numb will be evaluated via qPCR.

Increasing the level of GATA-3 protein has been shown to affect the final fate of T cell progenitors, allowing them to differentiate to mast cells if these precursors are placed on a system that support their growth [30]. On the other

hand, GATA-3 knockout progenitors fail to develop T cells [33]. These observations suggest that different levels of GATA-3 influence the commitment of progenitors to different lineages. Utilizing the technique developed by Banaszynski and colleagues, we will modulate the protein level of GATA-3 in hematopoietic progenitors [66]. In this technique, the leucine 106 in human FKBP12 protein was mutated to a proline (FKBP-L106P), effectively bestowing the protein with a destabilizing domain (DD) that can get degraded rapidly, along with any protein fused to it, when expressed in mammalian cells. Binding of the DD to its synthetic ligand (Shield-1) will stabilize it, allowing the protein fused with it to become functional in a Shield-1 dose-dependent manner (Figure 2). We will clone GATA-3 into a retroviral plasmid containing the DD of FKBP-L106P, followed by the generation of non-recombinant retrovirus in Phoenix ecotropic packaging cell [66]. DN2 cells generated from GATA-$3^{-/-}$ FL-HSC in OP9Dl1 co-cultures will be infected with the GATA-3:FKBP retrovirus, and the positive cells will be sorted by FACS onto OP9 and OP9Dl1 wells supplemented with different concentration of Shield-1 ligand (Shld-1). In these DN2 cells, the level of GATA-3 protein will be manipulated by the addition of the Shld-1 until it reaches a threshold level required to affect Notch-1 regulators. Cultured cells will be FACS analyzed for developmental progression beyond the DN2 stage, and the gene expression analysis will be done using qPCR technique described previously. Western blot analysis will be conducted to determine the protein level of GATA-3 required for the commitment of T cells as a response of the different concentration of Shld-1.

***Expected Results**:*

Since GATA-3 is required for the progression of early T cell progenitors beyond the DN2 stage, we expect that GATA-$3^{-/-}$ deficient DN2 cells expressing GATA-3:FKPB will develop into $CD4^{+}CD8^{+}$ DP cells in a Shield-1 dose dependent manner. At low concentrations of Shield-1, GATA-$3^{-/-}$ DN2 cells will not progress beyond the DN2 stage and possibly differentiate into B cells when cultured on OP9Dl1 stroma. As the concentration of Shield-1 ligand increases, the amount of functional GATA-3 protein will increase, shifting the differentiation capacity of the transduced DN2 cells toward the T cell lineage, generating $CD4^{+}CD8^{+}$ DP cells up to mature T cells. If the concentration of Shield-1 ligand increases beyond the required threshold for T-cell development, mast cell are expected to be generated [30].

Alternative Approach: Use different retroviral vector to deliver GATA-3.

This part of the proposal attempts to define a GATA-3 threshold level that will allow GATA-$3^{-/-}$ DN2 cells to progress forward with normal T-cell development. To achieve this goal, an alternative approach is to induce GATA-3 expression on these cells utilizing a bicistronic retroviral vector, in a manner analogous to Taghon and colleagues [30]. In this approach, the level of GATA-3 overexpression will depend on the titer of the produced virus. After retroviral transduction, the levels of GATA-3 expression will be evaluated by qPCR and western blot.

The data generated from these experiments will lead us to establish the mechanism by which GATA-3 and Notch-1 signals control the commitment towards the T cell lineage. This valuable finding will allow us to discover how early progenitors commit and differentiate into T cells, giving us insight into how these mechanisms can be manipulated for research and therapeutic purposes.

D- PRELIMINARY DATA:

Efficiency Analysis for the designed Primers:

The efficiency study for the primers used in the qPCR analysis is done to insure that all primers will work appropriately. The use of primers with the same amplification efficiency will allow for the accurate comparison of the expression of different genes of different samples. For this purpose, whole thymus cDNA was

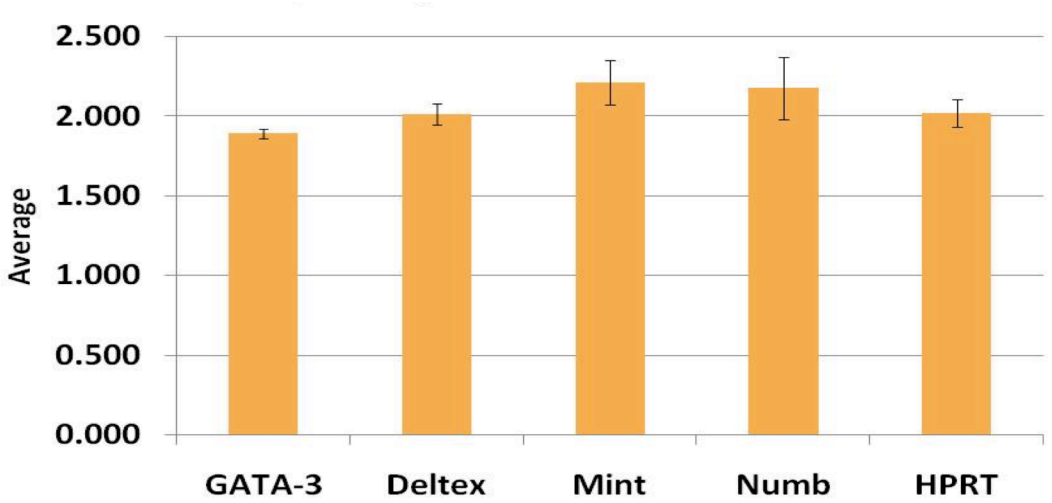

Figure 3: Primers Efficiency: Whole thymus cDNA used to evaluate the efficiency of individual primers.

used to evaluate the amplification efficiency of individual primer pairs in comparison to other primer pairs. The primers' efficiency was analyzed as described by Peixoto et al [67]. The statistical analysis for the PCR reaction for

each primer set shows that they have similar amplification efficiencies (Figure 3), and that there is no significant difference among these PCR reactions ($p>0.05$).

GATA-3 Binding Sites on Targeted Genes:

To determine if GATA-3 directly controls the regulation of Notch-1 regulators, we searched for GATA-3 binding sites on the promoter and 5' untranslated region of Deltex-1, Mint, Nrarp and Numb. The 1000 base pair sequence of the promoter and the 5' untranslated regulatory region of Deltex-1, Mint, Nrarp and Numb were searched by Transcription Element Search software (TESS) for the GATA-3 consensus binding sites (W)GATA(R) [68]. As it is

Factor	La	La/n	Lpv	Beg	Sequence
Deltex-1	10	1.67	0	848	WGATAR*
	10	1.67	0	677	YTATCW**
Numb	9.85	1.64	0.38	586	AGATAA*
	10	1.67	0	486	WGATAR*
	10	1.67	0	586	WGATAR*
Mint	10	1.64	0	272	YTATCW**
	9.85	1.67	0.48	272	TTATCT**
Nrarp	10	1.67	0	409	WGATAR*

Table 1: GATA-3 biding sites to targeted genes: TESS statistical analysis of Log-likelihood score (L*a)*, Approximate p-value for La score; (La/n), La/number of bases on the binding site; (L*pv)*, binding site from in the beginning of the query sequence (beg) and the matching sequence of binding. Binding site on the sense strand (*), Anti-sense strand (**). "W" represent A or T,"R" represent A or G,"Y" represent T or C.

shown in Table 1, there are two putative GATA-3 binding sites for Mint and Deltex-1, one site for Nrarp and three sites for Numb. The statistical analysis obtained from TESS for these sites shows that the log-likelihood score (L*a*) was very high for all sites, indicating that the sites are probably real. However, when evaluating these binding sites based on the approximate p-value for the L*a* score, the sites with value higher than 0.05 will be considered insignificant. Nevertheless, we will generate primers flanking the (W)GATA(R) sites on all regions for the four genes as well as those that will be obtained from the qPCR Array data in order to validate each site by PCR following ChIP analysis with anti-GATA-3 antibodies.

Transduction of DN Cells Using GATA3-shRNA-GFP:

A Banshee retroviral construct encoding GATA3-shRNA-GFP [58] is used to evaluate the level of GATA-3 expression needed to seal the commitment of DN2 cells toward the T cell lineage. The expression level of Notch-1 regulators will be evaluated on GATA-3 silenced DN2 cells. Figure 4 shows the results of an experiment where wild type DN cells were cocultured on OP9Dl1 stroma cells and then transduced with empty Banshee vector, or vector containing the GATA-3-shRNA-GFP. Supernatant from packaging cells treated with Lipofectamine alone was used as a negative control. We detected GFP expressing cells in the cultures transduced with the Banshee control vector, and the GATA-3-shRNA-GFP group but not on the Lipofectamine-alone control group. The development

of DN cells from the GFP+ and GFP- of Banshee control vector, and the GATA-3-shRNA-GFP show abnormal phenotypic development of the DN cells of the GFP+ cells with an increased number of DN2 cells on the GATA-3-shRNA-GFP transduced cells in comparison to the Banshee control vector. The expression level of GFP should correlate with the level of GATA-3 silencing on these cells.

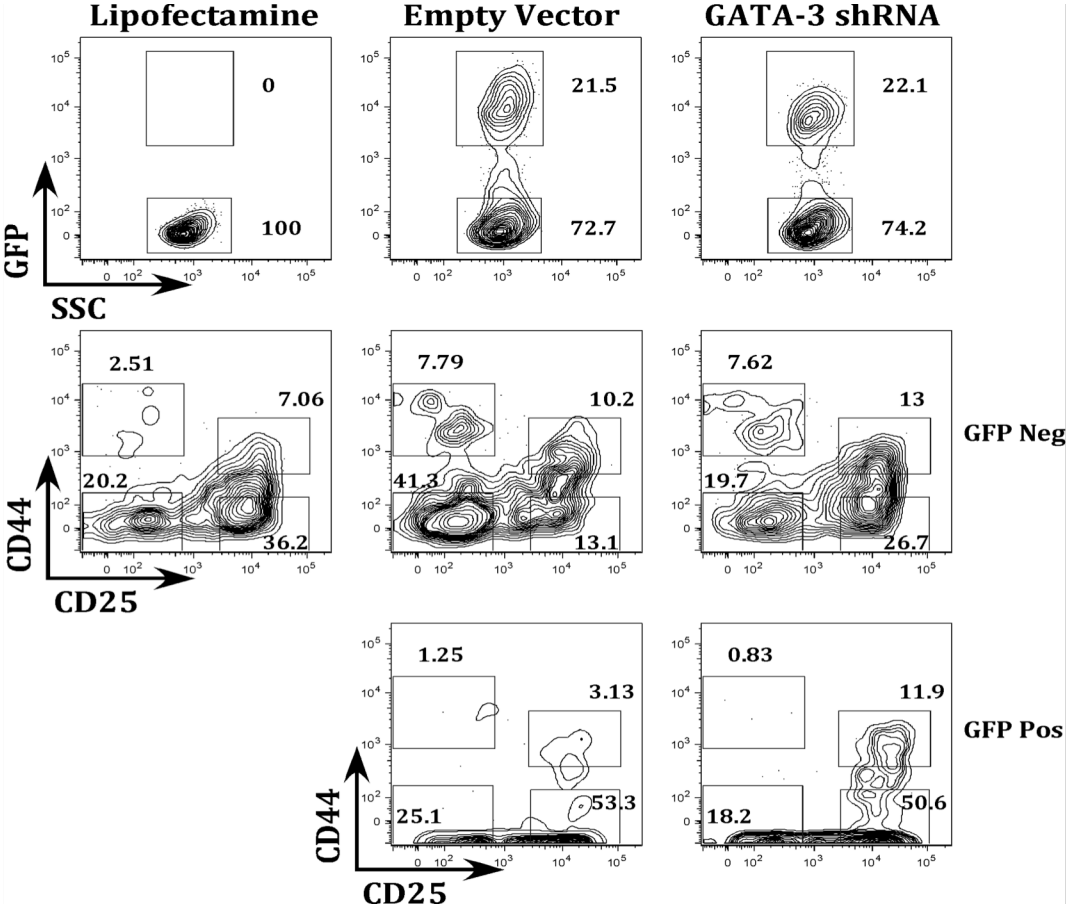

Figure 4: Flow Cytometry representation of the transduction of cocultured DN cells on OP9Dl1

***E- Timeline*:** The optimization of the techniques to be used in this project is in progress. Currently, we have the necessary instruments and scientific skills to complete this project within a 3-year period. Gene expression analysis for the

wild type mice is under way and the GATA3-shRNA construct for Aim 1b has been designed and tested. The q-PCR analysis for Notch-1 regulators for Aim 1 is on progress. The results from Aim 1 should be completed by the end of the first year. Generating the qPCR array data for Aim 2 will be started in the middle of the first year and be concluded and validated via ChIP assay by the second year. The construct of the FKBPL106P for GATA-3 has been generated and in the process of being tested. The work on Aim 3 will be started toward the middle of year 2 and expected to be completed eight months after that. Papers and chapters for the thesis will be written along the way.

F- MATERIALS AND METHODS:

Animals: Wild type C57Bl/6 mice were purchased from The Jackson Laboratories and bred on the vivarium facility at the University of California, Merced. Fetal liver from embryos of 14.5 days post coitum (dpc) will be used to conduct our experiments. GATA-$3^{-/-}$ embryos will be generated by mating GATA-$3^{+/nlslacZ}$ mice. To extend the life of the GATA-3 deficient embryos, the mother will be treated with 100 µg/ml Isoproterenol, 100 µg/ml L-Phenylephrine and 2 mg/ml Ascorbic acid (all from Sigma, Saint Louis, Missouri) in the drinking water, beginning at 8.5 dpc [35]. Fetal liver will be recovered from the embryos at 14.5 dpc, and GATA-$3^{-/-}$ embryos identified by PCR [69]. All experiments and handling of the mice will follow the guidelines approved by UC Merced's IACUC.

Antibodies: The following antibodies were purchased from Bio-Legends: PE anti-

mouse CD44 (clone IM7), PE anti-mouse Sca-1 (E13-161.7), APC and PECy5 anti-mouse CD3 (145-2C11), PECy5 and PECy7 anti-mouse CD4 (RM4-5), Biotin anti-mouse CD45.2 (clone 104), FITC anti-mouse CD117 (2B8), FITC and PECy5 anti-mouse GR-1 (RB6-8C5), PECy5 anti-mouse CD8a (53-6.7), PECy5 anti-mouse CD11b (M1/70), PECy5 anti-mouse CD19 (6D5), PECy5 anti-mouse NK1.1 (PK136), and PECy5 anti-mouse Ter119. Only APC anti-mouse CD25 (PC61) was purchased from eBiosciences.

Isolation of FL-HSC and the sorting of DN cells: Fetal liver from 14.5 dpc embryos are collected and processed for FL-HSC isolation. Before the addition of any antibodies, the FcγRIIIA/B receptors of the cells are blocked with anti-CD16/32 antibody (clone 2.4G2). Harvested cells will be stained with PECy5 conjugated anti-lineage antibodies (CD3, CD4, CD8, CD11b, CD19, GR1, NK1.1, and Ter119), and incubated at 4°C for 20 min. Excess antibody will be washed with FACS buffer, followed by anti-PE MACS magnetic beads staining according to the manufacturer's instructions. Following the 20-minute incubation, the cells will be washed and the Lin^+ fraction depleted using AutoMACS (Miltenyi Biotech). The Lin^- fraction will be stained with c-Kit and Sca-1 and the $Lin^-Sca\text{-}1^+c\text{-}Kit^+$(LSK), containing FL-HSCs, will be sorted.

To isolate DN cells, whole thymus will be stained with anti-CD4 and anti-CD8, followed by depletion of the $CD4^+$ and $CD8^+$ cells by AutoMacs. The $CD4^-CD8^-$ cells will be stained further with anti CD44 and CD25. DN1-DN4 cells

($CD44^{+}CD25^{-}$ for DN1, $CD44^{+}CD25^{+}$ for DN2, $CD44^{-}CD25^{+}$ for DN3, and $CD44^{-}CD25^{-}$ for DN4) will be sorted for molecular analysis into

Cell sorting will be conducted in a 3-laser, 11-parameter FACSAria (Becton Dickinson Biosciences), and collected data will be analyzed using FlowJo (version 7.2.5) flow cytometry software (Tree Star, San Carlos CA).

OP9Dl1 culture system: A modified version of the protocol developed by Schmitt et al., will be used to generate lymphocytes [36]. Fetal liver from 14.5 dpc embryos will be co-cultured with OP9Dl1 stroma on OP9Dl1 media (OPTI-MEM media + Glutamax, 20% FCS, 50 U/ml Penicillin, 50 ug/ml Streptomycin and 5.5 x 10^{-5} M β-mercaptoethanol), for a period of 14 days in the presence of 5 ng/ml of IL-7 and Flt3L as follows:

D0	D1	D2	D3	D4-5	D6	D7
-Prepare $3x10^{5}$ OP9Dl1 cells on 6-well plate in 3ml media.	-Remove the 3 ml media -Add $1x10^{5}$ FL-HSC to the OP9Dl1 into final volume of 3 ml media - Add 5 ng/ml of IL-7 and Flt3L	NO change	Add 3 ml of fresh media (total 6 ml to each well).	NO change	-Prepare new OP9Dl1 in 6 well (3 ml volume)	-Harvest lymphocytes by removing OP9Dl1 through 70 µm filter -Spin the cells 5 min at 1500g -Re-incubate the cells on new OP9Dl1 -Repeat from Day 1 to Day 7 (14 days total).

At Day 14, lymphocytes co-cultured with OP9Dl1 will be harvested and DN populations sorted as explained above. Sorted cell will either be used for qPCR analysis or for the retroviral transduction.

GATA-3 transfection and transduction; The GATA3-shRNA construct will be cloned into a Banshee vector containing GFP [58]. This construct will be transfected into Phoenix ectopic packaging cell line (a kind gift from Dr. Gary Nolan, Stanford University) by Lipofectamine 2000 transfection, following manufacturer's instructions (Invitrogen). Viral supernatant, collected 48 hrs post transfection, was used to transduce the FL-HSC cocultured on OP9Dl1 stroma in 24-well plates using OP9Dl1 media. The transduction process is conducted following the protocol developed by Costa et al., [70]. Briefly, $0.5x10^5$ cocultured FL-HSC cells on $0.5x10^5$ OP9Dl1 stroma will be centrifuged for 2 hrs at 2000 RPM at 32°C with infection cocktail that contains 1ml viral supernatant, 1ml fresh OP9Dl1 media, and 8 µg/ml polybrene, 5 ng/ml of Flt-3L and 5 ng/ml of IL-7. Plates will be incubated for 16 hrs at 32°C before replacing the media and further incubate it for total time of 48 hours at 37°C°. Transduced cells will be analyzed after 2 weeks as described above before sorting for the DN2 population based on their expression of GFP. Sorted cells will be used for the qPCR analysis

qPCR analysis: Total RNA extraction of the sorted cells using TRIzol reagent and DNase-I treatment as well as the synthesis of the cDNA template will be conducted according to the manufacturer's instruction (Invitrogen). q-PCR

analysis using Fast SYBR Green (Applied Biosystem) will be conducted in triplicates. Expression of the genes will be normalized to the housekeeping gene HPRT, and the resulting difference on the Ct values for each reaction will be compared to the difference in Ct values observed in the steady state as described above.

FKBPL106P, Transfection, and Transductions: FKBPL106P:GATA-3iHcRed-t construct will be used to transfect Phoenix ectopic packaging cell line following manufacture protocol of Lipofectamine 2000 (Invitrogen). Viral supernatant will be collected 48 hours post transfection and used to transduce the sorted DN2 of GATA-$3^{-/-}$ embryos in OP9DI1 media that contains different concentrations of Shield-1 ligand (1 μM, 500 nM, 100 nM, 50 nM, 10 nM and a 0.0 nM of Shld-1 as control), 8 μg/ml polybrene, 5 ng/ml of Flt-3L and 5 ng/ml of mrIL-7 by spinning at 2000 rpm, for 2 hrs at 32°C. Transduced cells will be FACS sorted based on their expression of iHcRed-t. Differentiation of the transduced cells beyond the DN2 stage is an indication of how much Shld-1 is required to induce GATA-3 that is required to seal the T cell commitment. Western blot analysis will be used to determine the protein level of GATA-3. Transduced DN2 cells while inducing the appropriate level of GATA-3 protein by the addition of the appropriate concentration of Shld-1 will generate DN3 population that will be sorted out and the gene expression analysis will be done using qPCR technique described previously.

Chromatin immunoprecipitation assay (ChIP): ChIP will be performed following the protocol developed by Nelson et al [65]. Briefly, $1x10^6$ DN2 cells will be cross-linked with 1.5% (wt/vol) formaldehyde. Following cross-linking, the cells will be lysed in IP buffer prepared as described [65] and sonicated to shear the chromatin. After sonication, the supernatant will immunoprecipitated with anti-GATA-3 specific antibodies in an ultrasonic water bath for 15 min at 4°C followed by precipitation with protein A-agarose beads. After washing, the immunoprecipitated complexes will be boiled to reverse the cross-linking and disassociate the beads. The supernatant containing the precipitated DNA will be collected and used for PCR [65].

Bibliography

1. Reya, T., et al., *Stem cells, cancer, and cancer stem cells.* Nature, 2001. **414**(6859): p. 105-11.
2. Quong, M.W., W.J. Romanow, and C. Murre, *E protein function in lymphocyte development.* Annu Rev Immunol, 2002. **20**: p. 301-22.
3. Rothenberg, E.V. and C.J. Dionne, *Lineage plasticity and commitment in T-cell development.* Immunol Rev, 2002. **187**: p. 96-115.
4. Godfrey, D.I., et al., *A developmental pathway involving four phenotypically and functionally distinct subsets of CD3-CD4-CD8- triple-negative adult mouse thymocytes defined by CD44 and CD25 expression.* J Immunol, 1993. **150**(10): p. 4244-52.
5. Zediak, V.P., I. Maillard, and A. Bhandoola, *Closer to the source: notch and the nature of thymus-settling cells.* Immunity, 2005. **23**(3): p. 245-8.
6. Porritt, H.E., et al., *Heterogeneity among DN1 prothymocytes reveals multiple progenitors with different capacities to generate T cell and non-T cell lineages.* Immunity, 2004. **20**(6): p. 735-45.
7. Wilson, A., M. Capone, and H.R. MacDonald, *Unexpectedly late expression of intracellular CD3epsilon and TCR gammadelta proteins during adult thymus development.* Int Immunol, 1999. **11**(10): p. 1641-50.
8. Ceredig, R., N. Bosco, and T. Rolink, *Problems defining DN2 thymocytes.* Immunol Cell Biol, 2008. **86**(7): p. 545-7.
9. Rothenberg, E.V. and T. Taghon, *Molecular genetics of T cell development.* Annu Rev Immunol, 2005. **23**: p. 601-49.
10. Radtke, F., A. Wilson, and H.R. MacDonald, *Notch signaling in T- and B-cell development.* Curr Opin Immunol, 2004. **16**(2): p. 174-9.
11. Artavanis-Tsakonas, S., M.D. Rand, and R.J. Lake, *Notch signaling: cell fate control and signal integration in development.* Science, 1999. **284**(5415): p. 770-6.
12. Kopan, R. and M.X. Ilagan, *The canonical Notch signaling pathway: unfolding the activation mechanism.* Cell, 2009. **137**(2): p. 216-33.
13. Radtke, F., et al., *Notch regulation of lymphocyte development and function.* Nat Immunol, 2004. **5**(3): p. 247-53.
14. Nam, Y., et al., *Structural basis for cooperativity in recruitment of MAML coactivators to Notch transcription complexes.* Cell, 2006. **124**(5): p. 973-83.
15. Amsen, D., et al., *Direct regulation of Gata3 expression determines the T helper differentiation potential of Notch.* Immunity, 2007. **27**(1): p. 89-99.
16. Matsuno, K., et al., *Deltex acts as a positive regulator of Notch signaling through interactions with the Notch ankyrin repeats.* Development, 1995. **121**(8): p. 2633-44.
17. Lehar, S.M. and M.J. Bevan, *T cells develop normally in the absence of both Deltex1 and Deltex2.* Mol Cell Biol, 2006. **26**(20): p. 7358-71.
18. Deftos, M.L., et al., *Notch1 signaling promotes the maturation of CD4 and CD8 SP thymocytes.* Immunity, 2000. **13**(1): p. 73-84.
19. Hoflinger, S., et al., *Analysis of Notch1 function by in vitro T cell differentiation of Pax5 mutant lymphoid progenitors.* J Immunol, 2004. **173**(6): p. 3935-44.
20. Pui, J.C., et al., *Notch1 expression in early lymphopoiesis influences B versus T lineage determination.* Immunity, 1999. **11**(3): p. 299-308.

21. Palaga, T., et al., *TCR-mediated Notch signaling regulates proliferation and IFN-gamma production in peripheral T cells.* J Immunol, 2003. **171**(6): p. 3019-24.
22. Amsen, D., et al., *Instruction of distinct CD4 T helper cell fates by different notch ligands on antigen-presenting cells.* Cell, 2004. **117**(4): p. 515-26.
23. Radtke, F., et al., *Deficient T cell fate specification in mice with an induced inactivation of Notch1.* Immunity, 1999. **10**(5): p. 547-58.
24. Han, H., et al., *Inducible gene knockout of transcription factor recombination signal binding protein-J reveals its essential role in T versus B lineage decision.* Int Immunol, 2002. **14**(6): p. 637-45.
25. Burch, J.B., *Regulation of GATA gene expression during vertebrate development.* Semin Cell Dev Biol, 2005. **16**(1): p. 71-81.
26. Tevosian, S.G., et al., *FOG-2: A novel GATA-family cofactor related to multitype zinc-finger proteins Friend of GATA-1 and U-shaped.* Proc Natl Acad Sci U S A, 1999. **96**(3): p. 950-5.
27. Fang, T.C., et al., *Notch directly regulates Gata3 expression during T helper 2 cell differentiation.* Immunity, 2007. **27**(1): p. 100-10.
28. David-Fung, E.S., et al., *Progression of regulatory gene expression states in fetal and adult pro-T-cell development.* Immunol Rev, 2006. **209**: p. 212-36.
29. Zhong, J.F., et al., *Gene expression profile of murine long-term reconstituting vs. short-term reconstituting hematopoietic stem cells.* Proc Natl Acad Sci U S A, 2005. **102**(7): p. 2448-53.
30. Taghon, T., M.A. Yui, and E.V. Rothenberg, *Mast cell lineage diversion of T lineage precursors by the essential T cell transcription factor GATA-3.* Nat Immunol, 2007. **8**(8): p. 845-55.
31. Georgescu, C., et al., *A gene regulatory network armature for T lymphocyte specification.* Proc Natl Acad Sci U S A, 2008. **105**(51): p. 20100-5.
32. Ting, C.N., et al., *Transcription factor GATA-3 is required for development of the T-cell lineage.* Nature, 1996. **384**(6608): p. 474-8.
33. Hendriks, R.W., et al., *Expression of the transcription factor GATA-3 is required for the development of the earliest T cell progenitors and correlates with stages of cellular proliferation in the thymus.* Eur J Immunol, 1999. **29**(6): p. 1912-8.
34. Pandolfi, P.P., et al., *Targeted disruption of the GATA3 gene causes severe abnormalities in the nervous system and in fetal liver haematopoiesis.* Nat Genet, 1995. **11**(1): p. 40-4.
35. Kaufman, C.K., et al., *GATA-3: an unexpected regulator of cell lineage determination in skin.* Genes Dev, 2003. **17**(17): p. 2108-22.
36. Schmitt, T.M. and J.C. Zuniga-Pflucker, *Induction of T cell development from hematopoietic progenitor cells by delta-like-1 in vitro.* Immunity, 2002. **17**(6): p. 749-56.
37. García-Ojeda, M.E., et al., *GATA-3 seals Notch-induced T cell commitment.* Manuscript in Preparation, 2009.
38. Izon, D.J., et al., *Deltex1 redirects lymphoid progenitors to the B cell lineage by antagonizing Notch1.* Immunity, 2002. **16**(2): p. 231-43.
39. Moloney, D.J., et al., *Fringe is a glycosyltransferase that modifies Notch.* Nature, 2000. **406**(6794): p. 369-75.
40. Liu, W.H. and M.Z. Lai, *Deltex regulates T-cell activation by targeted degradation of active MEKK1.* Mol Cell Biol, 2005. **25**(4): p. 1367-78.

41. Storck, S., et al., *Normal immune system development in mice lacking the Deltex-1 RING finger domain.* Mol Cell Biol, 2005. **25**(4): p. 1437-45.
42. Wilson, A., et al., *Normal hemopoiesis and lymphopoiesis in the combined absence of numb and numblike.* J Immunol, 2007. **178**(11): p. 6746-51.
43. Frise, E., et al., *The Drosophila Numb protein inhibits signaling of the Notch receptor during cell-cell interaction in sensory organ lineage.* Proc Natl Acad Sci U S A, 1996. **93**(21): p. 11925-32.
44. Guo, M., L.Y. Jan, and Y.N. Jan, *Control of daughter cell fates during asymmetric division: interaction of Numb and Notch.* Neuron, 1996. **17**(1): p. 27-41.
45. French, M.B., et al., *Transgenic expression of numb inhibits notch signaling in immature thymocytes but does not alter T cell fate specification.* J Immunol, 2002. **168**(7): p. 3173-80.
46. Sewell, W., et al., *Cyclical expression of the Notch/Wnt regulator Nrarp requires modulation by Dll3 in somitogenesis.* Dev Biol, 2009. **329**(2): p. 400-9.
47. Phng, L.K., et al., *Nrarp coordinates endothelial Notch and Wnt signaling to control vessel density in angiogenesis.* Dev Cell, 2009. **16**(1): p. 70-82.
48. Yun, T.J. and M.J. Bevan, *Notch-regulated ankyrin-repeat protein inhibits Notch1 signaling: multiple Notch1 signaling pathways involved in T cell development.* J Immunol, 2003. **170**(12): p. 5834-41.
49. Lamar, E., et al., *Nrarp is a novel intracellular component of the Notch signaling pathway.* Genes Dev, 2001. **15**(15): p. 1885-99.
50. Lahaye, K., S. Kricha, and E.J. Bellefroid, *XNAP, a conserved ankyrin repeat-containing protein with a role in the Notch pathway during Xenopus primary neurogenesis.* Mech Dev, 2002. **110**(1-2): p. 113-24.
51. Kuroda, K., et al., *Regulation of marginal zone B cell development by MINT, a suppressor of Notch/RBP-J signaling pathway.* Immunity, 2003. **18**(2): p. 301-12.
52. Li, J., et al., *The Spen homolog Msx2-interacting nuclear target protein interacts with the E2 ubiquitin-conjugating enzyme UbcH8.* Mol Cell Biochem, 2006. **288**(1-2): p. 151-7.
53. Yabe, D., et al., *Generation of a conditional knockout allele for mammalian Spen protein Mint/SHARP.* Genesis, 2007. **45**(5): p. 300-6.
54. Li, J., et al., *The C terminus of MINT forms homodimers and abrogates MINT-mediated transcriptional repression.* Biochim Biophys Acta, 2005. **1729**(1): p. 50-6.
55. Tsuji, M., et al., *Msx2-interacting nuclear target protein (Mint) deficiency reveals negative regulation of early thymocyte differentiation by Notch/RBP-J signaling.* Proc Natl Acad Sci U S A, 2007. **104**(5): p. 1610-5.
56. Adolfsson, J., et al., *Upregulation of Flt3 expression within the bone marrow Lin(-)Sca1(+)c-kit(+) stem cell compartment is accompanied by loss of self-renewal capacity.* Immunity, 2001. **15**(4): p. 659-69.
57. Livak, K.J. and T.D. Schmittgen, *Analysis of relative gene expression data using real-time quantitative PCR and the 2(-Delta Delta C(T)) Method.* Methods, 2001. **25**(4): p. 402-8.
58. Hernandez-Hoyos, G. and J. Alberola-Ila, *Analysis of T-cell development by using short interfering RNA to knock down protein expression.* Methods Enzymol, 2005. **392**: p. 199-217.

59. Zhu, J., et al., *Conditional deletion of Gata3 shows its essential function in T(H)1-T(H)2 responses.* Nat Immunol, 2004. **5**(11): p. 1157-65.
60. Marine, J. and A. Winoto, *The human enhancer-binding protein Gata3 binds to several T-cell receptor regulatory elements.* Proc Natl Acad Sci U S A, 1991. **88**(16): p. 7284-8.
61. Wingender, E., et al., *The TRANSFAC system on gene expression regulation.* Nucleic Acids Res, 2001. **29**(1): p. 281-3.
62. Wingender, E., et al., *TRANSFAC: an integrated system for gene expression regulation.* Nucleic Acids Res, 2000. **28**(1): p. 316-9.
63. Heinemeyer, T., et al., *Databases on transcriptional regulation: TRANSFAC, TRRD and COMPEL.* Nucleic Acids Res, 1998. **26**(1): p. 362-7.
64. Schug, J., *Using TESS to predict transcription factor binding sites in DNA sequence.* Curr Protoc Bioinformatics, 2008. **Chapter 2**: p. Unit 2 6.
65. Nelson, J.D., O. Denisenko, and K. Bomsztyk, *Protocol for the fast chromatin immunoprecipitation (ChIP) method.* Nat Protoc, 2006. **1**(1): p. 179-85.
66. Banaszynski, L.A., et al., *A rapid, reversible, and tunable method to regulate protein function in living cells using synthetic small molecules.* Cell, 2006. **126**(5): p. 995-1004.
67. Peixoto, A., et al., *Quantification of multiple gene expression in individual cells.* Genome Res, 2004. **14**(10A): p. 1938-47.
68. Ko, L.J. and J.D. Engel, *DNA-binding specificities of the GATA transcription factor family.* Mol Cell Biol, 1993. **13**(7): p. 4011-22.
69. Samson, S.I., et al., *GATA-3 promotes maturation, IFN-gamma production, and liver-specific homing of NK cells.* Immunity, 2003. **19**(5): p. 701-11.
70. Costa, G.L., et al., *Targeting rare populations of murine antigen-specific T lymphocytes by retroviral transduction for potential application in gene therapy for autoimmune disease.* J Immunol, 2000. **164**(7): p. 3581-90.

APPENDIX B

Multiplex single cell RT-qPCR analysis of fetal and adult murine long-term hematopoietic stem cells

Jesús Ciriza[1], Mufadhal Al-Kuhlani[1], Dominique Hall[1], Alison Lu[1], Joseph Robert De Sena[1], Marcos E. García-Ojeda[1].

[1]University of California, Merced, School of Natural Sciences.

Corresponding author:

Marcos E. García-Ojeda, PhD

University of California, Merced

School of Natural Sciences

5200 North Lake Road

Merced, CA 95343 USA

Tel. 209-228-6986

Fax. 209-228-4060

Email: mgarcia-ojeda@ucmerced.edu

Other Authors:

Jesús Ciriza, PhD

University of California, Merced

School of Natural Sciences

5200 North Lake Road

Merced, CA 95343 USA

Tel. 209-228-4378

Fax. 209-228-4060

Email: jciriza@ucmerced.edu

Mufadhal Al-Kuhlani
University of California, Merced
School of Natural Sciences
5200 North Lake Road
Merced, CA 95343 USA
Tel. 209-228-4378
Fax. 209-228-4060
Email: mal-kuhlani@ucmerced.edu

Dominique Hall
University of California, Merced
School of Natural Sciences
5200 North Lake Road
Merced, CA 95343 USA
Tel. 209-228-4378
Fax. 209-228-4060
Email: dhall@ucmerced.edu

Alison Lu
University of California, Merced
School of Natural Sciences
5200 North Lake Road
Merced, CA 95343 USA
Tel. 209-228-4378
Fax. 209-228-4060
Email: alu3@ucmerced.edu

Joseph Robert De Sena
University of California, Merced
School of Natural Sciences

5200 North Lake Road
Merced, CA 95343 USA
Tel. 209-228-4378
Fax. 209-228-4060
Email: jdesena@ucmerced.edu

Abstract

Murine long-term hematopoietic stem cells (LT-HSCs), with the $CD150^{+}CD48^{-}CD4^{-}Lineage^{-/low}$ phenotype, can be isolated by flow cytometry from fetal and adult tissues. However, the rare number of LT-HSC in fetal tissues precludes their gene expression analysis by classical molecular biology techniques. Here we present an affordable protocol to optimize and perform multiplex gene expression analysis from single cells by RT-qPCR. In this protocol, we analyze expression of 9 genes per single cell, but it can be easily scaled up to examine a larger number of genes. This technique can be adapted to analyze gene expression in other rare populations. Our results demonstrate the power of single cell multiplex gene expression analysis: demonstration of gene expression distribution within a defined phenotypic population, which would be otherwise masked by whole population analysis.

Keywords

Fetal hematopoietic cells, Long-term hematopoietic stem cells, single cell sorting by flow cytometry, single cell multiplex RT-qPCR, cell migration.

Introduction

Hematopoietic stem cells (HSCs) are characterized by their capacity to provide lifelong reconstitution of all blood cell lineages after transplantation into lethally irradiated recipients, calling this population long-term HSC (LT-HSCs) [1]. All functional HSCs are included within the Lineage$^-$Sca-1$^+$cKit$^+$ (LSK) population, but not all LSK have long-term repopulating activity. The LSK population can be subdivided further into three subsets: LT-HSCs, the short-term HSCs (ST-HSC), and the multipotential progenitors (MPP). The LT-HSCs, with the CD150$^+$CD48$^-$ CD41$^-$ phenotype, are the most immature cells within the LSK population, displaying long-term self-renewal potential [2,3]. LT-HSCs from the fetal liver and fetal bone marrow also have this phenotype [4-6]. The absolute number of LT-HSCs in the adult bone marrow is very low (about 4 LT-HSC per 10^7 marrow cells), with even lower numbers when fetal tissues are studied [4]. Traditional quantitative gene expression profiling studies of rare populations, such as LT-HSC, are done at the population level. This type of analysis provides the average expression pattern for a particular gene within the population masking differences in the gene expression distribution among members of that population [7]. Therefore, gene expression analysis of LT-HSC requires alternative approaches available for routine experimentation that produce more in depth data analysis [5].

The analysis of rare populations must be approached by single cell multiplex gene expression quantification. Three main methods have been

described for multiplex quantification of single cell gene expression: Digital RT-PCR [8], digital mRNA-Seq [9] and RT-qPCR [10]. Digital RT-PCR is a reliable strategy for single cell gene expression analysis that requires a digital array chip and Fluidigm Access Array™ [11]. Similarly, digital mRNA-Seq requires next generation sequencing systems, such as the SOLiD or Illumina systems [9,12]. The Fluidigm Access Array™ microfluidic systems and the next-generation sequencing systems are not often available in labs. On the other hand, RT-qPCR is a technique that only requires a traditional thermocycler and a qPCR system, making it a more accessible strategy for single cells gene expression studies. Single cell multiplex RT-qPCR consists of retrotranscription from a single cell followed by PCR preamplification and further quantification of genes of interest. The qPCR of the preamplified product can be performed in a semi-nested reaction [10] or by using the same primers utilized during the preamplification step [5]. Here, we present a protocol designed to quantify the expression of 9 genes from single LT-HSC, using identical primers in the PCR preamplification and quantification steps. Following isolation by FACS, single LT-HSCs are lysed by heat shock and the cDNA for the genes of interest obtained by retrotranscription with gene specific primers. The cDNA products undergo a 10-cycle PCR preamplification step with primer pairs for each gene of interest (Figure 1). This preamplification step has been shown to maintain the proportion of the original gene expression sample in an efficient, reproducible and unbiased way, decreasing the levels of technical noise [13].

Several requirements need to be met before performing the single cell multiplex RT-qPCR. First, the primers need to be designed carefully to avoid the formation of primer dimers and hairpin loops, in order to minimize primer competition during the multiplex reactions and ensure similar PCR amplification efficiencies for all the genes tested. All primers should have similar length (between 18-21 base pairs), melting temperatures and CG content, if possible hybridize across an intron (to avoid amplification of contaminating genomic DNA) and amplify products of similar sizes (between 100-150 base pairs).

After finding the gene sequences in Genbank [14], all primers can be designed by means of online software such as Primer3Plus [15] and primer dimer formation tested with PrimersList online software [16]. The gene specificity of each primer must be verified using NCBI's BLAST [17]. Following primer design, several analyses must be done in order to test the accuracy of the PCR amplification. Primer competition needs to be evaluated for each gene of interest in both retrotranscription and preamplification reactions by comparing the gene-specific amplification in a multiplex reaction containing all the primers versus amplification with only the primer pair specific for one gene [5]. The qPCR amplification efficiency and detection limit for each reaction also need to be determined. In this regard, cloning the PCR products amplified for each gene through a classical PCR cloning system will allow the preparation of 10-fold dilutions samples with known concentrations. With these samples, qPCR efficiency studies can be performed and the detection limit can be determined [5].

Primer pairs that result in similar qPCR amplification efficiencies are required in order to compare the expression of the different genes. If the reactions do not have similar qPCR amplification efficiencies, the primer pair needs to be redesigned and tested. Detection limits of 100 copies, corresponding to the expression of transcription factors, are sufficient for the multiplex reaction since lower values cannot be differentiated from intrinsic noise in the qPCR [18,19]. Lastly, it is important to test the ability of the technique to detect variations in the initial template concentration for each gene in the presence of a constant template concentration for the other genes of interest [5].

Once the retrotranscription and qPCR amplification have been optimized, the single cell gene expression quantification can be performed. Because the high cell-to-cell variation in the levels of all genes, absolute quantification is the best measurement to does comparing the expression of each single cell to a RNA or DNA standards. However when comparing the down- or upregulation of genes among a large number of individual cells, relative quantification can be a reasonable less expensive choice. In the following protocol, we describe a relative quantification procedure where a large number of single cells from a defined population (obtained from different tissues or experimental conditions) can be compared in order to evaluate simultaneously the variation in gene expression for several genes. This protocol formed the basis of our previous study of migration-related genes in LT-HSCs across different anatomical locations during development [5]. However, this technique could be applied to

cells from other populations as long as they are able to be single-cell sorted by either flow cytometry or another cell isolation technique such as limiting dilution [10,13]. Currently, our group is using this protocol to study the variation of gene expression in $CD4^{-}CD8^{-}$ double negative thymocyte subpopulations of genes important in T cell specification and commitment.

Materials

Reagents

1. C57BL/6 (B6) mice can be purchased from any breeding company and/or bred in house in sterile microisolator cages with sterile feed and autoclaved water, as required by UC Merced Institutional Animal Care and Use Committee.
2. M199+ media (Invitrogen, NY, cat. no. 11150059)
3. Fetal Bovine Serum, FBS (Atlanta Biologicals, GA, cat. no. S11550).
4. Dulbecco's phosphate buffered saline without calcium and magnesium, PBS (HyClone, UT, cat. no. SH30378.02)
5. Affinity Purified anti-mouse CD16/32 - blocks Fc binding (clone 93, e-Biosciences, CA, cat. no. 14-0161-82)
6. PE-Cy5 Anti-mouse CD3ε Antibody (clone 145-2C11, BioLegend, CA, cat. no. 100310)
7. PE-Cy5 Anti-mouse CD4 Antibody (clone RM4-5, BioLegend, CA, cat. no. 100514)
8. PE-Cy5 Anti-mouse CD8a Antibody (clone 53-6.7, BioLegend, CA, cat. no. 100710)
9. PE-Cy5 Anti-mouse CD11b Antibody (clone M1/70, BioLegend, CA, cat. no. 101210)
10. PE-Cy5 Anti-mouse CD19 Antibody (clone 6D5, BioLegend, CA, cat. no. 115510)

11. PE-Cy5 Anti-mouse NK-1.1 Antibody (clone PK136, BioLegend, CA, cat. no. 108716)
12. PE-Cy5 Anti-mouse Ter-119/Erythroid Cells Antibody (clone Ter-119, BioLegend, CA, cat. no. 116210)
13. PE-Cy5 Anti-mouse Ly-6G/Ly-6C (Gr-1) Antibody (clone RB6-8C5, BioLegend, CA, cat. no. 108410)
14. PE Anti-mouse Ly-6A/E (Sca-1) Antibody (clone E13-161.7, BioLegend, CA, cat. no. 122508)
15. APC Anti-mouse CD117 (c-Kit) Antibody (clone 2B8, BioLegend, CA, cat. no. 105812)
16. PE-Cy7 Anti-mouse CD150 (SLAM) Antibody (clone TC15-12F12.2, BioLegend, CA, cat. no. 115914)
17. FITC Anti-mouse CD48 Antibody (clone HM48-1, BioLegend, CA, cat. no. 103404)
18. FITC Anti-mouse CD41 Antibody (clone MWReg30, e-Biosciences, CA, cat. no. 11-0411-82)
19. RNaseOUT™ Recombinant Ribonuclease Inhibitor (Invitrogen, NY, cat. no. 10777-019)
20. BD™ CompBeads (BD Biosciences, NJ, cat. no. 552845)
21. TRIzol® (Invitrogen, NY, cat. no. 15596-018)
22. DNAse I (Invitrogen, NY, cat. no. 18068-015)
23. Gene-specific forward and reverse primers (100 mM concentration, Sigma-Aldrich Corp, TX)

24. SuperScript® III First-Strand Synthesis System for RT-PCR (Invitrogen, NY, cat. no. 18080-051)
25. Platinum® Taq DNA polymerase (Invitrogen, NY, cat. no. 10966-026)
26. 1x Fast SYBR® Green Master Mix (Applied Biosystems, CA, cat. no. 4385612)
27. UltraPure™ Distilled Water DNAse RNAse Free (Invitrogen, NY, cat. no. 109770-23)
28. Trypan Blue 0.4% (Invitrogen, NY, cat. no. 15250-061)

Equipment

1. Zeiss Stemi DV4 dissecting microscope (Zeiss, NY, cat. no. 435421-9901-000)
2. Cell Strainer (70 µm, BD Biosciences, CA, cat. no. 322350)
3. Syringe (5 ml, Becton Dickinson, NJ)
4. Syringe (1 ml, Becton Dickinson, NJ)
5. Syringe needle (25G, Becton Dickinson, NJ).
6. Centrifuge tubes (15 ml; BD Falcon, cat. no. 352097)
7. Round-bottom tube (5 ml; BD Falcon, cat. no. 352063)
8. Hemocytometer (Hausser Scientific, cat. no. 3500)
9. Low-Profile 0.2 ml 8-Tube Strips without Caps (Bio-Rad, CA, cat. no. TLS-0851EDU)
10. Optical Flat 8-Cap Strips (Bio-Rad, CA, cat. no. TCS-0803EDU)
11. Twin.tec® PCR plate 96, skirted (Eppendorf, NY, cat. no. 0030 128.672). We remove the tubes from these plates filling the empty frame with 0.2 ml

low profile thin-walled 8 tubes. This system allows sorting just the strips needed instead of a whole plate. Size higher to 0.2 ml cannot be used in the BD Biosciences FACSAria™ IIu cell sorter for single cell sorting.

12. MicroAmp® Fast Optical 96-well (0.1 ml) Reaction Plate with Barcode (Applied Biosystems, CA, cat. no. 4346906)
13. MicroAmp® Optical Adhesive Film (Applied Biosystems, CA, cat. no. 4311971)
14. BD Biosciences FACSAria™ IIu cell sorter (BD Biosciences, CA) controlled by BD FACSDiva™, v.6.1.3 software (Becton Dickinson, Franklin Lakes, NJ). We used the following solid-state lasers: Sapphire™ 488-20 (488 nm) and JDS Uniphase™ 1144-P (633 nm). Any FACS system with single cell sorting capacity and five-color analysis could be used, but the positioning of the single drop requires optimization and verification.
15. Nanodrop ND-1000 spectrophotometer (Thermo Scientific, MA)
16. Mastercycler EP gradient S thermocycler (Eppendorf, NY, cat. no. E950040025).
17. StepOnePlus qPCR System (Applied Biosystems, CA, cat. no. 4376600) controlled by StepOne™ software, version 2.0. We used the “quantitation Relative Standard Curve” set up with SYBR® Green Reagents and Fast (~40 minutes) run options of the system. Any qPCR system can be used, but this system allows the qPCR to run faster

18. AirClean®600 PCR Workstation (AirClean Systems, NC, cat. no. AC624LFUW)
19. 0.22 mm GV PVDF Membrane Stericup & Steritop (Millipore, MA, cat. no. SC00B10RE)
20. Dumont No. 5 super fine forceps (Roboz, MD, cat. no. RS-4955)
21. Mouse dissection tools.

Solutions and Buffers

1. Trypan Blue working solution (0.04%). Dilute 5 ml of Trypan Blue (0.4%) with 45 ml of PBS.
2. Propidium iodide (PI) stock. 1 mg ml^{-1} PI (Sigma-Aldrich) in PBS stored at -20°C.
3. FACS sorting buffer. Add 10 ml of heat inactivated FBS to 490 ml of PBS. Filter-sterilize in 0.22 μm Stericup and stored at 4°C.
4. Single cell sorting buffer: 20 units of RNAse OUT (0.5 ml of RNAse OUT) in 10 mM Tris-HCl, 25 mM KCl at pH 8.4 (0.25 ml of 10x RT buffer and 4.25 ml of water RNAse free). Prepare it in a PCR workstation and stored at -20°C.
5. Antibody dilution buffer: 0.09% sodium azide, 1% BSA in PBS. Store at 4°C.
6. Antibody cocktail: add 5 ml anti CD3 conjugated to PE-Cy5, 5 ml anti CD4 conjugated to PE-Cy5, 5 ml anti CD8 conjugated to PE-Cy5, 5 ml anti CD11b conjugated to PE-Cy5, 5 ml anti CD19 conjugated to PE-Cy5, 5 ml anti NK1.1 conjugated to PE-Cy5, 5 ml anti Ter119 conjugated to PE-Cy5,

5 ml anti Gr-1 conjugated to PE-Cy5, 5 ml anti Sca-1 conjugated to PE, 5 ml anti c-Kit conjugated APC, 5 ml anti CD150 conjugated to PE-Cy7, 5 ml anti CD48 conjugated to FITC, 5 ml anti CD41 conjugated to FITC in a final volume of 500 ml of FACS solution. Antibodies must be previously titrated to determine the appropriate concentration that gives the highest signal with the lowest background. They are diluted in the antibody dilution buffer to be used at a concentration 1:100.

7. Retrotranscription primer solution: add 0.5 ml of 10 mM dNTPs mix to1 ml of RT primers mix (mix contains RT primers for each gene studied at 10 mM). Prepare immediately before use. The volumes provided here are for one well. Scale your master mix accordingly

8. Retrotranscription mix solution: mix 0.5 ml of 10x RT buffer, 2 ml of 25 mM $MgCl_2$, 1 ml of 0.1 M DTT, 0.5 ml of 40 U µl-1 RNAse OUT and 0.5 ml of 200 U µl-1 SuperScript® III. Prepare immediately before use. All the reagents are provided in SuperScript® III First-Strand Synthesis System for RT-PCR. The volumes provided here are for one well. Scale your master mix accordingly.

9. Preamplification solution: mix 5 ml of 10x PCR Buffer, 1.5 ml of 50 mM $MgCl_2$, 1 ml of 10 mM dNTPs mix, 2 ml of forward and reverse primers mix (this mix contains similar volumes of 10 mM forward and 10 mM reverse primers for each gene studied), 0.5 ml of 5 U µl-1 Platinum® Taq DNA polymerase. All the reagents (except primers) are provided in Platinum®

Taq DNA polymerase kit. The volumes provided here are for one well. Scale your master mix accordingly. Prepare immediately before use.

10. qPCR solution: mix 10 ml of 2x Fast SYBR Master Mix, 0.4 µl of 10 mM forward primer (gene of interest), 0.4 ml of 10 mM reverse primer (gene of interest) and 4.2 ml of water RNAse free. Prepare immediately before use. The volumes provided here are for one well. Scale your master mix accordingly.

Methods

Single LT-HSCs flow cytometry sorting.

1 Mate breeder mice in the early evening and check vaginal plugs the following morning designated as 0.5 dpc.

2 Euthanize adult and pregnant mice at the gestation time of interest by CO_2 asphyxiation keeping embryos alive. All animal procedures must be performed in accordance with relevant authorities' guidelines and regulations

3 With scissor and forceps, dissect the femora and tibiae from adult mice and place them in ice-cold M199+ media supplemented with 2% FBS. From pregnant mothers, dissect out the uterus, rinse in ice-cold PBS and remove the embryos from uterus. Using fine forceps, separate the muscular wall of the uterus and visceral yolk sac from the embryo. Place embryos on ice-cold M199+ media with 2% FBS. Under an inverted microscope, carefully dissect fetal livers and fetal bones from embryos removing traces of other remaining tissues using Dumont No. 5 super fine forceps. Place these tissues in ice-cold M199+ media with 2% FBS.

4 Cut off both ends of adult bones and flush out bone marrow with a 25G needle and a 5 ml syringe containing ice-cold M199+ media with 2% FBS. Disaggregate adult marrow and fetal liver and bone marrow tissues on a 70 μm cell strainer using the rubber plunger of a 1 ml syringe. Transfer the single cells suspension to a 15 ml conical tube.

5 Centrifuge down cells for 5 min at 300g at 4°C with the brake on.

6 Carefully discard the supernatant and resuspend the pellet in 5 ml of ice-cold M199+ media containing 2% FBS. Count nucleated cells with a hemocytometer. Keep some cells as unstained controls for the flow cytometry analysis and instrument set up. Expect low cell numbers from the fetal bone marrow samples.

7 Centrifuge down cells for 5 min at 300*g* at 4°C with the brake on.

8 Carefully discard the supernatant and resuspend the cell pellet in 500 ml of FACS sorting buffer containing 6.25 ml of anti-mouse CD16/32 monoclonal antibody to block antibody-Fc receptor binding. Incubate for 5 minutes on ice.

9 Wash cells with 5 ml of ice-cold FACS sorting buffer and centrifuge for 5 min at 300*g* at 4°C with the brake on.

10 Resuspend pellet in 500 ml of Antibody cocktail and transfer to a 5 ml round-bottom tube. At this step, set up compensation samples by mixing BD™ CompBeads and 0.5 µl of fluorochrome-conjugated antibodies per fluorochrome used. Ensure that the BD™ CompBeads used bind to your antibody isotype.

11 Incubate for 30 minutes on ice in the dark.

12 Wash cells twice with 4 ml of ice-cold FACS sorting buffer by centrifuging for 5 min at 300*g* at 4°C with the brake on. In the second washing step, filter the samples through a 70 µm cell strainer before proceeding to the flow cytometer to avoid clogs while sorting.

13 Discard supernatant and resuspend pellets in 250 ml of ice-cold FACS sorting buffer.

14 Add Propidium iodide to a final concentration of 0.5 mg ml^{-1} just before analyzing the samples by flow cytometry. Keep one sample completely unstained as a control. Keep samples in the dark until they are ready to be analyzed and sorted.

15 Analyze and sort by BD FACSAria™ IIu cell sorter with settings shown in Table 1. Flow cytometry analyses of LT-HSCs and their sorting gates are shown in Figure 2.

16 Sort single LT-HSCs into Low-Profile 0.2 ml 8-Tube Strips containing 5 ml of single cell sorting buffer. Wells containing single cells must be spun down and can be frozen and stored for up to two months at -20°C **(See Note 1)**.

Single-Cell Multiplex RT-qPCR.

1 Add 100 ng of RNA extracted from bone marrow to wells containing only sorting buffer. These wells will be used as a positive control while wells containing only sorting buffer will be used as negative control **(See Note 2)**.

2 Heat-lyse single cells in a Mastercycler EP gradient S thermocycler at 65°C for 5 minutes followed by cooling at 4°C for a minimum of 5 minutes. Treat positive and negative samples in the same manner as the experimental samples.

3 Add 1.5 ml of the retrotranscription primer solution to each well and incubate in the thermocycler for 5 minutes at 65°C, followed by cooling down to 4°C.

4 Add 4.5 ml of retrotranscription mix solution to each well and incubate in the thermocycler for 50 minutes at 50°C followed by 5 minutes at 85°C. Cool down to 4°C.

5 Add 0.5 ml of RNaseH (2 U μl^{-1}) provided in the SuperScript® III First-Strand Synthesis System for RT-PCR. Incubate for 20 minutes at 37°C and cool down at 4°C.

6 Dilute samples by adding 29 ml of DNAse, RNAse free water. Dilution should be done immediately after retrotranscription to minimize the formation of primer dimers. At this step, wells can be frozen and stored for up to two months at -20°C.

7 Add 10 ml of preamplification solution to each well, place them in the thermocycler and perform the 10-cycle preamplification with the following conditions: 94°C for 45 seconds followed by 10 cycles, each cycle consisting on 94°C for 1 minute, 60°C for 1 minute and 72°C for 1 minute.

8 Transfer 45 ml of preamplified samples to a 1.5 ml microcentrifuge tube. Dilute by adding 180 ml of DNAse, RNAse free water. This dilution should be done immediately after preamplification to minimize the formation of primer dimers. Wells can be frozen and stored for up to two months at -20°C.

9 In a MicroAmp Fast Optical 96-Well Reaction Plate, dispense 5 ml of preamplified sample in triplicates wells. Add samples of positive controls and negative controls to triplicates wells

10 Add 15 ml of qPCR solution containing primers for the housekeeping gene to each well and perform a qPCR reaction in a StepOnePlus System with the

following conditions: 95°C for 10 minutes followed by 60 cycles, each cycle consisting on 95°C for15 seconds and 60°C for 1 minute. Add a melting curve analysis at the end of the reaction.

11 Compare the melting curves of the housekeeping gene for each single cell triplicate with the positive control. Wells with melting curve that does not match the positive control must be discarded (Figure 3).

12 Repeat step 9 for each gene to be studied using samples not discarded in step 11. Prepare qPCR solutions for each gene of interest as well as for the housekeeping gene. Figure 4 shows an example of an experimental 96-well plate design. Repeat this step until all single cells have been analyzed for all genes of interest. Add samples of positive and negative controls in triplicates wells for each gene studied.

13 Analyze the data with the StepOne™ software, version 2.0, applying the same threshold value to all the samples studied. Export C_t values from all the samples into a spreadsheet file. Single cells which melting curves do not match with the positive control's melting curve should be considered not detectable. Figure 5 shows an example of the detection of several genes following this procedure.

14 Choose one single cell randomly as reference sample to calculate $2^{-\Delta\Delta Ct}$. Figure 6 shows the $\log(2^{-\Delta\Delta Ct})$ distribution of VE-cadherin expression in 24 single fetal liver or adult LT-HSC.

This technology can be used to simultaneously examine the single-cell gene expression of multiple genes from any cell type. Figure 7 shows the expression of CD44 and CD25 markers on $CD4^{-}CD8^{-}$ double negative (DN) thymocytes. The DN population can be divided into DN1 ($CD44^{+}CD25^{-}$), DN2 ($CD44^{+}CD25^{+}$), DN3 ($CD44^{-}CD25^{+}$) and DN4 cells ($CD44^{-}CD25^{-}$). Single cells from the various DN subpopulations were sorted following similar parameters described in this protocol. Figure 8 shows the analysis of single DN1-DN4 cells sorted based on the phenotype shown in Figure 7. The single cell multiplex RT-qPCR protocol described in this manuscript was used to perform these analyses. However, a different qPCR machine was used demonstrating that this protocol works successfully for different genes and cell populations independently of the qPCR system used.

Notes

1. The abundance of the population to be sorted will influence the speed of the single cell sort. Therefore, sort into one to three 8-well strips instead of a whole 96-well plate, spinning down and freezing the samples to preserve the integrity of the RNA. Set up of the single cell sorting mechanism must be aligned in order to ensure that sorted single cells land in or near the sorting buffer.
2. After single cells sorting all the manipulation should be done in a ventilated PCR workstation to prevent contamination. Contaminations can be detected by negative controls giving same melting curve than positive control. If contamination is detected, all reagents must be replaced by new ones and pipetters cleaned as recommended by manufacturer.

Acknowledgement

The authors thank Mr. Roy Hoglund and the staff of the UC Merced Laboratory Animal Resource Center for mouse husbandry and care. This work was funded by the University of California, Merced start-up funds. J.C. was partially funded by a postdoctoral fellowship from the Government of Navarra, Spain and the California Institute for Regenerative Medicine Stem Cell Training Program Award (TG2-01163).

Conflict of interest

The authors declare that they have no conflict of interest.

References

1. Domen J, Weissman IL (1999) Self-renewal, differentiation or death: regulation and manipulation of hematopoietic stem cell fate. *Mol Med Today* 5 (5):201-208

2. Kiel MJ, Yilmaz OH, Iwashita T, Yilmaz OH, Terhorst C, Morrison SJ (2005) SLAM family receptors distinguish hematopoietic stem and progenitor cells and reveal endothelial niches for stem cells. *Cell* 121 (7):1109-1121

3. Wilson A, Trumpp A (2006) Bone-marrow haematopoietic-stem-cell niches. *Nat Rev Immunol* 6 (2):93-106

4. Ciriza J, Garcia-Ojeda ME (2011) Expression of migration-related genes is progressively upregulated in murine Lineage-Sca-1+c-Kit+ population from the fetal to adult stages of development. *Stem Cell Res Ther* 1 (2):14. doi:10.1186/scrt14

5. Ciriza J, Hall D, Lu A, De Sena JR, Al-Kuhlani M, Garcia-Ojeda ME (2012) Single-cell analysis of murine long-term hematopoietic stem cells reveals distinct patterns of gene expression during fetal migration. *PLoS One* 7 (1):e30542. doi:10.1371/journal.pone.0030542

6. Kim I, He S, Yilmaz OH, Kiel MJ, Morrison SJ (2006) Enhanced purification of fetal liver hematopoietic stem cells using SLAM family receptors. *Blood* 108 (2):737-744

7. Miyamoto T, Iwasaki H, Reizis B, Ye M, Graf T, Weissman IL, Akashi K (2002) Myeloid or lymphoid promiscuity as a critical step in hematopoietic lineage commitment. *Dev Cell* 3 (1):137-147. doi:S1534580702002010

8. Warren L, Bryder D, Weissman IL, Quake SR (2006) Transcription factor profiling in individual hematopoietic progenitors by digital RT-PCR. *Proc Natl Acad Sci U S A* 103 (47):17807-17812

9. Tang F, Barbacioru C, Wang Y, Nordman E, Lee C, Xu N, Wang X, Bodeau J, Tuch BB, Siddiqui A, Lao K, Surani MA (2009) mRNA-Seq whole-transcriptome analysis of a single cell. *Nat Methods* 6 (5):377-382. doi:10.1038/nmeth.1315

10. Peixoto A, Monteiro M, Rocha B, Veiga-Fernandes H (2004) Quantification of multiple gene expression in individual cells. *Genome Res* 14 (10A):1938-1947

11. Sanchez-Freire V, Ebert AD, Kalisky T, Quake SR, Wu JC (2012) Microfluidic single-cell real-time PCR for comparative analysis of gene expression patterns. *Nat Protoc* 7 (5):829-838. doi:10.1038/nprot.2012.021

12. Islam S, Kjallquist U, Moliner A, Zajac P, Fan JB, Lonnerberg P, Linnarsson S (2011) Characterization of the single-cell transcriptional landscape by highly multiplex RNA-seq. *Genome Res* 21 (7):1160-1167. doi:10.1101/gr.110882.110

13. Warren LA, Rossi DJ, Schiebinger GR, Weissman IL, Kim SK, Quake SR (2007) Transcriptional instability is not a universal attribute of aging. *Aging Cell* 6 (6):775-782

14. Benson DA, Karsch-Mizrachi I, Lipman DJ, Ostell J, Sayers EW (2010) GenBank. *Nucleic Acids Res*. doi:10.1093/nar/gkq1079

15. Untergasser A, Nijveen H, Rao X, Bisseling T, Geurts R, Leunissen JA (2007) Primer3Plus, an enhanced web interface to Primer3. *Nucleic Acids Res* 35 (Web Server issue):W71-74. doi:10.1093/nar/gkm306

16. Kalendar R, Lee D, Schulman AH (2011) Java web tools for PCR, in silico PCR, and oligonucleotide assembly and analysis. *Genomics* 98 (2):137-144. doi:10.1016/j.ygeno.2011.04.009

17. Morgulis A, Coulouris G, Raytselis Y, Madden TL, Agarwala R, Schaffer AA (2008) Database indexing for production MegaBLAST searches. *Bioinformatics* 24 (16):1757-1764. doi:10.1093/bioinformatics/btn322

18. Bengtsson M, Hemberg M, Rorsman P, Stahlberg A (2008) Quantification of mRNA in single cells and modelling of RT-qPCR induced noise. *BMC Mol Biol* 9:63

19. Todd R, Margolin DH (2002) Challenges of single-cell diagnostics: analysis of gene expression. *Trends Mol Med* 8 (6):254-257

Figure Legends

Figure 1. Schematic representation of the single cell multiplex RT-qPCR protocol. cDNA is obtained by retrotranscription reaction with specific primers after heat shock lyses of single cells. A preamplified product is produced by a 10-cycle PCR. Preamplified product is quantified by qPCR analysis with the same pair of primers used in the preamplification.

Figure 2. Identification and sorting of LT-HSCs by flow cytometry. Live, Lineage negative-to-low cells (gated in left panel) were analyzed for the expression of c-Kit and Sca-1 (center panel). The gate shows the Lineage$^{-/low}$ c-Kit^{+}Sca-1^{+} (LSK) population that contains HSCs. The LSK population was then analyzed for the expression of CD41 and CD48 versus CD150 (left panel). Gate shows LSK CD150^{+}CD41^{-}CD48^{-} LT-HSC population. Data shown as high resolution, unsmoothed pseudocolor plots, using Bi-Exponential scaling.

Figure 3. Housekeeping gene melting curve analysis in single cells. To determine which wells contained a single cell, the melting curve for the housekeeping gene (*Hprt*) for each single cell (red lines) is compared to a positive control (whole bone marrow RNA, blue lines). This analysis provides the single cell sorting efficiency. Moreover the melting curve analysis of negative samples (no RNA, yellow lines) can indicate the presence of contamination. Based on the *Hprt* melting curve analysis, we obtained single cell sorting efficiencies ranging between 80% (left panel) to 30% (right panel).

Figure 4. Example of an experimental 96-well plate design. Each 96-well plate allows for the simultaneous analysis of 3 experimental and housekeeping genes from six independent single cells, including positive and negative controls for each gene.

Figure 5. Expression of several genes detected by single cell multiplex RT-qPCR. Plots show examples of the qPCR amplification slopes and melting curves for nine genes analyzed from single LT-HSC (red lines) and compared with bone marrow positive control (blue lines). Genes studied: *Hprt*, *Cxcr4*, *Cdh5* (VE-Cadherin), *Cdh2* (N-cadherin), *Casr* (Calcium sensing receptor), *Itga4* (α4 integrin), *Itga5* (α5 integrin), *Itgal* (αL integrin), *Selplg* (PSGl1).

Figure 6. Distribution of VE-cadherin expression in single fetal liver and adult LT-HSCs. Each symbol represents the $\log(2^{-\Delta\Delta Ct})$ of VE-cadherin in single LT-HSCs from fetal liver and adult bone marrow. A single adult bone marrow LT-HSC was chosen randomly as reference to calculate the $\log(2^{-\Delta\Delta Ct})$. The black bar represents the average $\log(2^{-\Delta\Delta Ct})$ for the entire 24-cell LT-HSC group.

Figure 7. Identification and single cell sorting of double negative thymocyte populations by flow cytometry. Live cell suspension from $CD4^-CD8^-$ double negative (DN) thymocytes was stained with anti-CD44-PE and anti-CD25-APC antibodies. The DN subpopulations were identified and sorted based on their expression of CD44 and CD25: DN1, $CD44^+CD25^-$; DN2, $CD44^+CD25^+$; DN3, $CD44^-CD25^+$; DN4, $CD44^-CD25^-$.

Figure 8. Single cell gene expression distribution of Notch-related genes in DN thymocyte populations. Double negative thymocyte subpopulations were

analyzed for expression of the Notch-related genes *Dtx1* (Deltex), *Gata3*, *Spen* (Mint) and *Numb* by multiplex single cell RT-qPCR. For each gene, a single DN1 cell was chosen randomly as reference to calculate the log $2^{-\Delta\Delta Ct}$ for each single cell. Each plot shows 10 independent single cells for each DN subpopulation. *Hprt* was used as housekeeping gene. The black bar represents the average log($2^{-\Delta\Delta Ct}$) for the entire 10-cell DN group.

Figure 1

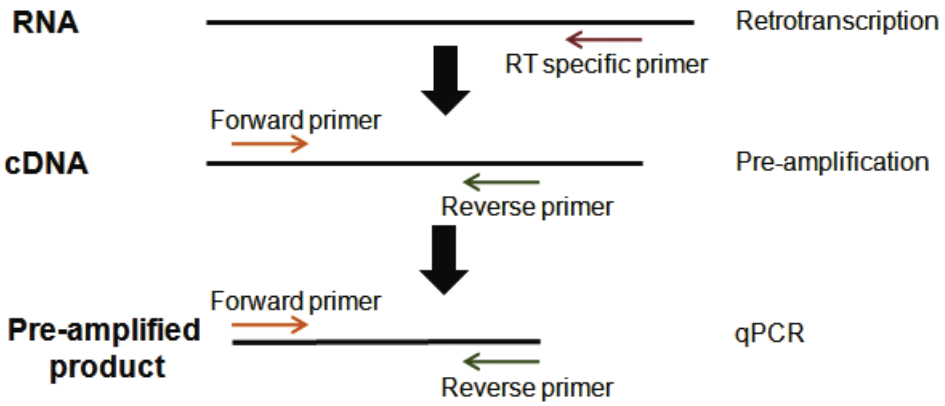

Figure 2

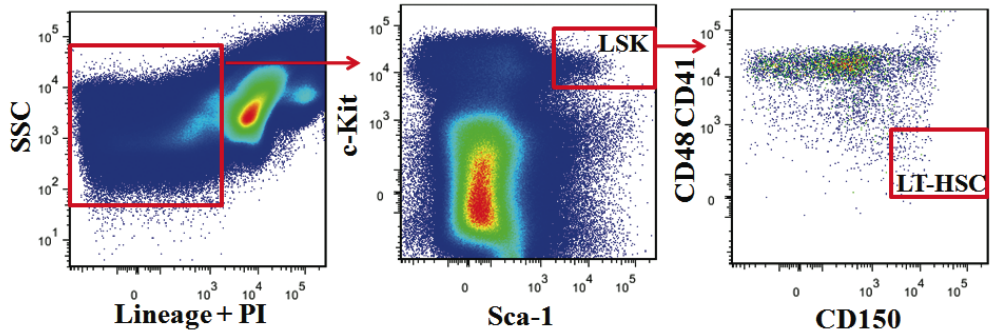

Figure 3

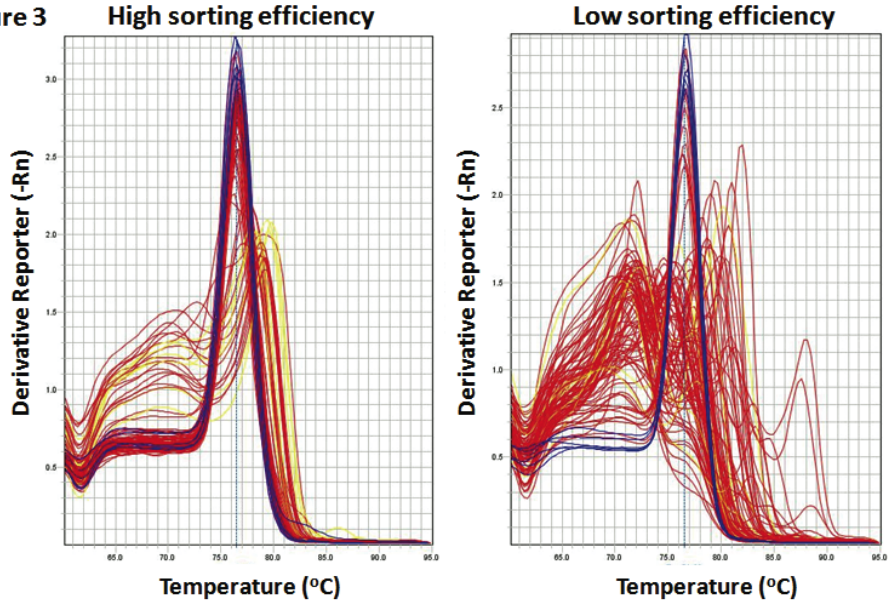

Figure 4

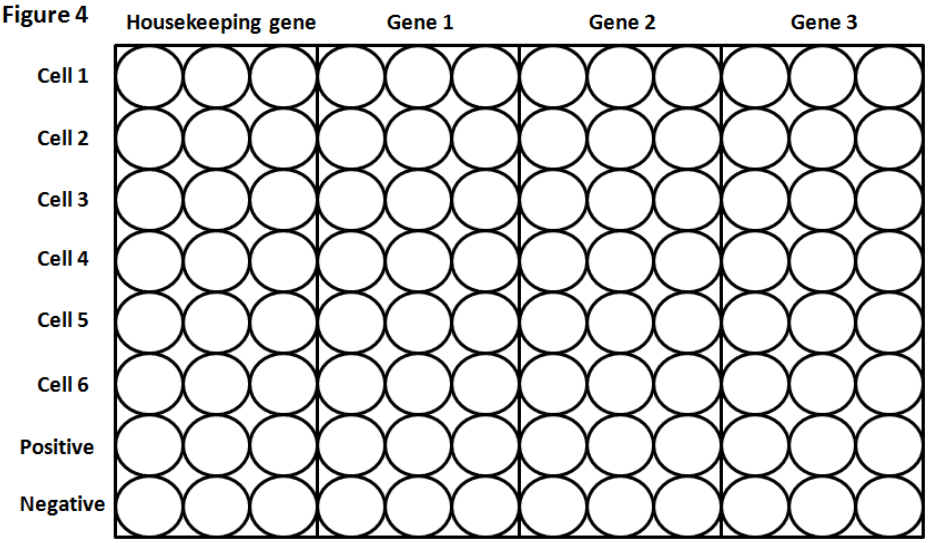

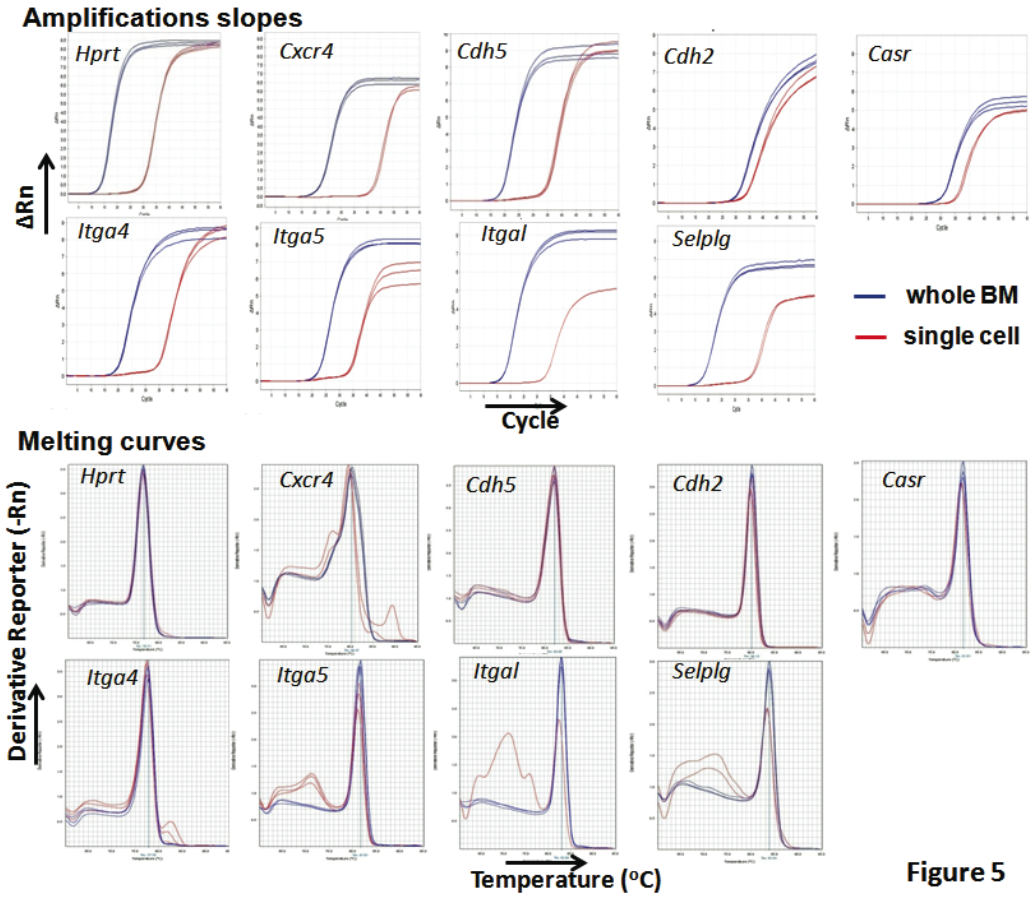

Figure 5

Figure 6

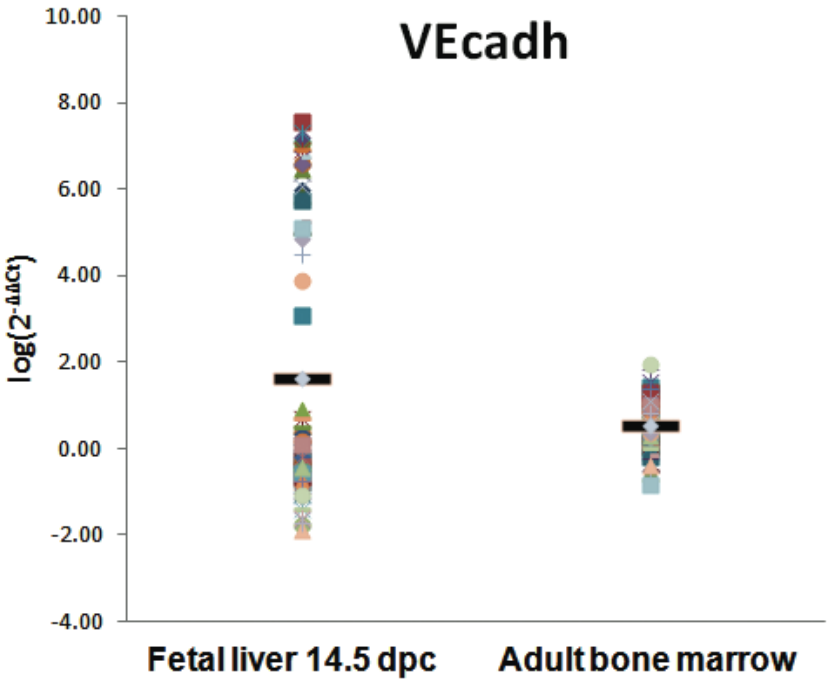

Figure 7

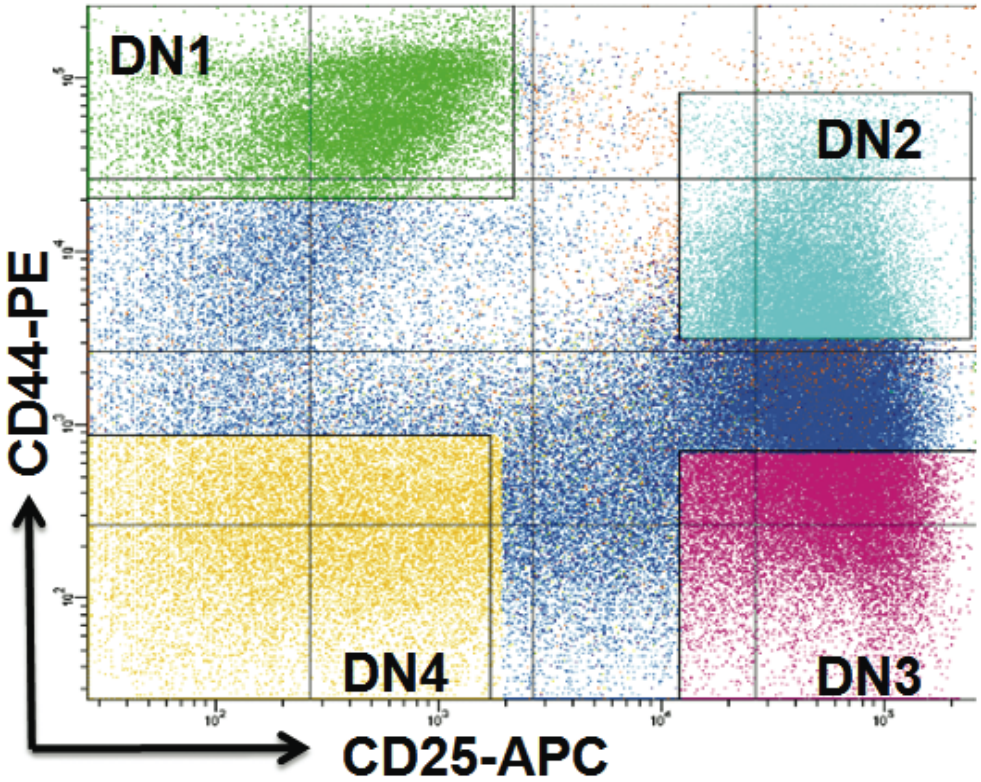

Figure 8

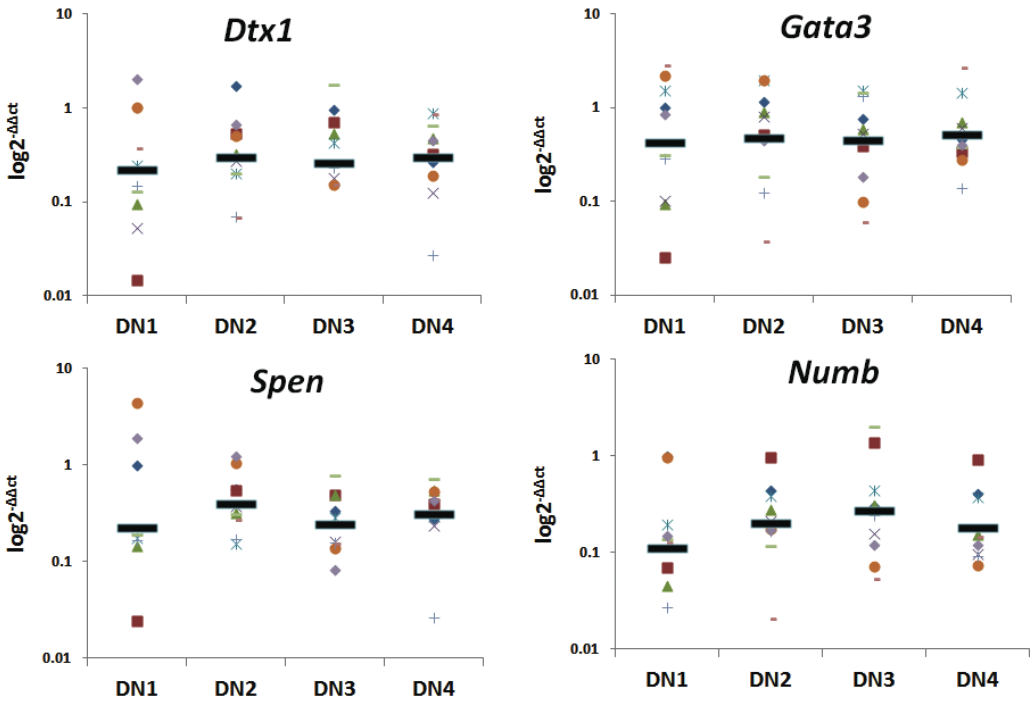

Table 1: BD FACSAria™ IIu cell sorter settings.

Fluorochrome	Excitation (nm)	Filter (nm)
FITC	488	530/30
PE-TR	488	610/20
PE-Cy7	488	780/60
PE	488	575/26
PE-Cy5/PI	488	695/40
APC-Cy7	633	780/60
APC	633	660/20
Alexa Fluor 430	407	530/30
DAPI	407	450/40

APPENDIX C

Single-Cell Analysis of Murine Long-Term Hematopoietic Stem Cells Reveals Distinct Patterns of Gene Expression during Fetal Migration

Jesu´ s Ciriza, Dominique Hall, Alison Lu, Joseph Robert De Sena, Mufadhal Al-Kuhlani, Marcos E. Garcı´a-Ojeda

OPEN ACCESS Freely available online

PLoS one

Single-Cell Analysis of Murine Long-Term Hematopoietic Stem Cells Reveals Distinct Patterns of Gene Expression during Fetal Migration

Jesús Ciriza, Dominique Hall, Alison Lu, Joseph Robert De Sena, Mufadhal Al-Kuhlani, Marcos E. García-Ojeda*

School of Natural Sciences, University of California Merced, Merced, California, United States of America

Abstract

Background: Long-term hematopoietic stem cells (LT-HSCs) migrate from the fetal liver (FL) to the fetal bone marrow (FBM) during development. Various adhesion and chemotactic receptor genes have been implicated in the migration of adult LT-HSCs. However, their role in the migration of fetal LT-HSCs is not clearly understood due, in part, to the rare number of these cells in fetal tissues, which preclude classical gene expression analysis. The aim of this study is to characterize the expression of migration related genes in fetal LT-HSC across different anatomical locations during development.

Methodology/Principal Findings: We isolated fetal LT-HSC from different developmental stages, as well as different anatomical locations, and performed single-cell multiplex RT-qPCR and flow cytometry analysis of eight molecules involved in adult LT-HSC migration. Our results show that the gene expression of the chemokine receptor *Cxcr4* in LT-HSC varies across developmental microenvironments and times, while the cadherin *Cdh2* (*Ncad*) and the calcium receptor *Casr* show higher gene expression and variability only in FBM at 17.5 days post coitum (dpc). The cadherin *Cdh5* (*Vecad*) maintains high expression variability only during fetal development, while the integrin subunit *Itga5 (α5)* increases its variability after 14.5 dpc. The integrin subunits *Itga4* (*α4*) and *Itgal* (*Lfa1*), as well as the selectin ligand *Selplg (Psgl1)*, did not show differences in their expression in single LT-HSCs irrespective of the developmental times or anatomical microenvironments studied.

Conclusions/Significance: Our data demonstrate that the expression pattern of phenotypically identical, single LT-HSCs fluctuates as a function of developmental stage and anatomical microenvironment. This is the first exhaustive gene expression comparison of migration-related molecules in fetal tissues across developmental times, enhancing the understanding of LT-HSC migration fate decisions during development.

Citation: Ciriza J, Hall D, Lu A, De Sena JR, Al-Kuhlani M, et al. (2012) Single-Cell Analysis of Murine Long-Term Hematopoietic Stem Cells Reveals Distinct Patterns of Gene Expression during Fetal Migration. PLoS ONE 7(1): e30542. doi:10.1371/journal.pone.0030542

Editor: Jose Alberola-Ila, Oklahoma Medical Research Foundation, United States of America

Received May 13, 2011; **Accepted** December 19, 2011; **Published** January 20, 2012

Funding: This work was funded by the University of California Merced start-up funds. JC was partially funded by a postdoctoral fellowship from the Government of Navarra, Spain and the California Institute for Regenerative Medicine Stem Cell Training Program Award (TG2-01163). The funders had no role in study design, data collection and analysis, decision to publish, or preparation of the manuscript.

Competing Interests: The authors have declared that no competing interests exist.

* E-mail: mgarcia-ojeda@ucmerced.edu

Introduction

Long-term hematopoietic stem cells (LT-HSCs) are characterized by their capacity to provide lifelong reconstitution of all blood cell lineages after transplantation into lethally irradiated recipients [1]. LT-HSCs in the fetal liver, as well as in the adult bone marrow (BM), can be identified by the Lineage$^{-/low}$Sca-1^{+}c-Kit^{+}CD150^{+}CD48^{-}CD41^{-} phenotype [2,3,4,5,6]. Hematopoietic stem cells follow a defined pattern of migration through different embryonic locations during development [7]. The yolk sack as well as the aorta, gonad and mesonephros (AGM) region serve as the sites of initial hematopoiesis by 7.5 and 10 dpc, respectively. Development continues by the colonization of the FL by 11.5 dpc, followed by the FBM by 17.5 dpc (FBM17.5, reviewed in references [7,8]). Interestingly, stem cells capable of long-term reconstitution circulate in the fetal blood as early as 12.5 dpc [8], leading to the hypothesis that circulating LT-HSC would colonize the FBM when a suitable microenvironment is present [8]. Alternatively, circulating LT-HSC might not possess the appropriate chemotactic receptor or adhesion molecule repertoire required for BM homing and migration until 17.5 dpc.

Several chemotactic receptors and adhesion molecules have been described in mice to play important roles in HSCs migration during development and adult life. The α-chemokine receptor CXCR4, specific for stromal-derived-factor-1α (SDF-1α or CXCL12), is one of the main molecules involved in LT-HSCs migration and retention in the BM [9,10,11,12]. Adult HSCs migrate continuously between the BM and blood, with SDF-1α/CXCR4 signaling as one of the main regulators of this process [13]. Cadherins are calcium-dependent, homophilic adhesion proteins that comprise another group of molecules involved in LT-HSC migration. VE-cadherin is expressed in fetal hematopoietic progenitors until they reach the FL and is no longer expressed after the HSCs have migrated to the adult BM [14]. N-cadherin is

expressed in both osteoblasts and quiescent HSCs [15] but its role in HSCs migration to the BM is not clear, as it has been shown that lack of N-cadherin expression does not affect stem cell maintenance [16,17]. Additionally, the seven transmembrane-spanning calcium-sensing receptor (CASR), which responds to extracellular calcium ion concentrations, has been described to participate in HSCs migration to the BM [18]. Adult mice deficient in *Casr* have reduced numbers of HSCs in the BM, but show no differences in HSC numbers in FL at 17.5 dpc (FL17.5) when compared with wild type controls [19].

Integrins, such as $\alpha_4\beta_1$ (VLA-4) and $\alpha_5\beta_1$ (VLA-5), are expressed in murine HSCs [20,21]. Fetal HSCs deficient in the integrin subunit β_1 do not colonize the FL or adult hematopoietic tissues. Adult integrin β_1-null HSCs fail to engraft the BM of irradiated recipient mice, remaining in circulation [22]. Furthermore, interfering with α_4 integrin adhesion reduces the ability of HSCs to home to the BM [20]. Integrins can also act in concert to increase HSC adhesion to BM, as evidenced by the collaboration of the $\alpha_L\beta_2$ integrin (leukocyte function antigen-1, LFA-1) with VLA-4 to increase HSCs adhesion [23]. Interestingly, exposure of HSCs to the chemokine SDF-1α upregulates the expression of VLA-4 and LFA-1, which in turn helps the HSCs to engraft in the BM [24]. The selectin family of adhesion proteins also mediates interactions between endothelial cells and HSCs. The P-selectin glycoprotein ligand-1 (PSGL1) mediates HSC rolling in the BM microvasculature [25]. This ligand participates in E-selectin progenitor homing by cooperating with α_4 integrin [26].

We hypothesize that the aforementioned chemotactic receptors and adhesion molecules could be modulated throughout development during the migration of LT-HSC from the FL to the FBM. Studying the genetic mechanisms of migration presents several technical challenges that hinder classical genetic analysis. For example, our previous work showed that the number of LT-HSC in fetal tissues is highly reduced compared to the adult BM [5], precluding traditional molecular analysis. Single cell multiplex gene expression analysis provides a powerful tool to circumvent this challenge. There are two main methodologies to analyze single cell multiplex gene expression: Digital RT-PCR [27] and RT-qPCR [28]. The digital RT-PCR method requires a system such as the Fluidigm Access Array™ System and digital array chips, an uncommon and expensive technology not available to many researchers. For our study, we chose to use multiplex single cell RT-qPCR (Figure 1A) for several reasons: First, this method only requires a classical thermocycler and a qPCR system, more common and affordable instruments than the Fluidigm Access Array™ System; Second, the low number of LT-HSCs isolated from the fetal tissues yields small amount of mRNA, restricting classical gene expression studies to a few, highly expressed genes [29]; Third, population qPCR analysis reflects the average expression of a gene of interest in a population, without providing information about the distribution of gene expression by individual cells [28,30,31]. Single cell multiplex RT-qPCR allows for the inexpensive, simultaneous quantification of several genes of interest, illustrating the gene expression distribution by single cells within the desired population.

Our results show that the single cell pattern of expression of various genes, such as *Cxcr4*, varies across developmental and anatomical locations. Moreover, expression of *Ncad* and *Casr* is upregulated in most FBM17.5 single cells, a pattern that differs greatly from the other microenvironments studied. Furthermore, the expression of *Vecad* is downregulated after 17.5 dpc, while the expression of *α5* increases after 14.5 dpc. Taken together, our data indicate that a phenotypically identical LT-HSC population displays a dynamic gene expression pattern that varies as a function of microenvironment and developmental times.

Results

Multiplex RT-qPCR accurately and specifically measures differences in gene expression from single cells

Determining amplification efficiencies and discarding possible competition between pooled primers in both the retrotranscription or pre-amplification reactions are essential to validate the accuracy of the single cell multiplex RT-qPCR technique. Our results show that there were no statistically significant differences when comparing qPCR amplification efficiencies for the nine genes tested ($P>0.5$, Tukey test, Figure 1B). We obtained the same Ct values when single and multiplex retrotranscription reactions (Figure 1C), as well as single and multiplex pre-amplification reactions (Figure 1D), were compared. We were also able to specifically detect the fluctuation in template concentration of the genes of interest independent of the presence of other gene templates (Figure 1E). Regression curve analysis obtained R^2 values greater than 0.99 for all studied genes, indicating high accuracy of amplification with a direct correlation between Ct value and template copy number (Figure 1F). Furthermore, we determined the limit of detection of the qPCR to be 100 copies for all genes studied, except *α4*, which had a detection limit of 1000 copies. Taken together, our data indicates that our multiplex RT-qPCR technique will allow us to accurately and confidently measure differences in gene expression from single cells.

LT-HSCs can be detected and isolated from fetal bone marrow at day 17.5 of gestation

Previously, we identified LT-HSCs by means of flow cytometry based on the Lineage$^{-/low}$Sca-1$^+$c-Kit$^+$CD150$^+$CD48$^-$CD41$^-$ phenotype from magnetically depleted, lineage negative FL14.5, FL17.5, FBM17.5 and adult BM samples. This protocol precluded us from obtaining single LT-HSC from FBM17.5 [5]. To circumvent this problem, we eliminated the magnetic lineage-depletion step from our procedure, allowing us to isolate single LT-HSCs from fetal bone marrow. Using flow cytometry, we identified live, Lineage negative, Sca-1 and c-Kit double positive cells that constitute the Lineage$^{-/low}$Sca-1$^+$c-Kit$^+$ (LSK) population (Figure 2A, upper and middle panels). We characterized LT-HSCs from the heterogeneous LSK population by gating cells with the CD150$^+$CD48$^-$CD41$^-$ phenotype (Figure 2A, lower panels). This approach allowed us to sort an average of 5 single LT-HSCs/embryo from FBM17.5 tissue. The rest of the samples provided sufficient single LT-HSC to fill a 96-well plate/sample.

We confirmed the presence of LT-HSCs from the different tissues studied by confocal microscopy (Figure 2B and Figure S1). We identified LT-HSCs, as defined by the CD150$^+$CD48$^-$CD41$^-$Lin^{neg} phenotype [2], in the FL14.5 and FL17.5 as well as in adult BM, detecting between 3–4 LT-HSCs/slide. However, LT-HSCs in the FBM17.5 were relatively rare, detecting about 1 LT-HSC per 5 slides. This experiment corroborated that the low number of LT-HSC in the FBM17.5 is not an artifact of flow cytometry but truly reflects the low frequency of these cells in this tissue. Overall, we were able to detect and isolate rare LT-HSCs from fetal tissues, particularly from FBM17.5 samples, for gene expression analysis.

Single LT-HSC display varied expression levels of migration-related genes depending on developmental time and anatomical location

We were interested in studying 8 genes described as essential for LT-HSCs migration: *Cxcr4, Vecad, Ncad, Casr, Itga4 (α4), Itga5 (α5), Itgal (Lfa1)* and *Psgl1*. We sorted single LT-HSCs from FL14.5, FL17.5, FBM17.5 and 4-week old adult BM to perform single cell

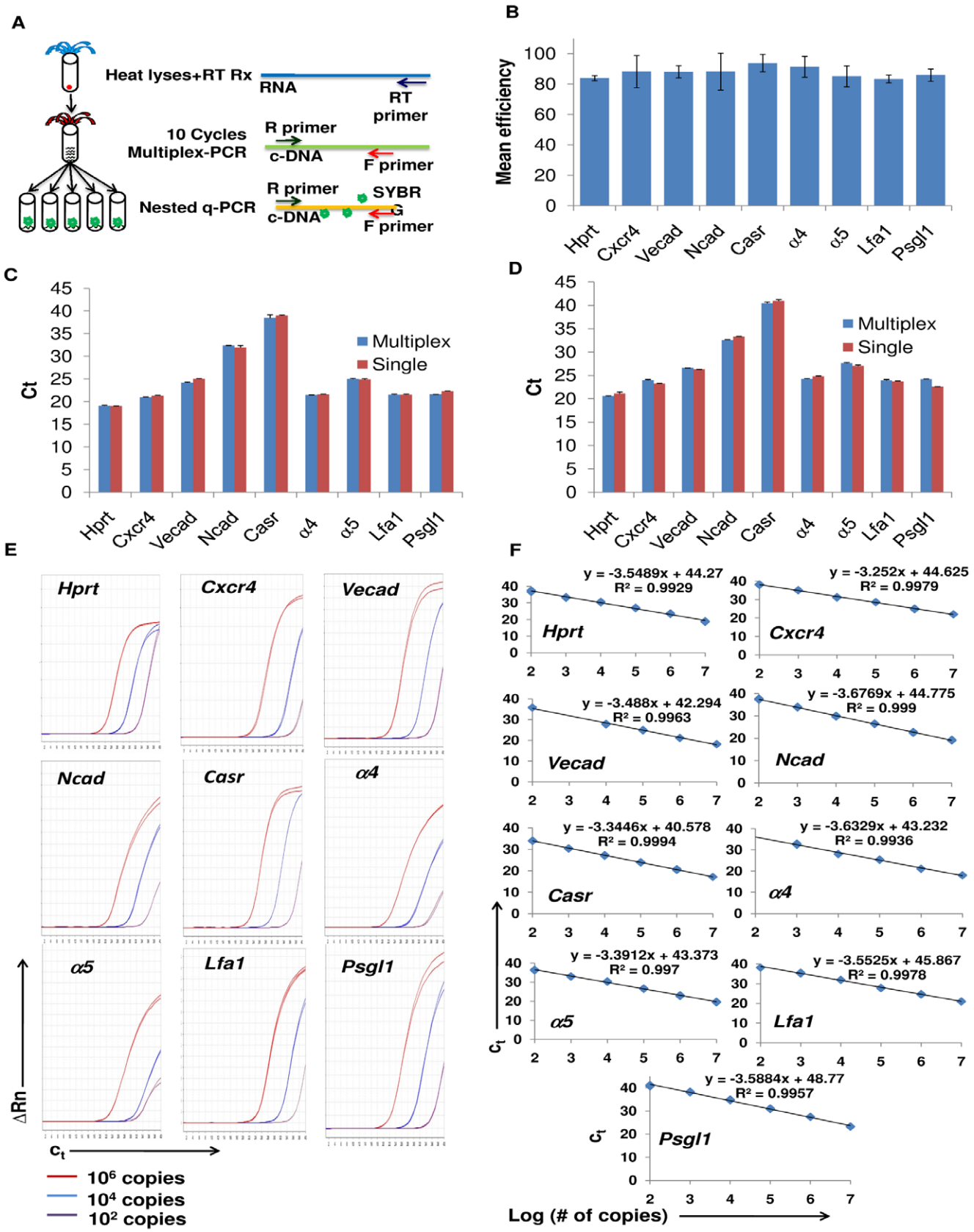

Figure 1. Validation of single-cell multiplex RT-qPCR. A) Schematic representation of the single cell multiplex RT-qPCR methodology. After lysing single cells by heating, cDNA is obtained by retrotranscription with as many specific primers as genes studied. The cDNA template is subjected to a 10-cycle pre-amplification reaction using a primer pair for each gene studied in order to maintain the linear ratio of the original sample. The pre-

amplified product is split into aliquots for qPCR analysis with SYBR®-Green using the same primer pairs as in the pre-amplification step. B) Efficiency of qPCR reactions after pre-amplification using 10-fold dilutions of standards did not show significant differences between the genes studied. C) Similar qPCR Ct values between samples using either single or multiplex RT primers indicate no primer competition during the retrotranscription reaction. D) Similar qPCR Ct values between samples using either single or multiplex primer pairs indicate no primer competition during the 10-cycle pre-amplification reaction. E) Quantification of varied copy number for a particular gene amplified in the presence of a constant number of plasmids for the other genes studied. For each reaction, 10^2 (purple line), 10^4 (blue line), or 10^6 (red line) plasmids were mixed with a constant number (10^4) of plasmids for the other eight genes studied. Gene specific multiplex qPCR amplification was then performed. Each reaction was performed in triplicate. F) Regression lines obtained from standard curves for each gene with the single cell RT-qPCR conditions. R^2-values were greater than 0.990 with detection limit of 100 copies for most genes.
doi:10.1371/journal.pone.0030542.g001

multiplex RT-qPCR. This technique was chosen due to the low number of LT-HSCs isolated from the fetal tissues studied, particularly the FBM17.5 [5]. Whole BM RNA and sorting buffer alone were used as positive and negative controls, respectively. For each time point, embryos from three independent pregnancies, as well as BM from three independent adults, were studied (a total of nine mice per time point). Following retrotranscription and pre-amplification, we analyzed the expression of *Hprt* in each well, confirming the presence of a single cell by comparing its melting curve to the positive control (Figure S2). Samples whose *Hprt* melting curves differed from the positive control were discarded. Moreover, the expression of the gene studied was considered non-detectable if its single cell qPCR melting curve did not correspond to its respective positive control (Figure S3). The threshold value for all the genes tested was set at 2.5 to differentiate real signal from qPCR noise. The reference sample used to calculate the $2^{-\Delta\Delta Ct}$ values for the entire cohort of single LT-HSCs was a randomly chosen, single sorted BM LT-HSC. The data were represented by box-and-whisker plots as $\log(2^{-\Delta\Delta Ct})$, displaying the gene expression distribution of single LT-HSCs at the different time points and microenvironments examined (Figure 3).

Our data showed that the median $\log(2^{-\Delta\Delta Ct})$ expression value for *Cxcr4* among the samples was similar except for FBM17.5, which displayed a lower median value (Figure 3A). However, the distribution of *Cxcr4* expression among single cells differed, with cells from the FL17.5 and adult BM having tighter distribution and the FL14.5 and FBM17.5 displaying greater distribution. The expression of *Vecad* showed a different profile, with similar median $\log(2^{-\Delta\Delta Ct})$ values in all the samples studied but a large single cell expression distribution only in the fetal tissues studied (Figure 3B). Interestingly, many single LT-HSCs in the FBM17.5 showed higher *Ncad* and *Casr* expression than the other fetal or adult microenvironments tested (Figure 3C–D). However, while the median $\log(2^{-\Delta\Delta Ct})$ value for *Ncad* in the FBM17.5 sample was similar to the other tissues, FBM17.5 LT-HSC had a higher $\log(2^{-\Delta\Delta Ct})$ median value for *Casr*.

We also studied the expression of α_4, α_5, and *Lfa1* integrins, as well as the vascular addressin *Psgl1*, in all the tissues tested. The integrin subunit α_4, which constitutes both the $\alpha_4\beta_1$ (VLA-4) and $\alpha_4\beta_7$ integrins, showed little expression differences among single LT-HSCs from the various microenvironments studied (Figure 3E). Conversely, the expression pattern of the integrin subunit α_5, which constitutes the $\alpha_5\beta_1$ (VLA-5), $\alpha_5\beta_5$ and $\alpha_5\beta_6$ integrins, was different among the samples studied. Only single LT-HSCs from FL14.5 had a tight α_5 expression distribution, as well as a lower median $\log(2^{-\Delta\Delta Ct})$ value. The median $\log(2^{-\Delta\Delta Ct})$ value observed in the other microenvironments varied, displaying a high expression value in the FL17.5 samples, decreasing to an intermediate expression value in the FBM17.5 sample, and further decreasing to a low expression value (comparable to the FL14.5 sample) in the adult BM LT-HSCs (Figure 3F). Lastly, no differences in *Lfa1* or *Psgl1* distribution or median $\log(2^{-\Delta\Delta Ct})$ values were detected between the microenvironments studied (Figure 3G–H). Our data show that we can successfully determine the expression levels of nine different genes from a single LT-HSC. Moreover, our analysis demonstrates gene expression variability among single cells within a phenotypically identical population, depending on developmental time and anatomical location.

Flow cytometry analysis of migration related proteins in fetal LT-HSC

We utilized flow cytometry to establish if the gene expression distributions observed by single cell multiplex RT-qPCR correlated with protein expression in the LT-HSCs populations studied. During data acquisition, only events that fell within a broad negative to medium Lineage/PI/CD41/CD48 gate and a medium to high CD150 gate were saved. For analysis of protein expression in the LT-HSC populations, we used stringent Lineage/PI/CD41/CD48$^{-/low}$ (Lin^{neg}) and $CD150^{high}$ ($CD150^{hi}$) gates (Figure 4A, upper and lower panels, respectively) [6]. This data acquisition strategy enabled us to obtain and analyze a statistically significant number of LT-HSCs ($Lin^{neg}CD150^{hi}$) from all of the tissues tested.

The cytometry data showed expression of CXCR4 in all the populations tested (Figure 4B), reflecting the broader distribution of *Cxcr4* expression observed by single cell multiplex RT-qPCR in LT-HSC from FL14.5 and FBM17.5 compared to FL17.5 and adult BM. VE-cadherin was expressed in most of the LT-HSCs from the fetal tissues analyzed, with the lowest expression in adult BM LT-HSCs (Figure 4C, Table S1). We found little expression of N-cadherin in the FL17.5 or adult BM LT-HSC, while a small population of FL14.5 and FBM17.5 LT-HSC expressed N-cadherin (Figure 4D). However, the mean fluorescence intensity (MFI) values for the FBM17.5 samples was almost double when compared to the MFI of the FL14.5 and other samples, indicating higher expression of N-cadherin in the FBM17.5 cells.

To examine the expression of integrins in LT-HSCs, we first gated the α_4 or α_5 positive populations, followed by analysis of β_1 expression, which comprise the VLA-4 and VLA-5 populations, respectively. The vast majority of the LT-HSCs from the FL14.5, FL17.5 and adult BM were $\alpha_4\beta_1^+$, while this integrin was expressed in about 30% of the FBM17.5 LT-HSCs (Figure 4E). These $\alpha_4\beta_1^+$ populations have a tight distribution, similar to the distribution observed by multiplex single cell RT-qPCR. About 70% of β_1^+ cells in FBM17.5 were α_4 negative, indicating that the FBM17.5 β_1^+ population includes other alpha integrin subunits. On the other hand, 7% of the $\alpha_5\beta_1$ expression was confined to the FL14.5 and FBM17.5 LT-HSC populations, with few $\alpha_5\beta_1^+$ cells found in the other samples (Figure 4F). This is contrary to the multiplex RT-qPCR data where only α_5 expression was evaluated.

Similarly to single cell RT-qPCR analysis, we did not observe differences in LFA-1 expression between microenvironments except for FBM17.5 LT-HSCs, where most of the cells were LFA-$1^{-/lo}$ (Figure 4G). Unfortunately, we were not able to analyze the expression of CasR and PSGL1 by flow cytometry, as the antibodies available for these molecules are not suitable for this

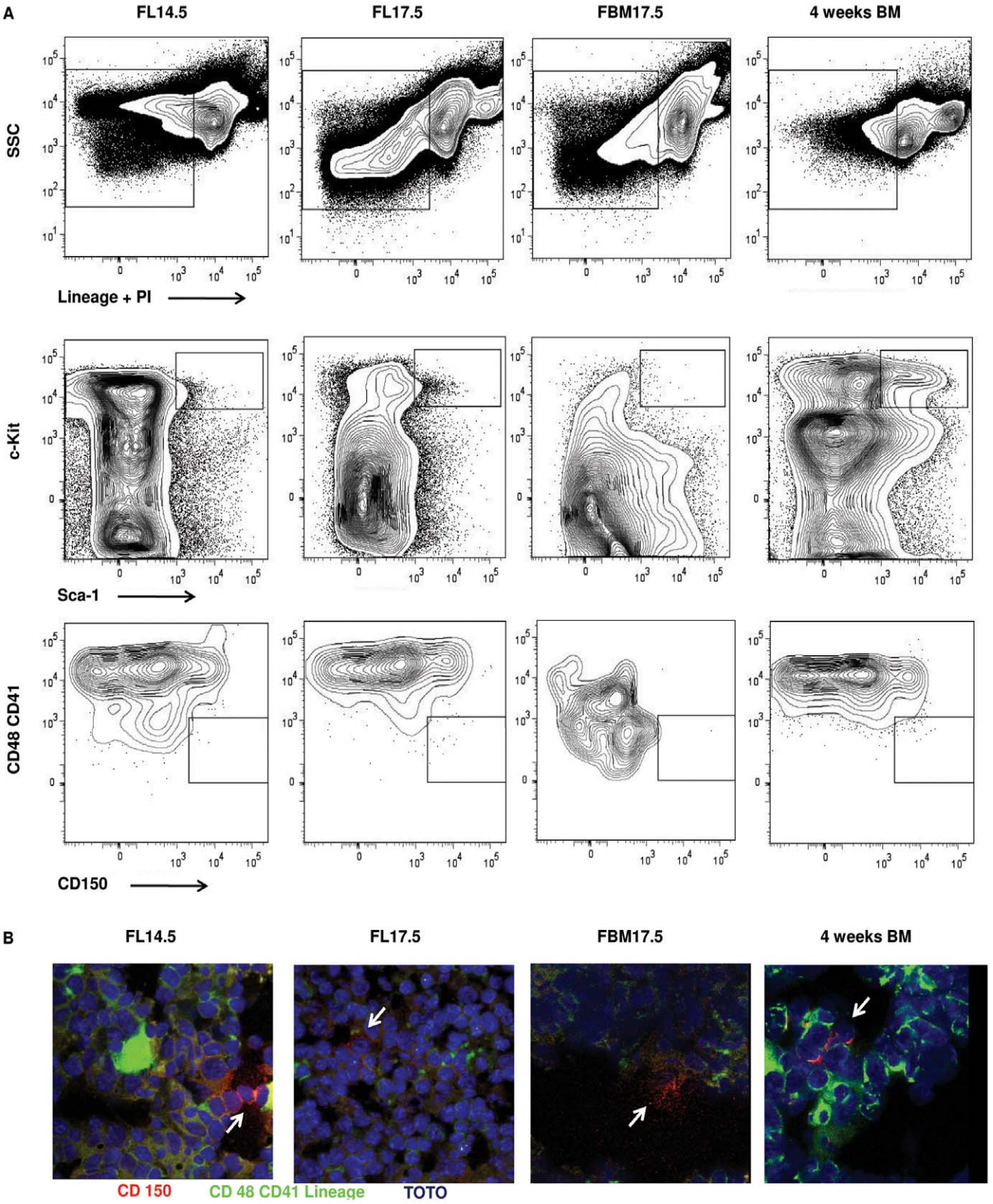

Figure 2. Identification of LT-HSC at different microenvironments by flow cytometry and confocal microscopy. A) Live, Lineage negative-to-low cells (gated cells in upper panels) were analyzed for the expression of c-Kit and Sca-1 (middle panels). Gates show the Lineage$^{-/low}$ Sca-1^{+}c-Kit^{+} (LSK) population, containing LT-HSC. The LSK population was then analyzed for the expression of CD150 versus CD41 and CD48 (lower panels). Gate shows LSK CD150^{+}CD41^{-}CD48^{-} LT-HSC. Data shown as 5% contour plots, using bi-exponential scaling and representative of three independent experiments. B) Immunohistochemistry of FL14.5, FL17.5, FBM17.5 and 4-week old adult BM. CD150 staining is shown in red while CD48, CD41 and lineage staining is shown in green. Blue staining represents nuclei marked with TOTO-3. CD150^{+}CD48^{-}CD41^{-}Lin^{-} LT-HSCs were identified as staining only in red with blue nuclear but not green (indicated by arrow).
doi:10.1371/journal.pone.0030542.g002

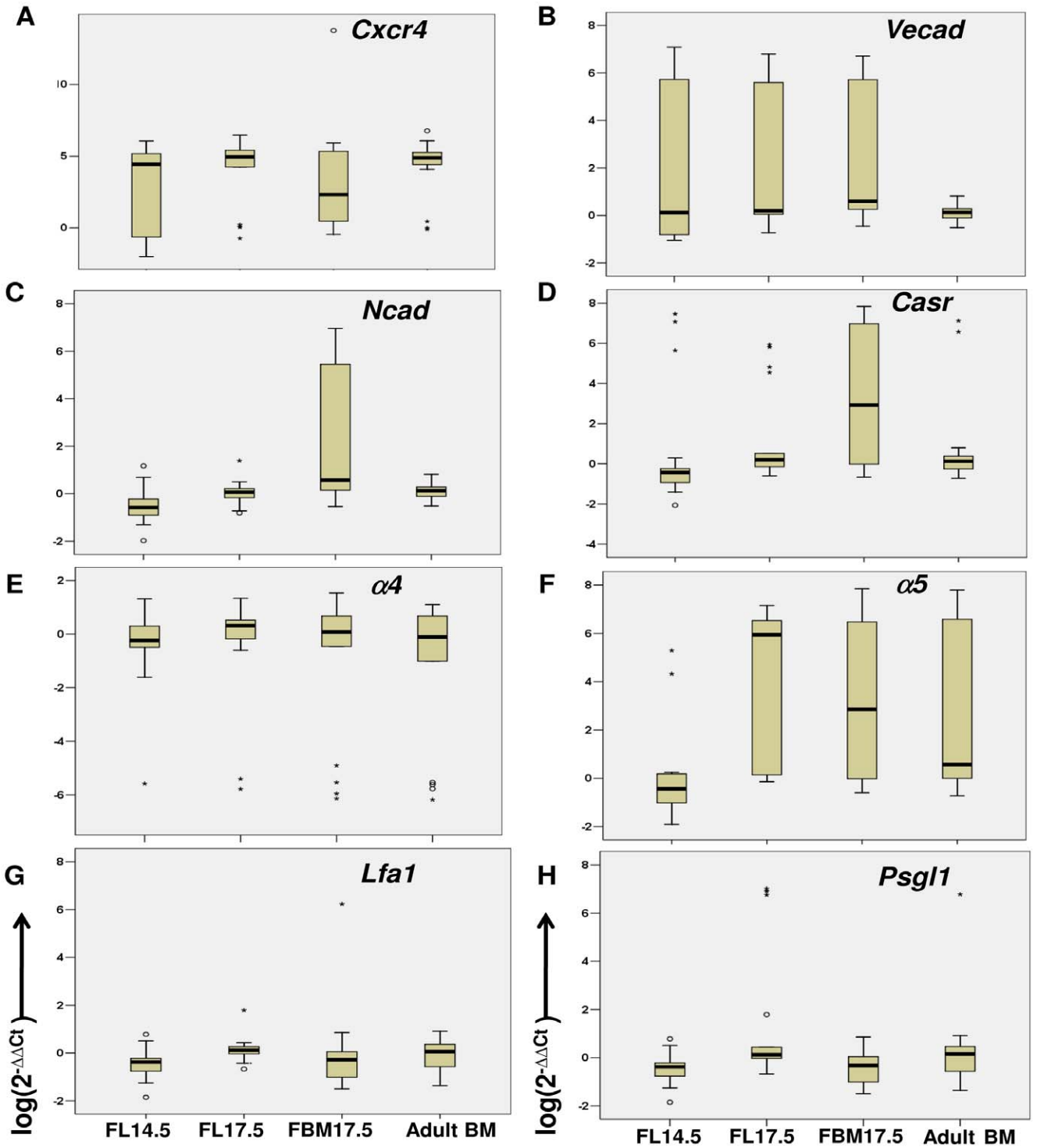

Figure 3. Representation of single LT-HSCs multiplex RT-qPCR analysis of genes related with their migration during development. Box plots represent the distribution of $\log(2^{-\Delta\Delta Ct})$ values of 72 single LT-HSCs from different microenvironments for each gene studied: A) *Cxcr4*; B) *Vecad*; C) *Ncad*; D) *Casr*; E) *α4*; F) *α5* G) *Lfa1* and H) *Psgl1*. Boxes represent the middle 50% of the data, localizing the 75th percentile in the upper boundary of the box and the 25th percentile in the lower boundary of the box. The median is shown as a bold line across the box. Vertical lines of the plot extending from the box indicate the minimum and maximum values. Circles indicate values between inner and outer fences, whereas asterisks indicate values beyond the outer fences. One single LT-HSCs from adult BM was randomly selected as reference sample.
doi:10.1371/journal.pone.0030542.g003

technique. Table S1 shows the mean fluorescence intensity for all the markers examined. Altogether, the flow cytometry data shows that the protein expression distribution in LT-HSC agrees with the overall single cell gene expression distribution observed by multiplex RT-qPCR among the developmental times and anatomical locations studied.

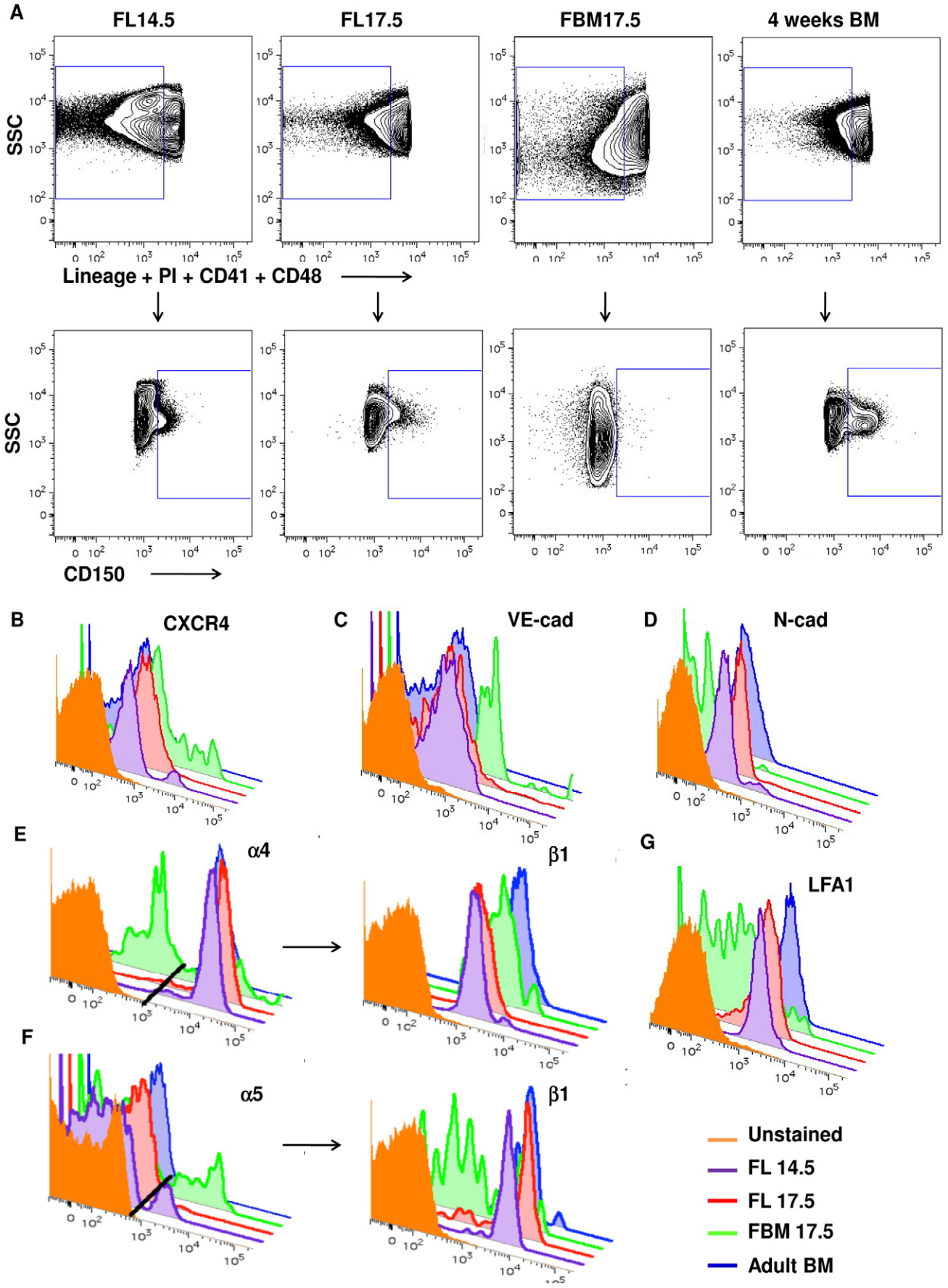
A
FL14.5
FL17.5
FBM17.5
4 weeks BM
SSC
Lineage + PI + CD41 + CD48
SSC
CD150
B
CXCR4
C
VE-cad
D
N-cad
E
α4
β1
F
α5
β1
G
LFA1
Unstained
FL 14.5
FL 17.5
FBM 17.5
Adult BM

Figure 4. Flow cytometry analysis of proteins related with migration of LT-HSCs during development. A) Live, Lineage negative-to-low, CD41 and CD48 negative cells (gated cells in upper panels) were analyzed for the expression of CD150 (lower panels). Data shown as 5% contour plots, using bi-exponential scaling. The $CD150^{+}CD41^{-}CD48^{-}$ $Lineage^{-/low}$ LT-HSC were analyzed for the expression of B) CXCR4; C) VE-cadherin; D) N-cadherin; E) VLA-4: $\alpha4^{+}$ cells were gated (left histogram, gate shown as dark line) and further analyzed for expression of β1 (right histogram); F) VLA-5: $\alpha5^{+}$ cells were gated (left histogram, gate shown as dark line) and further analyzed for expression of β1 (right histogram) and G) LFA-1. Histograms represent expression of molecules from LT-HSCs at different microenvironments and stages of development: orange, unstained; purple, FL14.5; red, FL17.5; green, FBM17.5; and blue, 4 weeks adult BM. Data representative of three independent experiments.
doi:10.1371/journal.pone.0030542.g004

Discussion

The molecular mechanisms that LT-HSCs use to migrate from the FL to the FBM are not well known, even when these cells follow an established pattern of migration during development [7]. The work presented here shows that we can isolate and determine the expression of eight migration-related genes from a single fetal LT-HSC by multiplex single cell RT-qPCR, accurately quantifying the single cell gene expression distribution within desired populations. We also begin to elucidate a pattern of adhesion molecules that might mediate homing of FL LT-HSC to the nascent BM vasculature as well as coordinate the migration of LT-HSC to the endosteal niche within the developing bone.

Miyamoto showed that single LSK ($Lineage^{-/low}Sca\text{-}1^{+}c\text{-}Kit^{+}$) cells had a promiscuous expression of multilineage-affiliated genes [32], indicating that cells within a population with similar cell surface phenotypes might have divergent genetic expression patterns leading to different cell fates. We examined LT-HSC (LSK $CD150^{+}CD48^{-}CD41^{-}$) from different anatomical locations and stages of development to quantitatively determine if a similar divergent gene expression pattern could be observed in migration-related genes. Our results demonstrate that single cells within the better-defined and more immature LT-HSC population still show a variable gene expression pattern. Nonetheless, we cannot rule out that the differences observed in our results might reflect expression differences among discrete sub-types within the LT-HSC population that inherently express these genes at different levels and not to transcriptional variability among phenotypically identical cells. Determining the single cell expression pattern of multiple housekeeping genes (for example *Actb*, *Gapdh*, and *Hprt*), believed to have more stable and uniform expression irrespective of the cells studied, could assess the latter possibility.

Studies on bone development have shown that successful migration of FL hematopoiesis to the FBM is dependent on normal embryonic bone formation [33] and endochondral ossification [34]. Initially, the primary skeleton is entirely cartilaginous [35], and the deposition of cartilage is orchestrated by the sequential maturation of chondrocytes (reviewed in [35,36,37]). As chondrocytes mature, they transition from a prehypertrophic state to a hypertropic state, secreting extracellular matrix that later becomes mineralized. The death of hypertrophic chondrocytes coincides with the initiation of the ossification process, which includes the vascularization of the bone, and the invasion of hematopoietic progenitors [37].

Our results support the idea that invasion of the fetal bone marrow by LT-HSC and other hematopoietic progenitors is a multi-step process involving chemotactic signals and multiple adhesion molecules [38] (Figure 5). Bone vascular endothelial cells constitutively express E-selectin, P-selectin, VCAM-1 and ICAM-1 in the absence of inflammation, making the BM endothelial microenvironment unique in its ability to recruit LT-HSC expressing PSGL-1, VLA-4 ($\alpha_4\beta_1$) and LFA-1 ($\alpha_4\beta_1$) [39,40]. Indeed, our data shows that VLA-4 (Figure 3E and Figure 4E) and PSGL-1 (Figure 3H) are expressed in LT-HSC and that their expression does not vary significantly from anatomical location or developmental time.

Circulating LT-HSCs engage E- and P-selectins [41] on the BM vascular endothelium through PSGL-1, tethering the LT-HSC to the vascular endothelium and allowing them to roll along the vessel wall. This initial contact facilitates CXCR4-SDF-1α engagement on the extravascular space. Signals from CXCR4 are required for the migration of LT-HSC into the fetal and adult BM [10,42,43]. Our data shows that FL17.5 LT-HSCs uniformly express *Cxcr4* (Figure 3A and Figure 4B), allowing them to respond to SDF-1α gradients. CXCR4 signals increase the affinity of the integrins LFA-1 and VLA-4 for their ligands (ICAM-1 and VCAM-1, respectively) [24]. Engagement of VCAM-1 by VLA-4 stabilizes the interaction of the vascular endothelium and the LT-HSC, causing the latter to stop rolling [38]. Together, CXCR4 and integrin signaling induces polarization and diapedesis of LT-HSC across the BM vascular endothelium, a process mediated by LFA-1 [24]. Our RT-qPCR data show that all LT-HSC tested, regardless of their tissue of origin or developmental time, express comparable levels of *Lfa1* (Figure 3G). Surface LFA-1 expression was corroborated by flow cytometric analysis on all the populations tested. However, a lower percentage of FBM17.5 LT-HSCs were $LFA\text{-}1^{+}$ (Figure 4G). Overall, our data suggests that PSGL-1, VLA-4, and LFA-1 are expressed at a constant level in all LT-HSC, independent of developmental time or anatomical location, and that these molecules might allow the LT-HSC to migrate into hematopoietic organs during development via vascular endothelial cell recognition.

After diapedesis, fetal LT-HSCs encounter the immature marrow microenvironment, where they interact with the basal lamina composed of extracellular matrix (ECM) proteins collagen type I, laminin and fibronectin [24]. They also interact via VLA-4 with $CXCL12^{+}$-reticular (CAR) cells surrounding the vessel [42], or to vascular endothelial niche cells via VE-cadherin [3,14]. Furthermore, LT-HSCs encounter both free Ca^{+2} [18,19] and SDF-1α gradients [11,44] that will direct them to the osteoblastic niche.

Our results show that most LT-HSC express levels of *Cxcr4* near the median of the FL14.5 sample. The large distribution and down-regulation of *Cxcr4* at this time reflects the fact that many LT-HSC are able to enter and leave the FL during this period of development. LT-HSCs with expression near the median might be retained in the FL since hematopoiesis is occurring in this organ at this developmental time. In contrast, *Cxcr4* expression in the FL17.5 shows a tight distribution near the median. At this time, the liver is transitioning from a hematopoietic to a hepatic organ [45] and many LT-HSCs are entering the circulation [8]. The tight distribution of *Cxcr4* at this time suggests that emigration of LT-HSC from the FL17.5 is mediated by a process other than down-regulation of CXCR4, such as decreased production of SDF-1α by FL stromal cells or proteolytic degradation of either SDF-1α or CXCR4 during the FL transition from a hematopoietic to a hepatic organ. In the FBM17.5, the distribution of *Cxcr4* expression resembles that of FL14.5 with a lower mean. SDF-1α plays a critical role in the attraction and retention of HSC in the BM during development [42]. CASR signaling increases the sensitivity of CXCR4 to SDF-1α in the presence of free Ca^{+2} [18], which results from the ossification of the bone at 17.5 dpc. In this

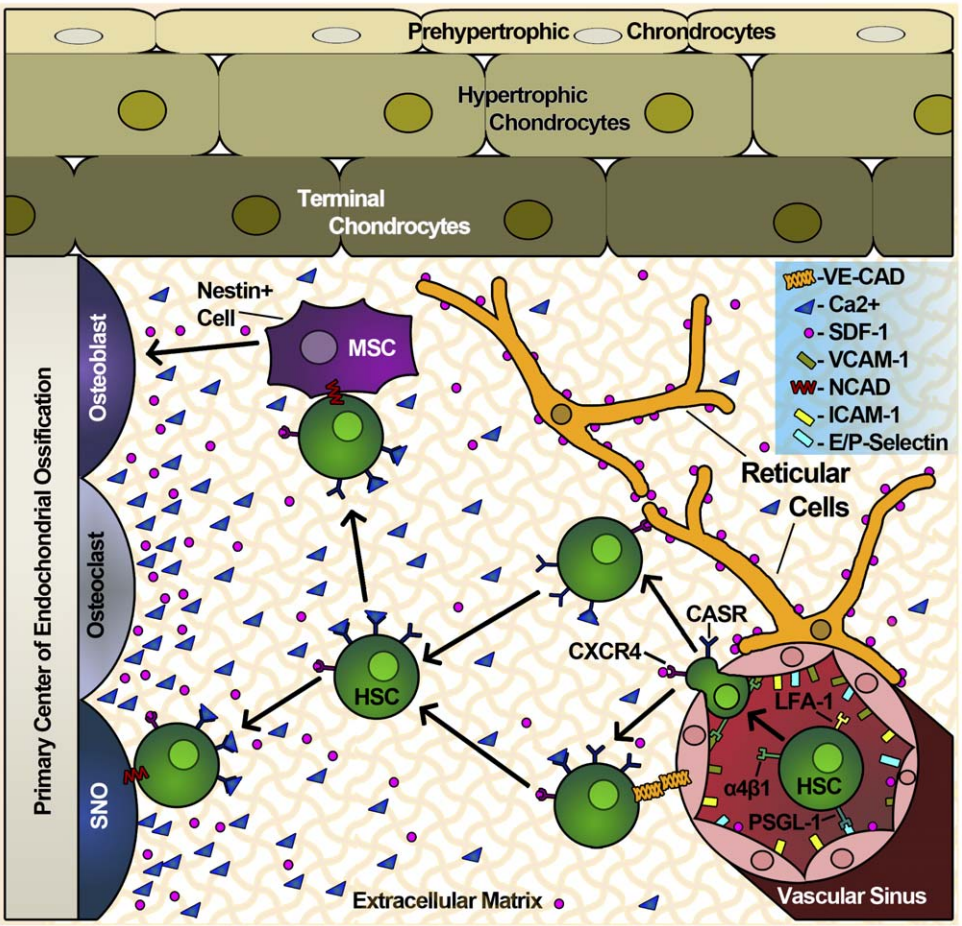

Figure 5. Model for the migration of LT-HSCs from the vascular niche to the endosteal niche. LT-HSC interact with bone marrow vascular endothelial cells via the PSGL-1/Selectin, allowing rolling on the vascular sinus. Stable LT-HSC adhesion occurs via VLA-4 binding VCAM-1, which also facilitates CXCR4/SDF-1α engagement and initiates endothelial transmigration. Once inside the BM, LT-HSCs interact with SDF-1α-producing reticular cells or with vascular endothelial cells. Detection of free Ca^{2+} gradients by CASR renders CXCR4 significantly more sensitive to SDF-1α, which is low in abundance [18]. Together, Ca^{+2} and SDF-1α gradients guide the LT-HSC to the endosteal niche, where they can interact with SNO (Spindle-shaped N-cadherin^{+}CD45^{-} osteoblastic) cells via N-cadherin. LT-HSC migration to the endosteum might ααααααoccur via VLA-5 interaction with fibronectin in the extracellular matrix or through the action of reticular cells directing the HSC within the BM.
doi:10.1371/journal.pone.0030542.g005

way, the lower expression of *Cxcr4* that may have impaired the LT-HSC's ability to colonize the FBM17.5 environment is mitigated by increased receptor sensitivity. *Cxcr4* is upregulated in the adult BM LT-HSC where it is expressed in a tight distribution around the medium, resembling that of the LT-HSCs in the FL17.5. In the case of the adult BM, the presence of high concentrations of SDF-1α helps retain the HSCs in the bone, stabilizing hematopoiesis. Outliers in the adult BM *Cxcr4* expression might represent cells that have down-regulated CXCR4 in order to leave the BM to populate other niches (Figure 3A).

Vecad displays high expression variability but similar median values in all the fetal tissues tested by single cell multiplex RT-qPCR, with its expression being more uniform in adult BM LT-HSC. This finding was confirmed by flow cytometry. Our data supports and complements studies where FL Thy-1^{low}Sca-1^{-}Lineage^{-}Mac-1^{-} cells, a population that includes LT-HSC and more mature progenitors, show decreased VE-cadherin expression by 16.5 dpc, and absence in adult BM cells [14]. We show that VE-cadherin expression is maintained in both FL and FBM samples at day 17.5 of gestation in Lineage$^{-/low}$CD150^{hi}CD48^{-}CD41^{-}, a more defined LT-HSC population. We propose that homotypic VE-cadherin interactions might play an important role in engaging LT-HSCs with both FL and FBM vascular endothelial niche cells during development. As the bone marrow develops into adulthood, the expression of *Vecad* diminishes (Figure 3B). This loss of VE-cadherin expression might reflect the emergence of endosteal and reticular niches as the bones are completely formed.

The role played by N-cadherin in LT-HSC interaction with its BM niches is controversial. It was previously described that N-cadherin does not play a role in adult LT-HSC adhesion to or maintenance by osteoblasts [16,17]. Recent transplantation studies have shown that loss of N-cadherin suppresses LT-HSC engraftment [46]. However, these studies did not evaluate the role of N-cadherin during fetal LT-HSC development, migration or maintenance. Our results showed that single FBM17.5 LT-HSCs express high *Ncad* levels. This suggests that N-cadherin might be required for the initial adhesion or maintenance of LT-HSCs in the FBM, an activity that is diminished when the adult bone is completely formed. Interestingly, CAR cells express low levels of N-cadherin [9], possibly facilitating their interaction with N-cadherin^{+} FBM LT-HSC. Moreover, studies in fetal bone

development show that N-cadherin is required for proper bone formation [47], and that early osteoblast development from mesenchymal stem cells can be induced through N-cadherin [48]. This raises the interesting possibility that N-cadherin expressing LT-HSC can positively influence the ontogeny of bone marrow osteoblasts during fetal development, in a manner analogous to fetal thymocytes being required for the development of the thymic medullary stroma [49,50].

Our data suggest that initial migration and colonization of the nascent bone marrow requires the coordinated expression of the chemokine receptor CXCR4 and adhesion molecules (Figure 5). Bone marrow vascular endothelial cells express VCAM-1, E-Selectin, P-Selectin and ICAM-1 constitutively. The PSGL-1/Selectin interaction slows LT-HSC and facilitates rolling on the vascular sinus. Stable LT-HSC adhesion to endothelial cells occurs via VLA-4 binding VCAM-1, which also facilitates CXCR4/SDF-1α engagement and initiates endothelial transmigration. Once inside the BM, LT-HSCs interact with SDF-1α-producing reticular cells or with vascular endothelial cells. They are also exposed to free Ca^{2+} and SDF-1α, which are significantly less abundant in the developing BM that in the adult BM [18,35]. Expression of CASR, the receptor for free Ca^{2+}, is increased and its signals render CXCR4 significantly more sensitive to SDF-1α [18]. Together, Ca^{+2} and SDF-1α gradients guide the LT-HSC to the endosteal niche, where they can interact with SNO (Spindle-shaped N-cadherin^{+}CD45^{-} osteoblastic) cells via N-cadherin. This migration might occur via the VLA-5 interaction with fibronectin in the extracellular matrix or by reticular cells directing the LT-HSC within the BM. As the BM develops and nears adulthood, *Casr* is downregulated, allowing maintenance of hematopoiesis since SDF-1α and free Ca^{2+} are abundant and BM hematopoiesis has been set into motion.

We have characterized the fetal single cell expression pattern of molecules important in migration of adult LT-HSC, and showed how this pattern fluctuates according to their developmental stage and anatomical location. Recently, embryonic stem cells have been differentiated into hematopoietic progenitors (ES-HP), which could be used in regenerative medicine of blood disorders [51,52]. However, the therapeutic capacity of ES-HP may be limited by their ability to home and engraft to the BM. We consider that the expression pattern of migration related genes shown in this study could be useful in predicting the migration potential of hematopoietic progenitors. The present study enhances our understanding of stem cell fate decisions during migration and has potential clinical relevance that could be applied to hematopoietic stem cell or ES-HP transplantation.

Materials and Methods

Mice

C57BL/6 (B6) mice were purchased from the Jackson Laboratories or bred in house and housed in sterile microisolator cages with sterile feed and autoclaved water. They were euthanized by CO_2 asphyxiation. The Institutional Animal Care and Use Committee (IACUC) at UC Merced approved all procedures.

Tissue Isolation

Breeder mice were mated in the early evening and were checked for vaginal plugs the following morning. The morning on which vaginal plugs were observed was designated 0.5 dpc. Fetal liver and limbs were dissected from fetuses at day 14.5 and 17.5 dpc and placed in cold M199+ media (Invitrogen, Grand Island, NY) with 2% of FBS (Atlanta Biologicals, Lawrenceville, GA). Single-cell suspensions were prepared by triturating the tissues through a 70 μm nylon mesh screen. At least three pregnant females were used for each time point. Those fetuses that appeared developmentally advanced or delayed in any age group were discarded. Adult BM obtained from the hind leg bones of 4-week old mice was flushed with a 25 G needle in cold M199+ media with 2% of FBS, filtered through a 70 μm nylon cell strainer, and immediately processed for staining.

For microscopy studies, fetal liver and limbs were dissected from fetuses at day 14.5 and 17.5 dpc. Adult BM was flushed from the hind bones of 4-week-old mice. All tissues were embedded in Tissue-Tek® O.C.T. Compound (Sakura Finetek USA, Inc, Torrance, CA). Slides of five micrometers sections of OCT embedded tissues were obtained from Cureline, Inc (Burlingame, CA). Slides were store at $-80^{\circ}C$ until being processed for confocal analysis.

Confocal Microscopy

Sample preparation and staining was performed as described by Kiel et al. [2], with some minor modifications (For details see Text S1).

Cell staining for flow cytometric sorting and analysis

Sample preparation for cell sorting was performed as described before [5], without magnetic depletion of Lineage positive cells (For details of antibodies, fluorochromes and methodology used, see Text S1). Plates containing sorted single cells and negative samples, were stored at $-20^{\circ}C$ for 2 month as maximum or until they were used for analysis.

For flow cytometry analysis, single cell suspensions from the different tissues were stained with anti-CD16/32 antibody to block FcγII/III receptors. Fc blockage was followed by a 15 minute staining with an antibody cocktail containing PE-Cy5-conjugated anti-CD3, anti-CD4, anti-CD8, anti-CD11b, anti-CD19, anti-NK1.1, anti-Ter119, anti-GR1, anti-CD41 and anti-CD48, PE-Cy7 conjugated anti-CD150, PE-conjugated anti-CD49d, Qdot605-conjugated anti-VE-Cadherin, biotin-conjugated anti-CD49e, FITC-conjugated anti-CD11a, PE-conjugated anti-CD49d, Pacific Blue-conjugated anti-CD29, APC-conjugated anti-CD148 and Qdot525-conjugated anti-N-Cadherin. After rinsing, samples were incubated with streptavidin-conjugated APC-Alexa Fluor 750. Propidium iodide (0.5 μg/ml final concentration) was added before analysis to exclude dead cells. At least 3×10^7 cells/sample were analyzed using a BD LSRII flow cytometer controlled by BD FACSDiva^{TM}, v.6.1.1 software (Becton Dickinson, Franklin Lakes, NJ). Unstained cells were used to evaluate autofluorescence. Each experiment was carefully compensated by single staining BD^{TM} compBeads (BD Biosciences, San José, CA) with the appropriate antibody:fluorochrome combination, using BD FACSDiva^{TM}. In all cytometry experiments, at least three samples were analyzed for each time point.

RNA isolation

RNA was extracted from 10^6 adult BM cells using Trizol (Invitrogen), following manufacturer's instructions. Following DNAse I (Roche, San Francisco, CA) treatment, the concentration of RNA was determined using a Nanodrop spectrophotometer (Thermo Scientific, Waltham, MA). The RNA was used as positive control and for the setup of the conditions for qPCR analysis as well as the validation of the single cell multiplex qPCR analysis.

Primer Design

Gene sequences for primers design were obtained from the nucleotide NCBI database [53]. Primer pairs were designed with Primer3Plus software [54], selecting oligos between 18–22 base pairs, which hybridized across introns, had similar melting temperatures, were ~50% G/C composition, and amplified amplicons of similar size. The percent G/C of the amplified products was determined with the Bioedit software, version 7.0.5.3. Formation of primer dimers was analyzed with Primer List (http://primerdigital.com/tools/PrimerList.html). Primers specificity was tested for each primer using NCBI BLAST search engine in the mouse genome [55]. The primers selected for these PCR reactions are listed in Table 1. All primers were purchased from Sigma-Aldrich Corp, TX.

Reverse Transcription

Sorted single cells lysed by heating at 65°C for 5 min. After cooling to 4°C, RNA from each single cell was incubated with 0.76 mM dNTPs (Invitrogen) and a cocktail containing 1.64 μM specific 3′ primers for each gene of interest for 5 minutes at 65°C. Subsequently, the RNA was retrotranscribed with 100 units of SuperScript™ III RT (Invitrogen) in a solution containing 40 units of RNase OUT™, 4.5 mM $MgCl_2$, 9 mM DTT, 13 mM Tris-HCl, 32.6 mM KCl at pH 8.4 for 50 minutes at 50°C and terminated by a 5-minute incubation at 85°C. After cooling the reaction at 4°C, the samples were treated with 1 U of RNaseH for 20 minutes at 37°C and stored at 4°C. All these reactions were run on a Mastercycler® ep gradient S thermocycler (Eppendorf, Hauppauge, NY). Negative samples (without cells) and positive controls (containing 100 ng of whole BM RNA) were run alongside each retrotranscription reaction. Similar conditions were used for validating the parameters of the single cell multiplex RT analysis with whole BM RNA except for competition analysis where either single or multiplex primers were added in the retrotranscription reaction.

Pre-amplification

All cDNAs obtained from retrotranscription reactions were diluted 4–fold in milliQ water, followed by pre-amplification with 0.05 U of Platinum® Taq DNA polymerase (Invitrogen) in 20 mM Tris-HCl (pH 8.4), 50 mM KCl, 1.5 mM $MgCl_2$, 0.2 mM dNTPs and a mix containing primers pairs specific for each gene of interest, at a final concentration of 0.022 μM/primer. PCR consisted of a first step of 94°C for 45 secs and 10 cycles of amplification (1 min at 94°C, 1 min at 60°C and 1 min at 72°C). Pre-amplification reactions were run on a Mastercycler® ep

Table 1. Primers used for single cell qPCR analysis.

Gene name and accession number	Primer name	Primer sequence (5′→3′)
Hprt	Hprt RT	CAAGGGCATATCCAACAACA
NM_013556	Hprt F	GGGGGCTATAAGTTCTTTGCT
	Hprt R	GGCCTGTATCCAACACTTCG
Cxcr4	CXCR4 RT	GACAAAGAGGAGGTCAGCCA
NM_009911	CXCR4 F	GTGCAGCAGGTAGCAGTGAA
	CXCR4 R	GGGTTCCTTGTTGGAGTCATAG
Vecad	VECad RT	CGGAGGGTTGTCATTCTCAT
NM_009868	VECad F	TGGTCACCATCAACGTCCTA
	VECad R	GCACAATGGACTCTTTCCCTAC
Ncad	NCad RT	AGGGTCTCCACCACTGATTCT
NM_007664	NCad F	ATGATCCAAATGCCCTGAAT
	NCad R	TTTGTCCGTGACAGTTAGGTTG
Casr	CASR RT	ATCCTGCCTGTGATGTTACG
NM_013803	CASR F	TATCCCCCAGGTGAGCTACG
	CASR R	GATCACTTCCACCACCTGCT
α4 integrin	VLA4 RT	CTTGAGAGGCGATCCACAT
NM_010576	VLA4 F	CACTCCAGCCGATCCTTCA
	VLA4 R	TGCAGGCAAGCTTCACTATG
α5 integrin	VLA5 RT	ACCTCCTGAGGTCTCCCATC
NM_010577	VLA5 F	ATCCTGTCCGCCACTCAA
	VLA5 R	GGTCATCTAGCCCATCTCCA
Lfa1	LFA1 RT	CCAGCGTCATTCCCAAGTA
NM_008400	LFA1 F	AGAAGCCACCATTTCCCTCT
	LFA1 R	TGCTTGTTCGGCAGTGATAG
Psgl1	PSGL1 RT	GTAGGGTCAGTGGTGGCAAT
NM_009151	PSGL1 F	CTGTCACTGAGGCAGAGTCGTT
	PSGL1 R	GTTCCCGGAGATGCACAG

Note: RT primers were used for retrotranscription reaction. Forward (F) and Reverse (R) primers were used for pre-amplification and qPCR reactions. Gene accession number for each gene obtained from NCBI database (http://www.ncbi.nlm.nih.gov/nuccore) [53].

doi:10.1371/journal.pone.0030542.t001

gradient S thermocycler (Eppendorf). Similar conditions were used for validating the parameters of the single cell multiplex RT-PCR analysis with either whole BM RNA or cloned PCR amplicons, except for competition analysis where either primer pairs or multiplex primer pairs were added in the reaction. For details concerning cloning of PCR amplicons, see Text S1.

Real-Time Quantitative PCR

Pre-amplified samples were diluted 5-fold before quantitative PCR studies. Real time qPCR was performed in 1× Fast SYBR® Green Master Mix (Applied Biosystems, CA) containing 5 µl of pre-amplified template and 200 nM of each specific primer pair in a StepOnePlus Real-Time PCR System (Applied Biosystems, Carlsbad, CA). After a 10 min denaturation step at 95°C, 60 cycles of amplification were performed as follows: 95°C for 3 seconds and 60°C for 30 seconds. Melting curves were generated after amplification with the following conditions: 95°C for 15 seconds, 60°C for 1 minute, a 0.3°C gradient increase and 95°C for 15 seconds. All genes, including the housekeeping gene *Hprt*, were analyzed in triplicates for each sample as well as the positive and negative controls. The same threshold value, falling on the exponential phase of the qPCR curve, was applied to all the samples amplified in order to determine the threshold cycle (C_t). A typical experiment consisted of analyzing twenty-four cells, which displayed the correct melting curve for *Hprt*, for each tissue sample studied. Each experiment was repeated in 3 independent pregnancies per developmental time studied or 3 adult mice. The amplification efficiency, specificity and limit-of-detection qPCR experiments were performed in triplicate samples using cloned PCR amplicons as template.

Data analysis

Flow cytometry data was analyzed using FlowJo software, version 7.2.4 or version 8.8.7 (TreeStar, Ashland, OR). Single cell quantification based in the $\Delta\Delta C_t$ method and qPCR efficiency calculations were performed using StepOne™ software, version 2.0. Confocal microscopy analysis was performed with EZ-C1 FreeViewer software, version 3.20. Tukey and Student *t*-test statistical analysis were performed using SPSS software, version 13.0.

Supporting Information

Figure S1 LT-HSC identification by confocal microscopy. The immunohistochemical images of FL14.5 (1st row), FL17.5 (2nd row), FBM17.5 (3rd row) and 4-week old adult BM (4th row) are shown. Staining by CD48, CD41 and lineage markers is shown in green (1st column), CD150 in red (2nd column) and nuclei marked by TOTO-3 in blue (3rd column). Merged images are shown in the 4th column. LT-HSCs were identified as $CD150^+CD48^-CD41^-Lin^-$ cells.
(TIF)

Figure S2 Verification of single cell RT-qPCR product by comparison of melting temperature curves for *Hprt*. Single cells were sorted into 8-well strips and subjected to multiplex RT-qPCR. The melting temperature curves for the *Hprt* product were used to confirm the presence of a single cell per well and to evaluate the integrity of the sample's mRNA. Blue lines show the melting temperature curve of wells containing the positive whole BM control (300 ng RNA/sample), red lines the sorted, single LT-HSC and yellow lines the sorting buffer alone control. Wells in which the melting curve of the *Hprt* product did not match the whole BM control were discarded.
(TIF)

Figure S3 Verification of single cell RT-qPCR product by comparison of melting temperature curves. The melting temperature curves for each single cell RT-qPCR product (red lines) were compared to the melting temperature curve of the positive whole BM control (blue lines, 300 ng RNA/sample).
(TIF)

Table S1 Mean Fluorescence Intensity (MFI) values.
(DOC)

Text S1 Supplemental Materials and Methods.
(DOC)

Acknowledgments

The authors thank Mr. Roy Hoglund and the UC Merced Laboratory Animal Resource Center staff for mouse husbandry and care, Mr. Raffi Petrosian and Drs. Michael Cleary, Jennifer O. Manilay, and Néstor J. Oviedo for their critical review of the manuscript, and Drs. Sophie Ezine, Amine Boudil and Luigi A. Warren for helpful discussions.

Author Contributions

Conceived and designed the experiments: JC MGO. Performed the experiments: JC DH AL JDS MAK MGO. Analyzed the data: JC DH AL MGO. Contributed reagents/materials/analysis tools: JC MGO. Wrote the paper: JC MGO.

References

1. Domen J, Weissman IL (1999) Self-renewal, differentiation or death: regulation and manipulation of hematopoietic stem cell fate. Mol Med Today 5: 201–208.
2. Kiel MJ, Yilmaz OH, Iwashita T, Yilmaz OH, Terhorst C, et al. (2005) SLAM family receptors distinguish hematopoietic stem and progenitor cells and reveal endothelial niches for stem cells. Cell 121: 1109–1121.
3. Kim I, He S, Yilmaz OH, Kiel MJ, Morrison SJ (2006) Enhanced purification of fetal liver hematopoietic stem cells using SLAM family receptors. Blood 108: 737–744.
4. Yilmaz OH, Kiel MJ, Morrison SJ (2006) SLAM family markers are conserved among hematopoietic stem cells from old and reconstituted mice and markedly increase their purity. Blood 107: 924–930.
5. Ciriza J, Garcia-Ojeda ME (2010) Expression of migration-related genes is progressively upregulated in murine Lineage-Sca-1+c-Kit+ population from the fetal to adult stages of development. Stem Cell Res Ther 1: 14.
6. Weksberg DC, Chambers SM, Boles NC, Goodell MA (2008) CD150- side population cells represent a functionally distinct population of long-term hematopoietic stem cells. Blood 111: 2444–2451.
7. Mikkola HK, Orkin SH (2006) The journey of developing hematopoietic stem cells. Development 133: 3733–3744.
8. Christensen JL, Wright DE, Wagers AJ, Weissman IL (2004) Circulation and chemotaxis of fetal hematopoietic stem cells. PLoS Biol 2: E75.
9. Sugiyama T, Kohara H, Noda M, Nagasawa T (2006) Maintenance of the hematopoietic stem cell pool by CXCL12-CXCR4 chemokine signaling in bone marrow stromal cell niches. Immunity 25: 977–988.
10. Zou YR, Kottmann AH, Kuroda M, Taniuchi I, Littman DR (1998) Function of the chemokine receptor CXCR4 in haematopoiesis and in cerebellar development. Nature 393: 595–599.
11. Nagasawa T, Hirota S, Tachibana K, Takakura N, Nishikawa S, et al. (1996) Defects of B-cell lymphopoiesis and bone-marrow myelopoiesis in mice lacking the CXC chemokine PBSF/SDF-1. Nature 382: 635–638.
12. Kawabata K, Ujikawa M, Egawa T, Kawamoto H, Tachibana K, et al. (1999) A cell-autonomous requirement for CXCR4 in long-term lymphoid and myeloid reconstitution. Proc Natl Acad Sci U S A 96: 5663–5667.
13. Kaplan RN, Psaila B, Lyden D (2007) Niche-to-niche migration of bone-marrow-derived cells. Trends Mol Med 13: 72–81.
14. Kim I, Yilmaz OH, Morrison SJ (2005) CD144 (VE-cadherin) is transiently expressed by fetal liver hematopoietic stem cells. Blood 106: 903–905.
15. Zhang J, Niu C, Ye L, Huang H, He X, et al. (2003) Identification of the haematopoietic stem cell niche and control of the niche size. Nature 425: 836–841.
16. Kiel MJ, Radice GL, Morrison SJ (2007) Lack of evidence that hematopoietic stem cells depend on N-cadherin-mediated adhesion to osteoblasts for their maintenance. Cell Stem Cell 1: 204–217.

17. Kiel MJ, Acar M, Radice GL, Morrison SJ (2009) Hematopoietic stem cells do not depend on N-cadherin to regulate their maintenance. Cell Stem Cell 4: 170–179.
18. Lam BS, Cunningham C, Adams GB (2010) Pharmacologic modulation of the calcium-sensing receptor enhances hematopoietic stem cell lodgment in the adult bone marrow. Blood.
19. Adams GB, Chabner KT, Alley IR, Olson DP, Szczepiorkowski ZM, et al. (2006) Stem cell engraftment at the endosteal niche is specified by the calcium-sensing receptor. Nature 439: 599–603.
20. Papayannopoulou T, Craddock C, Nakamoto B, Priestley GV, Wolf NS (1995) The VLA4/VCAM-1 adhesion pathway defines contrasting mechanisms of lodgement of transplanted murine hemopoietic progenitors between bone marrow and spleen. Proc Natl Acad Sci U S A 92: 9647–9651.
21. van der Loo JC, Xiao X, McMillin D, Hashino K, Kato I, et al. (1998) VLA-5 is expressed by mouse and human long-term repopulating hematopoietic cells and mediates adhesion to extracellular matrix protein fibronectin. J Clin Invest 102: 1051–1061.
22. Potocnik AJ, Brakebusch C, Fassler R (2000) Fetal and adult hematopoietic stem cells require beta1 integrin function for colonizing fetal liver, spleen, and bone marrow. Immunity 12: 653–663.
23. Papayannopoulou T, Priestley GV, Nakamoto B, Zafiropoulos V, Scott LM, et al. (2001) Synergistic mobilization of hemopoietic progenitor cells using concurrent beta1 and beta2 integrin blockade or beta2-deficient mice. Blood 97: 1282–1288.
24. Peled A, Kollet O, Ponomaryov T, Petit I, Franitza S, et al. (2000) The chemokine SDF-1 activates the integrins LFA-1, VLA-4, and VLA-5 on immature human CD34(+) cells: role in transendothelial/stromal migration and engraftment of NOD/SCID mice. Blood 95: 3289–3296.
25. Hidalgo A, Weiss LA, Frenette PS (2002) Functional selectin ligands mediating human CD34(+) cell interactions with bone marrow endothelium are enhanced postnatally. J Clin Invest 110: 559–569.
26. Katayama Y, Hidalgo A, Furie BC, Vestweber D, Furie B, et al. (2003) PSGL-1 participates in E-selectin-mediated progenitor homing to bone marrow: evidence for cooperation between E-selectin ligands and alpha4 integrin. Blood 102: 2060–2067.
27. Warren L, Bryder D, Weissman IL, Quake SR (2006) Transcription factor profiling in individual hematopoietic progenitors by digital RT-PCR. Proc Natl Acad Sci U S A 103: 17807–17812.
28. Peixoto A, Monteiro M, Rocha B, Veiga-Fernandes H (2004) Quantification of multiple gene expression in individual cells. Genome Res 14: 1938–1947.
29. Walter U, Franzke A, Sarukhan A, Zober C, von Boehmer H, et al. (2000) Monitoring gene expression of TNFR family members by beta-cells during development of autoimmune diabetes. Eur J Immunol 30: 1224–1232.
30. Raj A, Peskin CS, Tranchina D, Vargas DY, Tyagi S (2006) Stochastic mRNA synthesis in mammalian cells. PLoS Biol 4: e309.
31. Warren LA, Rossi DJ, Schiebinger GR, Weissman IL, Kim SK, et al. (2007) Transcriptional instability is not a universal attribute of aging. Aging Cell 6: 775–782.
32. Miyamoto T, Iwasaki H, Reizis B, Ye M, Graf T, et al. (2002) Myeloid or lymphoid promiscuity as a critical step in hematopoietic lineage commitment. Dev Cell 3: 137–147.
33. Wu JY, Scadden DT, Kronenberg HM (2009) Role of the osteoblast lineage in the bone marrow hematopoietic niches. J Bone Miner Res 24: 759–764.
34. Chan CK, Chen CC, Luppen CA, Kim JB, DeBoer AT, et al. (2009) Endochondral ossification is required for haematopoietic stem-cell niche formation. Nature 457: 490–494.
35. Lefebvre V, Bhattaram P (2010) Vertebrate skeletogenesis. Curr Top Dev Biol 90: 291–317.
36. Mazo IB, von Andrian UH (1999) Adhesion and homing of blood-borne cells in bone marrow microvessels. J Leukoc Biol 66: 25–32.
37. Mackie EJ, Ahmed YA, Tatarczuch L, Chen KS, Mirams M (2008) Endochondral ossification: how cartilage is converted into bone in the developing skeleton. Int J Biochem Cell Biol 40: 46–62.
38. Butcher EC (1991) Leukocyte-endothelial cell recognition: three (or more) steps to specificity and diversity. Cell 67: 1033–1036.
39. Jacobsen K, Kravitz J, Kincade PW, Osmond DG (1996) Adhesion receptors on bone marrow stromal cells: in vivo expression of vascular cell adhesion molecule-1 by reticular cells and sinusoidal endothelium in normal and gamma-irradiated mice. Blood 87: 73–82.
40. Schweitzer KM, Drager AM, van der Valk P, Thijsen SF, Zevenbergen A, et al. (1996) Constitutive expression of E-selectin and vascular cell adhesion molecule-1 on endothelial cells of hematopoietic tissues. Am J Pathol 148: 165–175.
41. Frenette PS, Subbarao S, Mazo IB, von Andrian UH, Wagner DD (1998) Endothelial selectins and vascular cell adhesion molecule-1 promote hematopoietic progenitor homing to bone marrow. Proc Natl Acad Sci U S A 95: 14423–14428.
42. Ara T, Tokoyoda K, Sugiyama T, Egawa T, Kawabata K, et al. (2003) Long-term hematopoietic stem cells require stromal cell-derived factor-1 for colonizing bone marrow during ontogeny. Immunity 19: 257–267.
43. Tzeng YS, Li H, Kang YL, Chen WC, Cheng WC, et al. (2010) Loss of Cxcl12/Sdf-1 in adult mice decreases the quiescent state of hematopoietic stem/progenitor cells and alters the pattern of hematopoietic regeneration after myelosuppression. Blood 117: 429–439.
44. Nagasawa T (2006) Microenvironmental niches in the bone marrow required for B-cell development. Nat Rev Immunol 6: 107–116.
45. Ayres-Silva Jde P, Manso PP, Madeira MR, Pelajo-Machado M, Lenzi HL (2011) Sequential morphological characteristics of murine fetal liver hematopoietic microenvironment in Swiss Webster mice. Cell Tissue Res 344: 455–469.
46. Hosokawa K, Arai F, Yoshihara H, Iwasaki H, Nakamura Y, et al. (2010) Knockdown of N-cadherin suppresses the long-term engraftment of hematopoietic stem cells. Blood 116: 554–563.
47. Castro CH, Shin CS, Stains JP, Cheng SL, Sheikh S, et al. (2004) Targeted expression of a dominant-negative N-cadherin in vivo delays peak bone mass and increases adipogenesis. J Cell Sci 117: 2853–2864.
48. Li H, Daculsi R, Grellier M, Bareille R, Bourget C, et al. (2010) Role of neural-cadherin in early osteoblastic differentiation of human bone marrow stromal cells cocultured with human umbilical vein endothelial cells. Am J Physiol Cell Physiol 299: C422–430.
49. Ritter MA, Boyd RL (1993) Development in the thymus: it takes two to tango. Immunol Today 14: 462–469.
50. Klug DB, Carter C, Gimenez-Conti IB, Richie ER (2002) Cutting edge: thymocyte-independent and thymocyte-dependent phases of epithelial patterning in the fetal thymus. J Immunol 169: 2842–2845.
51. Bradley JA, Bolton EM, Pedersen RA (2002) Stem cell medicine encounters the immune system. Nat Rev Immunol 2: 859–871.
52. McKinney-Freeman SL, Naveiras O, Yates F, Loewer S, Philitas M, et al. (2009) Surface antigen phenotypes of hematopoietic stem cells from embryos and murine embryonic stem cells. Blood 114: 268–278.
53. Benson DA, Karsch-Mizrachi I, Lipman DJ, Ostell J, Sayers EW (2010) GenBank. Nucleic Acids Res.
54. Untergasser A, Nijveen H, Rao X, Bisseling T, Geurts R, et al. (2007) Primer3Plus, an enhanced web interface to Primer3. Nucleic Acids Res 35: W71–74.
55. Morgulis A, Coulouris G, Raytselis Y, Madden TL, Agarwala R, et al. (2008) Database indexing for production MegaBLAST searches. Bioinformatics 24: 1757–1764.

APPENDIX D

Transcription Factor Complex AP-1 Mediates Inflammation Initiated by *Chlamydia pneumoniae* Infection

Anyou Wang, Mufadhal Al-Kuhlani, S. Claiborne Johnston,David M. Ojcius, Joyce Chou and Deborah Dean

Cellular Microbiology (2012) doi:10.1111/cmi.12071

Transcription factor complex AP-1 mediates inflammation initiated by *Chlamydia pneumoniae* infection

Anyou Wang,[1†] Mufadhal Al-Kuhlani,[2] S. Claiborne Johnston,[3] David M. Ojcius,[2] Joyce Chou[1] and Deborah Dean[1,4,5*]

[1]*Center for Immunobiology and Vaccine Development, Children's Hospital Oakland Research Institute, Oakland, CA 94609, USA.*

[2]*Health Sciences Research Institute and Molecular Cell Biology, University of California, Merced, CA 95340, USA.*

Departments of [3]*Neurology and*

[4]*Medicine, University of California School of Medicine, San Francisco, CA 94143, USA.*

[5]*Department of Bioengineering, University of California, Berkeley, CA 94720, USA.*

Summary

Chlamydia pneumoniae **is responsible for a high prevalence of respiratory infections worldwide and has been implicated in atherosclerosis. Inflammation is regulated by transcription factor (TF) networks. Yet, the core TF network triggered by chlamydiae remains largely unknown. Primary human coronary artery endothelial cells were mock-infected or infected with** ***C. pneumoniae*** **to generate human transcriptome data throughout the chlamydial developmental cycle. Using systems network analysis, the predominant TF network involved receptor, binding and adhesion and immune response complexes. Cells transfected with interfering RNA against activator protein-1 (AP-1) members FOS, FOSB, JUN and JUNB had significantly decreased expression and protein levels of inflammatory mediators interleukin (IL)6, IL8, CD38 and tumour necrosis factor compared with controls. These mediators have been shown to be associated with** ***C. pneumoniae*** **disease. Expression of AP-1 components was regulated by MAPK3K8, a MAPK pathway component. Additionally, knock-down of JUN and FOS showed significantly decreased expression of Toll-like receptor (TLR)3 during infection, implicating JUN and FOS in TLR3 regulation. TLR3 stimulation led to elevated IL8. These findings suggest that** ***C. pneumoniae*** **initiates signalling via TLR3 and MAPK that activate AP-1, a known immune activator in other bacteria not previously shown for chlamydiae, triggering inflammation linked to** ***C. pneumoniae*** **disease.**

Introduction

Inflammation is a natural biological response to stimuli such as microbial infection. Chronic inflammation, however, can lead to severe human diseases such as atherosclerosis and cancer (Karin *et al*., 2006). The extent of inflammation is tightly controlled by transcription factors (TFs). For example, the NF-κB complex of TFs mediates inflammation involved in antimicrobial bioprocesses and disease pathogenesis (Pikarsky *et al*., 2004). Yet, the key TFs that control inflammation initiated by a particular pathogen remain elusive.

Chlamydia pneumoniae is an obligate intracellular bacterial pathogen that is responsible for a high prevalence of upper and lower respiratory tract infections worldwide (Campbell and Kuo, 2004). *C. pneumoniae* has also been implicated in atherosclerosis based on compelling evidence from *in vitro* and animal studies in addition to data from human populations (Selzman *et al*., 2003; Belland *et al*., 2004; Campbell and Kuo, 2004). Some of the most persuasive evidence comes from the direct initiation or exacerbation of vascular lesions in rabbit and murine models in response to *C. pneumoniae* infection (Selzman *et al*., 2003; Belland *et al*., 2004; Campbell and Kuo, 2004).

Human hosts activate multiple TFs such as AP-1 and NF-κB that mediate inflammation (Dechend *et al*., 1999; Miller *et al*., 2000; Huang *et al*., 2008). The NF-κB complex has been regarded as a major TF complex in the regulation of inflammation caused by *C. pneumoniae* infection (Dechend *et al*., 1999). However, recent discoveries reveal that NF-κB is not necessary for the

Received 29 August, 2012; revised 15 October, 2012; accepted 10 November, 2012. *For correspondence. E-mail ddean@chori.org; Tel. (+1) 510 450 7655; Fax (+1) 510 450 7910.
†Present address: Human Genetics, David Geffen School of Medicine, University of California, Los Angeles, CA 90095, USA.

stimulation of inflammation during *Chlamydia trachomatis* infection (Misaghi *et al*., 2006; Le Negrate *et al*., 2008). This organism actually stimulates the formation of a protein complex, ChlaDub1, to inhibit NF-κB activation (Misaghi *et al*., 2006; Le Negrate *et al*., 2008), suggesting that NF-κB may not be the most important complex controlling inflammation initiated by chlamydiae (Le Negrate *et al*., 2008), although this has not yet been shown for *C. pneumoniae*. Nevertheless, with or without NF-κB, the human host activates a variety of inflammatory responses and releases various cytokines to cope with *C. pneumoniae* infection. For example, IL-8, which contains promoters for multiple TFs including binding sites for AP-1 and NF-κB, is released during *C. pneumoniae* infection of endothelial cells (Krull *et al*., 2004) and is linked to inflammatory disease development at this site (Campbell and Kuo, 2004; Krull *et al*., 2004). This suggests that at least one alternative TF complex other than NF-κB is activated in response to *C. pneumoniae*.

An obvious candidate is the AP-1 complex, a ubiquitous dimeric protein complex composed of Jun (e.g. JUN) and Fos (e.g. FOS) subfamilies (Curran and Franza, 1988). AP-1 is commonly activated during microbial infection with bacteria and viruses (Seo *et al*., 2004; Xie *et al*., 2005). In *in vitro* studies, *C. pneumoniae* infection of human vascular smooth muscle cells induced both NF-κB and AP-1 (Miller *et al*., 2000). In the murine model, the product of the immediate early gene c-Fos (FOS), a subunit of AP-1, is activated in the heart during *C. pneumoniae* infection (Huang *et al*., 2008).

Similar to NF-κB, AP-1 contains transcriptional regulator binding sites for most inflammatory mediators, and AP-1 can also bind promoters of inflammatory mediators independent of NF-κB during inflammation (Cho *et al*., 2001; Balasubramanian *et al*., 2003). Therefore, AP-1 independently mediates the release of inflammatory mediators such as IL8 (Yeo *et al*., 2004). AP-1 also interacts with other TFs to modulate expression of inflammatory mediators during infection with pathogens such as Group B Streptococcus (Vallejo *et al*., 2000). AP-1 functions vary depending on the combination of AP-1 complex components and conditions. The FOS and JUN complexes normally function as positive factors in regulating inflammation (Shaulian and Karin, 2002). However, the functional complexity of AP-1 remains largely elusive.

In the present study, we employed a systems biology network approach and identified AP-1 as the core complex modulating the fundamental processes of inflammation, including inflammatory signalling initiation, the signalling cascade and inflammatory mediator releases, in response to *C. pneumoniae* infection. The model predicted a role for TLR3 in initiating the inflammatory response, which was confirmed by infecting cells expressing different TLRs. Our results provide a unifying mechanism by which *C. pneumoniae* regulates inflammation.

Results

AP-1 members are the core components of a TF network Initiated by C. pneumoniae *infection*

To systematically decode a TF network involved in inflammation initiated by *C. pneumoniae* infection, we applied a protein-based network approach to analyse expression profiling altered by *C. pneumoniae* infection. We first assembled a protein interaction network by integrating the known protein-interaction databases as we previously published (Wang *et al*., 2010). We then mapped the network with the transcriptome data that was significantly altered by *C. pneumoniae* infection in HCAEC, a primary cell line used as a model for studying arthrosclerosis and *C. pneumoniae* infection (Molestina *et al*., 1998; Kaul and Wenman, 2001; Hogdahl *et al*., 2008). HCAEC were infected with live *C. pneumoniae* at five time points, representing the developmental cycle of the organism. The time points corresponded to bacterial attachment (5 min post infection), entry (25 min), initial transformation into metabolically active reticulate bodies and replication (2 h), metabolism and replication (24 h) and transformation into infectious particles for release and infection of adjacent cells (60 h). The transcription alterations during infection with living bacteria were compared with those from UV-treated *C. pneumoniae* and mock-infected HCAEC.

The TFs with significantly altered expression during *C. pneumoniae* infection were mapped to their corresponding proteins in the above network to integrate the gene expression profiling and network database as we previously described (Wang *et al*., 2010). The overlaid network became a dynamic TF network activated by *C. pneumoniae* infection (Figs 1A and 2).

To identify the key TFs in the infection model, we searched for the hubs and bottlenecks (Yu *et al*., 2007) in the TF network as we previously described (Wang *et al*., 2010). We systematically *in silico* knocked out each TF and examined their contribution to network connectivity – the distance between a node and every other node in the transmission range – calculated as the average number of neighbours (i.e. average distance). The TFs that contributed most to the connectivity of the network at 5 min were FOS (v-fos FBJ murine osteosarcoma viral oncogene homologue), EGR1 (early growth response) and MAP3K8 (mitogen-activated protein kinase kinase kinase 8) (Fig. 1B, grey bars). In addition, we further calculated the contribution of a single TF to the network diameter – the average of the shortest path length, which essentially characterized the network's interconnectivity (Wang *et al*., 2010). The longer the diameter, the less interconnectivity

there is in the network. Knocking out a hub (highly connected protein) would increase the diameter because of the loss of short paths in a network, whereas knocking out a bottleneck (node with many short paths going through them, analogous to key bridges that link subnetworks to a whole map network) (Yu *et al*., 2007), would decrease the diameter because the network would be broken down and the long path that normally links subnetworks would be lost. Knocking out FOS dramatically increased the network diameter (Fig. 1B, black bar), indicating that it is a hub in this network. However, knocking out SFPQ (splicing factor proline/glutamine rich – polypyrimidine tract binding protein associated) remarkably decreased the network diameter (Fig. 1B, black bar), and SFPQ also notably contributed to network connectivity (Fig. 1B, grey bar), suggesting that SFPQ is a bottleneck in this network. Deleting hub FOS (Fig. 2, green arrow) caused a huge loss in network connectivity. This suggested that the FOS hub and SFPQ bottleneck (Fig. 2, pink arrow) are critical co-ordinators in the network activated by *C. pneumoniae* at 5 min.

Similarly, the top 10 nodes that contributed to the network diameter for the rest of the time points are summarized in Fig. 1C. The top two hubs at 25 min were identified as FOS and AP-C (Activated Protein C), FOS and JUNB at 2 h, FOS and STAT1 at 24 h, and JUN and STAT1 at 60 h (Fig. 1C). Clearly, from the frequency of each TF in the entire profiling, FOS and JUN predominated in these dynamic networks, indicating that the AP-1 complex is likely the core component of the inflammatory network initiated by *C. pneumoniae*.

The microarray data have been deposited in GEO. The accession number is GSE27008 (http://www.ncbi.nlm.nih.gov/geo/query/acc.cgi?token=vduzheioawcigtm&acc=GSE27008).

AP-1 regulatory network

After deducing that the AP-1 complex is likely the core component of the inflammatory network stimulated by *C. pneumoniae*, we searched for additional members of the AP-1 regulatory network. We mapped the known protein–protein interactions with inflammatory genes that are associated with the AP-1 complex and that were significantly altered after *C. pneumoniae* infection of HCAEC (Fig. 3A). Special attention was paid to genes that have putative AP-1-binding motifs predicted from the motif-binding matrix (http://xerad.systemsbiology.net/MotifMogulServer/) with constraint criteria as shown in Fig. 4. Most of these inflammatory genes exhibit more than two putative AP-1 binding sites located within 3000 base pairs upstream of the transcriptional start sites. Examples are shown in Figs 3B and 4. The mapped network containing these AP-1 targets became an AP-1 regulatory network that was further classified into functional protein complexes based on gene functions and cellular locations in the gene ontology database (Fig. 3A) (http://www.geneontology.org). This network, then, contained a number of primary complexes central to inflammation, including receptor (yellow), binding and adhesion (green) and immune response (red) complexes (Fig. 3A). These protein interactions have largely been known to be dynamically activated by the AP-1 complex. For example, the features of inflammation induced by *C. pneumoniae* infections in *in vitro* studies and murine models, such as inflammatory mediators IL6, IL8, CD38 and TNFα (Selzman *et al*., 2003; Belland *et al*., 2004; Campbell and Kuo, 2004) and key signalling kinases like MAP3K8, were among the factors included in these complexes.

AP-1 complex mediates expressions of inflammatory mediators

To confirm the role of AP-1 in inflammation as predicted above, we experimentally examined the effect of AP-1 on the expression of inflammatory factors IL6, IL8, TNFα and CD38 during *C. pneumoniae* infection of HEp-2 and human peripheral blood monocytic leukaemia (THP-1; ATCC TIB-202) cells. siRNA designed against AP-1 members FOS, FOSB, JUN and JUNB (Table S1) were used to knock down expression of each in addition to the combination knock-down of FOS and JUN. The knock-down efficiency was determined by measuring gene expression alteration of IL6, IL8, TNFα and CD38 by qRT-PCR (Table S2).

siRNA treatment successfully knocked down at least 75% of the gene expression for AP-1 components FOS, FOSB, JUN and JUNB (Fig. 5A). Knock-down of AP-1 significantly reduced expression of almost all examined inflammatory factors (Fig. 5B–E) in both HEp-2 and THP-1 cells except for IL6 in THP-1 cells with FOS^- (Fig. 5D). Notably, the combined knock-down of AP-1 components produced, in general, a greater reduction of inflammatory gene expression than any single AP-1 member knock-down (Fig. 5B–E). For example, IL6 expression was not significantly altered under single FOS knock-down in THP-1 cells, but was dramatically repressed under the combination knock-down of FOS^-JUN^-. These findings suggested that AP-1 dimers are crucial TFs for inflammatory mediator release during *C. pneumoniae* infection.

The expression levels of selected inflammatory genes were also verified at the protein level using a Luminex multiplex protein quantitative assay (Fig. 5F). In general, results measured at the protein and mRNA level were consistent. Both FOS^- and JUN^- resulted in significantly lower protein levels of IL8 and TNFα compared with the

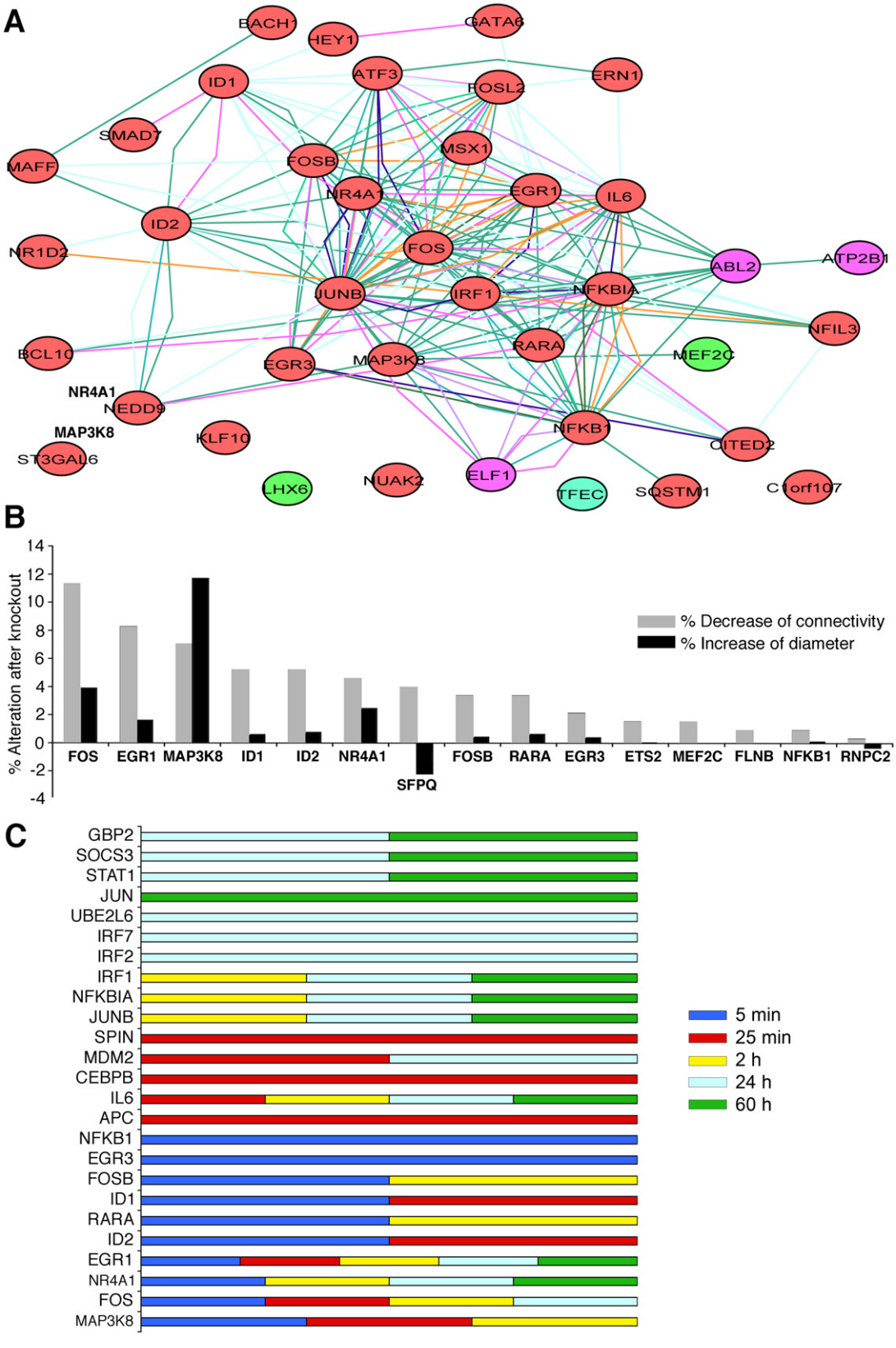

Fig. 1. AP-1 components dominate the transcription factor (TF) network initiated by *C. pneumoniae* infection of HCAEC.
A. AP-1 components, FOS, FOSB and JUNB dominate the TF network initiated by *C. pneumoniae* infection. The TF network was derived from a genome-wide protein interaction network overlapped with transcriptome data from this study (see *Experimental procedures*). Nodes and edges donate proteins and interactions respectively. The colour of the node represents the gene expression level: Red for upregulation, green for downregulation and violet for equivocal at 5 min.
B. The contribution of TFs to network connectivity and to the diameter of the network activated at 5 min post infection. TFs were systematically knocked out *in silico,* and the alterations in network connectivity (measured as average number of neighbours) and network diameter (measured as average shortest path length) were calculated (see *Experimental procedures*). The top TFs that contributed most to the network are shown. FOS and MAP3K8 contributed the most to both connectivity and diameter, respectively, suggesting that AP-1 dominates the TF network for *C. pneumoniae*.
C. Summary of the top 10 TFs from our transcriptome data at each time point that contributed the most to the diameter of the network activated at 5 min, 25 min, 2 h, 24 h and 60 h. From top to bottom, GBP2, SOCS3, STAT1, JUN, UBE2L6, IRF7 and IRF2 predominated in late infection (24 h and 60 h), while IRF1, NFKIA and JUNB were featured at 2 h, 24 h and 60 h. SPIN, MDM2, CEBPB and APC predominated at 25 min. EGR1, NR4A1, IL6 and FOS were primarily activated from 5 min to 24 h or to 60 h.

control. Together, our data suggest that AP-1 is a key TF complex regulating inflammation initiated by *C. pneumoniae* infection.

AP-1 complex mediates inflammatory signalling via TLR3 and MAP3K8

We next explored the mechanisms for AP-1 regulation of inflammation by examining the key inflammatory pathway regulated by AP-1 during *C. pneumoniae* infection. Inflammatory signalling is initiated by pattern recognition receptors (PRR), which then precipitate a signalling cascade via protein kinases. To identify crucial genes primarily involved in inflammation regulated by AP-1, we systematically screened genes with the highest correlation with AP-1 based on both the AP-1 target network (Fig. 3) and the mathematical model analysis of coexpression profiling. Gene expression alterations of all components of the AP-1 regulatory network (Fig. 3A) were measured by qRT-PCR for both overexpression of AP-1 (wild-type) and knock-down of AP-1 (FOS^-, JUN^- and combination FOS^-JUN^-) via siRNA during *C. pneumoniae* infection of HCAECs. A standard stepwise regression model was used to select genes with the largest partial correlation with AP-1. The results showed that AP-1 strongly associates with TLR3 and MAP3K8. Based on gene ontology (Fig. 3A), TLR3 appeared to be targeted by AP-1, while MAP3K8 appeared to be the key kinase for signalling transduction. We found that JUN and FOS knock-down significantly inhibited TLR3 expression (Fig. 6A) but not TLR4. TLR2 expression was similarly inhibited. By plotting the dynamic gene expression pattern of AP-1 components and MAP3K8 for 5 min, 25 min, 2 h, 24 h and 60 h, we found similar expression patterns between AP-1 complex TFs and MAP3K8 in HCAECs (Fig. 6B), which is consistent with the general regulatory pathway induced by pathogens as previously reported by Nijhara *et al*. (2001). Together, these data demonstrate that the AP-1 complex mediates inflammatory signalling via TLR3 and MAP3K8.

TLR3 regulates activation of NF-κB and expression of the chemokine IL8

TLR2 was previously shown to stimulate the innate immune response during infection by *Chlamydia muridarum* and *C. pneumoniae*, while TLR4 is thought to have no effect (Prebeck *et al*., 2001; Darville *et al*., 2003; Naiki *et al*., 2005; Cao *et al*., 2007). A role for TLR3 has been reported for infection of an oviduct cell line by the murine pathogen, *C. muridarum* (Derbigny *et al*., 2005; 2007; 2010) but never in animal studies. TLR3 effects on infection by the human pathogens, *C. trachomatis* or *C. pneumoniae*, have never been studied. Given our unexpected finding that the AP-1 complex regulates signalling via TLR3 during *C. pneumoniae* infection, we screened the TLRs likely to be involved in the response to *C. pneumoniae* using HEK293 cells that are stably transfected with control vector or human TLR2, TLR3 or TLR4. The cells, including control cells, stably coexpress an NF-κB-inducible SEAP (secreted embryonic alkaline phosphatase) reporter gene whose enzymatic activity can be conveniently and quantitatively monitored through a colorimetric assay.

As expected, HEK cells expressing NF-κB-induced reporter gene but not TLR (HEK-Null1) did not show NF-κB activation in response to stimulation with ligands for TLR2 (Pam3), TLR4 (LPS) or TLR3 (Pam3), or infection with C. *pneumoniae* (Fig. 7A). However, *C. pneumoniae* infection or Pam3-stimulation induced strong NF-κB activation in HEK-TLR2 cells, in agreement with previous reports. *C. pneumoniae* infection had no effect in HEK-TLR4 cells, although the positive control, LPS, stimulated NF-κB activation in these cells. *C. pneumoniae* infection had no effect at low multiplicity of infection (moi) in TLR3-expressing cells, but activated NF-κB at significant levels at an moi of 10 or 40. Even at the highest moi, there was no NF-κB in the HEK-Null1 cells.

The same cells were also used to measure IL8 gene expression during *C. pneumoniae* infection (Fig. 7B). IL8 expression in HEK-TLR3 cells was observed even at low moi of infection. Much higher levels of expression were

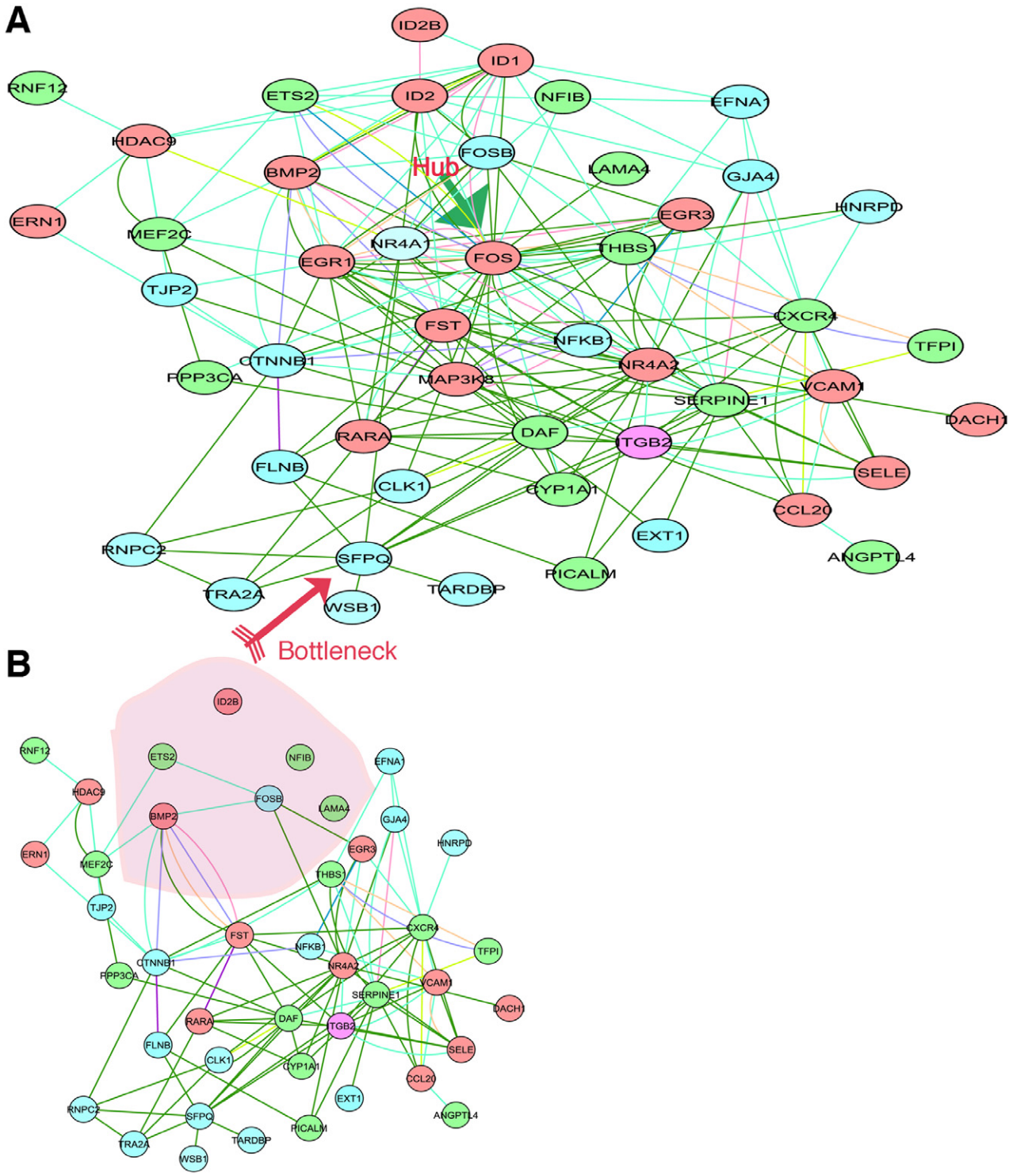

Fig. 2. *In silico* knockout of hubs and bottlenecks in the TF network.
A. Hubs and bottleneck and their neighbours for the wild-type network activated at 5 min. The green arrow highlights a hub (FOS). The pink arrow highlights a bottleneck (SFPQ).
B. The network was locally disconnected after the combination of knocking out the first five genes, FOS, EGR1, MAP3K8, ID1 and ID2, compared with the wild-type network shown in (A).

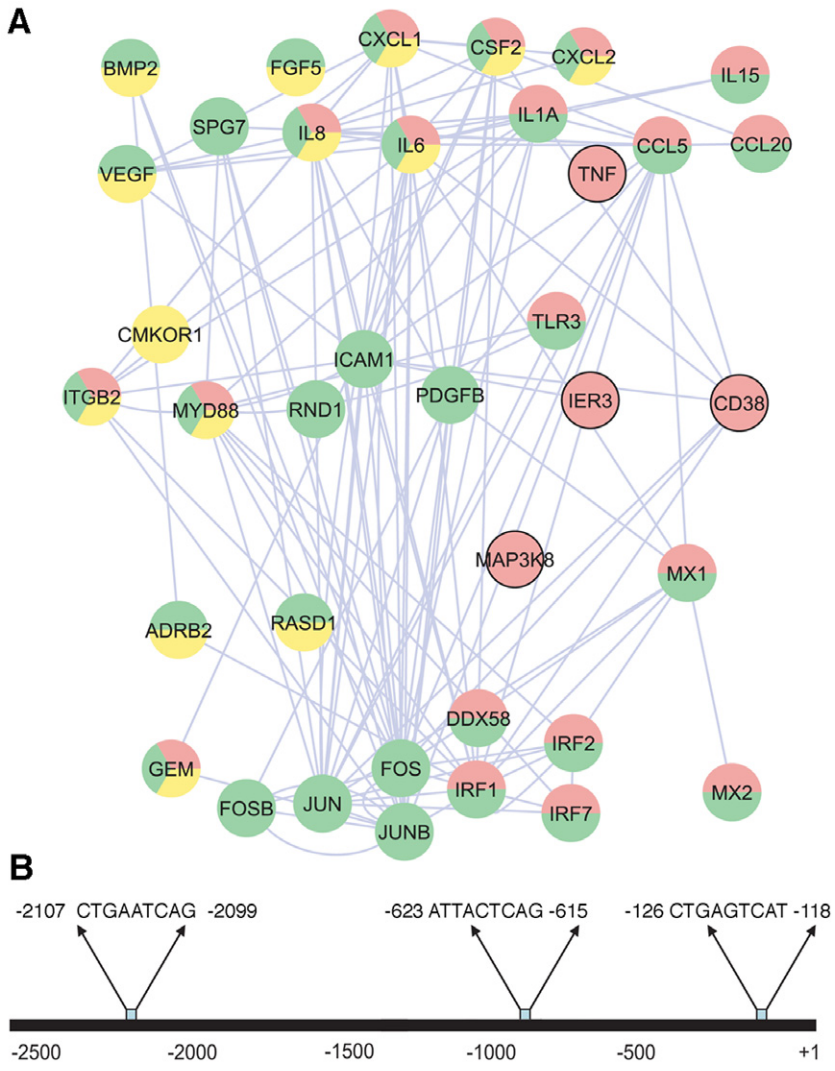

Fig. 3. AP-1 target gene predictions using the protein–protein interaction network and promoter sequence analysis.
A. Predicting AP-1-associated genes using the protein interaction network. The genes were determined from the network assembled from known transcription factor protein–protein interactions and transcriptome data as described in *Experimental procedures*. This network was organized by the gene ontology database, in which gene functions and localizations were included. AP-1 (nucleus) is predicted to interact with a number of major functional modules, including those for receptor complexes (yellow), immune response (red) and binding and adhesion (green).
B. Computational analysis of AP-1 binding sites for inflammatory mediators. These AP-1 binding sites were identified by scanning the 5′ upstream promoter regions of each gene with MotifMogul. For illustration, only the one for IL8 is shown; the rest are shown in Fig. 4.

found in HEK-TLR2 cells, also consistent with previous studies, although TLR3-dependent IL8 production during chlamydial infection has not been reported until now. *C. pneumoniae* infection, even at moi = 40, had no effect on IL8 expression in HEK cells in the absence of TLR.

Discussion

Inflammation is fundamentally modulated by TFs. However, the challenge has been to identify the critical TFs that regulate inflammation, because a complex network is usually activated during pathogenic infections. The NF-κB complex, a well-characterized TF complex, has been considered key in regulating inflammatory mediators (e.g. IL6 and IL8) during chlamydial infections (Gencay *et al*., 2003; Buchholz and Stephens, 2006). However, recent studies argue against this (Le Negrate *et al*., 2008). Significantly, chlamydial infection has been reported to interfere with NF-κB signalling (Lad *et al*., 2007; Le Negrate *et al*., 2008; Betts *et al*., 2009; Wolf *et al*., 2009).

In the present study, we employed a systems biology approach and found that AP-1 contributes to the major structure of the TF network initiated by *C. pneumoniae* infection (Fig. 1) and regulates many inflammatory mediators (Fig. 3). RNAi knock-down of single components of AP-1 or the AP-1 dimer combination significantly reduced the expression of inflammatory mediators, such as IL6, IL8, CD38 and TNFα, at both the mRNA and protein level (Fig. 5), although the latter levels were not as low as might be expected given the corresponding gene knock-down. The inflammatory mediator IL8 has been reported to be regulated by NF-κB, but IL8 release also occurs through the MAPK pathway independently of the NF-κB complex during *C. trachomatis* infection (Lad *et al*., 2007). Here, we revealed that IL8 is primarily regulated by AP-1. Our

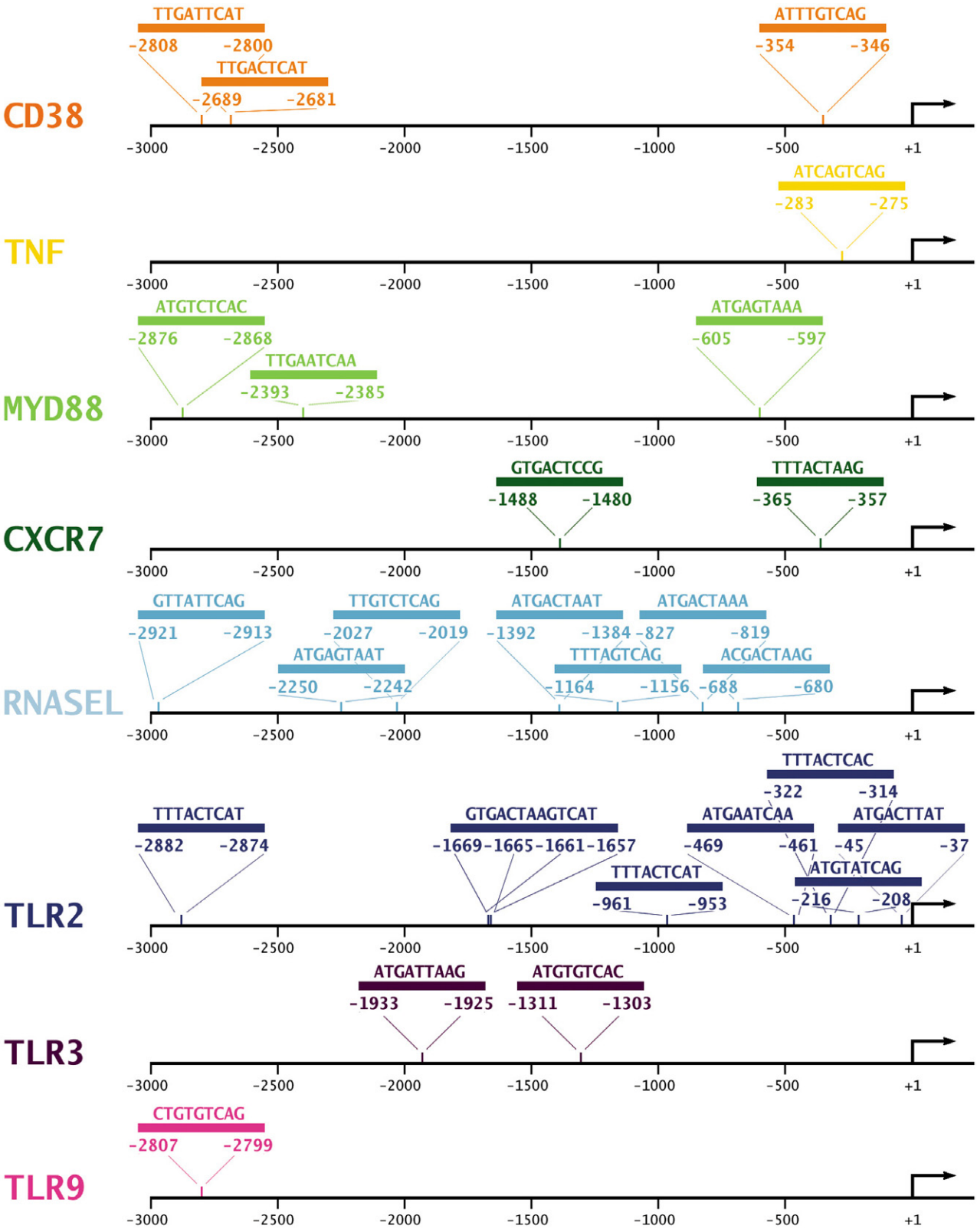

Fig. 4. AP-1 binding sites for inflammatory mediators predicted by MotifMogul. MotifMogul was used to predict AP-1 binding sites for inflammatory mediators as described in detail in *Experimental procedures*.

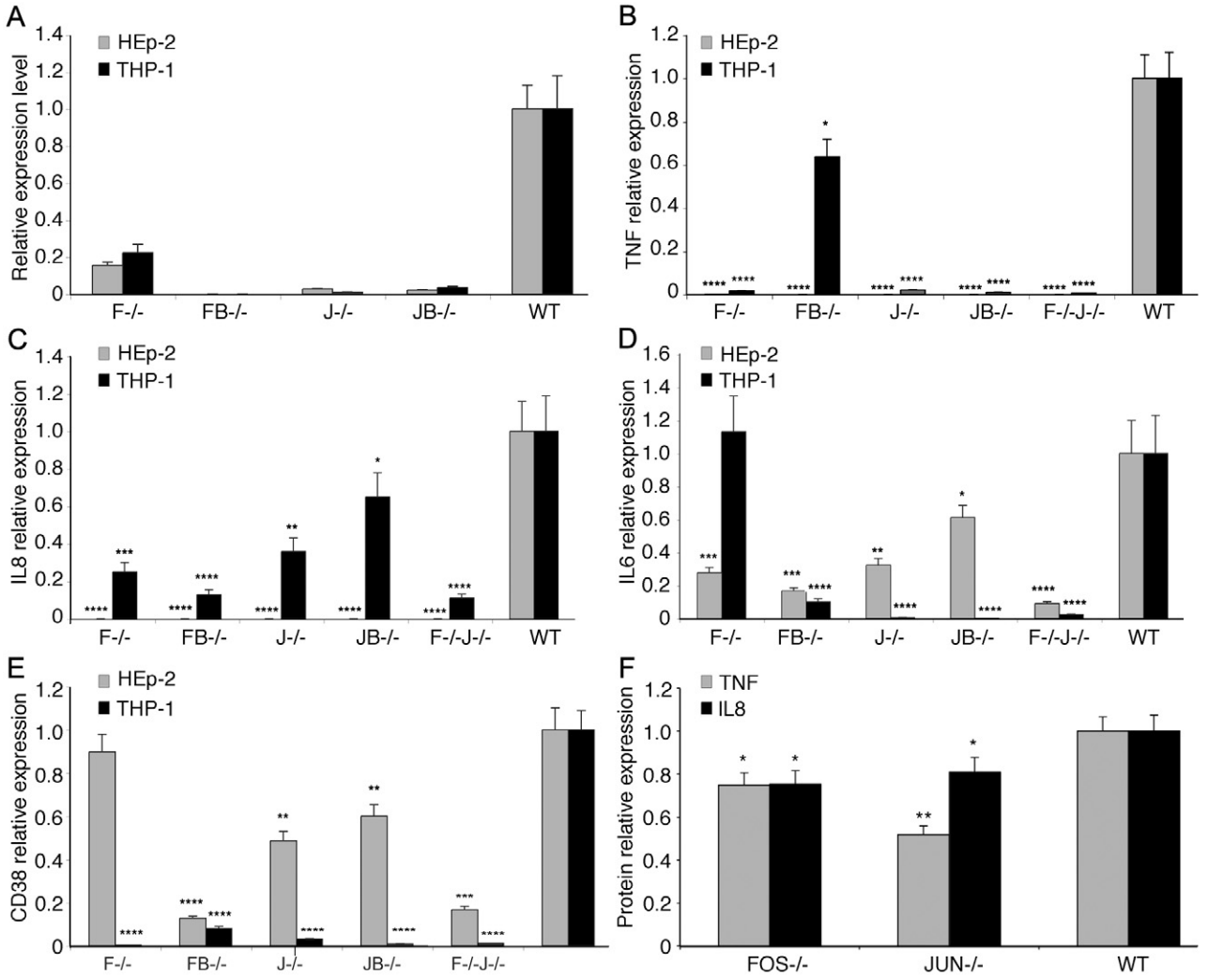

Fig. 5. AP-1 regulates gene expression of inflammatory mediators in *C. pneumoniae* infected HEp-2 and THP-1 cells.
A. AP-1 components FOS, FOSB, JUN and JUNB were knocked down by siRNA. The knock-down efficiency was determined by measuring gene expression alteration by qRT-PCR after siRNA knock-down of each AP-1 member (FOS, F–/–; FOSB, FB–/–; JUN, J–/–; JUNB, J–/–; FOS and JUN, F–/–J–/–) in *C. pneumoniae* infected HEp-2 and THP-1 cells. At least 75% of the gene expression of AP-1 members was knocked down when compared with the scrambled siRNA control.
B–E. Knock-down of AP-1 members FOS and JUN during *C. pneumoniae* infection significantly decreased key pro-inflammatory mediators TNF, IL8, IL6 and CD38, but not IL6, measured by qRT-PCR in both HEp-2 and THP-1 cells compared with wild-type (WT).
F. Knock-down of AP-1 components JUN and FOS downregulate inflammatory factors TNF and IL8 compared with WT measured during infection.
$^{*}P < 0.045$, $^{**}P < 0.01$, $^{***}P < 0.001$ and $^{****}P < 0.0005$.

findings suggest that AP-1 is a key TF complex that regulates the inflammatory network activated by *C. pneumoniae* infection.

AP-1 is a ubiquitous dimeric protein complex composed of different Jun (c-Jun, JunB and JunD) and Fos (c-Fos, Fra-1, Fra-2 and FosB) subfamilies (Curran and Franza, 1988) and commonly activated during microbial infection with bacteria and viruses (Seo *et al*., 2004; Xie *et al*., 2005). AP-1 complexes normally function as positive factors in regulating inflammation and the cell cycle. Yet, different combinations of AP-1 members express differential biological effects. While JUN, FOS and FOSB are often positively associated with inflammation, cell growth, cellular transformation, tumour formation and tumour progression, JUNB performs a negative regulatory role in mediating cell proliferation (Shaulian and Karin, 2002). AP-1 mediates the release of inflammatory mediators such as IL8 (Yeo *et al*., 2004) and regulates angiogenesis caused by pathogen infection as in the case of herpesvirus infection (Ye *et al*., 2007). AP-1 also interacts with other TFs to cope with pathogen development (Ravichandran *et al*., 2006) and modulates expression

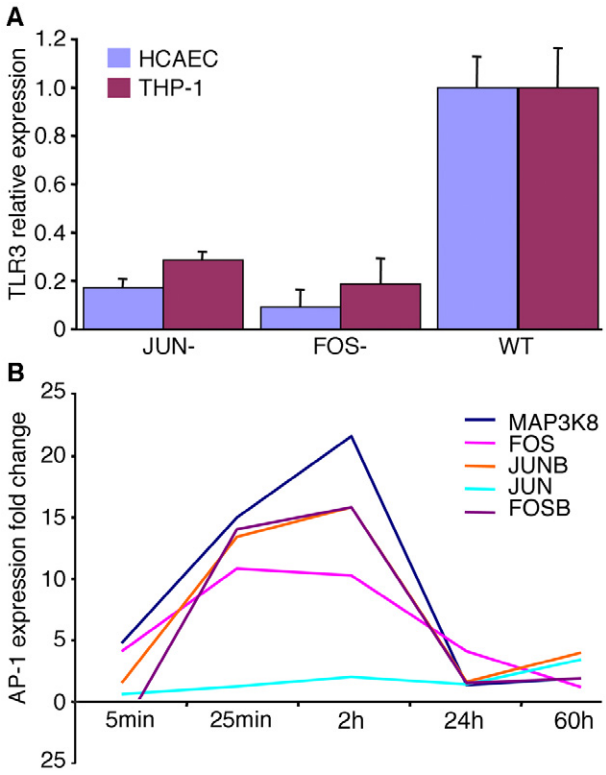

Fig. 6. AP-1 complex mediates inflammatory signalling via TLR3 and MAP3K8.
A. JUN and FOS knock-down by siRNA dramatically alters gene expression of TLR3 in *C. pneumoniae* infected HCAEC and THP-1 cells as measured by qRT-PCR.
B. Expression of AP-1 components correlates with MAPK signalling pathway during *C. pneumoniae* infection of HCAEC measured by both microarray and qRT-PCR.

of inflammatory mediators during infection with pathogens such as Group B Streptococcus (Vallejo *et al*., 2000). This suggests that the biological functions of AP-1 are complex and that much of its functional complexity remains to be elucidated.

The function of AP-1 is known to vary depending on cell type (Chinenov and Kerppola, 2001; Eferl and Wagner, 2003). We used three different cell types to examine the AP-1 function during *C. pneumoniae* infection and surprisingly, found that inflammatory mediators, IL6, IL8, CD38 and IFN, were primarily regulated by most of the AP-1 members examined here. In fact, other inflammatory mediators predicted in Fig. 3A were also regulated by at least one AP-1 member (either FOS or JUN) for a given cell line. This suggests that AP-1 likely regulates inflammation stimulated by *C. pneumoniae* infection. Our results nicely parallel the recent observations showing that AP-1 serves as a crucial modulator in regulating inflammation initiated by other pathogens such as Group B streptococcus, Herpes simplex virus 1 and *Helicobacter pylori* (Zachos *et al*., 1999; Vallejo *et al*., 2000; Wu *et al*., 2006).

The underlying molecular mechanism(s) whereby AP-1 mediates inflammation during infections remains largely unknown. Here, our data revealed that AP-1 is activated primarily from TLR3 and MAP3K8 signalling pathways during *C. pneumoniae* infection. TLR3 is a host PRR that recognizes dsRNA derived from many different viral pathogens (Takeuchi and Akira, 2009). The interaction of dsRNA with TLR3 and its ectodomain results in dimer formation and recruitment of TIR-domain-containing adapter-inducing interferon-β (TRIF) that initiates signalling pathways and ultimately downstream TF activation, including AP-1 (Botos *et al*., 2009). While dsRNA is commonly produced by viral replication and is not known to be associated with chlamydiae, we speculate that it is possible that the organism generates a unique molecular ligand that is recognized by TLR3. In a murine oviduct cell line that was infected with *C. muridarum*, TLR3 was expressed in infected cells and served as a trigger for IFNβ production (Derbigny *et al*., 2005), which was subsequently found to be dependent on interferon regulatory factor 3 (IRF3) and TRIF (Derbigny *et al*., 2007). Recently, the IFNβ response was shown to be dependent on TLR3 in the same cell line (Derbigny *et al*., 2010). In another study. *C. pneumoniae* induced foam cell formation was influenced by TLR2 and TLR4 but not TLR3 (Chen *et al*., 2008). Our data revealed that TLR3 as well as interferon regulatory factors were activated during *C. pneumoniae* infection (Fig. 3) and regulated by JUN and FOS (Fig. 6). AP-1 may regulate inflammation via regulating TLR3, which appears to be one key receptor initiating inflammatory signalling triggered by *C. pneumoniae* infection, although signalling initiated by TLR3 can cascade via various pathways (Vercammen *et al*., 2008).

In addition, our data showed that MAP3K8 is a key enzyme regulating AP-1 signalling during *C. pneumoniae* infection (Figs 2 and 4), which is consistent with previous reports showing that AP-1 is regulated by the MAPK pathway (Chinenov and Kerppola, 2001; Eferl and Wagner, 2003). Previous studies demonstrated that release of inflammatory mediators such as IL8 are dependent on the MAP pathway independent of NF-κB (Cho *et al*., 2001; Balasubramanian *et al*., 2003). We found that IL8 release was dependent on AP-1. Thus, our findings suggest a model wherein *C. pneumoniae* initiates inflammatory signalling via TLR3 and the MAPK pathway, which in turn activates AP-1, triggering inflammatory mediator and chemokine release that are linked to chlamydial disease (Darville *et al*., 2003; Buchholz and Stephens, 2006; Sessa *et al*., 2009).

The functions of different AP-1 components could vary considerably, as inducers or inhibitors depending on specific conditions. There are many pathways that can transmit the signalling, once initiated (Fig. 3). Our data showed that the FOS and JUN complex serves as a

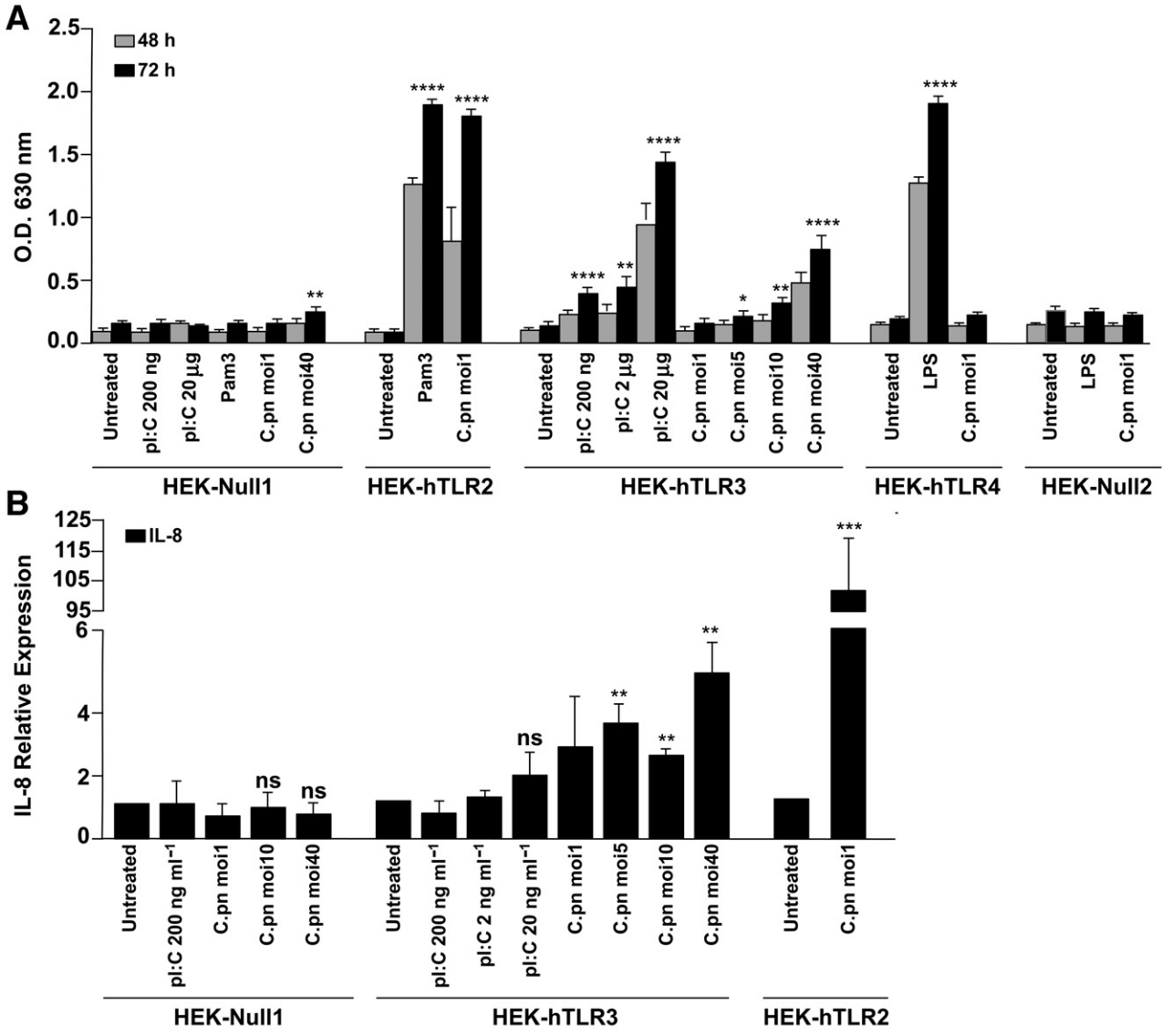

Fig. 7. TLR3 mediates NF-κB activation and IL8 expression.
A. Control HEK cells (HEK-Null) or HEK cells expressing TLR2, TLR3 or TLR4 were infected with *C. pneumoniae* (moi of 1, 5, 10 or 40) or stimulated with the TLR ligands, 5 mg ml^{-1} Pam3CSK4 (TLR2 ligand), 500 ng ml^{-1} LPS (TLR4 ligand) or 200 ng ml^{-1}, 2 mg ml^{-1} or 20 mg ml^{-1} poly(I:C) (TLR3 ligand) for 48 h or 72 h. NF-κB activation was assessed by measuring SEAP activity colorimetrically at 630 nm.
B. HEK cells expressing TLR3 or TLR2 were infected with *C. pneumoniae* at the indicated moi or stimulated with poly(I:C), and IL8 expression was measured by qPCR.
*$P < 0.045$, **$P < 0.01$, ***$P < 0.001$ and ****$P < 0.0005$.

central mediator in regulating inflammation initiated by *C. pneumoniae,* and this complex appears to perform its functions primarily via a potential feedback loop that may interact with TLR3 and MAP3K8. This does not exclude other TF complexes or other signalling pathway components that may be involved in the inflammatory process. In fact, many of the intermediate steps and components in the complex network (Fig. 3) remain to be experimentally discovered. However, we consider our results to be less biased than other biological and experimental conditions because they are drawn from a systems biology-based approach using established and primary cell lines, including experimental validation. Thus, our results are supporting a role for AP-1 in regulating inflammation induced by *C. pneumoniae*. Our findings lay the foundation for further research to expand our understanding of the AP-1 complex and other TF networks in *C. pneumoniae*-stimulated inflammation using appropriate animal models and *in vitro* model systems. In addition, our approach will be important for identifying immunotherapeutic markers as targets for interventions to prevent the inflammatory diseases caused by *C. pneumoniae* such as

atherosclerosis (Campbell and Kuo, 2004) and asthma (Hahn *et al*., 2012). Indeed, while there are many publications regarding the role of this pathogen in atherosclerosis, the present work may also be important in understanding the pathogenesis of asthma, given the growing body of evidence supporting an association between *C. pneumoniae* and asthma (Metz and Kraft, 2010; Olivares-Zavaleta *et al*., 2011; Senn *et al*., 2011; Hahn *et al*., 2012; Patel *et al*., 2012).

Experimental procedures

Network assembly

We combined existing network databases and systems network approaches using our previously described methods (Wang *et al*., 2010). Briefly, our network database included proteins and interactions from BIND (http://bond.unleashedinformatics.com/Action), DIP (http://dip.doe-mbi.ucla.edu/), HPRD (http://hprd.org/), PreBIND (http://www.blueprint.org/system/app/pages/search?scope=search-site&q=PreBIND), curated inflammatory disease databases (Calvano *et al*., 2005; von Mering *et al*., 2005; Reiss *et al*., 2005a,b), biocarta (http://www.biocarta.com/pathfiles/h_inflamPathway.asp, http://www.biocarta.com/pathfiles/h_LairPathway.asp), KEGG (http://www.genome.jp/kegg/pathway.html), EMBL human database (http://www.embl-heidelberg.de/) and two cytokine databases (http://www.siteseostats.net/site/cytokine.medic.kumamoto-u.ac.jp and http://people.bu.edu/gilmore/nf-kb/). This network was then used as a basis for building a *C. pneumoniae* network from whole human genome microarray data of *C. pneumoniae* infection of HCAEC over five experimental time points representing the developmental cycle of the organism (see below).

C. pneumoniae *propagation*

Chlamydia pneumoniae strain A03 (a gift from Dr James Summersgill) was previously isolated from the coronary artery of a patient with atherosclerosis (Ramirez, 1996). This clinical isolate was propagated in HEp-2 cells (ATCC CCL-23; Manassas, VA) following standard laboratory protocols as we have described previously (Ramirez, 1996; Molestina *et al*., 1998; Mukhopadhyay *et al*., 2004; Wang *et al*., 2010). Isolates were purified using 30% RenoCal centrifugation gradients as described (Li *et al*., 2005; Wang *et al*., 2010) to eliminate ~ 0.1% of contaminating human cellular material.

HCAEC culture and infection

The cell culture was performed using a previously reported method (Wang *et al*., 2010). Briefly, Endothelial Cell Basal Medium-2 with hEGF, Hydrocortisone, GA-1000, FBS, VEGF, hFGF-B, R3-IGF-1 and Ascorbic Acid (Clonetics™ EGM®-2-MV BulletKit, East Rutherford, NJ) were used to grow HCAEC (Clonetics™) according to the manufacturer's instructions. The cells were grown in T25 flasks in 37°C with 5% CO_2 to a confluence of ~ 80% and ~ 55%, respectively, for subsequent group 1 (0 min, 5 min, 25 min and 2 h) and group 2 (24 h and 60 h) infections with *C. pneumoniae*. A *C. pneumoniae* moi of 100 and 5 was used for group 1 and group 2 infections respectively. The higher confluence and moi for group 1 was used to ensure sufficient infection for a short period of *C. pneumoniae* growth for RNA extraction. The lower confluence and moi for group 2 allowed the cells to grow and for *C. pneumoniae* to infect these cells for the 24 h and 60 h time points in such a way that neither the cells nor *C. pneumoniae* would overgrow the cell culture system, which could result in apoptosis and loss of infection. For UV inactivation, *C. pneumoniae* was treated with a UV germicidal light for 3 h (30 w, 15 cm). HCAEC were infected as above with UV-treated *C. pneumoniae* at the same moi as for viable *C. pneumoniae*. Mock-infected HCAEC were used as controls for each time point.

RNA extraction, microarray hybridization and array detection

Infected and uninfected HCAEC at 0 min, 5 min, 25 min, 2 h, 24 h and 60 h post infection were trypsinized and collected by centrifugation. RNA was purified using the RNeasy RNA purification kit (QIAGEN, Valencia, CA), including an on column treatment with DNase to eliminate all traces of DNA, according to the manufacturer's instructions and as we have previously described (Gomes *et al*., 2005). Affymetrix Human Genome U133 Plus 2.0 Arrays, which contain over 47 000 transcripts that completely cover the whole human genome, were employed in this study. GeneChip® One-Cycle Target Labelling and Control Reagents (Affymetrix, Santa Clara, CA) were used to process RNA and for hybridization to the microarrays following the manufacturer's protocols. Briefly, cRNA was generated from total RNA. The resultant biotinylated cRNA was fragmented and hybridized to the microarrays. The arrays were washed, stained and scanned with the Affymetrix scanner using the manufacturer's recommended protocols as per the Stanford University Gene and Protein Expression Core Facility (Palo Alto, CA).

Network analysis

Network analysis was performed as we described in detail previously (Wang *et al*., 2010). Briefly, genes with significant alterations in gene expression compared with controls in the microarray (*t*-test, $P < 0.05$, as per the Bioconductor package) (Gentleman *et al*., 2004) were used to overlay the network described above. These overlaid networks became the inflammatory networks activated (up- and downregulated) by *C. pneumoniae*. The activated networks were decomposed into functional modules based on topological interconnection intensity and gene functions (http://www.geneontology.org/) (Bader and Hogue, 2003; Maere *et al*., 2005; Singhal and Domico, 2007; Singhal and Resat, 2007). Genes were classified according to the gene ontology database (http://www.geneontology.org/) (Garcia *et al*., 2007).

Standard stepwise regression, which adds and removes variables, was used to select the variables (genes, in our case). The basic method of stepwise regression is to calculate an *F*-statistic for each variable in the model (Hennekens and Buring, 1987). If the *F*-statistic for any variable is less than *F*, the variable with the smallest *F* is removed from the model. If no variable can be removed, the procedure attempts to add a variable. An *F*-statistic is calculated for each variable not yet in the model. The variable

with the largest *F*-statistic is then added, provided its *F*-statistic is larger than *F* to enter. Adding this variable is equivalent to choosing the variable with the largest partial correlation or the variable that most effectively reduces the error sum of squares. The regression equation is then calculated, results are displayed and the procedure continues to a new step. If no variable meets the criteria for addition to the network, the stepwise procedure is finished.

AP-1 binding sites were predicted using the motif Mogul (http://xerad.systemsbiology.net/MotifMogulServer/), with human stringent matrices, stringent MotifLocator Scans at 0.01%, $P < 0.05$, and others as per the default setting in the programs.

Small interfering RNA knock-down

Small interfering RNA (siRNA) knock-down experiments were performed as we previously described (Wang *et al*., 2010). Briefly, based on the results of the microarray analyses, siRNAs were selected to target AP-1 members, FOS, FOSB, JUN and JUNB (Table S1). To avoid cell line bias, RNAi experiments were also performed in HEp-2 and THP-1 cell lines in addition to HCAEC, which are primary cells. Since results were similar between THP-1 and HCAEC experiments, some experiments were performed with only HEp-2 and THP-1 cell lines owing to the difficulty in working with primary cells.

Cells were cultured to 60%, and siRNAs including scrambled siRNA as a control, were transfected at a 75 nM final concentration, using 0.45% Oligofectamine (Invitrogen, Carlsbad, CA) in a 48-well format. The plates were placed in a tissue culture incubator at 37°C and 5% CO_2. After 48 h of siRNA-mediated gene knock-down, the medium was removed and the cells were infected with *C. pneumoniae* at an moi of 5. After an additional 24 h of incubation as above, each experiment was analysed for quantitative gene expression and protein concentrations as described below. All experiments were performed in triplicate.

Quantitative RT-PCR

Quantitative RT-PCR was performed as we have previously described (Gomes *et al*., 2005; Wang *et al*., 2010). Total RNA was extracted using an RNeasy RNA isolation kit (QIAGEN). DNA was digested with RQ DNase (Promega, Madison, WI) at 37°C for 30 min, and cDNA was generated using a Reverse Transcription kit (ABI, Carlsbad, CA). Quantitative real-time reverse transcriptase PCR (qRT-PCR) was run using the Power SYBR Green PCR Kit (ABI) and reagents as we described (Gomes *et al*., 2005; Wang *et al*., 2010). The primers for each analyte are shown in Table S2. Each experiment contained negative controls including no template controls, mock-infected HCAEC, HEp-2 or THP-1 cell cDNA and RNA samples without RT. PCR parameters consisted of one cycle of 95°C for 15 min, followed by 40 cycles of PCR at 95°C for 15 s, 55°C for 30 s and 72°C for 30 s. The relative amount of target gene mRNA and 16S bacterial rRNA was normalized to beta-actin mRNA. These experiments were performed in triplicate.

Cytokine protein quantification

Cytokine concentrations for IL2, IL4, IL6, IL8, IL10, IL12, GM-CSF, IFNγ, TNFα and IL1β were tested using Bio-Plex 10-plex kits (Bio-Rad, Hercules, CA) as per the manufacturer's protocols. Briefly, 50 µl of cell culture supernatant for each sample was collected and assayed in duplicate. A range (1.95–32 000 pg ml^{-1}) of standards for each cytokine were resuspended in diluent and used to plot standard curves. Data obtained from Bio-Plex Manager software program (Bio-Rad) for standardization and standard curves were converted to Excel™ (Microsoft Corporation, Seattle, WA) to determine the final concentration for each protein.

NF-κB activity and chemokine expression in HEK-TLR cells

HEK-Blue SEAP reporter cell lines, Null1, Null2, hTLR2, hTLR3 or hTLR4 (Invivogen, San Diego, CA), were grown in T75 flasks with DMEM high glucose media supplemented with 10% FCS, 50 U ml^{-1} penicillin, 50 mg ml^{-1} streptomycin and selected with the appropriate antibiotic according to the manufacturer's instructions. Twelve hours prior to stimulation, 1×10^5 HEK-Blue cells per well (24-well plate) were plated. At ~ 50% confluency, cells were left untreated or infected with *C. pneumoniae* at an moi of 1, 5, 10 or 40; or treated with 0.2, 2.0 or 20 mg ml^{-1} poly I:C (pI:C), 5 mg ml^{-1} Pam3SCK4 or 0.5 mg ml^{-1} ultra pure *Escherichia coli* lipopolysaccharide (LPS) as indicated (Invivogen). Supernatants were collected at 48 and 72 hpi for the NF-κB activity assay. Whole cells were collected for RNA isolation (below) at 72 hpi.

Collected supernatants from each sample were mixed at a ratio of 9:1 with QUANTI-Blue solution (Invivogen) in a flat-bottom 96-well plate. The samples were incubated at 37°C for 2 h and then the secretion level of Secreted Embryonic Alkaline Phosphatase (SEAP) was measured at 630 nm using a spectrophotometer.

For measurement of cytokine gene expression by real-time PCR, mRNA was isolated from cells after the indicated treatments using the Qiagen RNeasy kit (QIAGEN) following the manufacturer's instructions. The synthesis of the complementary DNA (cDNA) template was conducted according to the manufacturer's instruction (TaqMan, Roche, Pleasanton, CA). qPCR analysis using Mx3000P (Stratagene, La Jolla, CA) was conducted in triplicates in a 20 ml final volume with Brilliant III Ultra-Fast SYBR Green qPCR master mix (Stratagene). Real-time PCR included initial denaturation at 95°C for 3 min, followed by 40 cycles of 95°C for 5 s, 60°C for 20 s, and one cycle of 95°C for 1 min, 55°C for 30 s, 95°C for 30 s. The average for each treatment was normalized to the activity of a house-keeping gene, GAPDH. The relative expression of IL-8 for each cell type was normalized to the untreated samples. The statistical analysis was carried out using the unpaired *t*-test where $*P < 0.045$, $**P < 0.01$, $***P < 0.001$ and $****P < 0.0005$. Data were collected from three independent experiments.

Acknowledgements

We would like to thank Iong Iong Ip, Jiaxin Li and Tigist Mehari for excellent technical assistance. This research was supported in part by the Pacific Vascular Foundation (to S.C.J. and D.D.) and by the National Institutes of Allergy and Infectious Diseases-sponsored Pathogen Functional Genomics Resource Center at JCVI (to D.D.) and by the National Institutes of Health Grant R01 AI098843 (to D.D.).

References

Bader, G.D., and Hogue, C.W. (2003) An automated method for finding molecular complexes in large protein interaction networks. *BMC Bioinformatics* **4:** 2.

Balasubramanian, A., Ganju, R.K., and Groopman, J.E. (2003) Hepatitis C virus and HIV envelope proteins collaboratively mediate interleukin-8 secretion through activation of p38 MAP kinase and SHP2 in hepatocytes. *J Biol Chem* **278:** 35755–35766.

Belland, R.J., Ouellette, S.P., Gieffers, J., and Byrne, G.I. (2004) *Chlamydia pneumoniae* and atherosclerosis. *Cell Microbiol* **6:** 117–127.

Betts, H.J., Wolf, K., and Fields, K.A. (2009) Effector protein modulation of host cells: examples in the *Chlamydia* spp. arsenal. *Curr Opin Microbiol* **12:** 81–87.

Botos, I., Liu, L., Wang, Y., Segal, D.M., and Davies, D.R. (2009) The toll-like receptor 3:dsRNA signaling complex. *Biochim Biophys Acta* **1789:** 667–674.

Buchholz, K.R., and Stephens, R.S. (2006) Activation of the host cell proinflammatory interleukin-8 response by *Chlamydia trachomatis*. *Cell Microbiol* **8:** 1768–1779.

Calvano, S.E., Xiao, W., Richards, D.R., Felciano, R.M., Baker, H.V., Cho, R.J., *et al*. (2005) A network-based analysis of systemic inflammation in humans. *Nature* **437:** 1032–1037.

Campbell, L.A., and Kuo, C.C. (2004) *Chlamydia pneumoniae* – an infectious risk factor for atherosclerosis? *Nat Rev Microbiol* **2:** 23–32.

Cao, F., Castrillo, A., Tontonoz, P., Re, F., and Byrne, G.I. (2007) *Chlamydia pneumoniae*-induced macrophage foam cell formation is mediated by Toll-like receptor 2. *Infect Immun* **75:** 753–759.

Chen, S., Sorrentino, R., Shimada, K., Bulut, Y., Doherty, T.M., Crother, T.R., and Arditi, M. (2008) *Chlamydia pneumoniae*-induced foam cell formation requires MyD88-dependent and -independent signaling and is reciprocally modulated by liver X receptor activation. *J Immunol* **181:** 7186–7193.

Chinenov, Y., and Kerppola, T.K. (2001) Close encounters of many kinds: Fos-Jun interactions that mediate transcription regulatory specificity. *Oncogene* **20:** 2438–2452.

Cho, N.H., Seong, S.Y., Choi, M.S., and Kim, I.S. (2001) Expression of chemokine genes in human dermal microvascular endothelial cell lines infected with *Orientia tsutsugamushi*. *Infect Immun* **69:** 1265–1272.

Curran, T., and Franza, B.R., Jr (1988) Fos and Jun: the AP-1 connection. *Cell* **55:** 395–397.

Darville, T., O'Neill, J.M., Andrews, C.W., Jr, Nagarajan, U.M., Stahl, L., and Ojcius, D.M. (2003) Toll-like receptor-2, but not Toll-like receptor-4, is essential for development of oviduct pathology in chlamydial genital tract infection. *J Immunol* **171:** 6187–6197.

Dechend, R., Maass, M., Gieffers, J., Dietz, R., Scheidereit, C., Leutz, A., and Gulba, D.C. (1999) *Chlamydia pneumoniae* infection of vascular smooth muscle and endothelial cells activates NF-kappaB and induces tissue factor and PAI-1 expression: a potential link to accelerated arteriosclerosis. *Circulation* **100:** 1369–1373.

Derbigny, W.A., Kerr, M.S., and Johnson, R.M. (2005) Pattern recognition molecules activated by *Chlamydia muridarum* infection of cloned murine oviduct epithelial cell lines. *J Immunol* **175:** 6065–6075.

Derbigny, W.A., Hong, S.C., Kerr, M.S., Temkit, M., and Johnson, R.M. (2007) *Chlamydia muridarum* infection elicits a beta interferon response in murine oviduct epithelial cells dependent on interferon regulatory factor 3 and TRIF. *Infect Immun* **75:** 1280–1290.

Derbigny, W.A., Johnson, R.M., Toomey, K.S., Ofner, S., and Jayarapu, K. (2010) The *Chlamydia muridarum*-induced IFN-beta response is TLR3-dependent in murine oviduct epithelial cells. *J Immunol* **185:** 6689–6697.

Eferl, R., and Wagner, E.F. (2003) AP-1: a double-edged sword in tumorigenesis. *Nat Rev Cancer* **3:** 859–868.

Garcia, M., Jemal, A., Ward, E.M., Center, M.M., Hao, Y., Siegel, R.L., and Thun, M.J. (2007) *Global Cancer Facts & Figures 2007*. Atlanta, GA: American Cancer Society.

Gencay, M.M., Tamm, M., Glanville, A., Perruchoud, A.P., and Roth, M. (2003) *Chlamydia pneumoniae* activates epithelial cell proliferation via NF-kappaB and the glucocorticoid receptor. *Infect Immun* **71:** 5814–5822.

Gentleman, R.C., Carey, V.J., Bates, D.M., Bolstad, B., Dettling, M., Dudoit, S., *et al*. (2004) Bioconductor: open software development for computational biology and bioinformatics. *Genome Biol* **5:** R80.

Gomes, J.P., Hsia, R.C., Mead, S., Borrego, M.J., and Dean, D. (2005) Immunoreactivity and differential developmental expression of known and putative *Chlamydia trachomatis* membrane proteins for biologically variant serovars representing distinct disease groups. *Microbes Infect* **7:** 410–420.

Hahn, D.L., Schure, A., Patel, K., Childs, T., Drizik, E., and Webley, W. (2012) *Chlamydia pneumoniae*-specific IgE is prevalent in asthma and is associated with disease severity. *PLoS ONE* **7:** e35945.

Hennekens, C.H., and Buring, J.E. (1987) Epidemiology in medicine. In *Medicine (Baltimore)*. Mayrent, S.L. (ed.). Boston, MA: Little, Brown and Co., pp. 1–383.

Hogdahl, M., Soderlund, G., and Kihlstrom, E. (2008) Expression of chemokines and adhesion molecules in human coronary artery endothelial cells infected with *Chlamydia* (Chlamydophila) *pneumoniae*. *APMIS* **116:** 1082–1088.

Huang, B., Dong, Y., Cheng, Y., Xie, Q., Lin, G., Wu, Y., *et al*. (2008) *Chlamydia pneumoniae* infection and hyperlipidaemia-induced expression of P50 and c-Fos in the heart of C57BL6J mice. *Acta Cardiol* **63:** 175–179.

Karin, M., Lawrence, T., and Nizet, V. (2006) Innate immunity gone awry: linking microbial infections to chronic inflammation and cancer. *Cell* **124:** 823–835.

Kaul, R., and Wenman, W.M. (2001) *Chlamydia pneumoniae* facilitates monocyte adhesion to endothelial and smooth muscle cells. *Microb Pathog* **30:** 149–155.

Krull, M., Kramp, J., Petrov, T., Klucken, A.C., Hocke, A.C., Walter, C., *et al*. (2004) Differences in cell activation by *Chlamydophila pneumoniae* and *Chlamydia trachomatis* infection in human endothelial cells. *Infect Immun* **72:** 6615–6621.

Lad, S.P., Li, J., Correia, J., Pan, Q., Gadwal, S., Ulevitch, R.J., and Li, E. (2007) Cleavage of p65/RelA of the NF-kappaB pathway by *Chlamydia*. *Proc Natl Acad Sci USA* **104:** 2933–2938.

Le Negrate, G., Krieg, A., Faustin, B., Loeffler, M., Godzik, A., Krajewski, S., and Reed, J.C. (2008) ChlaDub1 of *Chlamydia trachomatis* suppresses NF-κB activation and inhibits IκBα ubiquitination and degradation. *Cell Microbiol* **10:** 1879–1892.

Li, D., Vaglenov, A., Kim, T., Wang, C., Gao, D., and Kaltenboeck, B. (2005) High-yield culture and purification of *Chlamydiaceae* bacteria. *J Microbiol Methods* **61:** 17–24.

Maere, S., Heymans, K., and Kuiper, M. (2005) BiNGO: a Cytoscape plugin to assess overrepresentation of gene ontology categories in biological networks. *Bioinformatics* **21:** 3448–3449.

von Mering, C., Jensen, L.J., Snel, B., Hooper, S.D., Krupp, M., Foglierini, M., *et al*. (2005) STRING: known and predicted protein-protein associations, integrated and transferred across organisms. *Nucleic Acids Res* **33:** D433–D437.

Metz, G., and Kraft, M. (2010) Effects of atypical infections with *Mycoplasma* and *Chlamydia* on asthma. *Immunol Allergy Clin North Am* **30:** 575–585.

Miller, S.A., Selzman, C.H., Shames, B.D., Barton, H.A., Johnson, S.M., and Harken, A.H. (2000) *Chlamydia pneumoniae* activates nuclear factor kappaB and activator protein 1 in human vascular smooth muscle and induces cellular proliferation. *J Surg Res* **90:** 76–81.

Misaghi, S., Balsara, Z.R., Catic, A., Spooner, E., Ploegh, H.L., and Starnbach, M.N. (2006) *Chlamydia trachomatis*-derived deubiquitinating enzymes in mammalian cells during infection. *Mol Microbiol* **61:** 142–150.

Molestina, R.E., Dean, D., Miller, R.D., Ramirez, J.A., and Summersgill, J.T. (1998) Characterization of a strain of *Chlamydia pneumoniae* isolated from a coronary atheroma by analysis of the *omp1* gene and biological activity in human endothelial cells. *Infect Immun* **66:** 1370–1376.

Mukhopadhyay, S., Clark, A.P., Sullivan, E.D., Miller, R.D., and Summersgill, J.T. (2004) Detailed protocol for purification of *Chlamydia pneumoniae* elementary bodies. *J Clin Microbiol* **42:** 3288–3290.

Naiki, Y., Michelsen, K.S., Schroder, N.W., Alsabeh, R., Slepenkin, A., Zhang, W., *et al*. (2005) MyD88 is pivotal for the early inflammatory response and subsequent bacterial clearance and survival in a mouse model of *Chlamydia pneumoniae* pneumonia. *J Biol Chem* **280:** 29242–29249.

Nijhara, R., Jana, S.S., Goswami, S.K., Rana, A., Majumdar, S.S., Kumar, V., and Sarkar, D.P. (2001) Sustained activation of mitogen-activated protein kinases and activator protein 1 by the hepatitis B virus X protein in mouse hepatocytes *in vivo*. *J Virol* **75:** 10348–10358.

Olivares-Zavaleta, N., Carmody, A., Messer, R., Whitmire, W.M., and Caldwell, H.D. (2011) *Chlamydia pneumoniae* inhibits activated human T lymphocyte proliferation by the induction of apoptotic and pyroptotic pathways. *J Immunol* **186:** 7120–7126.

Patel, K.K., Anderson, E., Salva, P.S., and Webley, W.C. (2012) The prevalence and identity of *Chlamydia*-specific IgE in children with asthma and other chronic respiratory symptoms. *Respir Res* **13:** 32.

Pikarsky, E., Porat, R.M., Stein, I., Abramovitch, R., Amit, S., Kasem, S., *et al*. (2004) NF-kappaB functions as a tumour promoter in inflammation-associated cancer. *Nature* **431:** 461–466.

Prebeck, S., Kirschning, C., Durr, S., da Costa, C., Donath, B., Brand, K., *et al*. (2001) Predominant role of toll-like receptor 2 versus 4 in *Chlamydia pneumoniae*-induced activation of dendritic cells. *J Immunol* **167:** 3316–3323.

Ramirez, J.A. (1996) Isolation of *Chlamydia pneumoniae* from the coronary artery of a patient with coronary atherosclerosis. The *Chlamydia pneumoniae*/Atherosclerosis Study Group. *Ann Intern Med* **125:** 979–982.

Ravichandran, V., Sabath, B.F., Jensen, P.N., Houff, S.A., and Major, E.O. (2006) Interactions between c-Jun, nuclear factor 1, and JC virus promoter sequences: implications for viral tropism. *J Virol* **80:** 10506–10513.

Reiss, D.J., Avila-Campillo, I., Thorsson, V., Schwikowski, B., and Galitski, T. (2005a) Tools enabling the elucidation of molecular pathways active in human disease: application to Hepatitis C virus infection. *BMC Bioinformatics* **6:** 154.

Reiss, K., Maretzky, T., Ludwig, A., Tousseyn, T., de Strooper, B., Hartmann, D., and Saftig, P. (2005b) ADAM10 cleavage of N-cadherin and regulation of cell–cell adhesion and beta-catenin nuclear signalling. *EMBO J* **24:** 742–752.

Selzman, C.H., Netea, M.G., Zimmerman, M.A., Weinberg, A., Reznikov, L.L., Grover, F.L., and Dinarello, C.A. (2003) Atherogenic effects of *Chlamydia pneumoniae*: refuting the innocent bystander hypothesis. *J Thorac Cardiovasc Surg* **126:** 688–693.

Senn, L., Jaton, K., Fitting, J.W., and Greub, G. (2011) Does respiratory infection due to *Chlamydia pneumoniae* still exist? *Clin Infect Dis* **53:** 847–848.

Seo, J.H., Lim, J.W., Kim, H., and Kim, K.H. (2004) *Helicobacter pylori* in a Korean isolate activates mitogen-activated protein kinases, AP-1, and NF-kappaB and induces chemokine expression in gastric epithelial AGS cells. *Lab Invest* **84:** 49–62.

Sessa, R., Di Pietro, M., Schiavoni, G., Macone, A., Maras, B., Fontana, M., *et al*. (2009) *Chlamydia pneumoniae* induces T cell apoptosis through glutathione redox imbalance and secretion of TNF-alpha. *Int J Immunopathol Pharmacol* **22:** 659–668.

Shaulian, E., and Karin, M. (2002) AP-1 as a regulator of cell life and death. *Nat Cell Biol* **4:** E131–E136.

Singhal, M., and Domico, K. (2007) CABIN: collective analysis of biological interaction networks. *Comput Biol Chem* **31:** 222–225.

Singhal, M., and Resat, H. (2007) A domain-based approach to predict protein–protein interactions. *BMC Bioinformatics* **8:** 199.

Takeuchi, O., and Akira, S. (2009) Innate immunity to virus infection. *Immunol Rev* **227:** 75–86.

Vallejo, J.G., Knuefermann, P., Mann, D.L., and Sivasubramanian, N. (2000) Group B Streptococcus induces TNF-alpha gene expression and activation of the transcription factors NF-kappa B and activator protein-1 in human cord blood monocytes. *J Immunol* **165:** 419–425.

Vercammen, E., Staal, J., and Beyaert, R. (2008) Sensing of viral infection and activation of innate immunity by toll-like receptor 3. *Clin Microbiol Rev* **21:** 13–25.

Wang, A., Johnston, S.C., Chou, J., and Dean, D. (2010) A systemic network for *Chlamydia pneumoniae* entry into human cells. *J Bacteriol* **192:** 2809–2815.

Wolf, K., Plano, G.V., and Fields, K.A. (2009) A protein

secreted by the respiratory pathogen *Chlamydia pneumoniae* impairs IL-17 signaling via interaction with human Act1. *Cell Microbiol* **11:** 769–779.

Wu, J.Y., Lu, H., Sun, Y., Graham, D.Y., Cheung, H.S., and Yamaoka, Y. (2006) Balance between polyoma enhancing activator 3 and activator protein 1 regulates *Helicobacter pylori*-stimulated matrix metalloproteinase 1 expression. *Cancer Res* **66:** 5111–5120.

Xie, J., Pan, H., Yoo, S., and Gao, S.J. (2005) Kaposi's sarcoma-associated herpesvirus induction of AP-1 and interleukin 6 during primary infection mediated by multiple mitogen-activated protein kinase pathways. *J Virol* **79:** 15027–15037.

Ye, F.C., Blackbourn, D.J., Mengel, M., Xie, J.P., Qian, L.W., Greene, W., *et al*. (2007) Kaposi's sarcoma-associated herpesvirus promotes angiogenesis by inducing angiopoietin-2 expression via AP-1 and Ets1. *J Virol* **81:** 3980–3991.

Yeo, M., Park, H.K., Lee, K.M., Lee, K.J., Kim, J.H., Cho, S.W., and Hahm, K.B. (2004) Blockage of HSP 90 modulates Helicobacter pylori-induced IL-8 productions through the inactivation of transcriptional factors of AP-1 and NF-kappaB. *Biochem Biophys Res Commun* **320:** 816–824.

Yu, H., Kim, P.M., Sprecher, E., Trifonov, V., and Gerstein, M. (2007) The importance of bottlenecks in protein networks: correlation with gene essentiality and expression dynamics. *PLOS Comput Biol* **3:** e59.

Zachos, G., Clements, B., and Conner, J. (1999) Herpes simplex virus type 1 infection stimulates p38/c-Jun N-terminal mitogen-activated protein kinase pathways and activates transcription factor AP-1. *J Biol Chem* **274:** 5097–5103.

Supporting information

Additional Supporting Information may be found in the online version of this article:

Table S1. Gene and nucleotide sequences of small interfering RNA.

Table S2. Primers used for quantitative real-time PCR.